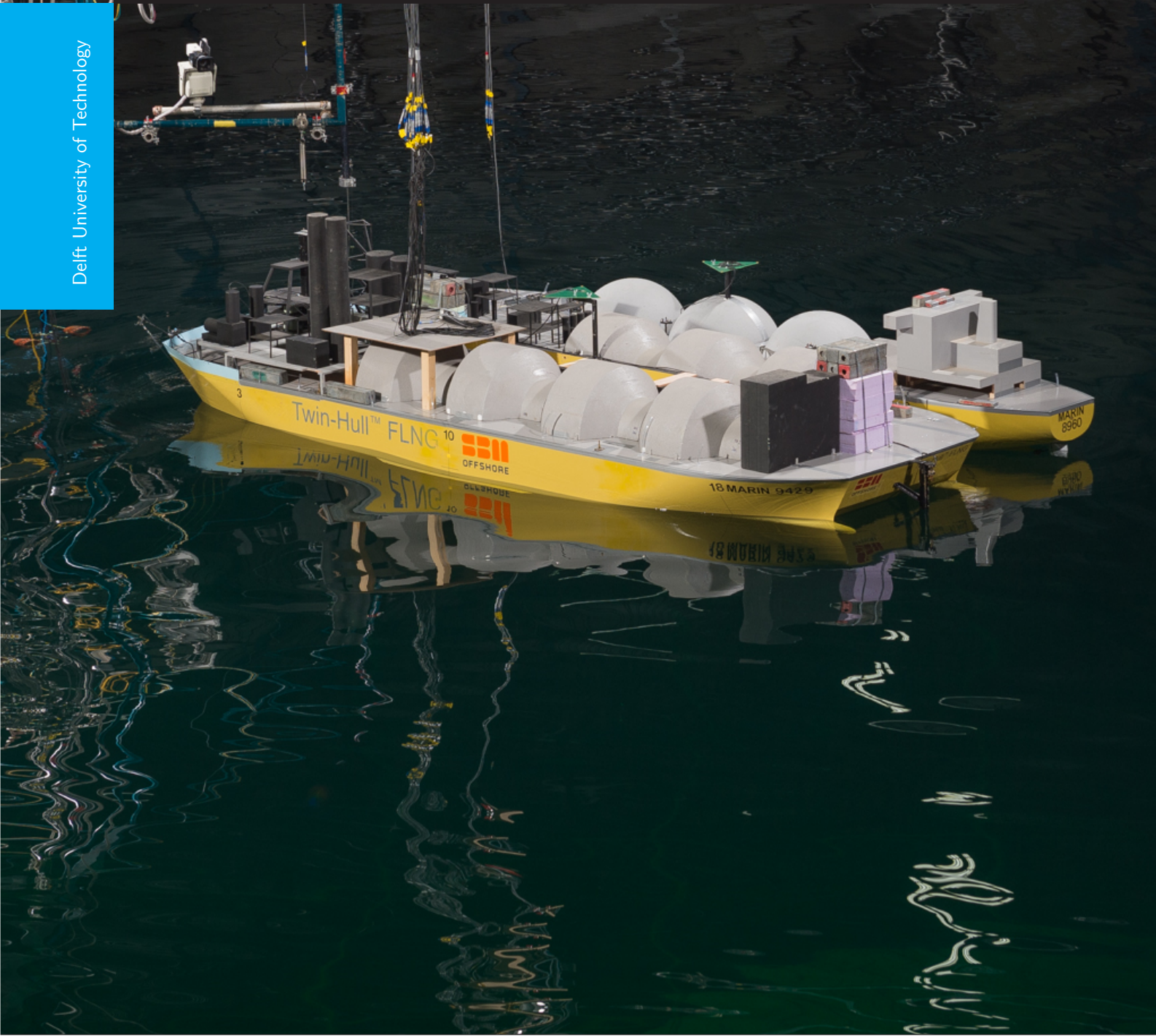


The relative motions of an FLNG and an LNG carrier in side-by-side arrangement

A numerical and experimental analysis

W.W. Quast



THE RELATIVE MOTIONS OF AN FLNG AND AN LNG CARRIER IN SIDE-BY-SIDE ARRANGEMENT

A NUMERICAL AND EXPERIMENTAL ANALYSIS

by

W.W. Quast

in partial fulfillment of the requirements for the degree of

Master of Science
in Offshore & Dredging Engineering

at the Delft University of Technology,
to be defended publicly on Wednesday April 8, 2015 at 11:00 AM.

Student number: 1309277
Thesis committee: Prof.dr.ir. R.H.M. Huijsmans Delft University of Technology
Ir. J. den Haan Delft University of Technology
Dr.ir. S. A. Miedema Delft University of Technology
Ir. T. Brinkel SBM Offshore
Ir. X. Schut SBM Offshore

PREFACE

This report contains my master's thesis research into the validation of side-by-side mooring analysis, using HydroStar , Ariane and scale model test data. This thesis is part of the Offshore Engineering & Dredging Engineering masters curriculum of the Delft University of Technology. Experiments were fulfilled at the MARIN Offshore Basin in Wageningen in February 2014. The research was carried out at SBM Offshore from February 2014 until March 2015. The supervising graduation committee consisted of the following persons:

Prof.dr.ir. R.H.M. Huijsmans	Delft University of Technology
Ir. J. den Haan	Delft University of Technology
Dr.ir. S. A. Miedema	Delft University of Technology
Ir. T. Brinkel	SBM Offshore
Ir. X. Schut	SBM Offshore

I would like to thank my whole committee for their time and effort in supporting me during the execution of this thesis, and especially Xavier Schut for his daily supervision and help. Furthermore I would like to thank SBM for the opportunity to perform my research in such a groundbreaking project as the Twin-hull FLNG.

Schiedam, March 23, 2015

Wouter Quast

EXECUTIVE SUMMARY

For future Floating Liquid Natural Gas vessel (FLNG) developments, SBM Offshore is considering systems for offloading of Liquid Natural GAS (LNG). The ability to offload LNG at minus 163 degrees Celsius from the Twin-Hull FLNG to an LNG Carrier (LNGC), is of high importance to the overall operability and economic viability of FLNG development. Side-by-side offloading is preferred above tandem offloading, due to the location of the (off-)loading manifolds on the LNG carrier. Furthermore the maximum distance for transporting the -163 degrees LNG is limited due to mechanical and thermal properties of offloading system components.

Traditionally, time-consuming physical model tests are being used to determine the side-by-side relative response of the FLNG and the LNGC, when subjected to specific waves forces. The aim of this thesis is to verify and validate the suitability of HydroStar and Ariane software models, to predict responses for the FLNG and the LNG carrier, by comparing the vessel response calculations to the results of model tests performed in the MARIN offshore basin. The calculated responses are performed both in frequency domain and in time-domain, which in both cases is much faster obtained compared to responses obtained by physical model tests. The relative manifold motions are a crucial design factor for the (off-)loading system.

A description of the MARIN offshore basin setups for soft-mooring and turret-mooring is given. Both setups are without the LNGC, so the FLNG is moored on its own inside the offshore basin. The responses obtained from these experiments are illustrated and compared. This study exposed unexpected outcomes for roll and especially the sway Response Amplitude Operator (RAO). The sway RAO shows an extreme peak value for the turret moored FLNG. This peak value is not observed in the soft mooring experiments. A theoretical description of HydroStar with the respective setups for the FLNG without the LNG Carrier is discussed. HydroStar does not account for a mooring-system so the same model is used both for the soft- as for the turret-mooring. The frequency response calculated by HydroStar corresponds more to the response observed in soft-mooring than to the response observed in turret-mooring. The HydroStar response does not show the extreme sway peak observed in turret-mooring experiments. Furthermore a sensitivity analysis by HydroStar concluded that the extra roll response of the FLNG in soft-mooring can be the result of a different weight distribution between the two vessels. Two different vessel setups were used in the turret- and soft-mooring experiments.

The response of the side-by-side setup is analyzed using HydroStar. The FLNG in SBS arrangement shows a similar response as to the FLNG alone, no extreme sway peak response is observed by HydroStar. Likewise, the response of the LNGC is about the same as the FLNG response. However the response obtained from MARIN for the FLNG in side-by-side (SBS) arrangement shows again no correlation for sway in the lower wave frequencies. This exceptional sway peak also applies for the sway response for the LNGC, observed in the offshore basin. The natural frequency of the turret mooring system does not come near this sway peak. Therefore the mooring system does not seem to be responsible for the observed sway motion amplification. Investigation on the effects of weight distribution, epsilon damping and linear viscous damping, showed that also these are not the source for the sway motion amplification. Possibly viscous phenomena are causing the observed sway behavior, which are neglected in HydroStar. HydroStar is not capable of calculating the sway RAO's for this typical mooring set-up. In order to "fit" the computed RAO's with the obtained experimental RAO's, the model has been tuned. The "tuned" RAO's are the RAO's computed by HydroStar except for the sway RAO. The "tuned" sway amplitude RAO and the "tuned" sway phase RAO are obtained from MARIN.

Subsequently, using Ariane multiple time domain analysis are executed, with the "untuned" and "tuned" RAO's as input. Their results consist of time traces of the relative manifold motions, which are compared with the manifold motions obtained from the MARIN experiments. The time domain analysis with "untuned" RAO's show satisfying correlations in X- and Z-direction, however the Y-direction (relative sway) does not correlate with the relative sway obtained in the offshore basin. For the "tuned" RAO's all six Degree of Freedom (DOF)'s do correlate, including the sway motions.

Due to insufficient experimental data, a true validation of the HydroStar SBS model and Ariane SBS model is not possible. Therefore it is recommended to perform additional side-by-side experiments in the MARIN offshore basin, which include appropriate parameters purposely designed for calculating the HydroStar SBS and Ariane SBS models.

ACRONYMS

CALM Catenary Anchor Leg Mooring.

CL Center Line.

COG Center of Gravity.

COOL Cryogenic Offshore Offloading and Loading.

DOF Degree of Freedom.

FFT Fast Fourier transform.

FLNG Floating Liquid Natural Gas vessel.

JONSWAP Joint North Sea Wave Project.

LC Load Case.

LNG Liquid Natural GAS.

LNGC LNG Carrier.

NDI Northern Digital Inc..

QTF Quadratic Transfer Function.

RAO Response Amplitude Operator.

SBM Single Buoy Mooring.

SBS side-by-side.

SPM Single Point Mooring.

VLCC Very Large Crude Carriers.

CONTENTS

Preface	iii
Executive summary	v
1 Introduction	1
1.1 Tandem offloading	1
1.2 Single point mooring offloading [1]	2
1.3 Onshore Offloading	3
1.4 Side-by-Side Offloading.	3
1.5 LNG Loading arms	4
1.6 Offloading hoses	4
1.7 Liquefied natural gas (LNG)	5
1.8 Availability of offshore LNG offloading	5
1.9 Loading arms or COOL hose operational envelope [2]	5
2 Thesis problem Analysis	7
2.1 Research question	7
2.2 Objectives.	7
3 Background	9
3.1 Axis and sign convention	9
3.2 Waves	10
3.2.1 Regular waves	10
3.2.2 Irregular waves.	10
3.2.3 Wave energy spectrum.	10
3.3 Relative vessel motions	11
3.4 Response Amplitude Operator	12
3.5 Velocity potential theory	13
3.6 Second order wave drift forces	13
3.7 Diffraction Theory	15
3.8 Forces and moments	15
3.9 Single body equation of motion.	16
3.10 Multi body equation of motion	16
4 MARIN experiments	19
4.1 Twin-Hull FLNG [3]	19
4.2 LNG Carriers	20
4.3 Set up and Model Characteristics	21
4.4 Instrumentation	22
4.4.1 Wave heights.	22
4.4.2 Motions of the model	23
4.4.3 Mooring lines	23
4.5 Mooring characteristics.	24
4.5.1 Turrent mooring	24
4.5.2 Side-by-side mooring	26
4.6 Wave calibration	26
4.7 Wave spectra	28
4.8 Shielding effects wind, current and waves.	30
4.9 Decay Tests	30
4.9.1 Mooring damping FLNG alone.	31
4.9.2 Mooring damping LNGC.	33

4.10 Motion translation	33
5 FLNG single vessel analysis	35
5.1 Introduction	35
5.2 FLNG alone in Hydrostar	35
5.2.1 FLNG in soft-mooring	35
5.2.2 FLNG in turret-mooring	37
5.3 Weight distribution	37
5.3.1 Sensitivity analysis on the weight distribution	40
6 Side-by-side diffraction analysis	43
6.1 Introduction	43
6.2 Hull geometries	43
6.3 Epsilon damping lid.	43
6.3.1 Conventional un-damped wave RAO.	45
6.3.2 Sensitivity analysis for wave RAO, by varying ϵ of the damping lid	45
6.3.3 Sensitivity analysis for motion RAO, by varying ϵ of the damping lid	46
6.4 Roll damping [4]	46
6.5 Headings	46
6.6 Frequency sensitivity	48
6.7 HydroStar side-by-side model results	48
6.7.1 FLNG RAO's	48
6.7.2 LNGC RAO's	50
6.8 MARIN results	50
6.9 QTF study	50
6.10 RAO tuning	52
7 Time-domain analysis	55
7.1 Introduction	55
7.2 Theory [5]	55
7.3 Decay tests	56
7.3.1 Damping.	56
7.3.2 Natural period	56
7.4 Relative motions	60
7.5 Environment O2	60
7.6 Case 1: "un-tuned" RAO's as input for Ariane	60
7.7 Case 2: "tuned" RAO's as input for Ariane	62
7.8 Fenders	62
7.9 Conclusion	62
8 Conclusions and recommendations	65
8.1 Introduction	65
8.2 Conclusions on the different motions measured in soft-mooring and turret-mooring	65
8.3 Conclusions on the discrepancies between the MARIN experiments frequency response and time-domain for the side-by-side arrangement	65
8.4 Recommendations	66
Bibliography	69
A Wave spectra	71
B Response spectra	75
C Frequency iteration response	83
D Viscous lid damping, ϵ damping	97
E Viscous roll damping	117
F Decay Plots	143
G Different QTF methods	147

1

INTRODUCTION

The significant growth in LNG production, export, import and transport has increased the demand for larger and more efficient facilities for LNG production. Traditionally, LNG import has been through onshore import and export terminals. These onshore terminals are having inherent safety risks and are meeting public resistance. Furthermore, large amounts of gas have been found in areas with a lack of infrastructure and in remote offshore areas, where subsea tiebacks are not possible or uneconomical. Therefore, LNG offshore production facilities as well as import and export terminals are gaining more and more interest. Both offshore production facilities and import and export terminals are at this moment under development. One of the greatest challenges for floating LNG plants and terminals is its offloading procedure. This should be executed in a fast and reliable way. The technical solutions for cryogenic liquefaction of natural gas and regasification of LNG on board an offshore floating platform are available, as well as the transfer in calm and sheltered conditions. However safe and reliable transfer of LNG in open sea conditions is not a proven concept. Due to the environmental conditions, which causes relative motions between vessels, the offloading system and the side-by-side mooring system should be able to overcome twelve degrees of freedom. The relative motions between the vessels are of crucial importance for the design of the mooring system and the (off-) loading system. Configurations possible for offloading are listed below:

- Tandem
- Side by side
- Catenary Anchor Leg Mooring
- Onshore offloading
- Soft mooring

The above mentioned techniques will be discussed in the following paragraphs.

1.1. TANDEM OFFLOADING

Tandem offloading which is illustrated in Figure 1.1 is a standard configuration for the unloading of a traditional Floating Production Storage Offloading unit (FPSO). Connecting the carrier with the use of a hawser to the stern of the FPSO will keep the vessel at a safe distance. Due to the turret moored FPSO, both vessels will take the optimal heading with respect to the environmental conditions while offloading. The FPSO's (off-) loading manifold is located at the aft of the vessel whereas, the manifold of the carrier can either be located at the fore or mid-ship. A floating or aerial offloading hose will enable the transfer of the cargo between the two vessels.

FPSO's which make use of a spread mooring system need additional tugs for tandem offloading. Due to the spread mooring of the FPSO, the carrier is not able to weather-vane. Therefore the carrier is assisted with one or more tugs to keep it on the right location.



Figure 1.1: Tandem offloading FPSO Xibomba



Figure 1.2: SBS offloading [6]

1.2. SINGLE POINT MOORING OFFLOADING [1]

Single Point Mooring (SPM) systems permit the vessel to weathervane while the vessel is moored to a floating buoy. A typical example for an SPM is the Catenary Anchor Leg Mooring (CALM) shown in figure 1.3. Such mooring systems consist of a floating buoy, turntable and catenary chain legs which are secured to anchors or piles on the seabed. One or two hawsers hold the carrier in place. The bearings in the turntable allow the carrier to weather-vane around the buoy. The fluid is transferred between the buoy to or from the vessel by means of a combined floating and sub-sea hose system. Different CALM designs have been developed, for a variety of applications, water depths and vessels ranging from small product carriers to Very Large Crude Carriers (VLCC).



Figure 1.3: CALM buoy[1]



Figure 1.4: Onshore offloading



Figure 1.5: Yoke mooring

1.3. ONSHORE OFFLOADING

For offloading near shore numerous mooring systems for offloading are available. Figure 1.4 illustrates a method for offloading a LNG carrier using offloading arms, while moored to a jetty. Usually this manner of offloading is performed in sheltered waters; resulting in low relative motions. Tugs may be used to manoeuvre the carrier in the correct place.

Yoke mooring systems as illustrated in figure 1.5 can either be connected to a jacket structure fixed to the seabed, or to a floating buoy. The Yoke has a shape of an 'A' and is suspended vertically by two mooring legs. The A frame is connected to the stern or aft of the vessel. These systems are in use for mooring, however they are not yet in operation for offloading. SBM Offshore designed a Soft Yoke Mooring and Offloading (SYMO) unit. The offloading unit is combined with the Mooring system integrated into a buoy at the stern of a FLNG. In this case the LNGC can remain moored in seas up to 5.5 significant wave height. A similar design is applied for Tandem mooring.

1.4. SIDE-BY-SIDE OFFLOADING

SBM Offshore has designed mooring systems like the enhanced side-by-side mooring shown in figure 1.2. This mooring system is designed to withstand sea states up to approximately 3.0 meters significant wave height. SBS moored vessels show different characteristics compared to tandem moored vessel. Hydrodynamic interaction between the vessels increases dramatically, which impacts on relative motions and drift forces due to the close proximity of the vessels. Today SBS offloading usually takes place in moderate climates, with prevailing low sea state. The relative manifold motions become a crucial design factor for the availability of SBS offloading. This orientation is a proven method and is widely used among offloading FPSO's. With the help of breast lines, spring lines and fenders the carrier is attached at the side of the FPSO. The fenders and lines can only withstand a certain amount of elongation/ compressing, therefore the understanding of relative motions between these vessels is crucial. The offloading of the cargo is done with the help of loading arms or through a flexible cargo hose, which is connected at both ends to the mid-ship manifolds. LNG Carriers unlike oil tankers, are typically designed for offloading with hard arm operations. The manifolds on

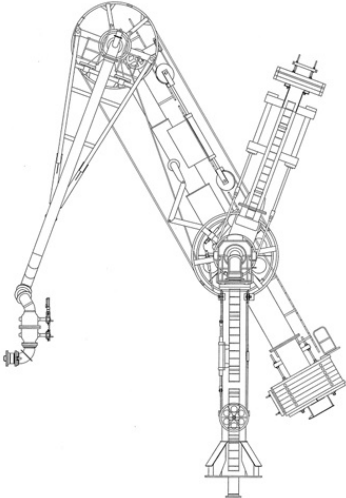


Figure 1.6: Chicksan Marine Loading System

most LNGC are located midship, as described in Section 4.2. Further more their cranes and chain stoppers for offloading offshore are not suited for tandem operations. Therefore it is anticipated that side-by-side operations will be favored for LNG carriers and so this thesis is focused on relative motions during side-by-side mooring of an FLNG and an LNGC.

1.5. LNG LOADING ARMS

Loading arms such as the Chicksan marine loading system displayed in figure 1.6 have been around since the fifties [7]. Their main use is for ship to shore offloading. Multiple arms can be placed next to each other for offloading very large carriers. The arms consists of several rigid tubes, designed so they can handle cryogenic temperatures. Multiple swivel joints connect the tubes and ensure the connecting piping is not subjected to large stress levels. The swivel joints on the loading arm are one of the most crucial components and must be checked routinely to ensure safe operation. The Chicksan loading arms are equipped with a Powered Emergency Release System (PERS). These release systems disconnects the piping from the LNG carrier almost instantly when stress levels become to high. Before disconnect, the isolation valves on each side of the system close, preventing an LNG spill. When disconnected the arm manoeuvres away from the ships connection. The loading arm is a loading system which could also be used for SBS offloading. For such a design the relative motions between the manifolds, during an offloading operation are needed as input for the design.

1.6. OFFLOADING HOSES

The flexible hose is a key component for a swivel-less transfer system for LNG. Multiple companies have designed cryogenic flexible hoses. Technip designed two Cryogenic flexible hoses; Mark 1 and Mark 2. Mark 1 is designed for an aerial connection whereas Mark 2 is a connection used for floating conditions. The physical difference between the pipes is recognized throughout the different material properties used for the layer buildup.

For (off-) loading SBM Offshore has also developed a flexible hose, called the Cryogenic Offshore Offloading and Loading (COOL) hose. This hose is specially designed for offloading LNG while the hose is floating in sea water. The hose is based on proven concepts and is compliant with the relevant applicable international standards. The main components of the COOL hose are shown in Figure 1.7. Unfortunately this hose cannot yet be applied for tandem offloading due to length restrictions. The hose might be usable for SBS offloading when the outer insulation is removed, reducing its minimal bending radius. This makes the hose more flexible. However for such a design the relative motions between the vessels are still a crucial design factor. Therefore this thesis focuses on determining the relative manifold motions.

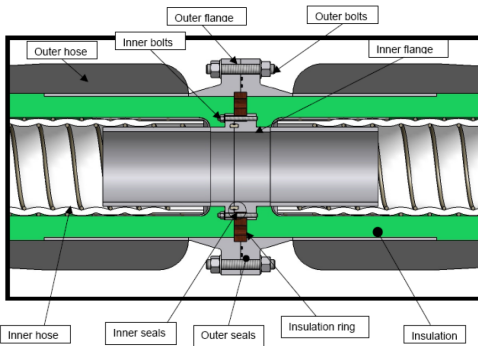


Figure 1.7: Isolated COOL hose main components

	Mark1	Mark2
Normal export flow speed	7 m/s	7 m/s
Maximum allowable working pressure	12 bar	18 bar
Cryogenic burst pressure	>> 60 bar	>> 90 bar
Design temperature	-163°C	-163°C
Minimum temperature	-196°C	-196°C
Internal diameter	14" to 18"	14" to 18"
Storage radius for 16" ID	4.5 m	5.0 m
Nominal operating life	10 years	10 years
Applicable standard	EN-1474	EN-1474

Table 1.1: Properties Technip's Cryogenic flexible hoses

1.7. LIQUEFIED NATURAL GAS (LNG)

The main advantage of LNG is the ease of transport and storage of gas. When gas is liquefied, it is about 600 times less voluminous than natural in gaseous state. This creates an energy density which is around 60% of that of diesel fuel, which makes LNG a cost efficient way to transport gas over large distances where a gas pipeline infrastructure does not exist. An additional benefit of LNG is its non-toxic and non-corrosive properties. The liquefaction of gas involves purification by removal of the condensates, CO₂ and acids followed by the cooling of gas in several stages until liquefaction is achieved. The temperature when liquefied is approximately -163 degrees Celsius.

1.8. AVAILABILITY OF OFFSHORE LNG OFFLOADING

The window of opportunity for LNG side-by-side offloading operations, also known as "offloading operability", is defined as a probability set at a randomly selected time period with given metocean criteria, during which offloading can be done in a successful and safe manner. The ability to offload LNG at minus 163 degrees Celcius from the FLNG to an LNGC is of high importance to the overall operability and thereby economic viability of an FLNG development. One of the crucial components in the SBS mooring system are the lines and fenders, which keep the vessels at the correct distance and make sure the vessels do not collide. Their design is crucial for the determination of the offloading operability. More factors determining this offloading operability are, wave height, wave direction, wave frequency, current, wind, hull design,

1.9. LOADING ARMS OR COOL HOSE OPERATIONAL ENVELOPE [2]

Either a COOL hose or an FMC hard arm can be used for side-by-side offloading. The offloading system has to be designed such that the operating envelope can cope with the relative motions including the static and dynamic height difference between the position of the manifold on the FLNG and the manifold on the LNGC. The operating envelope is defined as containing a connection zone, an operating zone, maximum drift zone and a mechanical limit.

The connection zone includes all the different positions between the manifolds in which the offloading system is capable to make a secure connection. The operating zone is defined as the connection area plus

the minimum allowable drift to continue transfer operations. The drift is the result of the relative motions between the FLNG and the LNGC and is depending on environmental conditions, vessel heading and the resulting vessel responses of the FLNG and the LNGC. This thesis focuses on determining the operating zone in a particular sea-state.

2

THESIS PROBLEM ANALYSIS

2.1. RESEARCH QUESTION

The primary goal of this research was initially to design a side-by-side LNG offloading system that can cope with predefined relative motions. However the complexity of the study on determining the relative motions was underestimated, due to unexpected results. Therefore the final goals had to be adjusted. For SBM's issues related to side-by-side mooring, the following research questions have been drawn up and will be answered in this thesis:

- Is there a difference between the first order motions measured in soft-mooring and turret-mooring configuration?
- What are the discrepancies in terms of first order motions, between the Side-by-side mooring tests result compared with the HydroStar frequency response output?
- What is the implication of the discrepancies in first order motions on the time domain simulations in Ariane?

2.2. OBJECTIVES

The following objectives for the research have been set to ensure that the above research questions will be answered:

- Verification of the HydroStar & Ariane model
- Validation of the HydroStar & Ariane model
- Identification of possible improvements to the Ariane model

Verification is used to confirm that the software's numerical model accurately represents the developer's conceptual description of the model and the solution of the model. The method to do so is by using several sensitivity studies to verify the changes in output when altering input parameters and comparing with theoretical results. Validation is used to confirm the degree to which the numerical model is an accurate representation of the real world. However there is no real word data available yet for this research, so the data used is from available physical scale model experiments done at MARIN. The steps of validating the model are as follows:

- Simulating the same sea states as carried out at MARIN by the Ariane model.
- Setting up a thorough comparison between the sea-states run in the numerical model and the results from the sea-states at MARIN.

3

BACKGROUND

This chapter is reserved for the overall picture and the definitions used for this study. A summarized description of the basic theory on waves and of a floating structure in waves is presented.

3.1. AXIS AND SIGN CONVENTION

A vessel's motions about the Center of Gravity (COG) can be decomposed into translations and rotations as shown in Figure 3.1. The vessel is fitted with a right handed coordinate system with its x-axis pointing in the direction of the bow and its z-axes which points upwards.

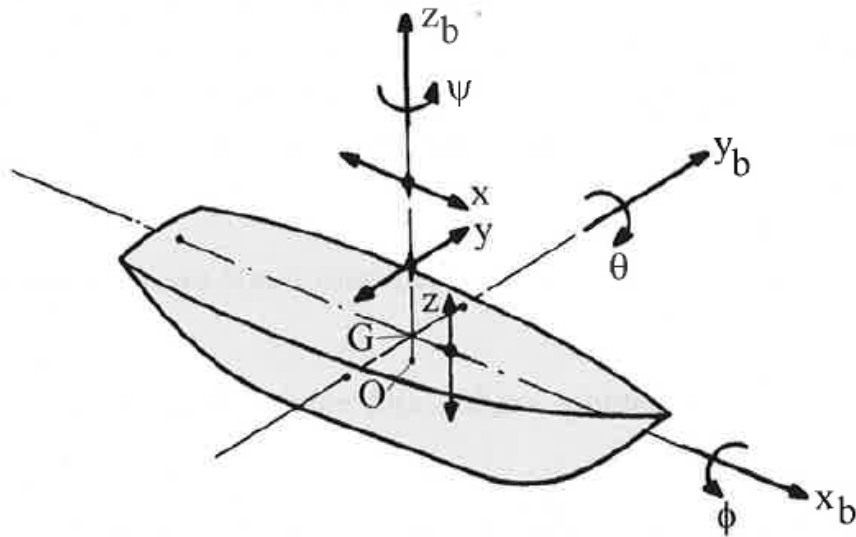


Figure 3.1: Definition of ship motions in six degrees of Freedom
[8]

There are three types of translations recognized in the x -, y -, and z -direction

- surge in x -direction, positive towards the bow
- sway in y -direction, positive towards port side
- heave in z -direction, positive upwards

There are three type of rotations about x –, y – and z – axis, (positive in the direction of the arrows depicted in Figure 3.1)

- Rotation around the front to back axis (x axis) is called roll
- Rotation around the side to side axis (y axis) is called pitch
- Rotation around the vertical axis (z axis) is called yaw

3.2. WAVES

Environmental loads such as waves acting on a vessels, causes a response. Therefore it is necessary to analyze the incoming waves in order to determine the wave loads.

3.2.1. REGULAR WAVES

When a harmonic regular wave moves in a positive x -direction, the wave profile can be expressed as function of both a space dependent term x and a time-dependent term t as follows:

$$\zeta = \zeta_a \cos(kx - \omega t) \quad (3.1)$$

where

- $\zeta(t)$ = surface elevation [m]
- ζ_a = wave amplitude component [m]
- ω_n = $2\pi/T$, frequency of wave component n [rad/s]
- k = $2\pi/\lambda$, the wave number [rad/m]

3.2.2. IRREGULAR WAVES

The sea does not consist of a single harmonic wave, but is built up from multiple harmonic waves summed together. In order to describe the sea surface as a stochastic process the assumption is made that the wave amplitude repeats its-self after an (long) interval. The wave elevation in figure 3.2 (in the time domain) of a long-crested irregular sea-state, propagating along the positive x axis, can be written as the sum of a large number of regular wave components (in the frequency domain):

$$\zeta(t) = \sum_{n=1}^N \zeta_a \cos(k_n x - \omega_n t + \varepsilon_n) \quad (3.2)$$

where

- ε_n = phase angle of wave component n [rad]
- k_n = wave number component [rad/m]

When enough Fourier series terms are included, the entire time record at a certain point can be reproduced using equation 3.2.

3.2.3. WAVE ENERGY SPECTRUM

The Fourier series in Equation 3.2 can be transformed into an energy density spectrum. First the mean square value can be found: $\overline{\zeta_{a_n}^2}$. When $\zeta(t)$ is an irregular signal without prevailing frequencies, the average values $\overline{\zeta_{a_n}^2}$ close to ω_n will not change much as a function of the frequency; $\overline{\zeta_{a_n}^2}$ is a continuous function. Now it is possible to setup the elevation as a spectrum which gives the amplitude per frequency interval:

$$S_\zeta(\omega_n) \cdot \Delta\omega = \sum_{\omega_n}^{\omega_n + \Delta\omega} \frac{1}{2} \zeta_{a_n}^2(\omega) \quad (3.3)$$

where

- $S_\zeta(\omega_n)$ = wave spectrum [m^2/s]

In the spectrum the phase angle term is irrelevant and can therefore be discarded. Letting $\Delta\omega$ decrease down to almost zero results in the definition of the wave energy spectrum $S_\zeta(\omega_n)$:

$$S_\zeta(\omega_n) \cdot d\omega = \frac{1}{2} \zeta_{a_n}^2(\omega) \quad (3.4)$$

A schematic representation of the transformation from time domain towards frequency domain is presented in Figure 3.3.

Several studies have attempted to describe wave frequency spectra in a standard form. One such standard form is, the Joint North Sea Wave Project (JONSWAP). This is a spectral formulation for fetch-limited wind generated seas:

$$S_\zeta(\omega) = \frac{320 \cdot H_{1/3}^2}{T_p^4} \cdot \omega^{-5} \cdot \exp\left\{\frac{-1950}{T_p^4} \cdot \omega^{-4}\right\} \cdot \gamma^A \quad (3.5)$$

where

- γ = peakedness factor
- A = $\exp\left\{-\left(\frac{\omega}{\omega_p} - 1\right)^2\right\}$
- $\omega_p s$ = $\frac{2\pi}{T_p}$, circular frequency at spectral peak
- σ = a step function of ω : if $\omega < \omega_p$ then: $\sigma = 0.07$
if $\omega > \omega_p$ then $\sigma = 0.009$

The variance σ^2 is equal to the area under the spectrum:

$$\sigma_\zeta^2 = \int_0^\infty S_\zeta(\omega) \cdot d\omega \quad (3.6)$$

For a given spectrum the significant wave height can be estimated using:

$$H_{1/3} = 4 \cdot \sqrt{m_{0\zeta}} \quad (3.7)$$

where

- $H_{1/3}$ = Significant wave height [m]
- $M_{0\zeta}$ = Zeroth moment of the given spectrum [m^2]

3.3. RELATIVE VESSEL MOTIONS

When a vessel is subjected to regular waves, the resulting translations and rotations about the COG can be defined by the following co-sinus equations:

$$\begin{aligned} \text{Surge: } x &= x_a \cos(\omega t + \varepsilon) \\ \text{Sway: } y &= y_a \cos(\omega t + \varepsilon) \\ \text{Heave: } z &= z_a \cos(\omega t + \varepsilon) \\ \text{Roll: } \phi &= \phi_a \cos(\omega t + \varepsilon) \\ \text{Pitch: } \theta &= \theta_a \cos(\omega t + \varepsilon) \\ \text{Yaw: } \psi &= \psi_a \cos(\omega t + \varepsilon) \end{aligned} \quad (3.8)$$

in which ω , t and ε are the circular wave frequency [rad/sec], time [s] and the phase shift respectively.

When these motions about the COG are known, superposition is used in order to calculate the motions in any other point on the vessel. An initial assumption must be made: the rotations ϕ, θ and ψ are to be small. In reality the FLNG an LNGC will have small rotations, due to its size and the relative calm sea-state at which offloading is performed. This assumption is necessary for the following linearisation:

$$\begin{aligned} \sin \phi &\approx \phi \\ \cos \phi &\approx 1.0 \end{aligned} \quad (3.9)$$

Using the above linearisation, the absolute harmonic motions at a certain point $P(x_b, y_b, z_b)$ on the vessel are given by:

$$\begin{aligned} x_p &= x - y_b \psi + z_b \theta \\ y_p &= y + x_b \psi - z_b \phi \end{aligned}$$

$$z_p = z - x_b \theta + y_b \phi \quad (3.10)$$

in which x, y, z, ϕ, θ and ψ are the motions of and about the CoG.

The above motions are obtained by linear superposition of three harmonic motions, therefore the resultant motions should become harmonic too e.g. z_p becomes

$$z_p = h_a \cos(\omega t + \varepsilon_{h\zeta}) \quad (3.11)$$

where h_a and $\varepsilon_{h\zeta}$ are respectively the motion amplitude and the phase shift with respect to the wave elevation at the CoG. Further evaluations shows h_a and $\varepsilon_{h\zeta}$ can be written as:

$$h_a = \sqrt{(h_a \sin \varepsilon_{h\zeta})^2 + (h_a \cos \varepsilon_{h\zeta})^2}$$

$$\varepsilon_{h\zeta} = \arctan \left\{ \frac{h_a \sin \varepsilon_{h\zeta}}{h_a \cos \varepsilon_{h\zeta}} \right\} \text{ with: } 0 \leq \varepsilon_{h\zeta} \leq 2\pi \quad (3.12)$$

The vertical velocity and acceleration at the chosen point on the vessel is determined by taking the first and second derivatives with respect to time of equation 3.11:

$$\begin{aligned} \dot{z}_p &= \{wh_a\} \cdot \cos(\omega t + \{\varepsilon_{h\zeta} + \frac{\pi}{2}\}) \\ \ddot{z}_p &= \{\omega^2 h_a\} \cdot \cos(\omega t + \{\varepsilon_{h\zeta} + \pi\}) \end{aligned} \quad (3.13)$$

3.4. RESPONSE AMPLITUDE OPERATOR

When a vessel is subjected to waves, the vessel will respond in a specific way. This paragraph elaborates on the way the response is calculated. The equation of motion of a heaving vessel is represented by Newton's 2nd law; a mass term and the hydrodynamic loads on the left had side and the total Froude-Krilov wave force on the right hand:

$$(m + a)\ddot{z} + b\dot{z} + cz = a\ddot{\zeta} + b\dot{\zeta} + c\zeta \quad (3.14)$$

where

- m = mass vessel [kg]
- a = added mass vessel [kg]
- z = vertical displacement [m]
- b = hydrodynamic damping coefficient [kg/s]
- c = restoring spring coefficient [kg/s²]

$a\ddot{\zeta}$ and $b\dot{\zeta}$ are considered to be corrections on the Froude-Krilov due to diffraction of the waves. For heave the response of a vessel to a regular wave excitation is given as:

$$z = z_a \cos(\omega t + \varepsilon_{z\zeta}) \quad (3.15)$$

Substituting equations 3.15 and 3.1 into equation of motion 3.14 yields:

$$\begin{aligned} z_a \{c - (m + a)w^2\} \cos(\omega t + \varepsilon_{z\zeta}) - z_a \{bw\} \sin(\omega t + \varepsilon_{z\zeta}) \\ = \zeta_a e^{-kT} \{c - aw^2\} \cos(\omega t) - \zeta_a e^{-kT} \{bw\} \sin(\omega t) \end{aligned} \quad (3.16)$$

by further evaluation of the above formula and by equating two in-phase and two out-of-face terms, one obtains two formula's with two unknowns:

$$\begin{aligned} Z_a \{c - (m + a)w^2\} \cos(\varepsilon_{z\zeta}) - \{bw\} \sin(\varepsilon_{z\zeta}) &= \zeta_a e^{-kT} \{c - aw^2\} \\ Z_a \{c - (m + a)w^2\} \sin(\varepsilon_{z\zeta}) - \{bw\} \cos(\varepsilon_{z\zeta}) &= \zeta_a e^{-kT} \{bw\} \end{aligned} \quad (3.17)$$

Taking the squares of the above equations subsequently taking the sum, results in the heave amplitude:

$$\frac{z_a}{\zeta_a} = e^{-kT} \sqrt{\frac{\{c - aw^2\}^2 + \{bw\}^2}{\{c - (m + a)w^2\}^2 + \{bw\}^2}} \quad (3.18)$$

by elimination of $Z_a/\zeta e^{-kT}$ one obtains the phase shift:

$$\varepsilon_{z\zeta} = \arctan \left\{ \frac{-mbw^3}{(c - aw^2)\{c - (m + a)w^2\} + \{bw\}^2} \right\} \quad (3.19)$$

- The heave amplitude $\frac{z_a}{\zeta_a}(w)$ is also referred to as RAO. The five other RAO's for the remaining DOF's can be calculated in the same manner as for heave. RAO's will be used throughout this thesis to analyze the motions of both the FLNG and the LNGC.

3.5. VELOCITY POTENTIAL THEORY

The velocity potential Φ function can be written as a space dependent term and a harmonic time-dependent term:

$$\Phi(x, y, z, t) = \phi(x, y, z) e^{i\omega t} \quad (3.20)$$

The above equations is an expression which has the property that the velocity component (u, v, w) for a point within the domain in any chosen direction equals the velocity potential's derivative of this point in any chosen direction. The potentials at the hull of the vessel have to satisfy the following boundary conditions:

- Substitution of the potentials into the continuity equation, resulting in the Laplace equation(the flow is assumed to be continuous and in-compressible):

$$\frac{\partial^2 \Phi}{\partial x^2} + \frac{\partial^2 \Phi}{\partial y^2} + \frac{\partial^2 \Phi}{\partial z^2} = 0 \quad (3.21)$$

- Seabed boundary condition, the seabed is assumed to be impermeable, so there is no vertical flow possible:

$$\frac{\partial^2 \Phi}{\partial z^2} = 0 \text{ at } z = -h \quad (3.22)$$

h is the distance from mean water level towards seabed

- Free surface boundary condition, at the surface the pressure is the same as the atmospheric pressure. The vertical velocity of the water particle is the same as the velocity of the free surface:

$$\frac{\partial^2 \Phi}{\partial t^2} + g \frac{\partial \Phi}{\partial z} = 0 \quad (3.23)$$

- Kinematic boundary condition on the oscillating body surface

$$\frac{\partial \Phi}{\partial n} = v_n(x, y, z; t) \quad (3.24)$$

- Radiation Condition, which states that the radiation potential value tends to zero at large distance from the vessel:

$$\lim_{R \rightarrow \infty} \Phi_j = 0 \quad (3.25)$$

where R is the distance from the vessel and Φ_j the radiation potential.

3.6. SECOND ORDER WAVE DRIFT FORCES

All the above information is focused on first order behavior. However vessels positioned in irregular waves, vibrate also in a low-frequency region. These low-frequency motions have been studied and described in a thesis written by J.A. Pinkster [9] and is titled 'Low frequency second order wave exciting forces on floating structures'.

Second order motions are caused by non-linear elements in the wave loads, the low-frequency wave drift forces, in combination with spring characteristics of the mooring system. Generally, a moored ship has a low natural frequency in sway, surge and yaw as well as very little damping at such frequencies. Large amplitudes

could occur at resonance frequencies, therefore the major part of the ships dynamic displacement and resulting loads on the mooring system can be caused by these low frequency excitation. The second order-wave drift force consists of a so called mean wave drift force and low-frequency wave drift force. The mean wave drift force in combination with currents, wind and the mooring system determine the equilibrium position of the vessel. This equilibrium position is for the horizontal modes of motion and the yaw angle of the vessel in the earth-bound coordinates.

The fluid force exerted on a body, relative to the $G - (x, y, z)$ system of axes can be calculated by the Froude-Krylov formula:

$$\vec{F}_{FK} = - \iint_S p \cdot \vec{N} \cdot dS \quad (3.26)$$

where

- \vec{F}_{FK} = Froude-Krylov force
- S = wetted surface of the floating body
- N = instantaneous normal vector to the surface element dS

and p is the pressure at a point in the fluid according to the non-linear Bernoulli equation:

$$p = -\rho g X_3 - \rho \frac{\partial \Phi}{\partial t} - \frac{1}{2} \rho (\vec{\nabla} \Phi)^2 \quad (3.27)$$

where

- $-\rho g X_3$ = Hydrostatic part, with X_3 is positive upwards in the earth-bound axis coordinate system, with its origin at the mean free surface
- Φ = fluid potential

Assuming that a body carries out first order wave frequency motions and low frequency order motions about a mean position, normal vector and pressure can both be expressed as the sum of a hydro-static, first order and second order term. The expression for the total second order force becomes:

$$\begin{aligned} \vec{F}^{(2)} &= \vec{F}_A^{(2)} + \vec{F}_B^{(2)} + \vec{F}_D^{(2)} \\ &= m \cdot R^{(1)} \cdot \vec{X}_G^{(1)} \\ &\quad + \iint_{S_0} \left\{ \frac{1}{2} \rho (\vec{\nabla} \Phi^{(1)})^2 + \rho \frac{\partial \Phi^{(2)}}{\partial t} + \rho \vec{X}^{(1)} \cdot \vec{\nabla} \frac{\partial \Phi^{(1)}}{\partial t} \right\} \cdot \vec{n} \cdot dS \\ &\quad - \oint_{wl} \frac{1}{2} \rho g (\zeta_r^{(1)})^2 \cdot \vec{n} \cdot dl \end{aligned}$$

Where $\vec{F}_A^{(2)}$ is the contribution due to the products of first order angular motions and inertia forces (rotations of first order forces). $\vec{F}_B^{(2)}$ Is the integration of the second order pressure over the constant part of the wetted surface of the body. And $\vec{F}_D^{(2)}$ is due to the relative wave height contribution. The expression for the total second order moment becomes:

$$\begin{aligned} \vec{M}^{(2)} &= I \cdot R^{(1)} \cdot \vec{X}_G^{(1)} \\ &\quad + \iint_{S_0} \left\{ \frac{1}{2} \rho (\vec{\nabla} \Phi^{(1)})^2 + \rho \frac{\partial \Phi^{(2)}}{\partial t} + \rho \vec{X}^{(1)} \cdot \vec{\nabla} \frac{\partial \Phi^{(1)}}{\partial t} \right\} \cdot (\vec{x} \times \vec{n}) \cdot dS \\ &\quad - \oint_{wl} \frac{1}{2} \rho g (\zeta_r^{(1)})^2 \cdot (\vec{x} \times \vec{n}) \cdot dl \end{aligned}$$

In which I is the mass moment of inertia about the considered body axis of the vessel. The wave drift force in irregular waves results in a response in phase with the envelope of the wave group. The wave envelope of an irregular wave elevation time trace, is a smooth curve outlining its extreme values. Figure 3.4 shows the composition of Wave drift forces which are obtained by an irregular wave record.

The curve for the wave drift force consists of a slowly varying part about a mean wave drift force (Figure 3.4). The component which contributes the most to the drift force is the second-order load that is only function of a quadratic product of the first-order wave field and responses. Considering the wave amplitude, this may also be expressed spectrally in Equation 3.4, the second order mean wave drift force is formulated as [8]:

$$F_{mean}^{(2)} = 2 \int_0^\infty S_\zeta(\omega) \cdot P(\omega, \omega) \quad (3.28)$$

where $P(\omega, \omega)$ is known as the mean drift force coefficient in regular waves.

3.7. DIFFRACTION THEORY

It is generally accepted that for engineering purposes the diffraction theory, described in this section, can be applied for structures in regular or irregular sea-states.

Several software programs are available which are based on the diffraction theory. For example HydroStar, DELFRAC and DIFFRAC. The programs use the same theory but the solving method at the panels can be different.

The software program used for this study is HydroStar. HydroStar is a software tool Developed by Bureau Veritas to evaluate 1st & 2nd order wave loads and induced motions of one or several ships or other marine structures of any type in deep and finite water depths. In HydroStar the linearized velocity potential problem is solved using three-dimensional source distribution techniques. The fluid is assumed to be an ideal fluid, meaning it is in-compressible, non-viscous and irrotational and without surface tension. The mean wetted part of the vessel hull is approximated by an imported mesh model of the vessel(s). Each element represents a distribution of source singularities and contributions to the velocity potential describing the fluid around the vessel, described in Section 3.5. The input for HydroStar consists of:

- Geometry of vessels, imported with a mesh
- Mass, position of COG's and radii of inertia about the tree axis
- Water depth
- Wave frequencies and direction

Floating vessels, which have greater dimensions than 0.2 times the wave length must account for wave forces, because the incoming wave field is influenced by the presence of the floating bodies. This phenomenon modifies the wave pattern en thereby the wave body interactions. The method used to calculate the wave force including the diffraction phenomenon is by using the general wave theory conditions and additional boundary conditions (Equations 3.21, 3.22, 3.23, 3.24 and 3.25). The equation of motion can then be solved with linear fluid potential consisting of:

$$\Phi(x, y, z, t) = \sum_{j=1}^6 \Phi_j + \Phi_w + \Phi_d \quad (3.29)$$

where Φ_j is the radiation potential for the six body motions, Φ_w the incident undisturbed wave potential and Φ_d the diffraction potential of the undisturbed wave on a fixed body [8]. The potential due to a motion at a point on the wetted surface can be determined by a distribution of a single source on the wetted surface and a function called the Green's function:

$$\phi_j(x, y, z) = \frac{1}{4\pi} \iint_{S_0} \sigma_j(\hat{x}, \hat{y}, \hat{z}) \cdot G(x, y, z, \hat{x}, \hat{y}, \hat{z}) \cdot dS_0 \text{ for } j = 1, \dots, 7 \quad (3.30)$$

in which:

- $\phi_j(x, y, z)$ is the time independent potential function
- $\sigma_j(\hat{x}, \hat{y}, \hat{z})$ is the complex source strength
- $G(x, y, z, \hat{x}, \hat{y}, \hat{z})$ Green's function of the pulsating source $\sigma_j(\hat{x}, \hat{y}, \hat{z})$ in a point located at $(\hat{x}, \hat{y}, \hat{z})$ in the potential $\phi_j(x, y, z)$. This green function satisfies the Laplace equation, the linearized boundary conditions at the seabed and on the free surface and the radiation condition at infinity.

The integral represents a distribution of sources, sinks and dipoles on the surface. The panels in the mesh are small enough to assume the fluid pressure is constant over each element. Since the panel method is based on linear potential theory, and thus ideal fluid, viscous effects are neglected.

3.8. FORCES AND MOMENTS

The fluid pressure around the vessel is calculated with the now know potential function:

$$p = -\rho \frac{\partial \Phi}{\partial t} - \rho g z \quad (3.31)$$

next the first order forces and moments can be calculated by integrating the pressure over the wetted surface of the vessel:

$$\vec{F} = - \iint_S (p \cdot \vec{n}) \cdot dS \quad (3.32)$$

$$\vec{M} = - \iint_S p \cdot (\vec{r} \times \vec{n}) \cdot dS \quad (3.33)$$

in which \vec{n} is the outward normal vector on surface dS and \vec{r} the position vector of surface dS .

The response for a single oscillating body in the direction j with a velocity potential ϕ_j the hydrodynamic mass (M_{kj}) and damping (B_{kj}) coefficients are defined as:

$$M_{kj} = -\Re e \left\{ \rho \iint_s \phi_j \frac{\partial \phi_k}{\partial n} \cdot dS \right\} \text{ and } B_{kj} = -\Im m \left\{ \rho \omega \iint_s \phi_j \frac{\partial \phi_k}{\partial n} \cdot dS \right\} \quad (3.34)$$

3.9. SINGLE BODY EQUATION OF MOTION

The response of a single floating structure in waves in the frequency domain is generally described by means of a mass-spring system. Assuming a linear system in six degree of freedom, such analysis represents the equation of motions as:

$$\sum_{j=1}^6 (m_{kj} + a_{kj}) \ddot{x}_j + b_{kj} \dot{x}_j + c_{kj} x_j = F_k \quad (3.35)$$

where:

- x_j = motion in j-direction
- k, j = subscripts of hydrodynamic property in the k-mode as a result of motion in the j-mode
- m_{kj} = mass or inertia
- a_{kj} = added mass coefficient
- b_{kj} = damping coefficient
- c_{kj} = spring coefficient
- F_k = Wave force for mode k (k = 1 to 6, for the six DOF)

3.10. MULTI BODY EQUATION OF MOTION

In case of multiple bodies which are hydrodynamically and/or mechanically coupled, the approach mentioned above needs to be solved in a coupled matrix equation. The bodies can be subject to wave-induced forces, hydrodynamic reaction forces and mechanical coupling effects (either linear or non-linear). In case of a two-body system, this system has 12 DOF and becomes:

$$[M] \ddot{\vec{X}} + [B] \dot{\vec{X}} + [K] \vec{X} = \vec{F}(t) \quad (3.36)$$

- $[M]$ = Combined mass and added mass matrix
- $[B]$ = Damping matrix
- $[K]$ = Stiffness matrix of mooring system
- $\vec{F}(t)$ = Total dynamic force acting on structure
- $\ddot{\vec{X}}$ = System's acceleration vector
- $\dot{\vec{X}}$ = System's velocity vector
- \vec{X} = System's displacement vector

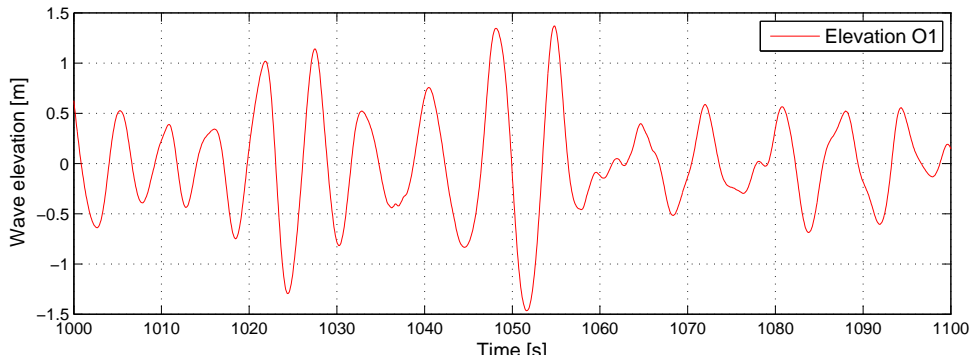


Figure 3.2: Surface elevation of an irregular wave

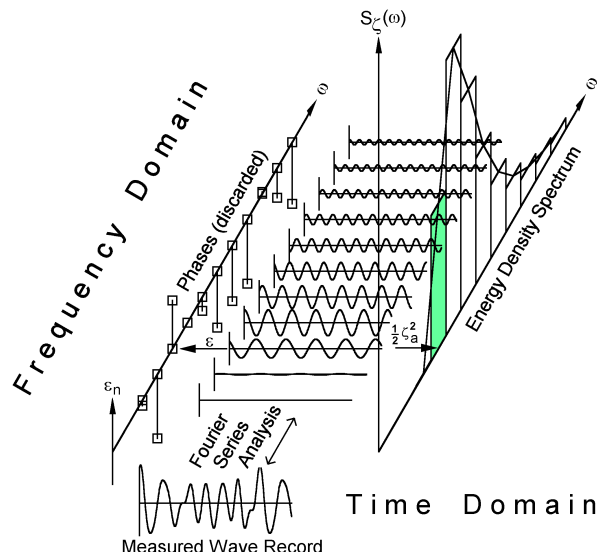


Figure 3.3: From time trace to spectrum

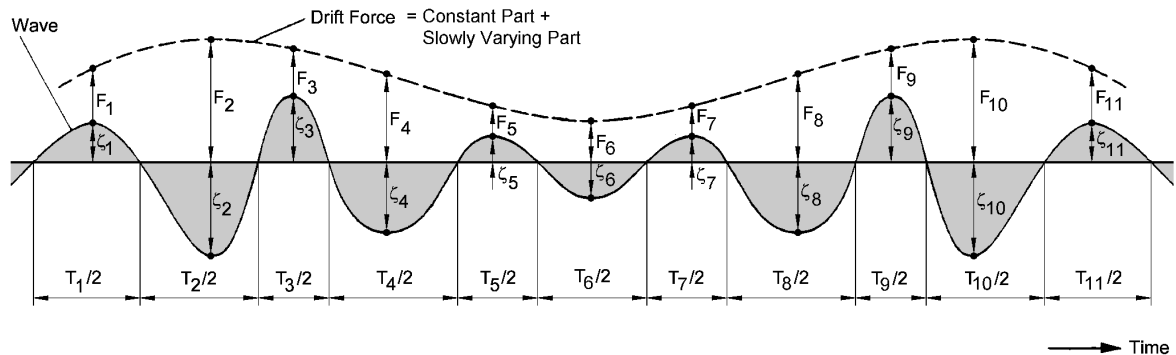


Figure 3.4: Wave drift forces obtained from a wave record

4

MARIN EXPERIMENTS

In February 2014 SBM Offshore in cooperation with MARIN performed side-by-side experiments, with an Twin-hull FLNG and an LNGC. The mooring test campaigns were intended to gain confidence in the numerical results of mooring loads and offsets. Additional the side-by-side tests were carried out for a feasibility check; whether offloading is possible. The experimental data can be used for validation of the relative motions obtained in the simulations run by HydroStar and Ariane. An additional purpose for the tests was to analyze mooring loads of the "full scaled" mooring system. This chapter elaborates on the experiments performed at MARIN.

4.1. TWIN-HULL FLNG [3]

The FLNG used for the model tests consists of two converted LNG carriers. Conversion of a single existing LNG carrier to an FLNG will not be feasible because of the lack of deck space and load carrying capacity, for topsides and oil storage. A solution for this problem, which Single Buoy Mooring (SBM) adopted is to connect two existing LNG tankers to each other. This Twin-Hull design concept addresses mid-scale gas fields that cannot be economically exploited by big floaters. The stern section of the Twin-Hull accommodates the internal turret. The process facilities are located on the aft deck, whereas the renewed accommodation block is on the other extreme side of the vessel, the original bows. Figure 4.1 depicts an overview of the Twin-Hull in the fully loaded condition. Table 4.3 shows the FLNG's main dimensions. In practice the FLNG will be fully loaded or almost fully loaded on arrival of the LNG carrier. For this thesis the FLNG is considered to be fully loaded; having the maximum load of LNG on board prior to its offloading procedure. The FLNG is considered to be in its maximum Load Case (LC).

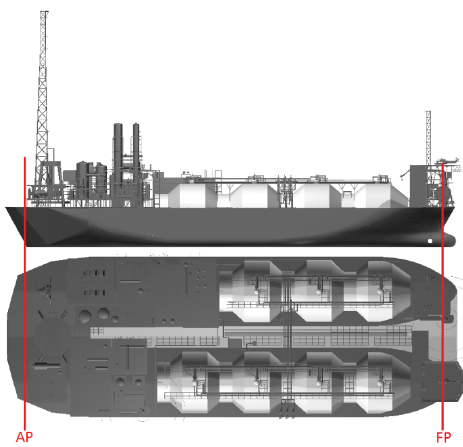


Figure 4.1: General arrangement Twin-Hull[3]

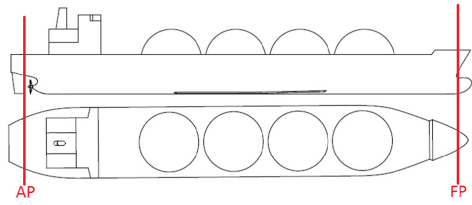


Figure 4.2: LNGC[3]

Ship Name	Type	Manifold distance to Midship [m]
Sunken BITT	Membrane	1.5
Al KHAZNAH	Moss	-3.5
Al KHOR	Moss	30.5
Al RAYYAN	Moss	30.7
SS AMAN	Membrane	0
SS BANSHU MARU	Moss	30.9
SS DWIPUTRA	Moss	-15.46
GIMJ	Moss	12.875
GOLAR FREEZE	Moss	27
GOLA SPIRIT	Moss	21.5
HANJIN PYEONG TAEK	Membrane	5.5
HA VFRU	Moss	-1.541
S/S Methane arctic	Membrane	6.45
Methane Princess		-3.47
Golar Spirit	Moss	-
Kristen ASCLEPIUS	Membrane	-0.9
Hyundai Utopia	Moss	15.7
Hoegh Gandria	Moss	27.68
SS Kotowaka Maru	Moss	25.6
Laieta		4.793
Hoegh Gangria	Moss	27.68
Inchon	Membrane	-9.3

Table 4.1: LNGC's manifold longitudinal location from midship[10]

4.2. LNG CARRIERS

Up to this date more than 180 LNG carriers have been built. The volume of the cargo ranges from less than 2000 m³ to about 150000 m³. All carriers have their manifolds located starboard and/or port side depending on their design. The longitudinal location of the LNGC's offloading and loading manifold plays a crucial role in the relative motions between the two vessels. Placing the manifold as close as possible to the vessel's COG will have a positive effect on reducing the motions of the manifold itself. The manifold's lateral spacing from the vessel's side is universal and amounts to 3.5 meters, whereas the longitudinal placement of the manifold differs from ship to ship. Table 4.1 shows an overview of the longitudinal location of the manifold of several LNG carriers. As shown in the table above, the longitudinal location is defined as the distance of the manifold to the midship. Notice the maximum longitudinal manifold distance for the Membrane and Moss tankers, which is 9.3 m and 30.9 m respectively. The manifold location on the Moss tanker is restricted to the gaps between the spherical cargo holds. For this thesis the assumption is made that the manifold is located midship, a lateral distance of 0 meters from the side, and an elevation of 1.20 meters. Figure 4.2 and table 4.3 represent the layout and the main specifications of the LNG carrier in the minimal loading case used for this study. In practice most LNG carriers sailing towards the FLNG do not have any LNG on board. For this thesis the LNGC is considered to be totally empty, having no LNG on board prior to its loading procedure. The LNGC is considered to be in its minimal LC.

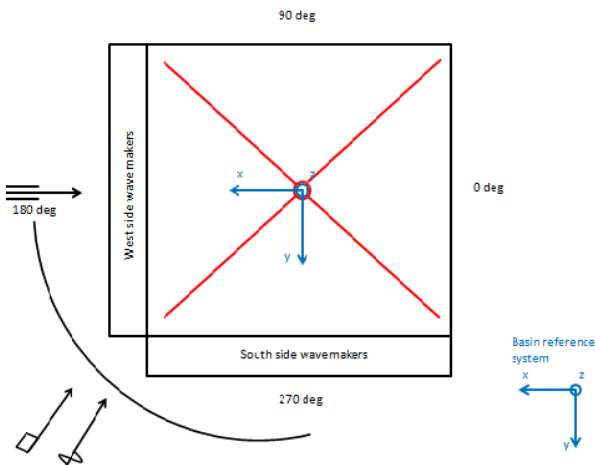


Figure 4.3: Basin reference system.

[11]

Quantity	Model	Prototype	Ratio
Linear Dimensions	1 m	60 m	λ
Areas	1 m^2	3600 m^2	λ^2
Volumes	1 m^3	216000 m^3	λ^3
Time	1 s	7.746 s	$\sqrt{\lambda}$
Velocities	1 m/s	7.746 m/s	$\sqrt{\lambda}$
Accelerations	1 m/s^2	1 m/s^2	1
Mass	1 kg	221.4 tons	$\rho \lambda^3 / 1000$
Forces	1 N	2171.93 kN	$\rho g \lambda^3 / 1000$
Moments	1 Nm	130316 kNm	$\rho g \lambda^4 / 1000$
Stiffness	1 N/m	36.2 kN/m	$\rho g \lambda^2 / 1000$

Table 4.2: Scaling factors

4.3. SET UP AND MODEL CHARACTERISTICS

The MARIN offshore basin measures 46 meters x 36 meters and has a movable floor to adjust the water depth. For the side by side experiments carried out, the water depth is set to 10.1 meters, which scales to 600 meters in reality.

All results from the model tests are converted from the model scale values applying Froude's law of similitude [12]. The applied scale factor is $\lambda = 60$. The relevant conversion factors are presented in Table 4.2.

The Twin Hull model consists of two separate models; an upper part and a lower part. The separate parts were used in previous experiments; one for wind loads the other for current loads respectively. For the experiments which were executed in February 2014 the models had to be glued together in order to have a uniform body. The model shown in figure 4.4 is reproduced at scale 1:60.

The following properties were reproduced to scale:

- External geometry
- Equivalent mass of the floater and the position of the center of gravity
- Mass moments of inertia
- Draft of the floaters
- Topsides

All elements are built to scale, with mass properties values staying within the 2%, as specified by SBM Offshore. The dimensions of the FLNG and the LNGC are listed in Table 4.3. The design of the LNGC is chosen such that it represents a general design of what a carrier looks like these days.



Figure 4.4: Twin Hull in Offshore Basin at MARIN

Table 4.3: Dimensions FLNG & LNGC

		FLNG LC-MAX	LNGC LC-MIN
Volume	[m ³]	246800	76032
Displacement	[ton]	252971	77932.8
x_{turret} from mid-ship	[m]	114.42	-
Lpp	[m]	267	274
Beam	[m]	103	44.2
Draft	[m]	10.5	9
LCG	[m]	131.23	137.62
KG	[m]	18.8	11.51

4.4. INSTRUMENTATION

During the side-by-side model tests multiple factors have been measured. The relevant measured factors for this thesis are model movements, wave heights and line/fender loads. All of these factors were sampled at a rate of 100 Hz model scale. Table 4.2 concludes the sample rate corresponds to 12.91 Hz full scale.

4.4.1. WAVE HEIGHTS

Resistance type wave probes located on the side of the FLNG were used to measure the relative motion of the model respect to the water and the wave elevation in the basin. The location of these wave probes are illustrated in Figure 4.5.

Wave probes were also used during the calibration phase, a detailed explanation on this phase can be found in Section 4.6. The locations of these wave probes are illustrated in Figure 4.6.

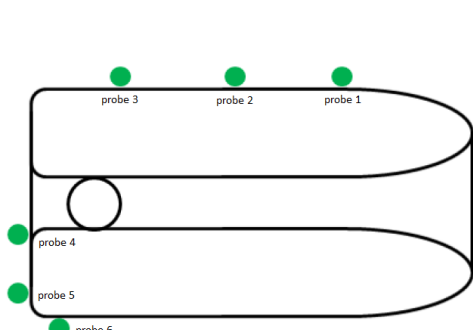


Figure 4.5: Position of the probes installed on the FLNG deck

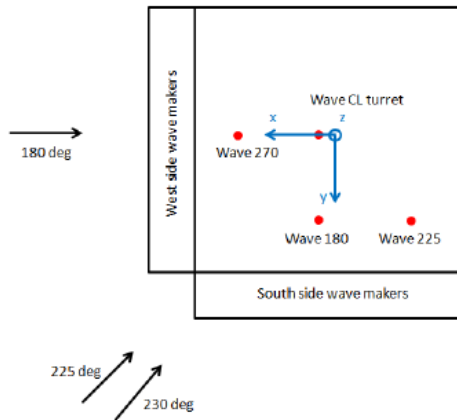


Figure 4.6: Position of the probes in the basin

4.4.2. MOTIONS OF THE MODEL

A Northern Digital Inc. (NDI) Certus optical tracking system was installed on the turret, to measure the six degree of motion of the FLNG. The system consists of three light sources mounted in a triangular formation, the 'Target'. This target is tracked by a 'Krypton' camera mounted on a carriage above the two vessels. For the LNGC a second target was installed on the deck. The absolute accuracy of these systems is within 1 millimeter at model scale.

4.4.3. MOORING LINES

All 20 mooring lines, including breast and spring lines were equipped with transducers which could measure the in-line tensions.

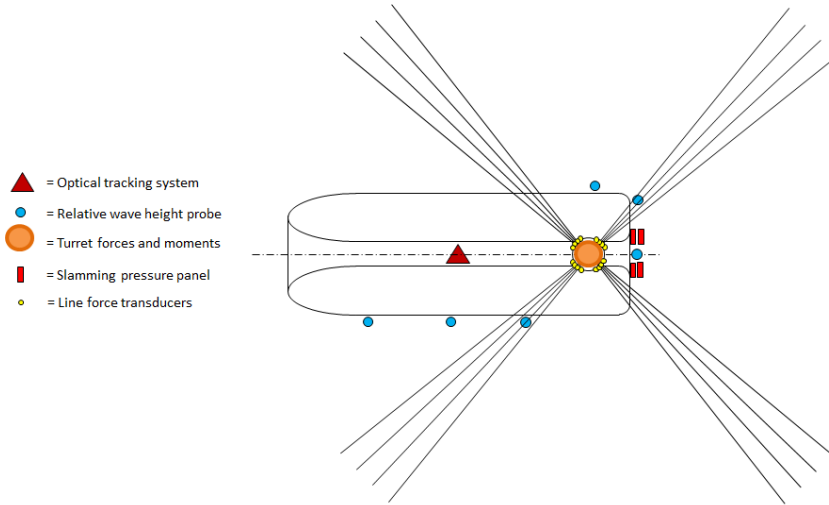


Figure 4.7: Turret-mooring configuration

Table 4.4: Restoring forces

Offset m	In line		In between
	X+Y+ dir. [kN]	X+ dir. [kN]	Y+ dir. [kN]
0	0	0	0
18	4726	4625	4663
42	11575	11172	11117
72	22110	20668	20621
102	36069	32655	32649
126	51253	44159	44280

4.5. MOORING CHARACTERISTICS

MARIN performed multiple mooring experiments which are of great use for this thesis. In this section the set up of the turret-mooring and side-by-side mooring is elaborated.

4.5.1. TURRENT MOORING

As mentioned above, the FLNG is moored to the bottom of the tank, with a full scale mooring system, which consists of a 16 line catenary system, bundled in groups of four. No truncation is needed. Each line is composed of a large bottom chain connected to the anchor points, a steel wire and a top chain that was connected to the fairleads on the chain table of the FLNG. The full scale mooring system was designed for the water depth of 600 meters and the lines were spread in a circle of 1200 meters of radius around the center of the turret of the FLNG. The layout of the mooring system can be found in the Figure 4.7. Furthermore the restoring forces generated by the mooring lines with multiple offsets are presented in Table 4.4. The in-line force is the reaction force on the turret when the turret has an off set in the direction of a line bundle. The in between force, is the restoring force when the vessel is positioned in the middle of two mooring line bundles. As for the side by side experiments the vessel is dragged by drift forces 'in line'.

The natural period of the system is defined by:

$$T = 2\pi \sqrt{\frac{m + m_a}{k}} \quad (4.1)$$

with m the mass of the FLNG, m_a the added mass and k the theoretical stiffness of the mooring system. The added mass is calculated by HydroStar, the values are obtained from diffraction calculations elaborated in section 3.7. Assuming the mooring system is linear for small offsets and the maximum turret offset never exceeds 18 meters, the theoretical mooring stiffness can be obtained from Table 4.4. Using Equation 4.1 and the above values the natural period of the mooring system is calculated and presented in Table 4.5.

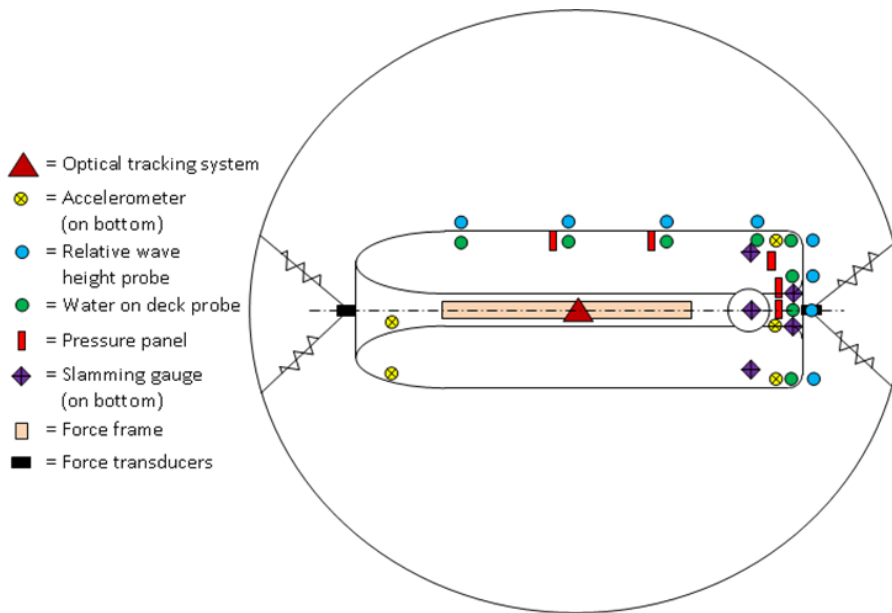


Figure 4.8: Soft-mooring configuration

Table 4.5: Theoretical mooring stiffness & Natural frequencies

	restoring force @ 18m [kN]	mooring stiffness [kN/m]	mass FLNG [tonnes]	added mass for surge [tonnes]	natural period [s]	natural frequency [rad/s]
in line	4726	263	252971	17636	201.72	0.0311
in between	4625	257	252971	17636	203.91	0.0308

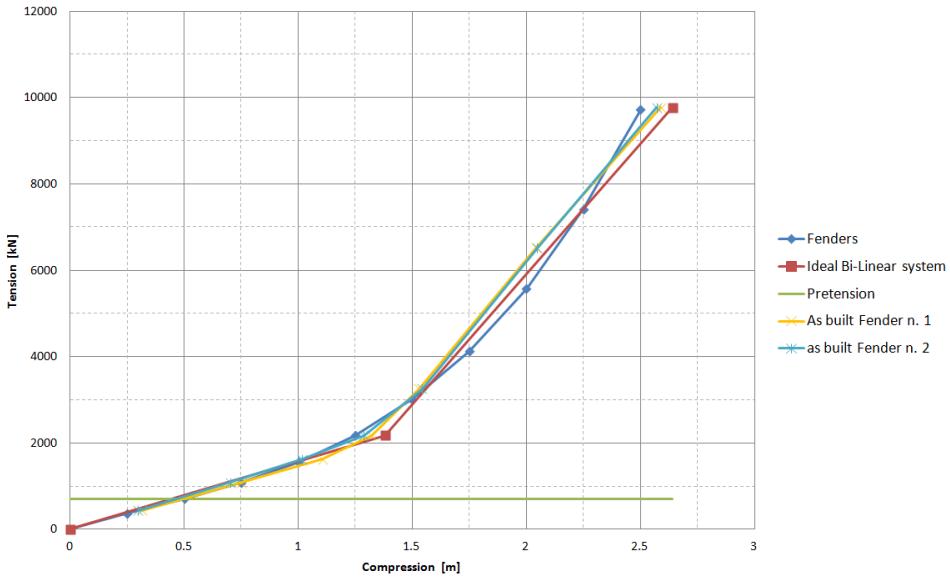


Figure 4.9: Characteristics of Fenders

4.5.2. SIDE-BY-SIDE MOORING

For the side-by-side mooring system, a traditional system is used. Containing four fenders, eight breast- and eight spring-lines. However the system in the MARIN offshore basin is simplified to a system composed of two fenders, two breast lines and 2 spring lines. The simplified system is modeled in such a way that each line represents in reality four lines and 1 fender represents 2 fenders. Each fender is build up from two springs connected in series in order to have a bi-linear tension-elongation relation. One linear spring would not be realistic. This accounts also for the breast and spring lines. Figure 4.9 represents the as built characteristics of the fenders. The spring and breast line characteristics can be found in Figures 4.10 and 4.11 respectively.

Ayman B. Mahfouz preformed offloading analysis for side-by-side offloading [13]. He studied the Hydrodynamic interactions between the two vessels depending on the lateral distance between the two vessels. Therefore Ayman studied three spacing distances, representing one two and triple fender diameter at 4.5 m, 9.0 m and 13.5 m respectively. The report concludes the following: "The heave motion for FLNG an LNGC are independent of the spacing, distance, while surge, sway and pitch are dependent on of it. As the spacing distance increase, these motions increase." This distance for the experiments at MARIN is determined by the fenders, used for LNG side by side mooring. The fenders which are modeled are produced by the company Yokohama [14], shown in figure 4.12and have a diameter of 4.5 meters when not compressed.

When the breast and spring lines are pre-tensioned, the diameter of the fenders are reduced to 4 meters. Thus the gap between the vessels equals 4 meters in its equilibrium position. This distance corresponds to the single fender spacing, which Ayman B. Mahfouz investigated. The green line in Figure 4.9 represents the pretension in the mooring system. The non linear curve represents the restoring force of the fender. Notice the large increase in the restoring force when the fender is compressed from 0.5 meters to 1.5 meters; the tension increases from 712 kN to 3000 kN. For a compression of 1 meter the fenders restoring force increases by a factor of 4. Therefore it is crucial to determine the relative motions between the vessels especially for sway. One meter additional sway can cause the fenders to fail. The orientation of the fenders and breast-/spring-lines are depicted in Figure 4.13.

4.6. WAVE CALIBRATION

Before the side-by-side model experiments could be performed, the required wave spectra had to be calibrated. Calibration is executed in order to measure the exact waves wind and currents which the models will encounter during the experiments at a predefined location in the basin. The time trace conducted at the calibration tests are used for the description of the incoming waves. This paragraph elaborates on the calibrations steps which were conducted.

Irregular waves were tested for a total duration of 27 minutes and 30 seconds model scale which corre-

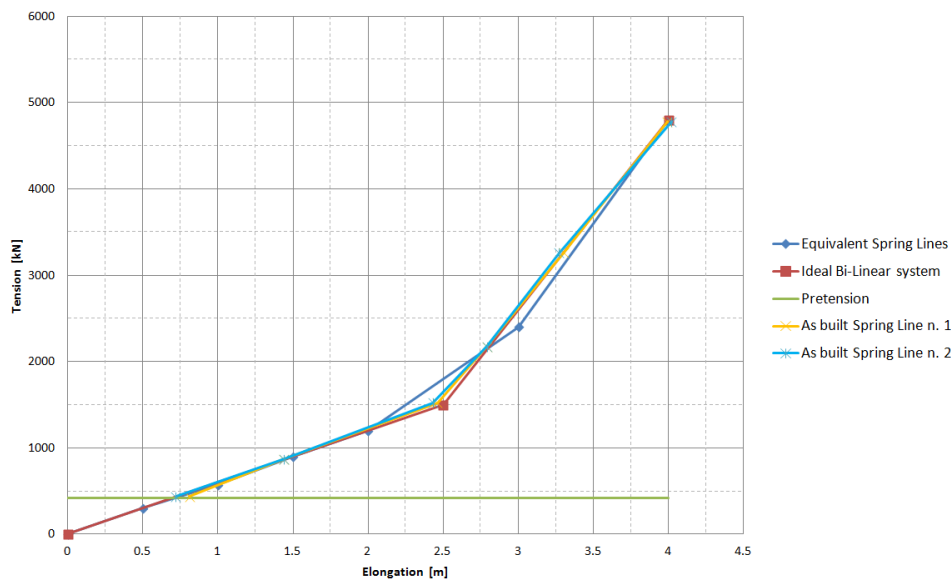


Figure 4.10: Characteristics of spring lines

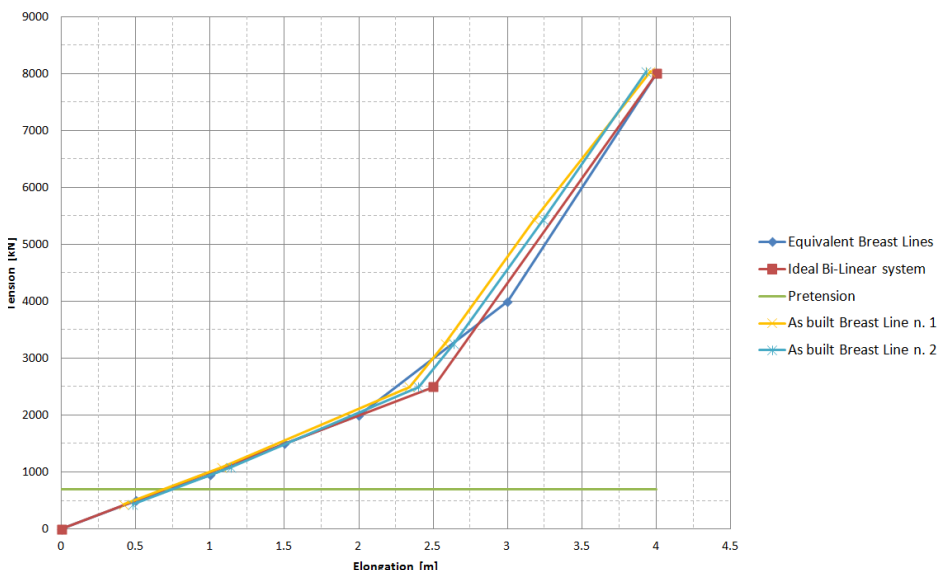


Figure 4.11: Characteristics of breast lines

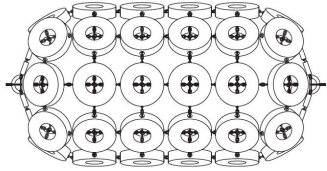


Figure 4.12: Modeled Yokohama fender used for side by side mooring
[14]

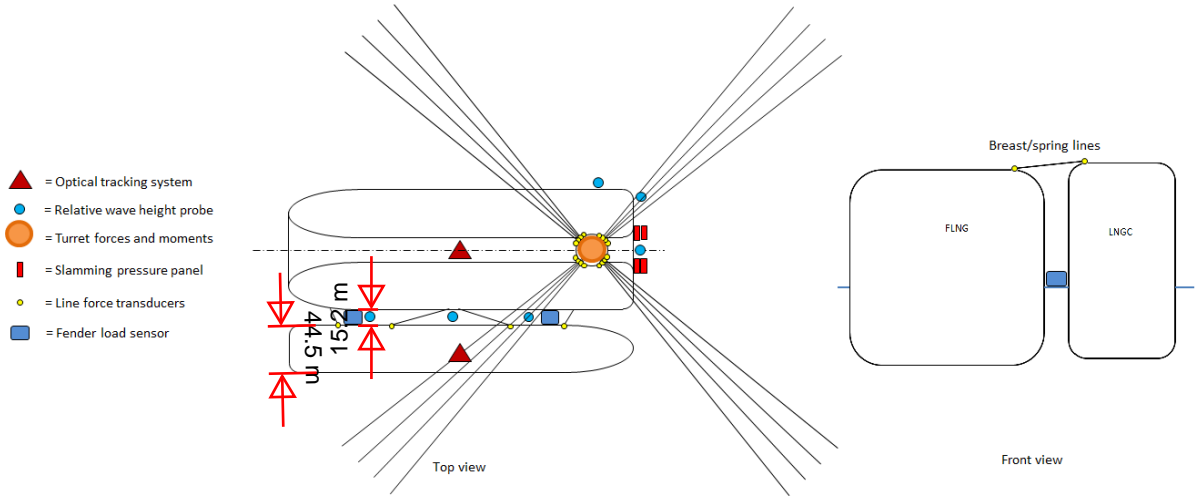


Figure 4.13: Side-by-side orientation, top & front view

sponds to 3 hours and 30 minutes in real life. These waves were measured at four resistance wave probes, which were installed at the locations illustrated in Figure 4.6. The first half an hour was meant for the buildup of the spectrum, the remaining 3 hours were considered to be a reasonable amount of time to get all the frequencies of the spectrum. At the end of each calibration run the value of the peak period and the area of the spectrum was determined, which is proportional to the significant wave height of the sea state. When these values differ more than 5% of the predefined significant wave height the run was restarted with an adapted significant wave height. Usually three corrections where needed in order to reach the satisfying level of accuracy of the output spectrum.

4.7. WAVE SPECTRA

Table 4.6 shows the relevant data of the side-by-side experiments preformed at the MARIN offshore basin. The experiments are preformed such that both vessels are allowed to freely weathervain around the FLNG's turret. There is no weathervaining possible for the experiments containing an angle in their title. This angle represents the angle at which the FLNG is fixed in the MARIN offshore basin.

The measured time records, by a wave probe, represent an irregular wave, which in turn can be seen as a superposition of a series of sinusoidal waves explained in Section 3.2.2. Using equation 3.4 and the surface elevations of the experiments it is possible to plot the wave spectra, shown in figure 4.15. The time trace measured by the wave probe Center Line (CL), depicted in figure 4.6 is used for calculating motion RAO's for both the FLNG and LNGC in Chapter 6. The location of this wave probe is near the center of the offshore basin. However to calculate a correct motion RAO of a vessel the wave probe should be positioned at the COG's location, or an Fast Fourier transform (FFT) is used in order to reconstruct the wave to the COG's location. Note, irregular waves in a perfect basin should show the same spectra when measured with probes which are located in a close vicinity. However the spectra in Figure 4.15 show great discrepancies, meaning the wave's energy is not equal across the MARIN offshore basin. This can be due to extra wave reflections within the basin or dis-functioning wave makers. Due to this inconsistency of wave spectra within the basin, a reconstruction of the O2 wave at the vessels COG using an FFT will therefore not be reliable. The wave spectra of the remaining experiments can be found in Appendix A.

Table 4.6: Side by side experiments

Environment	Environments						
	Hs [m]	Tp [s]	Wave	Current	Wind		
			θ [deg]	Uc [m/s]	θ_c [deg]	Uw [m/s]	θ_w [deg]
O1WC 230 deg	2.5	7	230	0.5	180	10	250
O1	2.5	7	230	0	180	0	250
O1WC	2.5	7	230	0.5	180	10	250
O1WC 190 deg	2.5	7	230	0.5	180	10	250
O1WC 180 deg	2.5	7	230	0.5	180	10	250
O2	2.5	17	230	0	180	0	250
O2WC	2.5	17	230	0.5	180	10	250
O2WC 200 deg	2.5	17	230	0.5	180	10	250

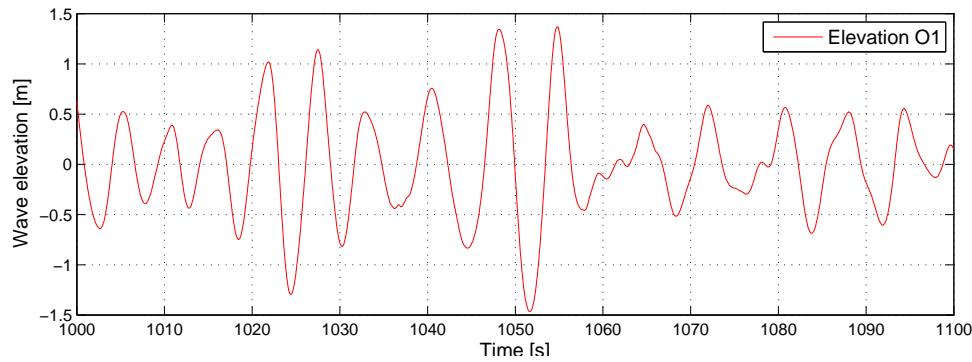


Figure 4.14: O1 wave elevation

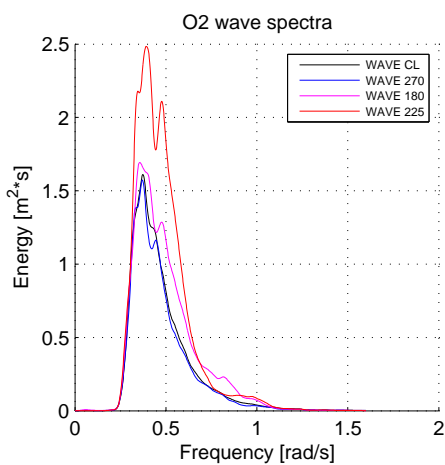


Figure 4.15: wave spectra

Table 4.7: Measured natural periods & frequencies from decay tests

		Natural periods T_0 [s]	Natural frequency [rad/s]
FLNG	In between (X dir.)	202.96	0.031
	In between (Y dir.)	203.61	0.031
	Roll	11.62	0.540
	Pitch	12.67	0.496
LNGC	Surge	53.58	0.117
	Sway	32.55	0.193
	yaw	35.38	0.177
	Roll	11.46	0.548
	Pitch (free floating)	10.02	0.627

Environment O2 has mainly energy in its lower frequencies, ranging from 0.25 rad/sec until 1.6 rad/s. The spectrum peaks at 0.37 rad/sec which corresponds to the given peak period (T_p) of 17 seconds. Note, all spectra were intended to be a JONSWAP. However environment O1 does not have the known shape of a JONSWAP. The high frequency waves beyond 1.3 rad/s have been missed out due to the limit of the wave generators in the MARIN offshore basin. Environment O2 does not include wind or current. Therefore no shielding effects due to current and wind will be influencing the motions of the vessel.

4.8. SHIELDING EFFECTS WIND, CURRENT AND WAVES

All SBS experiments conducted include wind and currents apart for O1 and O2. Including wind and current effects into the Ariane model requires wind and current coefficients. MARIN provided SBM Offshore with the coefficients from wind tunnel tests for the FLNG alone and for the LNGC alone. The coefficients do not include any shielding effects. Using these coefficients will result into inaccurate motions during the SBS calculations. Therefore this thesis will focus on the experiments without wind and current, especially on the O2 environment. Incoming waves can, depending on the angle of attack, first impact the FLNG before proceeding to the LNGC. The LNGC is thereby partially shielded by the FLNG. How much will largely depend on the separation distance between the FLNG and LNGC. When performing the diffraction calculations in HydroStar, the wave shielding is taken into account properly.

4.9. DECAY TESTS

Decay tests at MARIN have been performed in order to determine the natural frequencies of both the Twin Hull and the LNGC. MARIN conducted the tests in three main phases:

- **Phase 1:** Roll and pitch decay tests were first conducted with the free floating models in order to quickly verify if the roll period was comparable to the predicted one. These tests were done with another verification of the correctness of the weight distribution.
- **Phase 2:** Surge (in-between and in line with the bundles of the mooring system), roll and pitch decay tests were performed on the FLNG alone, connected to the mooring system.
- **Phase 3:** Surge, sway and yaw decay tests were performed on the LNGC connected to the Twin Hull in the side-by-side arrangement. For these experiments the FLNG was fixed to its zeroing position to the center of the basis.

For these phases the natural periods and frequencies are determined and listed in Table 4.7. These values are obtained from the decay tests at MARIN and can be compared with the theoretical values in Table 4.5, the results show satisfying similarities.

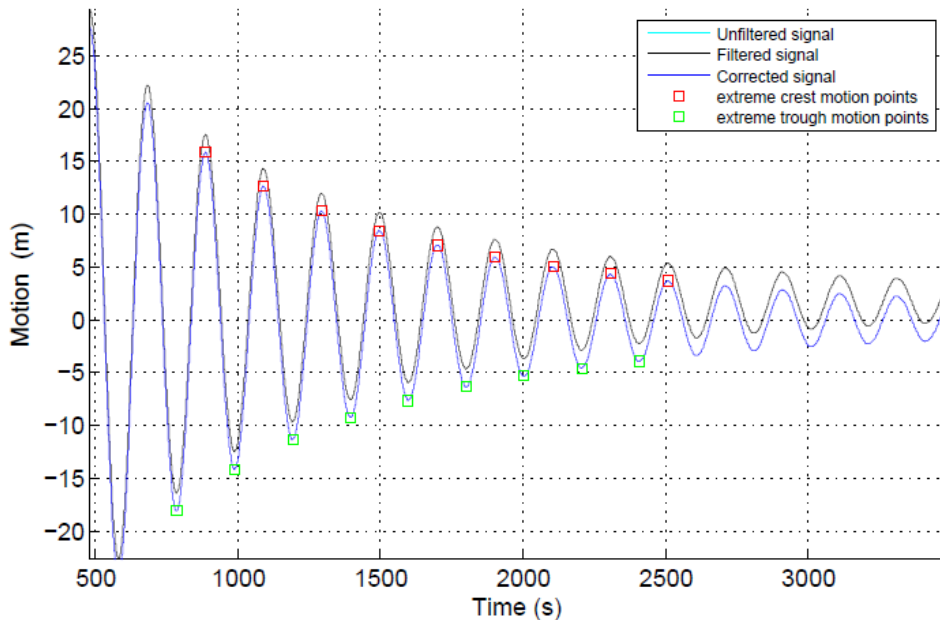


Figure 4.16: Surge decay - FLNG alone - signal plot

4.9.1. MOORING DAMPING FLNG ALONE

Phase 2 has been used for the calibration of the mooring damping values of the FLNG alone. The method used in order to calculate the damping values is briefly explained below.

The first step in order to calculate the damping values is to plot the motions of the FLNG during the decay tests, this plot is presented below, in Figure 4.16. Next the dimensionless damping coefficient is determined: this is the decrease in amplitude divided by the mean motion amplitude, as show in the equation 4.2.

$$\text{dimensionless damping coefficient} = \frac{\phi_n - \phi_{n+1}}{\frac{1}{2}(\phi_n + \phi_{n+1})} \quad (4.2)$$

where

ϕ = amplitude of cycle

n = number of cycle

$\frac{1}{2}(\phi_n + \phi_{n+1})$ = mean motion amplitude

Subsequently, the dimensionless damping values can be plotted against the mean motion amplitude, for surge the results are illustrated in Figure 4.17. Now it is possible to determine the angle q , and p which is the value where the line intersects the y-axes. The values p and q are used to calculate the linear and quadratic damping coefficients with the help of Equation 4.3 and 4.4.

$$b^1 = 2 * p * \frac{\nabla + a_{11}}{T_0} \quad (4.3)$$

$$b^2 = \frac{3}{8} * q * (\nabla + a_{11}) \quad (4.4)$$

where:

b^1 = Linear damping

b^2 = Quadratic damping

∇ = Vessel displacement [tonnes]

T_0 = Natural period for surge [s]

a_{11} = Added mass for surge [tonnes]

The PQ plot in Figure 4.17 has an angle, meaning there is quadratic damping present. In-turn this means equation 4.4 is preferred. However the software Ariane, used for time domain analysis does not have an input option for quadratic damping, so a compromised surge linear decay signal plot is proposed, presented in Figure 4.18. Notice, the compromised surge decay for Ariane has about the same amplitude, however the period is slightly increased in the Ariane plot.

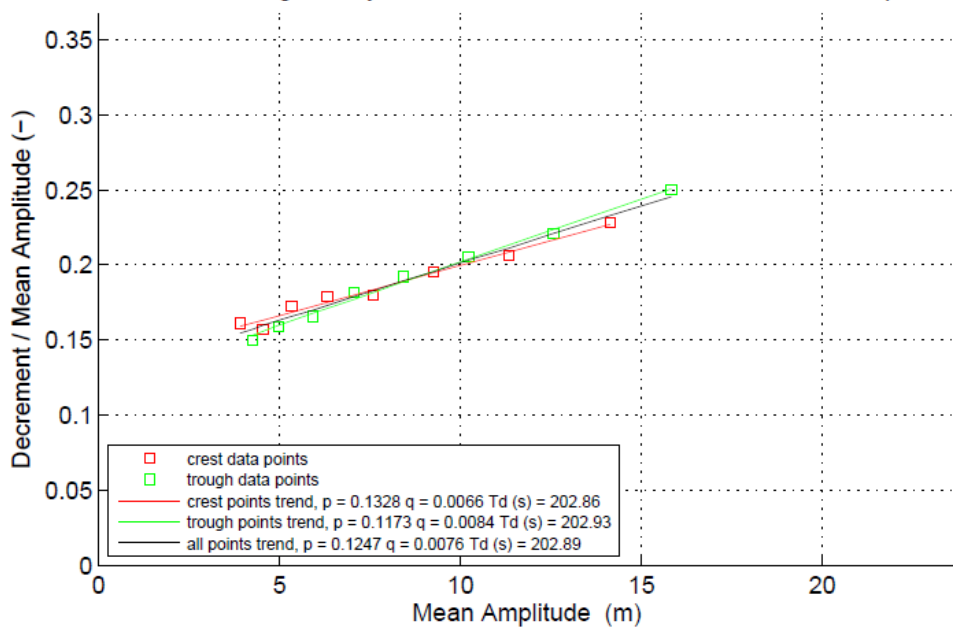


Figure 4.17: surge decay - FLNG alone - PQ plot

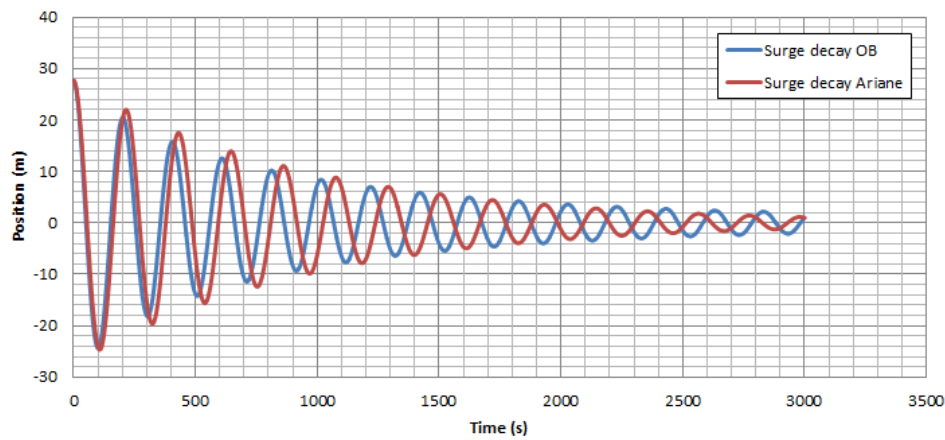


Figure 4.18: Surge decay - compromised - signal plot

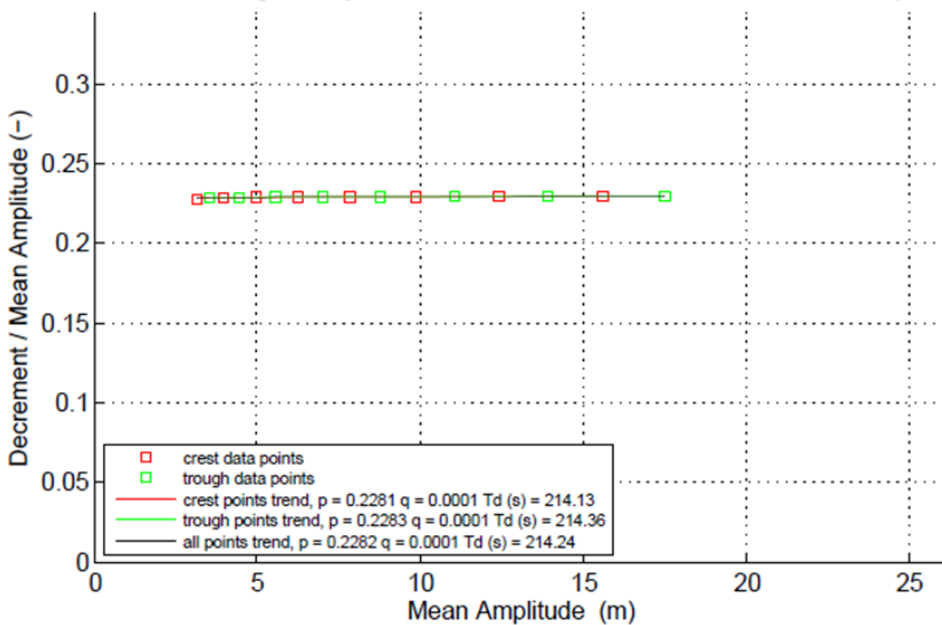


Figure 4.19: Compromised surge decay - PQ plot

Table 4.8: Damping coefficients FLNG alone

		b_{moor}	b_{diff}	b^1
Surge	[kg/s]	5.76E+05	1.53E+02	5.76E+05
Sway	[kg/s]	5.76E+05	2.10E+02	5.77E+05
Yaw	[kg ² /s]	5.76E+05	3.08E+02	7.55E+09

Next the PQ plot for the Surge Ariane decay is plotted in Figure 4.19. Note, the trend is a horizontal line, meaning the damping is linear and Equation 4.3 can be used for calculating the total surge damping. By subtracting the damping computed by diffraction in surge, the damping done by the mooring system is calculated. Damping from diffraction calculation is explained in Chapter 3. Note that diffraction damping is significantly smaller than damping from the mooring system. This is because there is lot more water displaced by the mooring system than by the hull when the vessel moves. The FLNG's mooring damping in yaw, or 'turret damping' is expressed by the following Equation 4.5.

$$\text{Linear yaw damping} = \frac{Lpp^2}{12} * b_{diff} + b_{moor} * x_{turret}^2 \quad (4.5)$$

where b_{diff} , $b_{mooring}$ and x_{turret} are the damping by diffraction, damping by the mooring line and the total linear damping respectively. Damping results for the FLNG alone are displayed in Table 4.8.

4.9.2. MOORING DAMPING LNGC

Phase 3 is intended for the understanding of the mooring system between the two vessels. The natural periods and natural frequencies provided by Marin have been listed in Table 4.5. From these results the decay and PQ plots can be constructed, these plots have been displayed in Appendix F. From the plots and using the same method as done in the previous paragraph the damping coefficients can be calculated. The LNGC damping values are displayed in Table 4.9.

4.10. MOTION TRANSLATION

The optical tracing system, also known as the "Target" used on-board the FLNG is placed on deck at mid-ship location. The local coordinates for the target are: (0, -8.34, 55.56). Many of the motions and moments mentioned throughout this report are referred to the COG of the full scale vessels, this accounts for the FLNG as well as for the LNGC. Section 3.3 explains how to calculate the linearized translations from COG to another location. However in this case the motions at the COG are unknown. In order to calculate the motions of the

Table 4.9: Damping coefficients LNGC

	p [-]	T_0 [s]	$a_{xx} + \nabla$ [kg]	b^1
Surge	1.2448	53.58	8.13E+07	3.78E+06 [kg/s]
Sway	0.557	32.55	9.91E+07	3.39E+06 [kg/s]
Yaw	0.8436	35.38	1.24E+11	5.90E+09 [kg ² /s]

FLNG COG and LNGC COG, Equation 4.6 is used. Note this equation does not linearize for small angles. As opposed to Section 3.3.

$$\begin{bmatrix} X_{COG} \\ Y_{COG} \\ Z_{COG} \end{bmatrix} = \begin{bmatrix} X_{target} \\ Y_{target} \\ Z_{target} \end{bmatrix} + \begin{bmatrix} D_{11} & D_{12} & D_{13} \\ D_{21} & D_{22} & D_{23} \\ D_{31} & D_{32} & D_{33} \end{bmatrix} \cdot \begin{bmatrix} A \\ B \\ C \end{bmatrix} \quad (4.6)$$

where A, B and C are the distances from the target toward the COG. For the FLNG the distance toward COG is (-2.27, 8.34, -35.2) respectively. X_{target} , Y_{target} and Z_{target} are the basin fixed (global) measured coordinate of the target. φ , θ and ψ are chosen to be the roll, pitch and yaw angles respectively, then the rotation matrix is given by:

$$\begin{aligned} D_{11} &= \cos \psi \cos \theta - 1 \\ D_{12} &= -\sin \psi \cos \varphi + \cos \varphi \sin \theta \sin \psi \\ D_{13} &= \sin \psi \sin \varphi + \cos \varphi \cos \psi \sin \theta \\ D_{21} &= \sin \psi \cos \theta \\ D_{22} &= \cos \psi \cos \varphi + \sin \psi \sin \theta \sin \varphi - 1 \\ D_{23} &= -\cos \psi \sin \varphi + \cos \varphi \sin \psi \sin \theta \\ D_{31} &= -\sin \theta \\ D_{32} &= \cos \theta \sin \varphi \\ D_{33} &= \cos \theta \cos \varphi - 1 \end{aligned}$$

5

FLNG SINGLE VESSEL ANALYSIS

5.1. INTRODUCTION

Before we move on to the side-by-side relative motions analysis, a thorough examination must be done on the first order motions of the FLNG alone, meaning there is no LNG Carrier moored next to the FLNG. SBM Offshore performed in cooperation with MARIN experiments in the offshore basin regarding sea-keeping. For these experiments two different mooring systems were used in order to keep the FLNG onto its required location. From October throughout November 2013 the soft-mooring experiments took place. Secondly the turret-moored see-keeping experiments were performed in February 2014, this was at the same time when the side-by-side experiments were carried out. The first order motions were calculated by diffraction software HydroStar, and are validated by the results of the above mentioned sea-keeping experiments.

5.2. FLNG ALONE IN HYDROSTAR

The dimensions of the FLNG listed in Tabel 4.3 are used for the "FLNG alone" analysis and are implemented into HydroStar. The mesh is provided by SBM Offshore and consists of a total of 3972 panels. An assumption is made that for a wide based vessel like the FLNG, the linear roll viscous damping is 1% of its critical damping. For the evaluation of the first order motions, a study is done on the RAO's over multiple frequencies. The headings used in the MARIN offshore basin for the soft- and turret-mooring experiments were 0 and 2 degrees respectively. HydroStar is set to calculate the RAO's at steps of 2.5 degrees. Therefore the calculated RAO for headings at which the waves encounter the vessel are chosen at 0 and 2.5 degrees. The discrepancy of 0.5 degrees can be neglected. Using the same wave angels for HydroStar as for the wave angle at MARIN makes it possible to compare the RAO's. The amplitude RAO's computed by HydroStar are plotted against the wave frequencies and presented in figure 5.1.

Note, for surge, heave and Pitch the curve with a heading of 2 degrees is plotted on top of the 0 degree curve, meaning these motions for the two headings remain the same and only the blue curve is visible. For the sway, roll and yaw only minor discrepancies are visible. For a wave with incoming angle of 0 degrees, the sway, roll and yaw RAO's are zero, the curve is a straight line at an amplitude of 0 m/m or deg/m. These DOF's are obvious zero for all frequencies when the vessel's hull is symmetric over the width of the ship. When the angle of attack is increased to 2 degrees, the sway, roll and yaw motions increase slightly. Sway has a maximum amplitude of 0.1 m/m at a wave frequency of 0.1 rad/s, whereas the roll RAO peaks with an amplitude 0.05 deg/m at about 0.6 rad/s.

5.2.1. FLNG IN SOFT-MOORING

The objectives of the soft-mooring campaign were to gain confidence in numerical results (RAOs, QTFs) for the FLNG and to study complex non-linear phenomena such as green water and bottom slamming on the single vessel. The configuration of the mooring is illustrated in 4.8. Two springs on the bow and two springs on the stern are used in order to keep the vessel on its location.

The RAO's for all six DOF's are obtained from the experiments and plotted in figure 5.2. These results can be used in order to validate the computed HydroStar RAO's for the single vessel, which are calculated in the previous section. Note in the figures the different curves represent different environments. The different

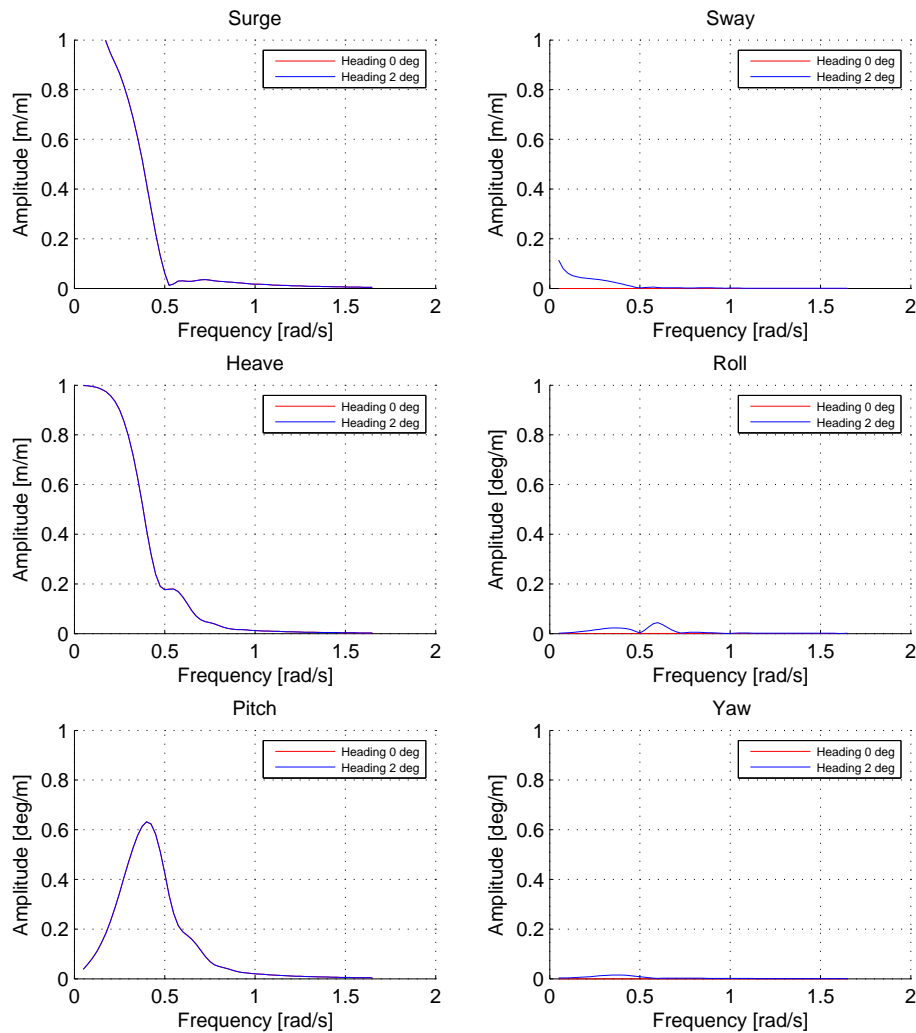


Figure 5.1: HydroStar RAO computations for FLNG alone

environments encountered the vessel with the same wave angle, causing the RAO's to have about the same curvature, no significant discrepancies can be observed.

The next step is to compare the RAO with the HydroStar computed RAO's, the red curves in Figure 5.1. The experimental RAO's have been plotted between 0.3 rad/s and 1 rad/s. No data is available outside the mentioned frequency range. This is because the wave energy is about 0 at these frequencies. From the plotted figures it is obvious to notice that the vessels sways more in the basin than is calculated by Hydrostar, especially around the frequency band from 0.4 rad/s to 0.6 rad/s. Also the roll and yaw amplitude is more around these frequencies than calculated in the basin. Roll has a peak of 0.3 deg/m at the COG. This roll can add almost 0.25 meters of extra sway at manifold location. These discrepancies can be due to the imperfections in the tank. In the offshore basin the imperfections can cause wave spreading. Wave spreading means the wave does not come from one specific heading, in this case 0 degrees. In the tank this specific heading is not achievable and the wave heading might be spread out over a range from, e.g. 3 to 357 degrees. In HydroStar the model is said to be perfect, no wave spreading and no viscous effects, so no yaw roll and sway is computed in head waves. The FLNG has a rather unconventional length/beam ratio of 2.5. Comparing this to a "normal" hull, the LNGC has a ratio is 6.2. The low ratio for the FLNG could mean the vessel encounters more viscous effects in reality, which are neglected in HydroStar. This concludes, the discrepancies between computed and experimental RAO's are significant, so the soft-mooring system or the tank imperfection or extra viscous effects in the tank influence the RAO's in a significant way.

5.2.2. FLNG IN TURRET-MOORING

The intentional objectives of the turret-mooring campaign were to gain confidence in numerical results for mainly mooring loads and offsets. The results are of special interest, because they can also be used for analyzing whether the type of mooring has effect on the first order motions. This analysis will answer the first research question from Section 2.1. The turret mooring system used for the configuration is illustrated in figure 4.7. Similar to the soft-mooring experiments, multiple tests with different environments have been subjected onto the vessel. The vessel is moored by the turret, so the vessel orientates itself in the most optimal position, the heading with the least resistance. With perfect conditions the heading would be zero degrees, however in the turret-mooring experiments the average wave heading was 2 degrees.

The RAO's for all six DOF's are obtained from the experiments and plotted in Figure 5.3. The RAO's have been plotted between 0.25 rad/s and 1.25 rad/s. No data is available outside the mentioned frequency range. This is because the wave energy is about 0 at these frequencies. For surge, heave, pitch and yaw the results are similar to both soft-mooring experiments as the HydroStar computations. Having the same peaks at the same frequencies. For roll the amplitude RAO seem to have a slight increase at frequencies between 0.25 and 0.7 rad/s, compared to the HydroStar calculation. However this increase seems to be slightly less than the roll RAO's from soft-mooring experiments. During the soft-mooring experiments the FLNG had a slightly different weight distribution. This is further elaborated in Section 5.3. The major discrepancy is observed for sway, which has a large peak between 0.25 rad/s and 0.5 rad/s. With a maximum RAO of 0.75 m/m, which is significant especially in almost head-waves. This peak is neither observed in HydroStar nor in the soft-mooring results. This concludes that the vessel sways significantly more in turret-mooring configuration. The natural frequency of the mooring system is obtained in Section 4.9 and is 0.031 rad/s, this does not come close to the frequency range of the peak observed for sway. The sway peak is a wave frequent phenomenon, because the wave energy peaks at the same frequency, as depicted in 4.15. One reason for the extra sway phenomenon could be weave spreading, however this extremely high peak is not visible in the soft-mooring RAO's. Therefore the above results conclude that the turret-mooring system might be impacted by significant viscous effects for sway which are neglected by the RAO computations of HydroStar.

5.3. WEIGHT DISTRIBUTION

The setup between soft- and turret-mooring differed not only in the type of mooring but also in the weight distribution on board of the FLNG. The FLNG for the soft-mooring experiments consisted of two hulls mounted together with a force frame in the middle, displayed in Figure 4.8. This force frame was used in order to calculate the internal forces, between the two hulls. The frame represented a significant weight on the FLNG. For the turret and side-by-side mooring experiments, this force frame was replaced by a wooden block. This effected the weight distribution on the FLNG, such that the COG shifted. Therefore extra weight blocks were added on the hull for the turret-mooring experiments. These weight blocks adjusted the COG back its original position. However the exact distribution is not known, potentially impacting the mass/inertia matrix

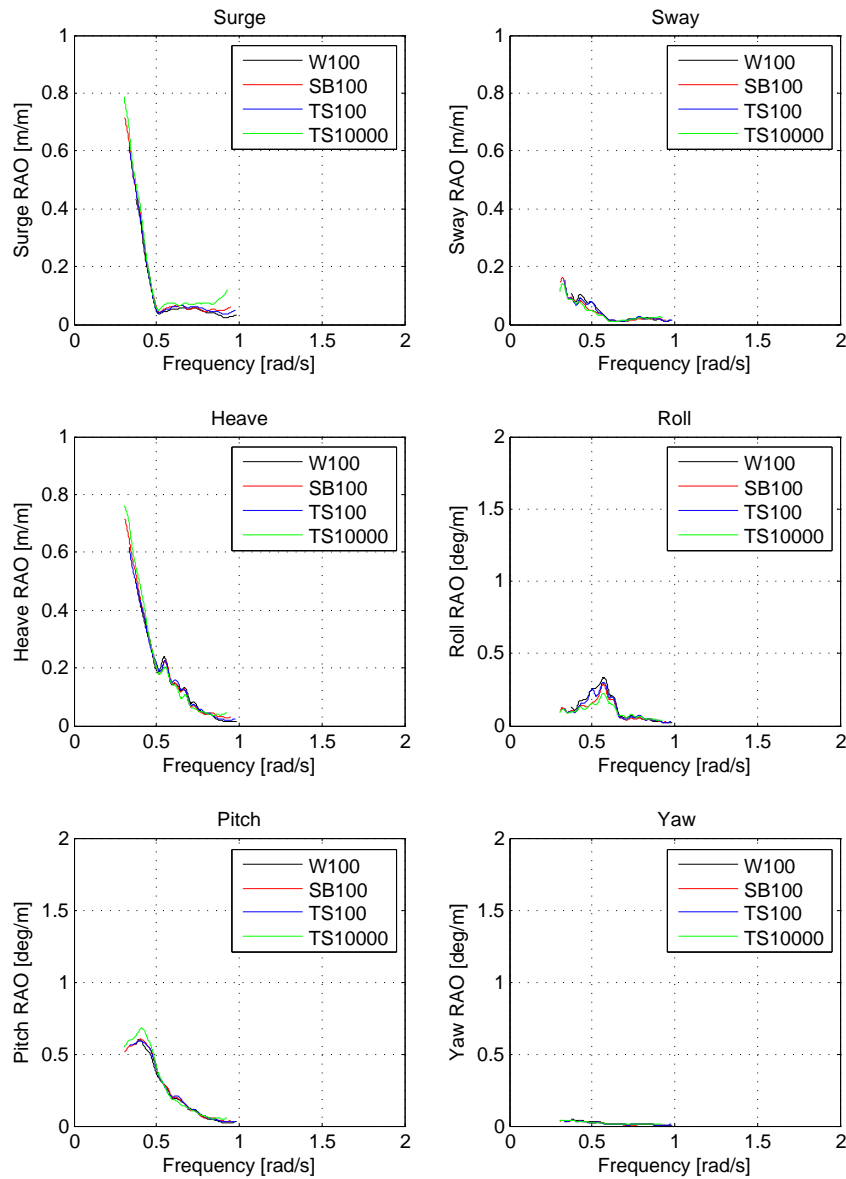


Figure 5.2: MARIN soft-mooring RAO for FLNG alone

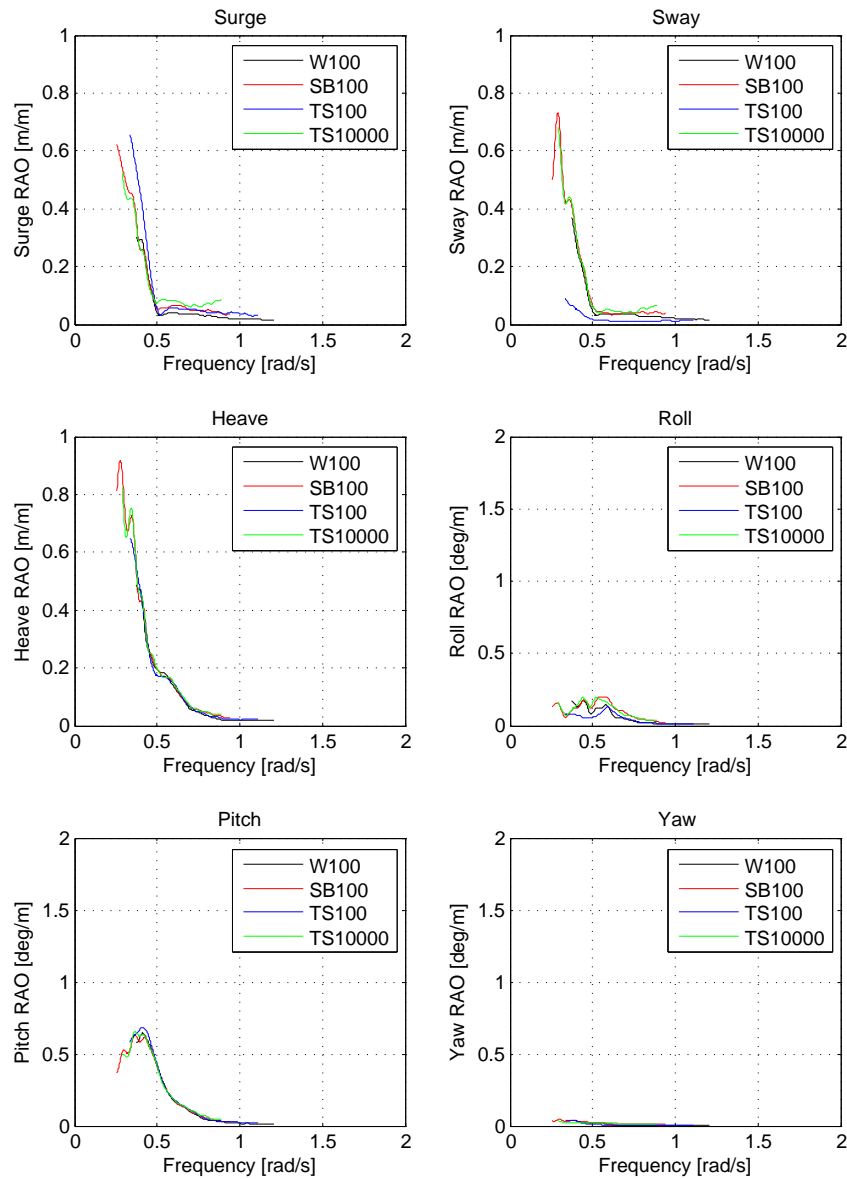


Figure 5.3: MARIN turret-mooring RAO for FLNG alone

Table 5.1: Coordinates weight points

	Weight point 1		Weight point 2		
	x-coordinate	y-coordinate	x-coordinate	y-coordinate	
case 1	0	-51.5	269	51.5	
case 2	40	-40	229	40	
case 3	400	-20	169	20	
case 4	120	-10	149	10	

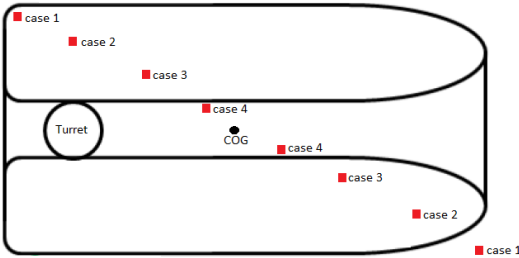


Figure 5.4: Weight point cases

from Equation 3.35. Therefore it cannot be determined whether the difference in roll RAO's is related to the difference in weight distribution, unless a sensitivity test is performed on the distribution. The sensitivity test conducted is explained briefly in the following paragraph.

5.3.1. SENSITIVITY ANALYSIS ON THE WEIGHT DISTRIBUTION

The goal of the sensitivity test is to determine whether the weight distribution can have an effect on the roll RAO. In the previous HydroStar calculation all mass and inertia coefficients in the mass matrix of the equation of motion 3.35, are set to 0, except for the diagonal coefficients; $m_{11}, m_{22}, m_{33}, m_{44}, m_{55}$ and m_{66} . This means there is no coupling between two motions in the system. This sensitivity analysis consists of 4 different cases, having a different weight distribution for the FLNG. The weight of the FLNG is concentrated on two different points of the vessel. Their coordinates are listed in Table 5.1 and depicted in Figure 5.4. Positioning the weight points in this manner will add coupling coefficients in the mass matrix of Equation 3.35.

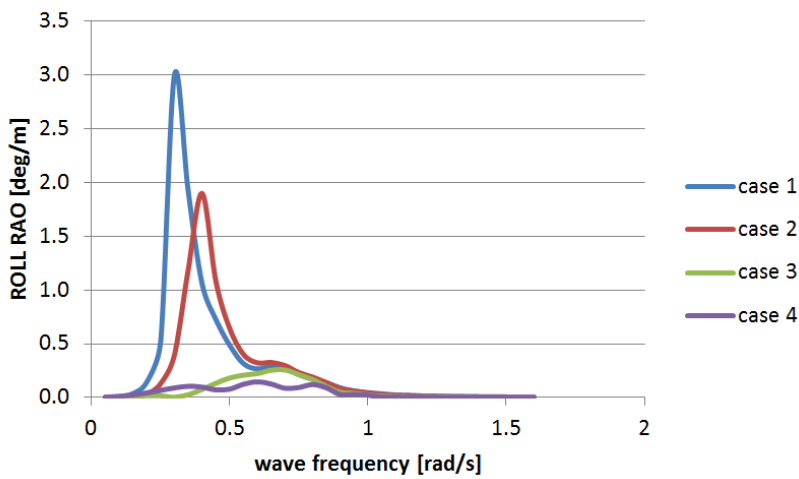


Figure 5.5: Roll RAO for the multiple weight distributions

In each case the total weight of the FLNG is split up into two separate points. The COG remains for each case in the exact same location. Next the roll RAO is determined for each case with the help of HydroStar. For this simulation the waves will encounter the FLNG head-on. Figure 5.5 shows the plot of the roll RAO for the 4 different cases. From this figure it is clearly visible that the FLNG will start rolling when the weight of

the FLNG is a non-uni formal distributed. Especially in the most extreme case number 4. For this case the vessel will roll a maximum of 3 degrees in head waves. Case 3 corresponds the most to the Roll response of the FLNG in Figure 5.2, heaving an RAO of 0.3 deg/m. From these results it can be concluded that the extra roll response of the FLNG in soft-mooring is due to a different weight distribution when compared to the FLNG in turret-mooring.

6

SIDE-BY-SIDE DIFFRACTION ANALYSIS

6.1. INTRODUCTION

Due to the complicated geometry of the FLNG and LNGC no simple analytical solution exists and numerical simulations are necessary. The diffraction software HydroStar, used in previous chapters is also used to calculate the response of the side-by-side oriented vessels. HydroStar is an in-house tool used by SBM Offshore and is developed by Bureau Veritas. The program provides a complete solution for first order wave diffraction and radiation problems. Furthermore the Quadratic Transfer Function (QTF) of second order low-frequency wave loads on a floating body can be computed. The relevant output generated by HydroStar used for computing relative motions are the RAO's with the corresponding phase shift, both represented in the frequency domain. Comparing the results from the diffraction calculations with the results from the model basin experiments, requires a computer model which represents the conditions used in the basin experiments as realistic as possible. The same set up for the main dimensions, hull shape, moments of inertia, water depths and environments will be applied to the model. The computation of the response is done in two phases:

- **Phase 1** Frequency domain (HydroStar), similar method as in Chapter 5
- **Phase 2** Time domain (Ariane), elaborated in Chapter 7

The frequency domain is considered straightforward, relatively simple and in practice widely used during the initial design stage. For this stage the system is assumed to be linear, such that this behavior is linear related to its displacement, velocity and acceleration. However in this system there are several complications which violate this linear assumption. For instance, forces and moments due to mooring lines, fenders and second order wave loads. Therefore the second phase is used for a more critical approach, including these non-linear effects. Section 3.7 elaborates on the theory used for the software program HydroStar. This chapter describes how the side-by-side model is built up, and which parameters are used for the HydroStar model.

6.2. HULL GEOMETRIES

A panel distribution of the FLNG and LNGC is provided by SBM Offshore. This is a mesh which has the same hull shape as the modeled vessels used in the experiments of MARIN. Their dimensions can be found in Table 4.3. The FLNG is composed of two identical LNGC's mounted together with additional spacing between the hulls, however this spacing is filled, so it does not have a catamaran hull shape. The complete geometries of the FLNG and LNGC have been visualized with the help of a software package called HSGVM, this package is included in HydroStar. HSGVM is a program which is capable to turn a list of panels and nodes with matching coordinates into a mesh, displayed below in Figure 6.1. The mesh of both hulls consist of a total of 8067 panels, with 532 segments along the waterline.

6.3. EPSILON DAMPING LID

Motion calculation for two vessels in close proximity is more complex compared to a single vessel. Complications lies in the hydro-mechanic interactions, causing resonance behavior of the waves in the gap between the vessels to be over-predicted using HydroStar. Viscous effects and friction on the hull are assumed to be

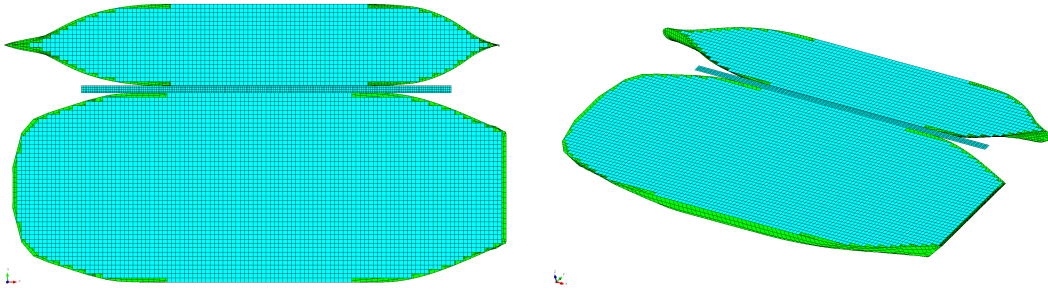


Figure 6.1: Mesh of the Twin-Hull, the LNG carrier and damping lid

contributing to reducing the wave elevations in the gap between the hull, as mentioned above in Chapter 3 (this is not taken into account in the diffraction theory). Over-prediction of wave elevation in the gap, will result in larger sway motion. The first component which contributes the most to this drift force is quadratic related to the relative wave height in the waterline. In order to damp the QTF's the water motions are to be damped in the gap between the vessels. A so called "epsilon" free surface lid can be used for the gap between the FLNG and the LNGC, in order to suppress the non-realistic high wave elevations between the two floating bodies. In this method a damping value is added to the free surface by means of a damping parameter. The method is based on the implementation of a damping force at the meshed free surface in between the two floating bodies. In the fluid a rotational free damping force is applied as described by R.H.M. Huijsmans [15]:

$$F = \mu \nabla \Phi \quad (6.1)$$

where Φ is the velocity potential, which is explained in Section 3.7. μ is the damping parameter. From Bernoulli it follows that the wave elevation at the free surface is:

$$\zeta = -\frac{1}{g} \Phi_t - \frac{1}{2g} \nabla \Phi \nabla \Phi - \frac{1}{g} \mu \Phi \quad (6.2)$$

At the free surface lid the boundary condition modifies to:

$$\frac{\partial \phi}{\partial z} - (1 - i\varepsilon) \frac{\omega^2}{g} \phi = 0 \quad (6.3)$$

in which ω is the wave frequency. The non dimensional parameter ε is related to the damping μ by:

$$\varepsilon = \frac{\mu}{\omega} \quad (6.4)$$

The free surface condition of the conventional approach, no-lid, the rigid lid and the damping lid, are summarized in table

Table 6.1: Free surface boundary equations

Conventional	Rigid lid	Damping lid
Undamped wave elevation	No wave elevation	Damed/tuned wave elevation
$\frac{\partial \phi}{\partial z} - \frac{\omega^2}{g} \phi = 0$	$\frac{\partial \phi}{\partial n} = 0$	$\frac{\partial \phi}{\partial z} - (1 - i\varepsilon) \frac{\omega^2}{g} \phi = 0$

The 'epsilon' coefficient in the damping lid Equation 6.3, can be varied in order to adjust the permeability of the lid, resulting in the damping of the wave elevation. Complete elimination of the waves in the gap results in a wave response which will be too low, likewise the QTF response which will be too low. Therefore complete elimination of the wave gap is unrealistic and the method preferred in this thesis is the "epsilon" lid method, also known as the energy dissipating method. The geometry of the lid added to the model is visible in Figure 6.1. The zone's dimensions are defined by the vessels length and the gap between the vessels, which corresponds in this model to a dissipation damping lid area of 4x202 meter.

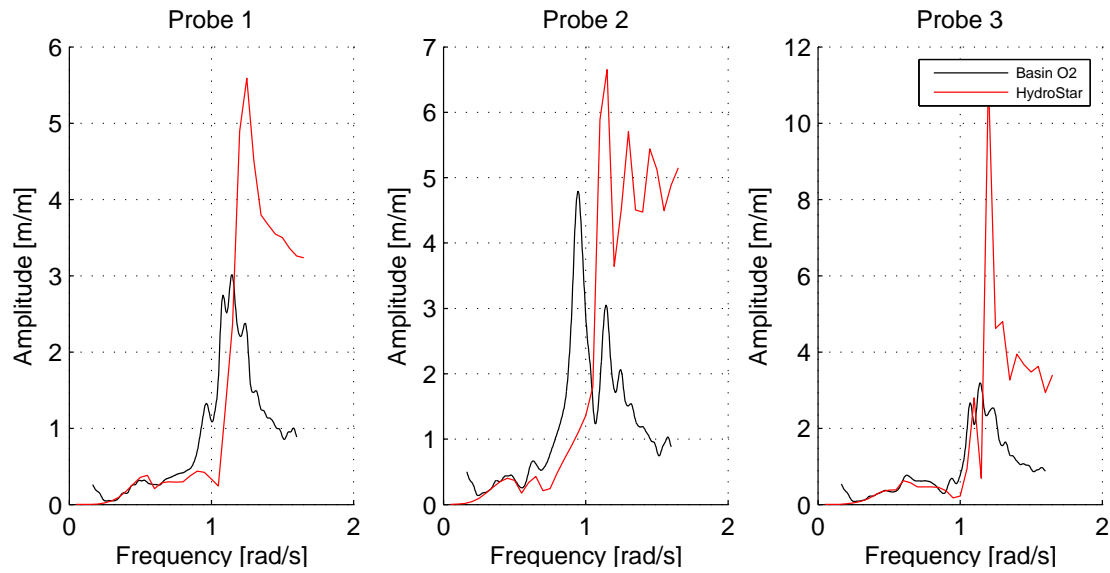


Figure 6.2: Wave RAO's for probe 1,2,3 obtained by MARIN and calculated by HydroStar

6.3.1. CONVENTIONAL UN-DAMPED WAVE RAO

Wave heights have been measured during the model basin experiments at three positions within the gap along the vessels hull, displayed in figure 4.5. At these positions the conventional un-damped wave RAO's have also been calculated by HydroStar. Both results are plotted in a wave RAO response figure, per wave probe in Figure 6.2. This figure shows the wave RAO of the experiment with environment O2. Additional wave RAO's of the remaining environments can be found in the Appendix D.

The wave elevation response of the HydroStar results show similar characteristics as the wave elevation registered during model basin experiments, but in certain frequency range large discrepancies are observed. In long waves the calculations are almost exactly the results of the model basin experiments, but in the higher frequency range, between 1.2 rad/s and 1.8 rad/s the calculated waves are considerably higher than the offshore basin experiments obtained. A peak around certain frequencies in the offshore basin is observed, but results from calculations over-predict this peak considerably. The peaks are corresponding to waves which are in resonance in between the vessels. Furthermore the amplified wave height is very sensitive to the position over the length of the water line. In the basin the highest wave response is measured at probe 2, mid-ship. However HydroStar calculates the peak at probe 3, which is more to the stern of the FLNG. The incoming wave will encounter probe 3 at first.

6.3.2. SENSITIVITY ANALYSIS FOR WAVE RAO, BY VARYING ϵ OF THE DAMPING LID

RAO's of the wave elevations of the HydroStar calculations with a damping lid between the vessels are compared with the experimental wave elevations measured in the MARIN basin. The wave RAO's for all wave probes and environments can be found in Appendix D. The RAO for wave probe 3 is illustrated in Figure 6.3, the black curve represents the wave RAO of environment O2 tested in the MARIN basin. Multiple "epsilon" iterations calculated by HydroStar have been plotted within this same figure. From this Figure 6.3 the best corresponding 'epsilon' can be chosen. Results clearly show a trend in the peak of the wave elevation. The "epsilon" damping has a greater effect on the frequency range where the resonance peak is observed, in the frequency range between 1.2 rad/sec and 1.4 rad/sec. This means the "epsilon" damping is occurring in the resonant frequency range. From Figure 6.3 and the remaining probes in Appendix D. It can be concluded that the iteration with $\epsilon = 0.2$ gives the best fit.

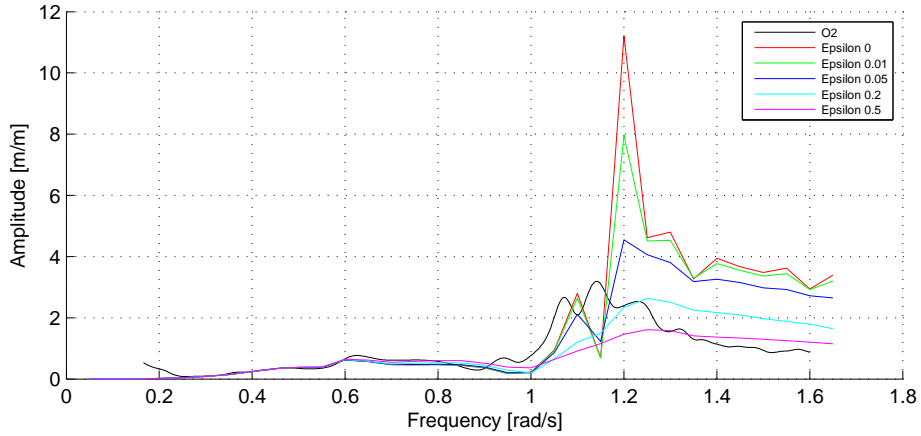


Figure 6.3: Sensitivity test on wave RAO by varying ϵ at probe 3

6.3.3. SENSITIVITY ANALYSIS FOR MOTION RAO, BY VARYING ϵ OF THE DAMPING LID

In the previous section the epsilon is fitted by means of the wave response in the gap between the two vessels. This same method, used in order to check which "epsilon" value fits best to the 1st order motions of the vessels. Multiple iterations with the "epsilon" value have been conducted, in order to calculate the motion RAO. In figure 6.4 the iterations are plotted.

Similar to the wave RAO sensitivity tests, the results show a clear trend in the damping of the roll motion. Additional the resonance peak at approximately 1.2 rad/s is visible. All iterations follow the same trend except at this resonance peak. A larger ϵ corresponds to more damping and a lower resonance peak. The iterations done for the remaining five degrees of freedom and other environments have been plotted in Appendix D. Note that for surge, pitch and yaw the "epsilon" iterations for both vessels do not show any variation. However for sway and heave, there is a similar resonance peak visible as the one in 6.4. The overall choice made for best fitted epsilon value is once again $\epsilon = 0.2$. Concluding from previous paragraph and from Section 6.3.2, ϵ is set to 0.2 in the final SBS HydroStar model.

6.4. ROLL DAMPING [4]

Damping calculated by HydroStar is based on the potential flow theory, meaning the damping is caused by the generation of waves, which dissipates energy from the moving structure. However the effects of fluid viscosity such as skin friction and vortices are not taken into account throughout the diffraction calculations. Viscosity increases the damping for roll to such an extent that it can't be neglected. The horizontal motions (Surge, Sway, Yaw) are usually out of resonance in common sea conditions. In these cases viscous damping does not play an important role, so the potential theory correctly evaluates the amplitudes of these motions. The only modes which may enter the resonance area are the motions in heave, pitch and roll direction. For these motions the viscous damping is essential. HydroStar offers the option to add a percentage of critical roll damping to a specific vessel. This percentage is the linear damping calculated by diffraction from the critical damping. Several iterations have been performed, by varying different linear damping percentages. The results have been plotted against the actual roll RAO's measured in the offshore basin at MARIN. Figure 6.5 represents the iterations done. A clear trend is visible, a small peak for the FLNG and a large peak for the LNGC, both around the frequency of 0.7 rad/sec. This peak decreases when the linear damping is increased. The best fit is 1% percent of critical roll damping for the FLNG and 8 % for the LNGC. Additional sensitivity plots on linear viscous damping are listed in Appendix E.

6.5. HEADINGS

HydroStar computes RAO's for a selected heading range. In order to know its response for different angles of the vessels, the range is selected to be from 0 to 360 degrees. The resolution, also known as the heading

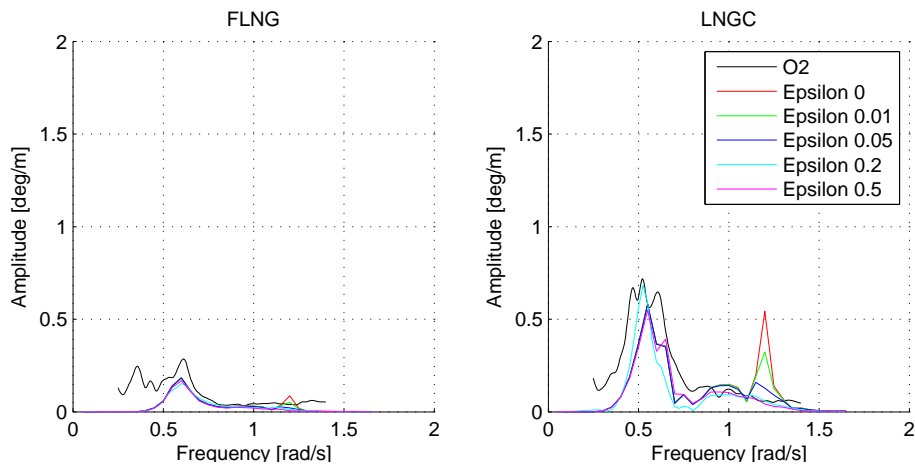


Figure 6.4: Sensitivity test on the vessel's roll RAO, by varying ϵ

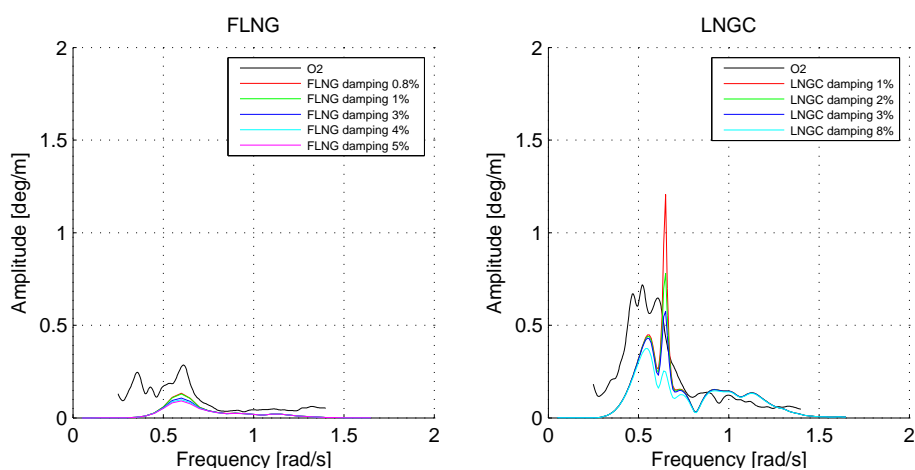


Figure 6.5: Sensitivity test on the vessel's roll RAO, by varying the percentage of linear viscous damping

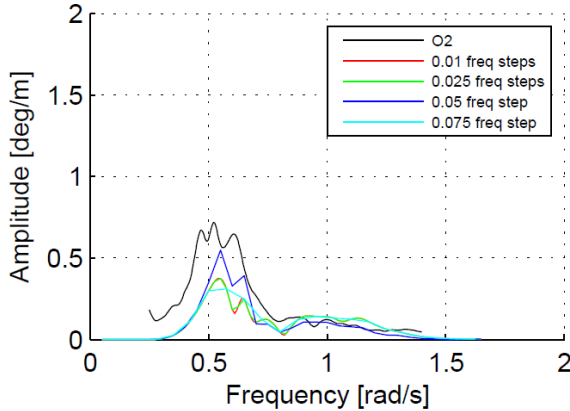


Figure 6.6: Frequency iteration for the LNGC in roll

steps, determine how many heading calculations HydroStar will compute. Choosing the resolution a factor two higher means the computation time will take twice as long. Therefore the heading steps are optimized for this thesis research, and determined to be in steps of 2.5 degrees. Therefore for each diffraction run by HydroStar, the response for 144 headings are computed.

6.6. FREQUENCY SENSITIVITY

As the diffraction runs executed by HydroSTAR are a time consuming part of the simulation, the chosen frequency resolution is crucial. If a small frequency step is chosen, e.g steps of 0.01 rad/sec these simulations will take significantly longer compared to simulations run with steps of 0.075 rad/s. However when a large frequency step is chosen, it might be the case that some crucial RAO resonance peaks will be left out. Figure 6.6 shows a plot of multiple frequency steps. The frequency steps 0.075 and 0.05 rad/s have not yet converged. As apposed to the 0.01 and 0.025 steps, their plots have converged on top of each other. The remaining frequency steps can be found in Appendix C. For the final model the frequency step is set to 0.025 rad/s.

6.7. HYDROSTAR SIDE-BY-SIDE MODEL RESULTS

All necessary input data for the HydroStar SBS model are known. In this section the results of this model are presented.

6.7.1. FLNG RAO'S

The RAO's which will be analyzed will be compared with the results from the O2 experiment, performed in the MARIN offshore basin. The average wave heading in this experiment is 3 degrees, which is almost head-on. The three degrees is measured from the stern of the FLNG. In the side-by-side configuration, the setup with the LNG carrier alongside the FLNG, is not a symmetric set up, due to the FLNG which is being moored by a turret and a full 16 line catenary system onto the seabed. This means that the carrier exerts an extra yaw moment around the turret. The extra yaw moment forces the vessels to turn to a wave angle of 3 degrees. For HydroStar the nearest heading calculated is 2.5 degrees (measured from the stern), this is due to the chosen heading steps in Section 6.5. The half of a degree difference does not have a great effect on the resulting RAO comparison, this difference can therefore be neglected. The calculated HydroStar RAO's are plotted in Figure 6.7.

Comparing these values with the calculated HydroStar RAO's for the FLNG alone (Figure 5.1) at a wave heading of 2 degrees, show great similarities for all six DOF's. Almost no sway is calculated, only when the frequency approaches zero, than the sway RAO peaks at 0.1 rad/sec. Yaw is similar for the single FLNG almost zero at any frequency. The only discrepancy noticeable is the peak for roll at a frequency of 0.6 rad/sec. This peak is due to the hydrodynamic iterations in the gap between the vessels. These iterations creates an extra roll moment at frequencies where lid-damping does not have an effect.

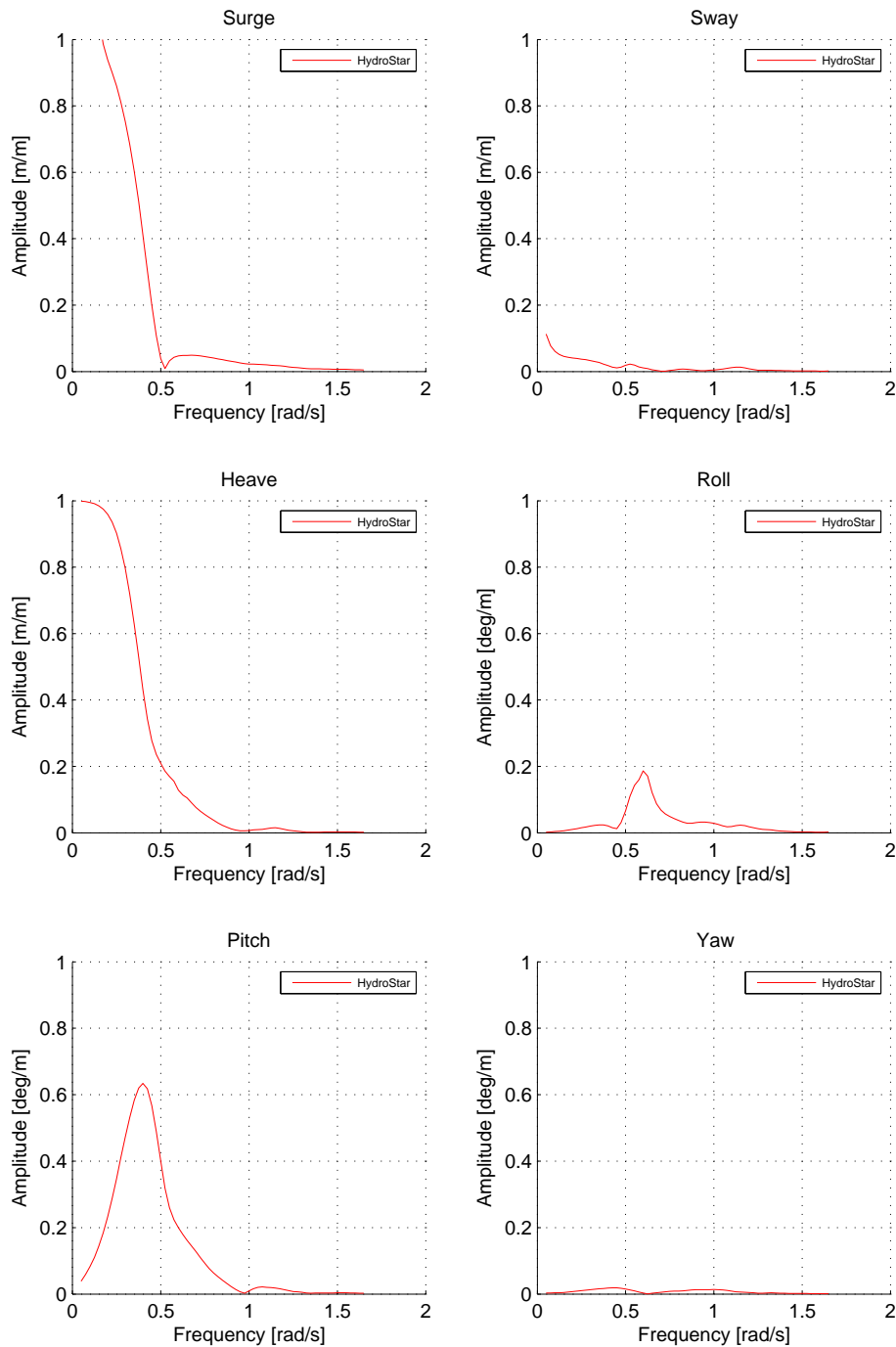


Figure 6.7: HydroStar RAO computations for FLNG in side-by-side configuration

6.7.2. LNGC RAO's

The RAO's for the LNG Carrier, with wave heading 2.5 degrees (measured from its bow) are presented in Figure 6.8. The calculated motions for the LNGC have the same trend as the FLNG. One obvious difference is the peak for roll at 0.55 rad/sec. This peak is at the same frequency for the FLNG, but the amplitude is three times greater. The difference of this peak is due to the geometry of the vessels. The breath-draught (B/T) ratio influences the potential damping for roll. The greater the ratio, the more potential damping the vessel encounters. The FLNG has a *B/T* ratio of 9.8 which is much greater than the LNGC ratio of 4.9. This concludes that the FLNG must have greater potential damping in roll, due to more waves being generated. Therefore the LNGC has less potential damping and will have a greater roll amplitude at its natural frequency. In addition, the mass of the LNGC is significantly less, this will result in larger roll motions.

6.8. MARIN RESULTS

The next step was the post processing of the results from the side-by-side experiments. MARIN provided SBM Offshore raw data files with a set of 70 sensors capable of measuring movements and wave elevations near and on the vessels. Similar to the turret- and soft-mooring tests all the six DOF's can be obtained from this data. RAO's from the obtained experiments are computed by the following transfer function:

$$\left| \frac{Z_a}{\zeta_a}(\omega) \right| = \sqrt{\frac{S_z}{S_\zeta}(\omega)} \quad (6.5)$$

Where $\frac{Z_a}{\zeta_a}$, $S_z(\omega)$ and S_ζ are the heave RAO, heave response spectrum and the wave spectrum respectively. The wave spectra are obtained in Section 4.7. The response spectra of all six DOF's of both vessels are listed in Appendix B. The resulting RAO's for experiment O2 are presented in combination with the HydroStar calculated RAO's in Figure 6.10. Note, the black curve in the figures represent the MARIN RAO's. The RAO's are plotted for frequencies ranging from 0.25 rad/sec to 0.35 rad/sec. Outside this frequency range the spectral wave energy is too low, meaning the RAO's will become inaccurate. Validating RAO's for motion simulations is normally done with the help of a so called white noise experiment. The wave spectrum to which a model vessel is subjected in a white noise experiment consists of a random signal with a constant energy spectrum over a chosen frequency band. Figure 6.9 shows an example of such a wave spectrum. The main advantages for validating RAO's with a white noise spectrum is that the wave energy is evenly distributed over the frequencies, resulting in a favorable output in the desired RAO's over the chosen frequencies.

No white noise tests were performed during the side-by-side experiments in the MARIN offshore basin. The RAO's in this thesis could only be calculated with a high degree of certainty around the resonance peaks, corresponding for environment O2 with a peak period of 17 seconds. In this range there is enough wave energy, as depicted in Figure 4.15. The next step is to compare the MARIN RAO's in Figure 6.10 with the soft- and -turret moorings in Figures 5.2 and 5.3. For surge, heave, roll, pitch and yaw the side-by-side experimental RAO's show similar curves to both the turret- as the soft-mooring experiments. However the sway RAO shows a large peak between 0.25 rad/sec and 0.5 rad/sec. The peak is not observed in the soft-mooring experiments, nonetheless this peak is observed for sway in turret-mooring experiment, in figure 5.3. This raises the possibility that the extra sway which is being measured has an effect on the way the vessel is moored.

The RAO's from HydroStar for the side-by-side orientation are included in 6.10, showing matching curves for surge, heave, pitch and yaw, when comparing these to the experimental MARIN curves. However the sway RAO's do not correlate in the frequency range from 0.25 rad/s to 0.5 rad/s. The calculated RAO shows a similar curve as calculated for soft- and turret-mooring, almost no sway amplitude in head-waves for all frequencies. For a vessel with a perfect symmetric hull, subjected to head-waves, no sway should be recorded. For the SBS experiments the wave angle is 3 degrees (in HydroStar this angle is 2.5 degrees), meaning there should be some sway, which is calculated as presented in the Figures 5.1 and 6.10. At 0.5 rad/sec the computed sway RAO is about 0.02 m/m, which corresponds to 0.05 meters in an offloading sea state with an H_s of 2.5 meters.

6.9. QTF STUDY

There are multiple methods available for calculating the QTF's:

- **Near field:** This method, as described by Pinkster [9], provides a second order description of the boundary conditions for the velocity potential. Via Bernoulli, Equation 3.27, the pressure is calculated and integrated over the hull to obtain the second order loads.

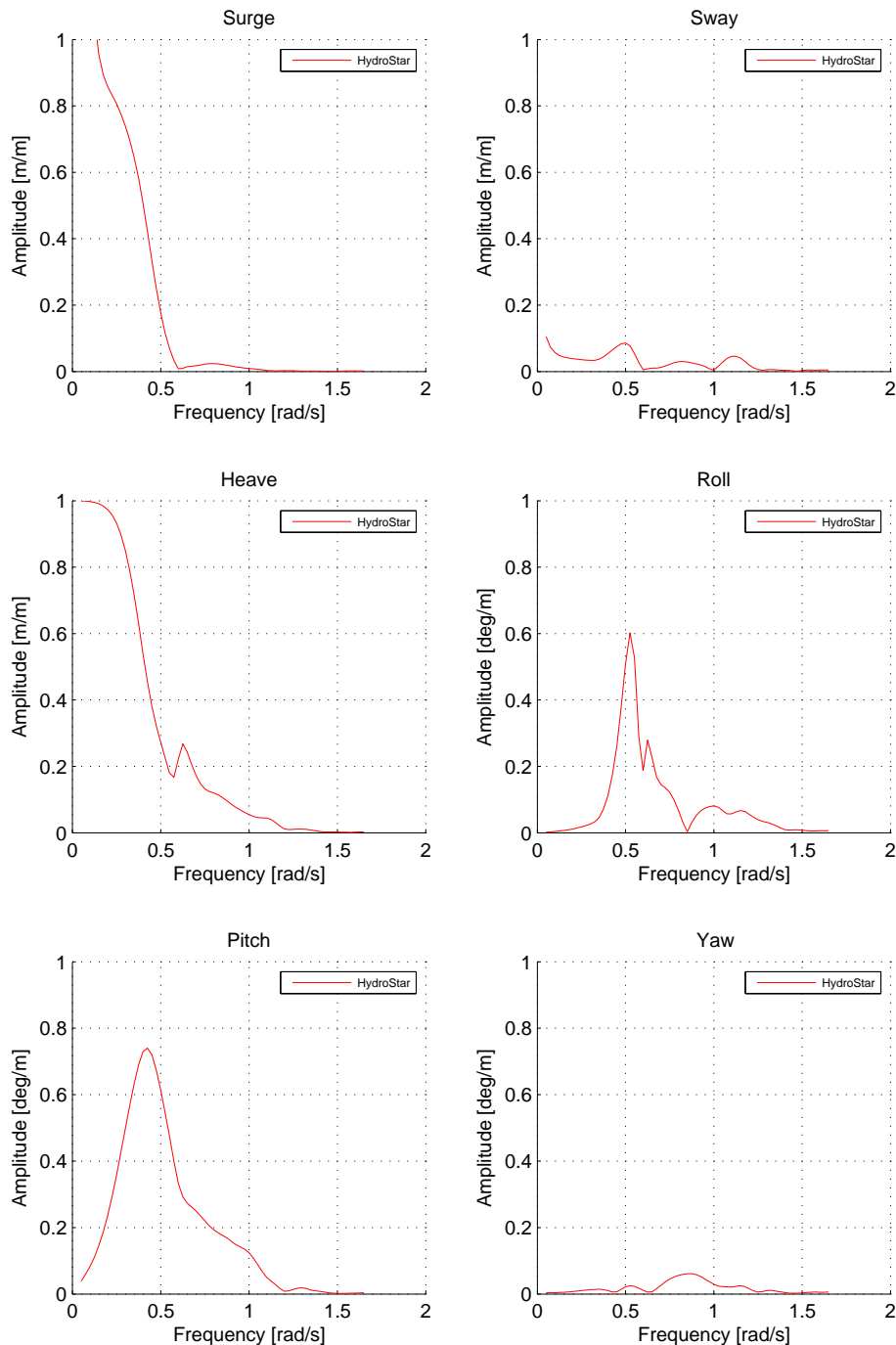


Figure 6.8: HydroStar RAO computations for LNGC in side-by-side configuration

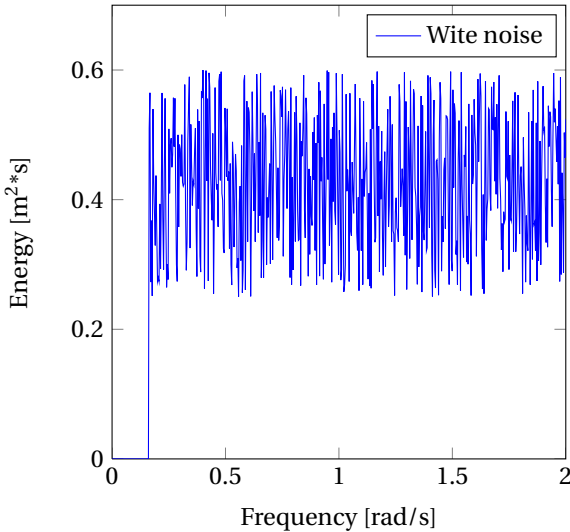


Figure 6.9: White noise spectrum

- **Far field:** This method is used to obtain expressions for the mean wave drift forces and moments. These expressions of the mean wave forces in regular waves are determined using equations for conservation of momentum in the fluid. The momentum is considered in a predefined surface area S away from the vessel. Adding the results of regular waves allows us to obtain results for an irregular sea surface. Only the horizontal terms can be determined.
- **Middle field:** This method describes the loads, on a control surface at a certain distance from the vessel. To determine the flow potential a panel method is used, done within the control surface. This formulation combines the advantages of both near field and far field formulation, providing good numerical precision and the possibility of accessing to all components of drift loads and low frequency loads (QTF's) as the near field formulation.

HydroStar can make use of all three methods above. In order to prove whether the methods converge, the QTF's for surge and sway calculated by the three methods are illustrated in Figure 6.11.

The side-by-side experiments executed in the MARIN offshore basin did not include regular wave tests. Without regular wave tests it is not possible to determine the QTF or mean drift force on the vessels in side-by-side arrangement. Therefore the QTF's determined by HydroStar cannot be verified. It is recommended to perform regular wave tests during future side-by-side experiments.

6.10. RAO TUNING

The calculated sway RAO for both the FLNG as for the LNGC show significantly less sway motion than the experimental sway RAO. Assuming the sway RAO from the experiments corresponds more to full scale motions, a logical step is to tune the sway RAO from HydroStar until it matches the RAO's from the experiments. The method used in this thesis is: to determine the amplitude and phase RAO from the MARIN experiments for both vessels, and implement these into the calculated sway RAO values. The resulting "tuned" sway HydroStar RAO is presented in 6.12. The phase is measured assuming the COG of the FLNG is positioned right above the location where the CL wave probe (Figure 4.6) is located. However in reality and in the experiments, the vessel tends to drift away from this position. Therefore the COG is never on this exact location, meaning there could be an additional phase shift. The extra phase shift is not measured during the MARIN experiments. Using an FFT the measured wave can be split into amplitude and phase, which makes it possible to reproduce the wave at a different location. However the wave energy tends to have quite a different spectrum at different locations in the tank, as was observed in Figure 4.15. Having different energy spectra for the same experiment in the offshore basin, means a reconstruction of a wave on a different location will not give a reliable outcome.

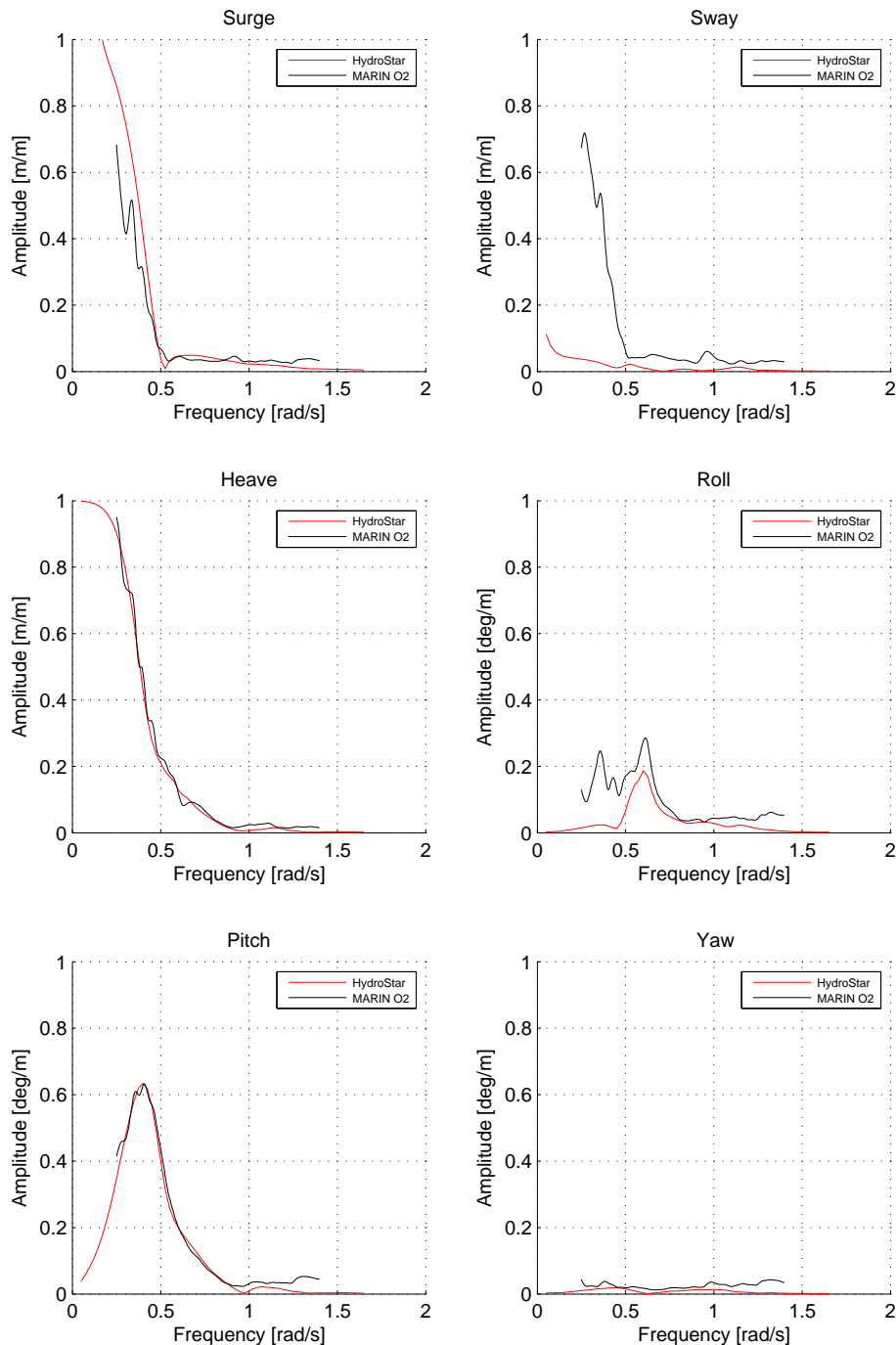


Figure 6.10: SBS MARIN & HydroStar RAO's for the FLNG

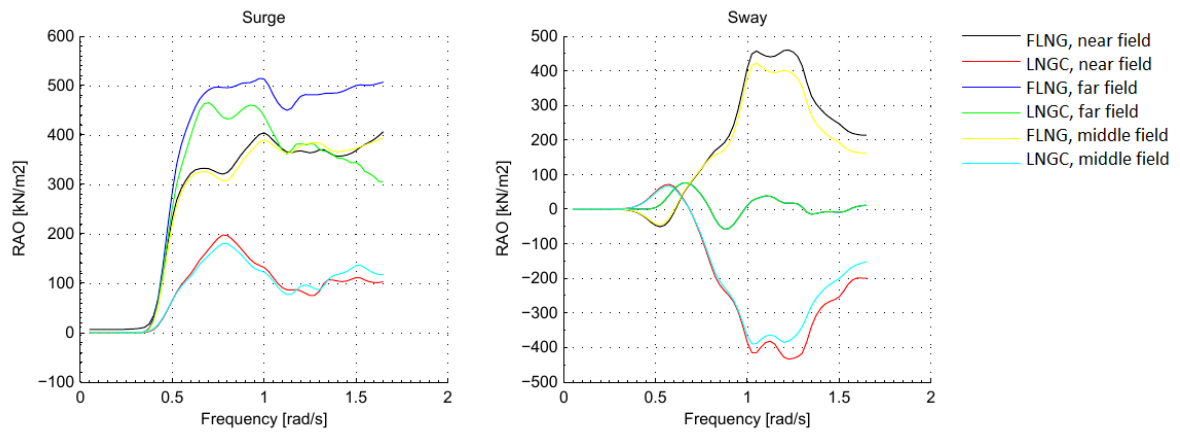


Figure 6.11: QTF's for surge & sway, with head-on waves

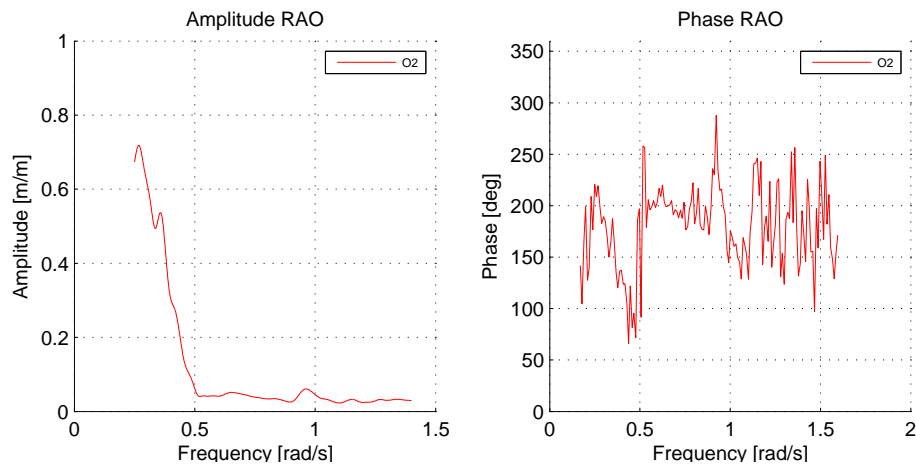


Figure 6.12: Tuned HydroStar sway RAO for FLNG

7

TIME-DOMAIN ANALYSIS

7.1. INTRODUCTION

The system is linear when the vessels behave linear related to their displacement, velocity and accelerations. If the system complies with these requirements, then the system can be studied in the frequency domain. However in order to increase the accuracy of the model, nonlinear components are added. Examples of nonlinear components are mooring lines, fenders and second order wave loads. Including these nonlinear components into the model will make the frequency domain approach no longer valid. This chapter presents the time-domain solutions of the numerical model. Using Ariane the two vessels can be moored in the same manner as done in the offshore basin at MARIN. Ariane can determine the equilibrium position of both vessels under influence of external forces, wind waves and currents. For these vessel positions the program is able to calculate the resultant mooring line tensions and thus all parameters which characterize the behavior of the individual lines. The experiment with environment O2 is used in this chapter as the base case and will be used to compare with the calculated RAO's.

7.2. THEORY [5]

The determination of the position of the vessels is done in two steps. First the low frequency response of the moored vessels is obtained by numerical resolution in the time domain of the vectorial differential Equation:

$$[M] \{\ddot{X}\} = \sum \{F(t)\} \quad (7.1)$$

where:

$\{X\}$ is the three-component vector characterizing the global coordinates X and Y of the COG and the heading ϕ of the vessels.

$$[M] = \begin{bmatrix} m & 0 & 0 \\ 0 & m & 0 \\ 0 & 0 & I_{\phi\phi} \end{bmatrix}$$

which is the horizontal mass matrix of the vessel calculated at its COG. With components that are the actual mass of the vessel for surge and sway motions m and moment of inertia $I_{\phi\phi}$.

$$\{F(t)\} = \begin{Bmatrix} F_{GX}(t) \\ F_{GY}(t) \\ M_{GZ}(t) \end{Bmatrix}$$

is the vector containing the horizontal loads applied to the COG of the vessel at instant t , which are contributing to the low frequency response i.e. F_x is:

$$F_x = F_{Hx} + F_{Mx} + F_{Bx} + F_{Dx} + F_{Wx} + F_{Cx} \quad (7.2)$$

where:

F_H	hydrodynamic wave loads
F_M	mooring loads
F_B	damping loads
F_D	wave drift force
F_W	wind loads
F_C	wind loads
F_O	current loads

For F_y and F_ϕ equation 7.2 is similar only x is replaced by y or ϕ respectively.

Next comes the calculation of the wave frequency response (1st order response, calculated in 6) which is added to the numerical integration of the low frequency response. At each time step, the six wave frequency motions of the vessel's COG are added to its low frequency position. The vessels 1st order response is calculated by multiplying each component of the wave signal with the RAO of the COG of the vessel. In this process it is assumed that wave frequency motions are not significantly influenced by the variations of the mooring stiffness with low frequency motions. The motions of a vessel subjected to linear waves can be computed using the equations in table 7.1.

Table 7.1: Motions of a vessel submitted to an linear wave

surge	$aR_x(\omega, \alpha)\cos(\omega t + \Phi_x(\omega, \alpha))$
sway	$aR_y(\omega, \alpha)\cos(\omega t + \Phi_y(\omega, \alpha))$
yaw	$aR_z(\omega, \alpha)\cos(\omega t + \Phi_z(\omega, \alpha))$
roll	$aR_\theta(\omega, \alpha)\cos(\omega t + \Phi_\theta(\omega, \alpha))$
pitch	$aR_\phi(\omega, \alpha)\cos(\omega t + \Phi_\phi(\omega, \alpha))$
yaw	$aR_\psi(\omega, \alpha)\cos(\omega t + \Phi_\psi(\omega, \alpha))$

In the table above, R and Φ are the amplitude RAO and Phase RAO respectively. These factors only depend on the wave frequency and the relative vessel heading to the incidence wave. The amplitude and phase RAO have been determined in section 3.7.

7.3. DECAY TESTS

In Ariane the decay tests which are performed at MARIN can be reproduced in order to verify the damping values calculated in Section 4.9. In this section the tuning is presented for the LNGC.

7.3.1. DAMPING

In 4.9 the linear damping values are presented. These values can be used as input for the Ariane 7 model. The damping loads are proportional to the absolute speed of the vessel according to the following formulae:

$$\begin{aligned} F_{Bx} &= B_{xx}\dot{x} \\ F_{By} &= B_{yy}\dot{y} \\ F_{B\psi} &= B_{\psi\psi}\dot{\psi} \end{aligned}$$

where B_{xx} , B_{yy} and $B_{\psi\psi}$, are the damping coefficients for surge, sway and yaw respectively.

However using this values will result in just linear mooring damping, which can result in too little damping. Therefore the model's decay should be evaluated. The decay tests done at MARIN can be reproduced in Ariane in order to verify the models damping coefficients. The calculated damping coefficients for surge, sway and yaw in 4.9 are used as the base-case. By slightly varying the p value, from equation 4.3 several adjusted damping values are calculated. Multiple iterations have been performed with different damping values. The results of these decay iterations are illustrated in figure 7.1 to 7.3. The plots illustrate decay tests for surge, sway and yaw, tested in the Offshore Basin at MARIN and calculated iterations from the Ariane model.

From the plots the best p fit is selected. The corresponding optimal damping value's are listed in Table 7.2:

For sway, the damping is correctly calculated, meaning the value has not been tuned. This concludes the damping is mostly linear. However for surge the optimized damping is decreased significantly from a value of 3.78E+06 to 2.12E+06 meaning there was too much damping.

7.3.2. NATURAL PERIOD

The side-by-side natural periods of the mooring system can be evaluated from figure 7.1 to 7.3. The results are listed in Table 7.2 and compared to the natural periods obtained from the decay tests at MARIN.

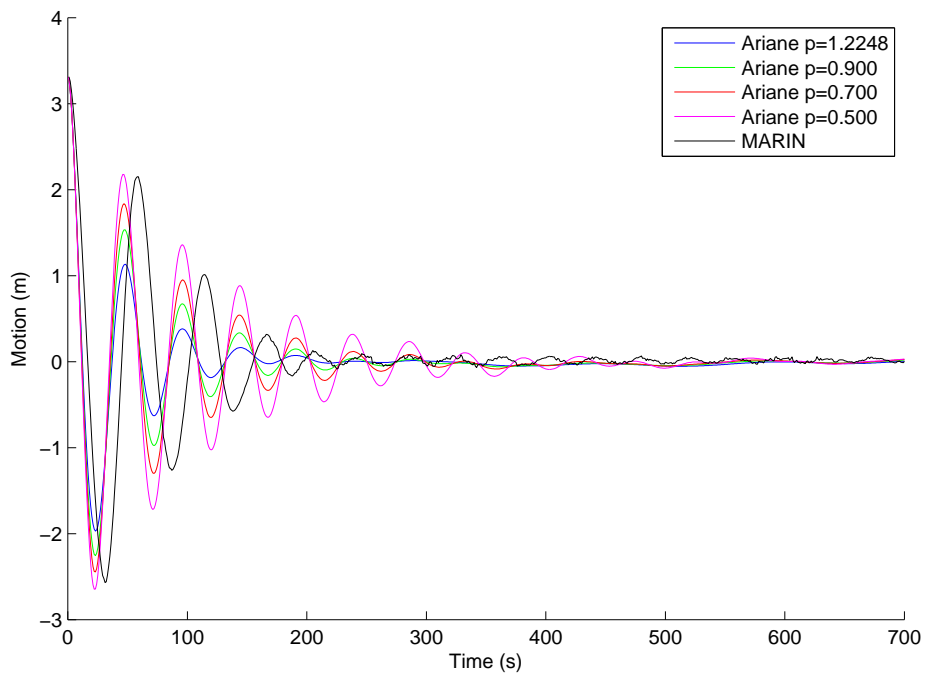


Figure 7.1: Ariane LNGC surge decay - damping iterations

Table 7.2: Optimized damping values

	calculated p	optimized p	optimized damping	MARIN natural freq [s]	Ariane natural freq [s]
surge	1.2448	0.700	2.12E+06	53.58	48.5
sway	0.557	0.557	3.39E+06	32.55	32
yaw	0.8436	2.000	1.40E+10	35.38	33.5

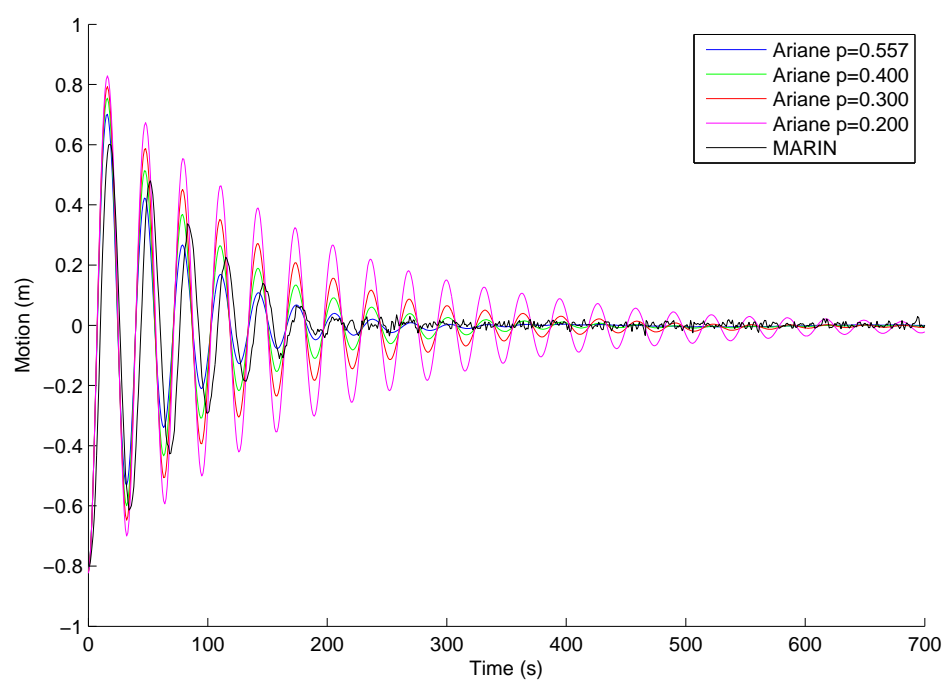


Figure 7.2: Ariane LNGC sway decay - damping iterations

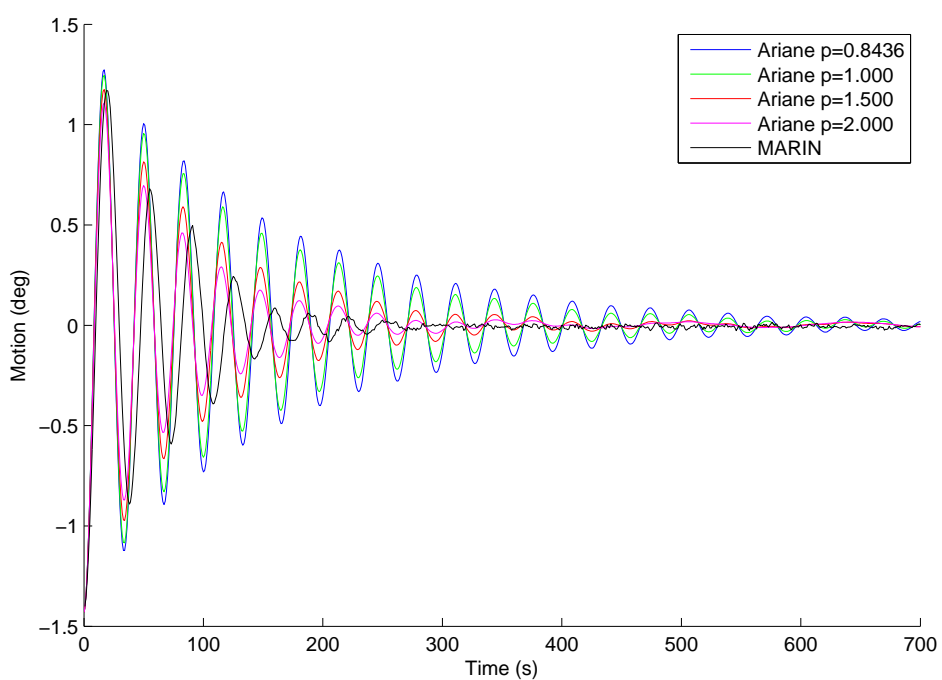


Figure 7.3: Ariane LNGC yaw decay - damping iterations

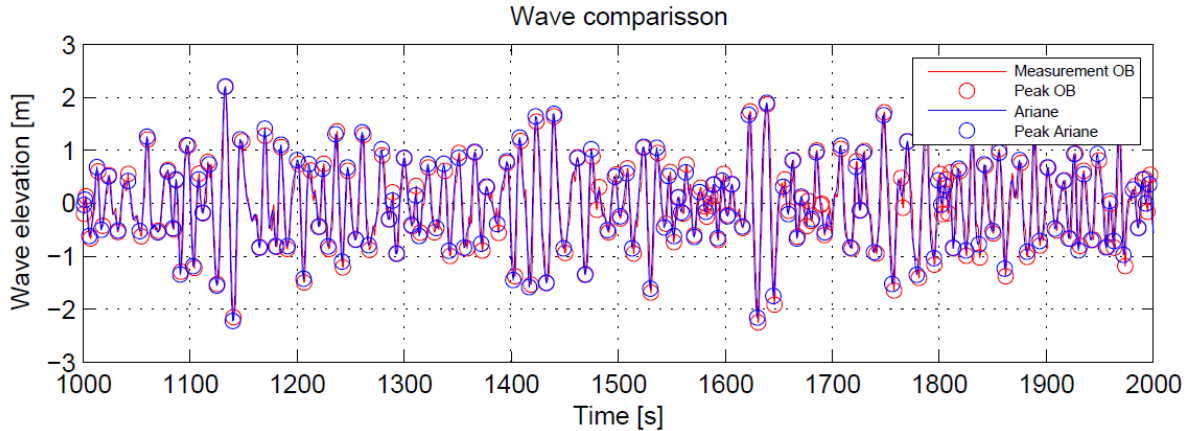


Figure 7.4: O2 wave timetrace

7.4. RELATIVE MOTIONS

The most important motions for this thesis are the motions between the manifolds of the FLNG and LNGC. To calculate these motions the RAO's from HydroStar are used as the input for Ariane, then with Ariane a time trace of relative manifold motions is computed. In this paragraph an analysis is done on the two different cases.

- **Case 1:** RAO's are used as input for Ariane which are calculated by the diffraction software HydroStar without tuning.
- **Case 2:** RAO's are used as input for Ariane which are calculated by the diffraction software HydroStar with tuning. The experimental RAO's for sway are taken as input in Ariane.

7.5. ENVIRONMENT O2

Figure 7.4 illustrates the reconstructed wave for the Ariane calculations. The reconstructed wave can be compared with the measured wave in the MARIN basin. The reconstructed wave is spot on. The reconstruction of the wave is done with the help of an FFT. There are no wind and no current forces for this Environment.

7.6. CASE 1: "UN-TUNED" RAO'S AS INPUT FOR ARIANE

Using the RAO's calculated by HydroStar without tuning will result in a time-traces presented in Figure 7.5. In the same figure the time trace is plotted of the MARIN experiments. X,Y and Z represent the relative distances for surge, sway and heave, between the manifolds. L is the total absolute distance between the manifolds.

For the relative manifold X distance, an offset of about 0.5 meters is notable. The mean offset in Ariane is calculated at 0 meters. This difference is due to the inaccuracy in the experimental set up. The model is built at a scale of 1:60, so this means an offset in the offshore basin corresponds to only $0.5/60 = 0.008$ meters model scale. Furthermore the extra drag due to the fenders discussed in Section 7.8 has an jerking effect on the relative surge motions, causing the extra peaks near 1180, 1460 and 1650 seconds.

For the relative manifold Y distance, a significant discrepancy is noticeable in the amplitude. Both time traces have an mean around 4 meters, due to the pretension in the fenders en mooring lines. However the maximum in the offshore basin is 5.36 meter whereas Ariane calculates a maximum of 4.24 meters. This relative large discrepancy is due to the sway RAO's calculated by HydroStar, visualized in Figures 6.7 and 6.8. From the figure it can be concluded that there is almost no sway calculated as opposed to the measured MARIN tests.

For the relative manifold Z distance the curves show favorable similarities, with a mean around 1.5 meters and both peak with a maximum of around 1.9 meters.

For the absolute relative distance L, a significant discrepancy is noticeable in the amplitude. This is due to the absence of sway in both vessels. The absolute relative distance is calculated by equation 7.3:

$$L = \sqrt{X^2 + Y^2 + Z^2} \quad (7.3)$$

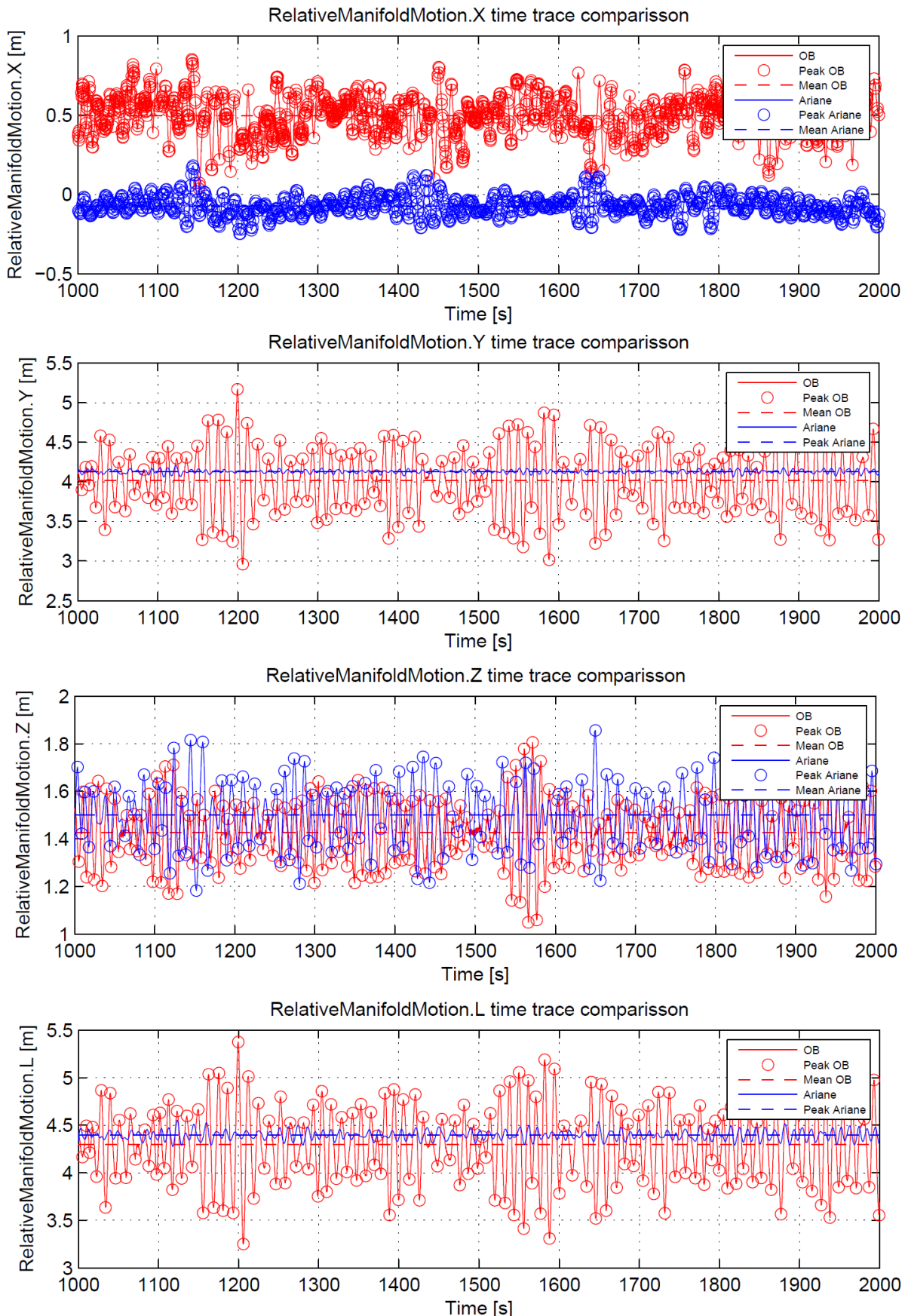


Figure 7.5: Relative manifold distance for X, Y, Z and the absolute distance L. Un-tuned RAO's as input

Table 7.3: Statistical results of the relative manifold motions of the Ariane models

	Ariane "un-tuned"		Ariane "tuned"		MARIN	
	Mean	Max	Mean	Max	Mean	Max
Realative manifold distance X [m]	-0.07	0.18	-0.07	0.19	0.5	0.95
Realative manifold distance Y [m]	4.13	4.24	4.13	5.75	4.02	5.36
Realative manifold distance Z [m]	1.5	1.92	1.5	1.97	1.43	1.88
Realative manifold distance L [m]	4.4	4.61	4.4	5.96	4.3	5.68

7.7. CASE 2: "TUNED" RAO'S AS INPUT FOR ARIANE

Tuning the RAO is done by replacing the calculated sway RAO for the experimentally obtained sway RAO. The output of the calculated sway RAO consists of arrays containing RAO's for each heading step and frequency step. In the experiment with environment O2 one wave-heading is observed. For the FLNG the waves encounter the vessel at an average angle of three degrees. The LNGC is orientated 180 degrees in the opposite direction, therefore the average angle of attack of the waves for the FLNG is 177 degrees. The corresponding array's, (2.5 degrees for the FLNG and 177.5 degrees for the LNGC) are replaced with the corresponding sway RAO's obtained from the experiment at MARIN. The resulting RAO's for the FLNG are plotted in Figure 6.12. The next step is to simulate the motions by using these "tuned" RAO's as input in Ariane. The resulting time-traces are presented in Figure 7.6.

For the relative manifold X distance, an offset of about 0.5 meters is notable. This offset is similar to the offset obtained for the relative X distance in Section 7.6. Concluding, the tuning of the sway does not influence the relative surge motions.

For sway there is a different conclusion, as the relative Y distance shows favorable similarities when comparing the "tuned" RAO's with the measured RAO's from the MARIN offshore basin. The mean value of the calculated "tuned" RAO's is 4.13 meters whereas the mean value from MARIN is 4.02 meters. The maxima show a slight difference as Ariane calculates a maximum Y distance of 5.75 meters whereas the MARIN maximum is 5.36 meter. There are 4 peaks in the total time trace where the calculated distance reaches near the peak of 5.75 meters, meaning the rest of the time-trace shows a trend which is also observed at MARIN. Concluding, the relative Y distance is influenced by tuning the sway RAO. For the relative manifold Z distance time-trace, there is no difference observed compared to case 1. A slight mean offset of 1.5 meters for Ariane and 1.43 meters for the offshore basin experiments. They both peak around 1.9 meters.

The absolute relative distance must increase due to the increase of Y, which is indeed reflected in the plot of the relative manifold motion L time-trace. Having about the same mean value and showing the about the same amplitudes. The statistical data of the experiment O2 and both "tuned" and "un-tuned" calculations are presented in Table 7.3.

7.8. FENDERS

Figure 7.7 shows a time trace of the calculated load on fender 1. The natural period in which the fender load oscillates about its mean is 25 seconds. This is considerably longer than the wave period of 17 seconds shown in Figure 7.4, this concludes the modeled fender reacts to motions with a frequency of 0.25 rad/sec.

During the side-by-side experiments in the Offshore basin, the fenders exerted a forces in both the X as in Y direction. The force in X direction caused the vessels to have jerky motions, which effected the motion in X direction. The jerky motions were also noticed when the SBS MARIN experiments took place and can be seen on the videos taken from the tests. Additionally the jerky motions can be seen in Figure 7.5. This plot is a time trace of the relative sway motion at the manifold's location. Irregular peaks at around 1180 seconds, 1460 seconds and 1650 are observed. These peaks are due to the jerky motions in X direction. Ariane does not have a function for friction fender force in X direction, so these peak motions are neglected, as can be seen in 7.5. Furthermore the fenders are modeled for lower frequency motions around 0.25 rad/s.

7.9. CONCLUSION

With the 1st order response of the FLNG and the LNGC being discussed in Chapter 6, this study shows that the 1st order response for the calculated sway RAO's seemed too low. This chapter confirmed that this 1st order response has indeed got an effect on the final relative motion time traces between the vessels. Ariane highly underestimates the sway motions, due to the low sway RAO input. This underestimation can be com-

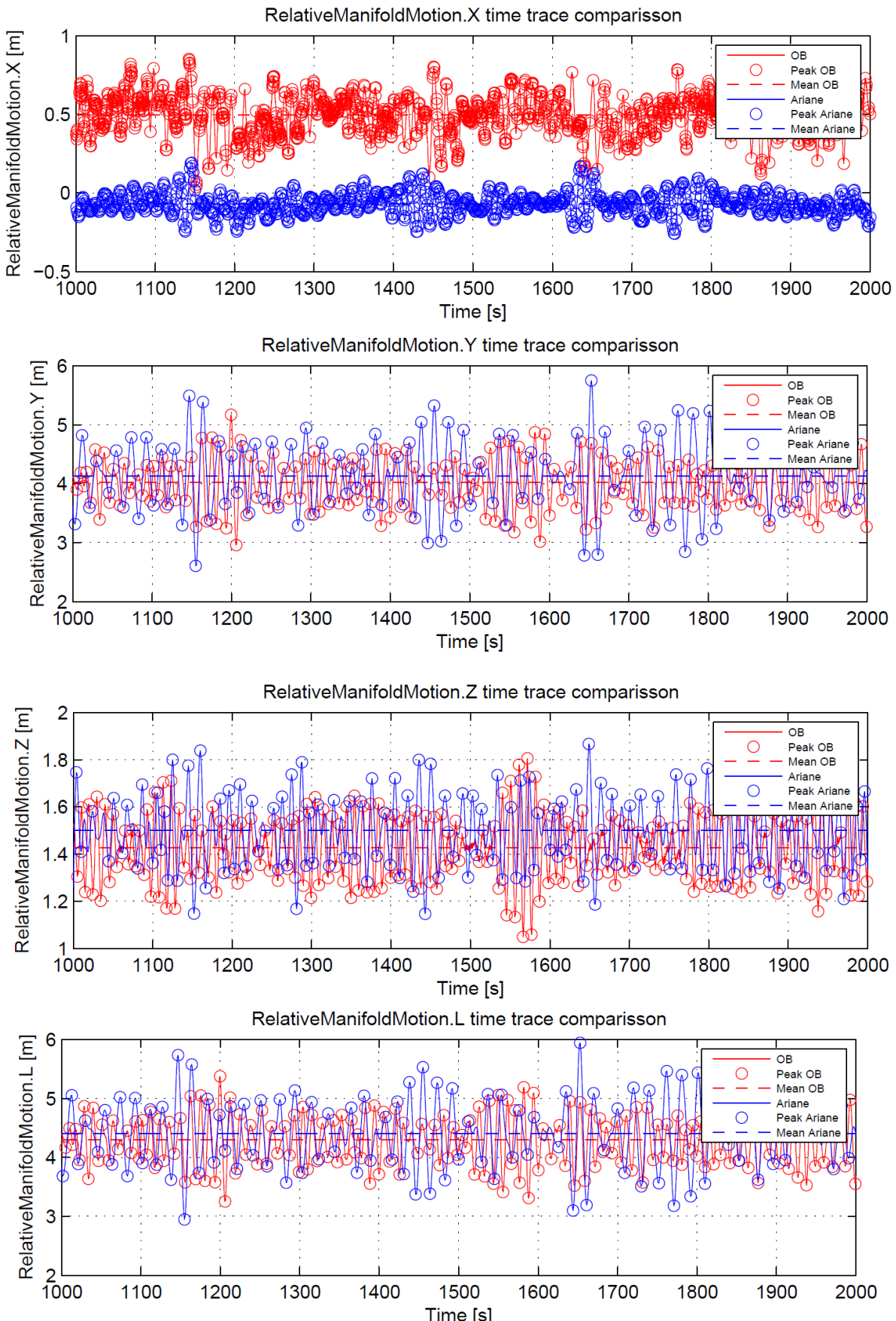


Figure 7.6: Relative manifold distance for X, Y, Z and the absolute distance L. Tuned RAO's as input

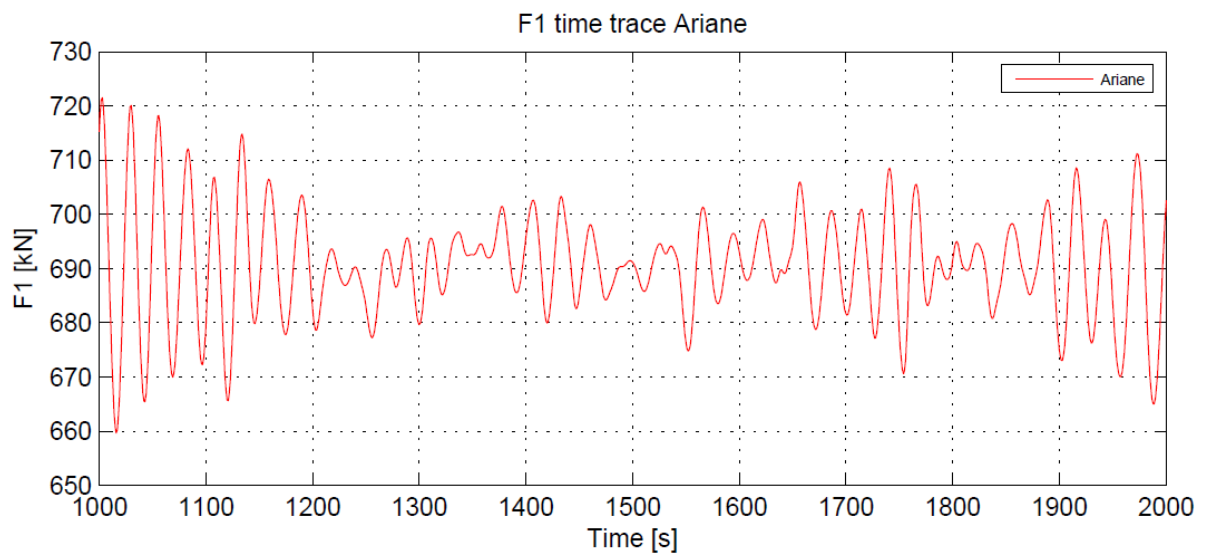


Figure 7.7: Ariane dender loads

pensated by tuning the sway RAO's such that it matches the exact measured sway from the MARIN basin. This will increase the overall sway motions. The intention of the study was to find an accurate re-presentable model which could account for wind, current waves and any angle of attack. It should be recognized that this "tuned" model is only applicable for head waves, without wind and current.

8

CONCLUSIONS AND RECOMMENDATIONS

8.1. INTRODUCTION

This chapter reflects on the whole thesis and attempts to answer the research questions defined in Chapter 1 the main questions consisted of three main pillars:

- Is there a difference between the first order motions measured in soft mooring and turret mooring configuration?
- What are the discrepancies in terms of first order motions, between the Side-by-side mooring tests result compared with the HydroStar frequency response output?
- What is the implication of the discrepancies in first order motions on the time domain simulations in Ariane?

The first question can primarily be answered using the single vessel study of Chapter 5. The in-depth understanding of the discrepancies between the side-by-side mooring test results and the HydroStar results have been explained in detail in Chapter 6. The last question has been answered by the help of a full motion comparison which has been conducted for two cases in Chapter 7.

8.2. CONCLUSIONS ON THE DIFFERENT MOTIONS MEASURED IN SOFT-MOORING AND TURRET-MOORING

The soft-mooring and turret-mooring show similar responses for surge, heave, pitch and yaw. The roll response for the soft-mooring test turns out to have a slightly higher maximum amplitude, due to different weight distribution on the vessel. The other discrepancy is observed for sway. For turret-mooring the maximum amplitude peaks with a factor 3 times greater than the sway response in soft-mooring. The natural frequency of the turret mooring system does not come near this sway peak. Therefore the mooring system should not be causing sway motion amplification. Investigation on the effects of weight distribution, epsilon damping, linear viscous damping, showed that these were not the source for the sway motion amplification either. Unfortunately Hydro-star is not capable of calculating these sway RAO's for this typical mooring set-up. Hydrostar does not take viscous effects into account, which possibly is causing the observed sway inconsistencies. The underlying mechanism has not been found, so that it remains uncertain whether the unconventional length/beam ratio of 2.5 plays a role in this.

8.3. CONCLUSIONS ON THE DISCREPANCIES BETWEEN THE MARIN EXPERIMENTS FREQUENCY RESPONSE AND TIME-DOMAIN FOR THE SIDE-BY-SIDE ARRANGEMENT

When the fenders are compressed from 0.5 meters to 1.5, due to the sway of the vessels, the restoring force increase with a factor of 4. Even more compression can cause the fender to fail, that is why the sway motion is so important for SBS mooring. The MARIN test for SBS mooring showed a significant peak for sway. The

same response is in the basin test for the FLNG alone, again this response is not seen in the calculation results by HydroStar. Therefore Hydrostar does not seem to properly capture the first order response on the vessels moored by a turret, in this typical setup. In Chapter 6 a method is introduced for tuning the calculated RAO's to fit the RAO's measured at the MARIN offshore basin. The tuned sway RAO's showed an acceptable correlation with the measured sway RAO's from the MARIN offshore basin. The intention of the study was to find an accurate representative model which could account for wind, current waves and any angle of attack. This study only extended as far as that the "tuned" model which is only applicable for head waves, without wind and current. The mooring test campaigns carried out at MARIN were intended to gain confidence in the numerical results of mooring loads and offsets. The additional side-by-side tests were for feasibility checks; whether SBS offloading was even possible. This study showed that the tests at MARIN were not designed to deliver the results necessary for the accurate side-by-side mooring calculations and has further demonstrated that additional experimental data are required for the validation of the RAO predictions for all wave headings.

8.4. RECOMMENDATIONS

Due to insufficient available data for a complete side-by-side model in the time-domain, it is recommended to perform additional SBS experiments in the Offshore basin. The experiment should focus on the following items:

- **Wave probes**

During the side-by-side experiment used for this thesis, one wave probe was used for wave calibration. However this wave probe was not at the location of either the COG of the FLNG nor the COG of the LNGC. Having the wave probe not at the COG's position will cause an incorrect phase shift. This phase shift cannot be adjusted by reconstructing the wave using an FFT because the spectral energy in the tank differed along multiple wave probes. Accordingly an exact reproduced COG time trace with Ariane is not possible. For future side-by-side experiments it is recommended to use two wave probes, one probe at the location of the FLNG's COG, and the other at the COG of the LNGC.

- **White noise tests**

The RAO's in this thesis could only be calculated with a high degree of certainty around the resonance peaks. No white noise tests were performed during the side-by-side experiment. White noise experiments are necessary in order to accurately compute RAO's over a larger frequency range. For future experiments it is recommended to perform these white noise tests for accurate RAO computations.

- **Friction fenders**

During the side-by-side experiments the fenders exerted forces in both the X as in Y direction. The force in X direction caused the vessels to have jerky motions, which effected the motion in X direction. This friction fender force in X direction is neglected in the Ariane model. For future research it is recommended to also implement this additional force to increase the accurateness of the surge motions. Another alternative is to adjust the fenders which are used in future experiments, in such a way there is no force in X direction. This could be done by adding a wheel bearing on the fender's arm, which will be the contact point to the hull of the LNGC. This will cutback the friction force in X-direction.

- **Viscous effects**

Additional research must be carried out on viscous effects around the hulls. These viscous effects might contribute to the observed sway inconsistencies between the calculated and experimental response of the FLNG, which has a unconventional wide hull.

- **Weight distribution**

The soft- and turret mooring experiments explained in Chapter 5 made use of 2 different weight distributions for the FLNG. This different weight distribution effected the roll RAO's. It is recommended to perform additional soft- and turret mooring experiment, but with an FLNG which has the same weight distribution and the same environments in both experiments.

- **Wind and current**

The Ariane model built for this thesis focuses on one experimental environment O2, which resulted in a relative wave angle of 3 degrees onto the FLNG. This environment was without wind and current. To improve the model, an advise is to further investigate the effects of wind and current onto the model. MARIN already provided SBM with current and wind coefficients for each vessel separately. However

these coefficients take no note for shielding effects. Additional experiments for determining shielding effect on current and wind is advised. When the correct coefficients are known, additional wave headings can be implemented into the model.

- **Regular waves**

The SBS experiments used for this thesis did not include regular wave tests. Without regular wave tests it is not possible to determine the QTF or mean drift force on the vessels in SBS arrangement. It is recommended to perform regular wave tests during future SBS experiments.

BIBLIOGRAPHY

- [1] SBM, *Catenary anchor leg mooring*, .
- [2] H. W. K. B. W. K. M. S. Kim, H. S. Jeong and J. K. Eom, *Improvement method on offloading operability of side-by-side moored flng*, Proceedings of the Twenty-second (2012) International Offshore and Polar Engineering Conference (2012).
- [3] X. Schut, *Turret trl3 basis of design report*, (2014).
- [4] J. M. Orozco, *A practical procedure for the evaluation of the roll motions of fpo including the non potential damping*, OTC 14234 (2002).
- [5] B. Veritas, *Theoretical manual ariane7*, (2007).
- [6] J.-P. Q. Wim van Wijngaarden and L. Pescio, *Loading and offloading of lng in open seas*, (2002).
- [7] W. Scott, *Care and maintenance of chicksan valves and swivel joints*, (2010).
- [8] J. Jornee and W. Massie, *Offshore Hydromechanics* (TU Delft, 2012).
- [9] J. A. Pinkster, *Low frequency second order wave exciting forces on floating structures*, (1980).
- [10] S. of International Gas Tankers & Terminal Operators Ltf, *LNG Ship Data Book* (Society of International Gas Tankers & Terminal Operators Ltf, 1997).
- [11] I. Y. P. Ir. C. Lena, *Sbm twin hull mooring and side by side tests*, (2014).
- [12] X.-B. C. Jean-Robert Fournier, Mamoun Naciri, *Hydromechanics of two side-by-side vessels experiments and numerical simulations*, (2006).
- [13] P. Ayman B. Mahouz, PH.D., *Offloading availability analysis for side-by-side flng and lnc*, Proceedings of the 17th offshore symposion (2012).
- [14] *Yokohama pneumatic ship fenders*, .
- [15] A. V. Wellemijn H. Pauw, Rene H.M. Huijsmans, *Advances in the hydromechanics of side-by-side moored vessels*, Offshore Mechanics and Artic engineering (2007).

A

WAVE SPECTRA

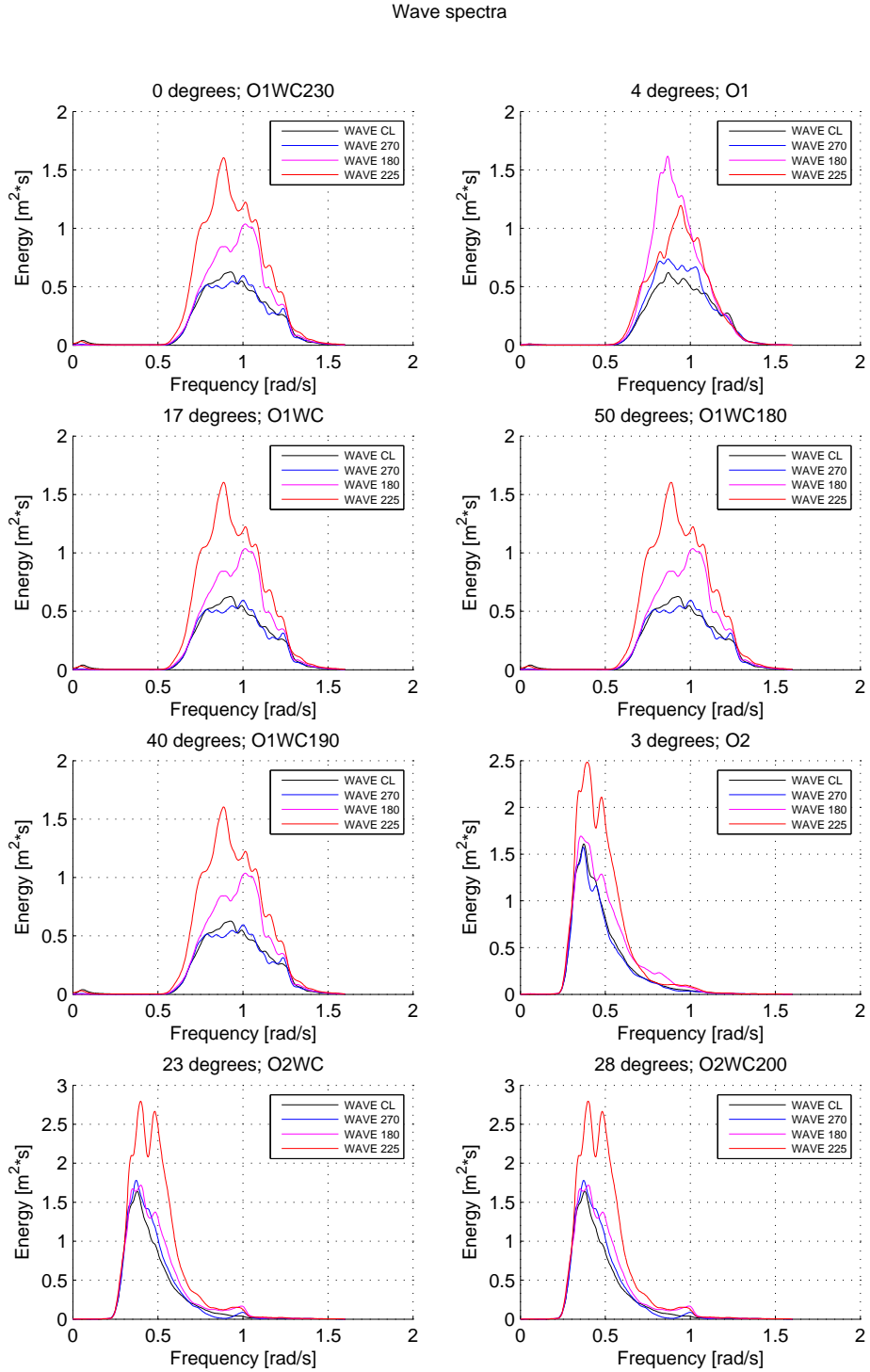


Figure A.1: Wave spectra of all probes and all SBS experiments

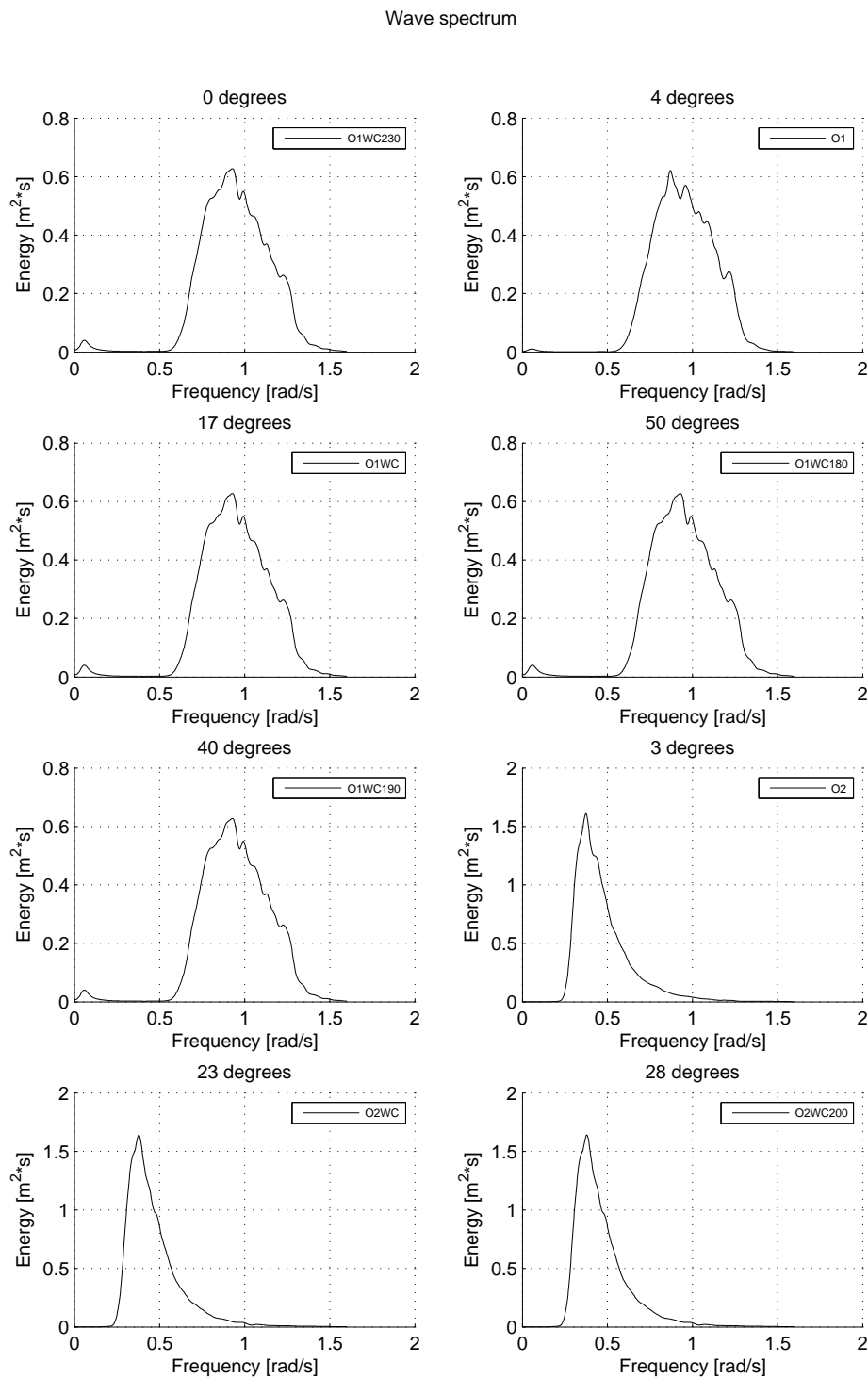
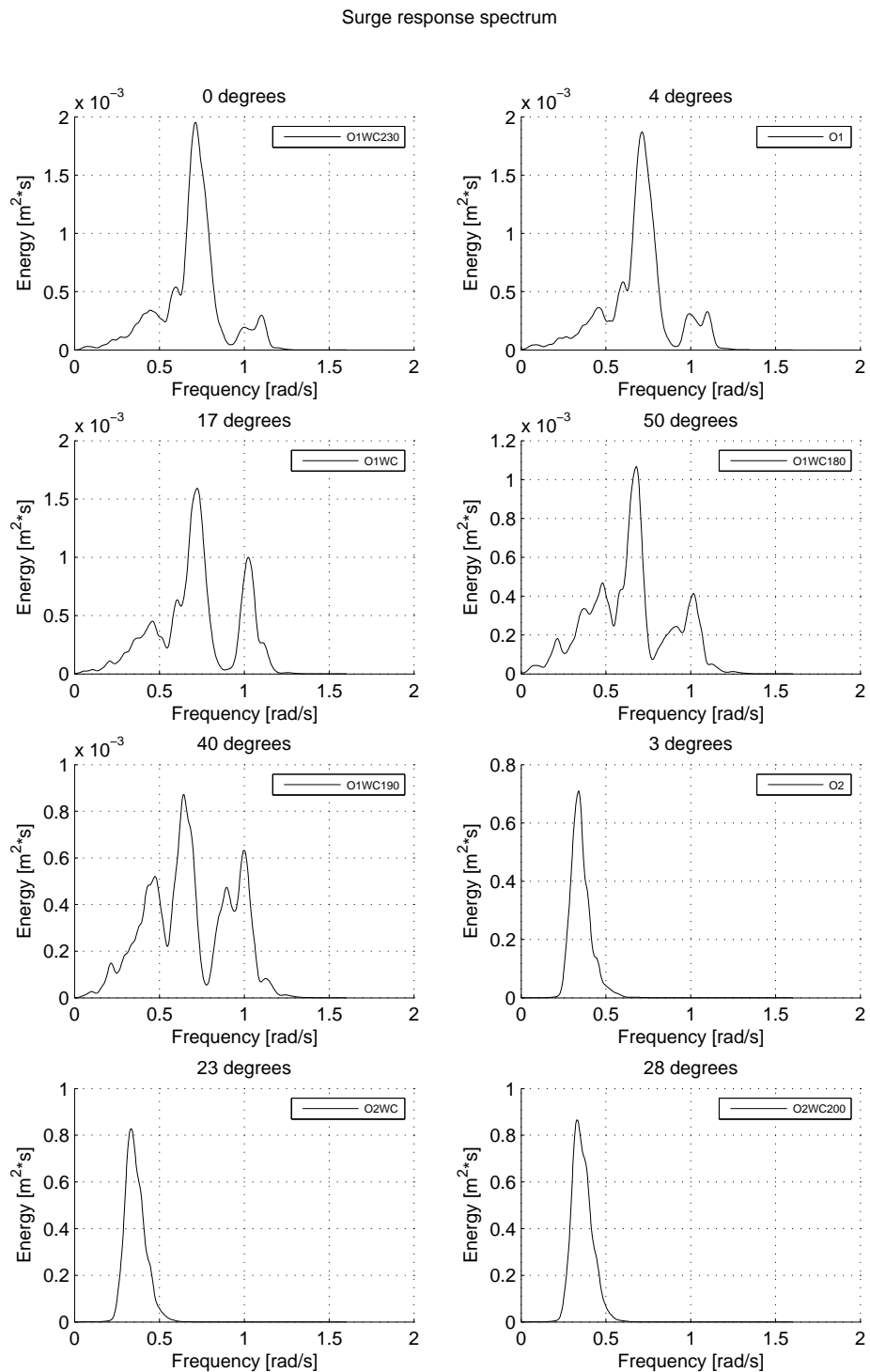


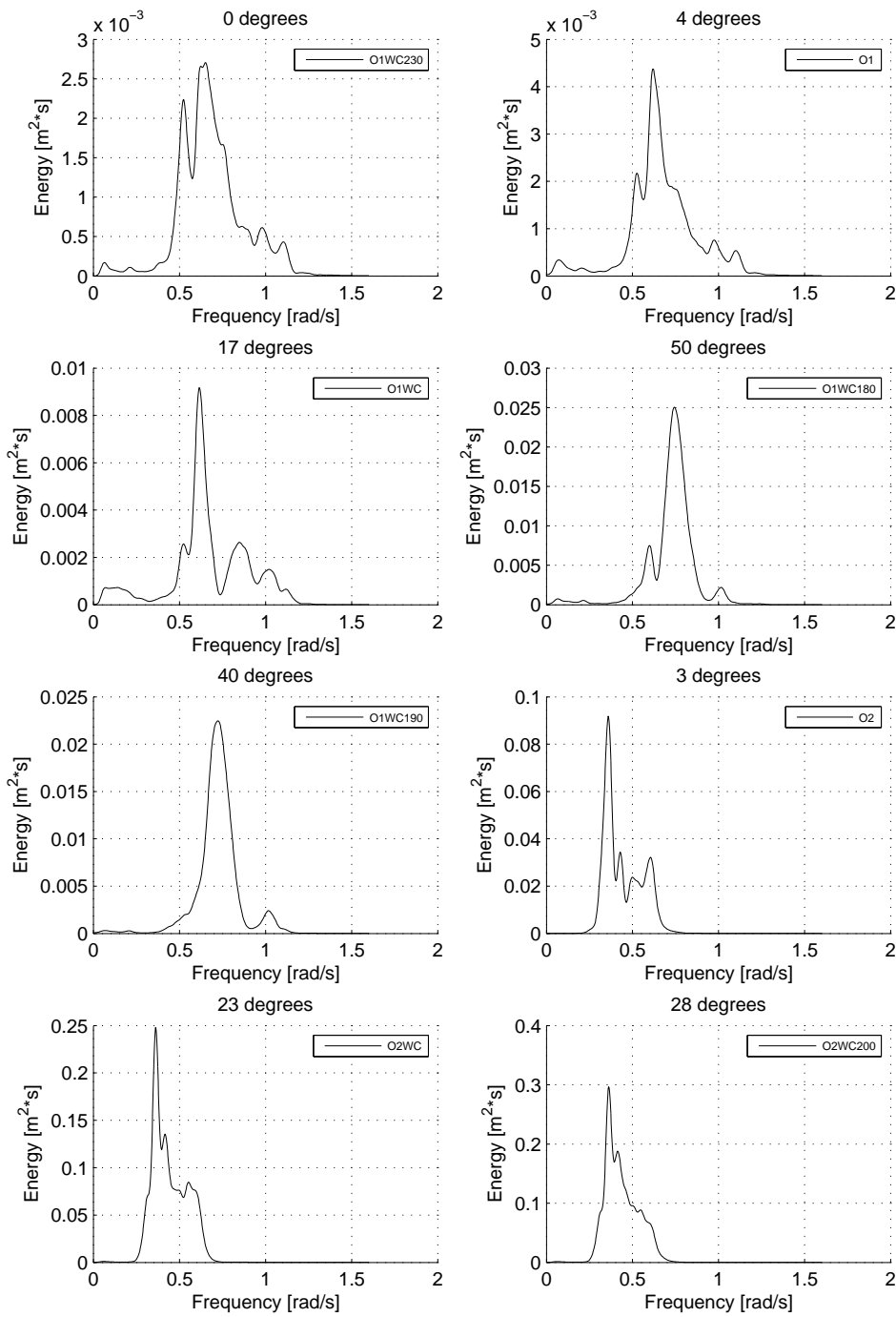
Figure A.2: Wave spectra of center line wave probe of all SBS experiments

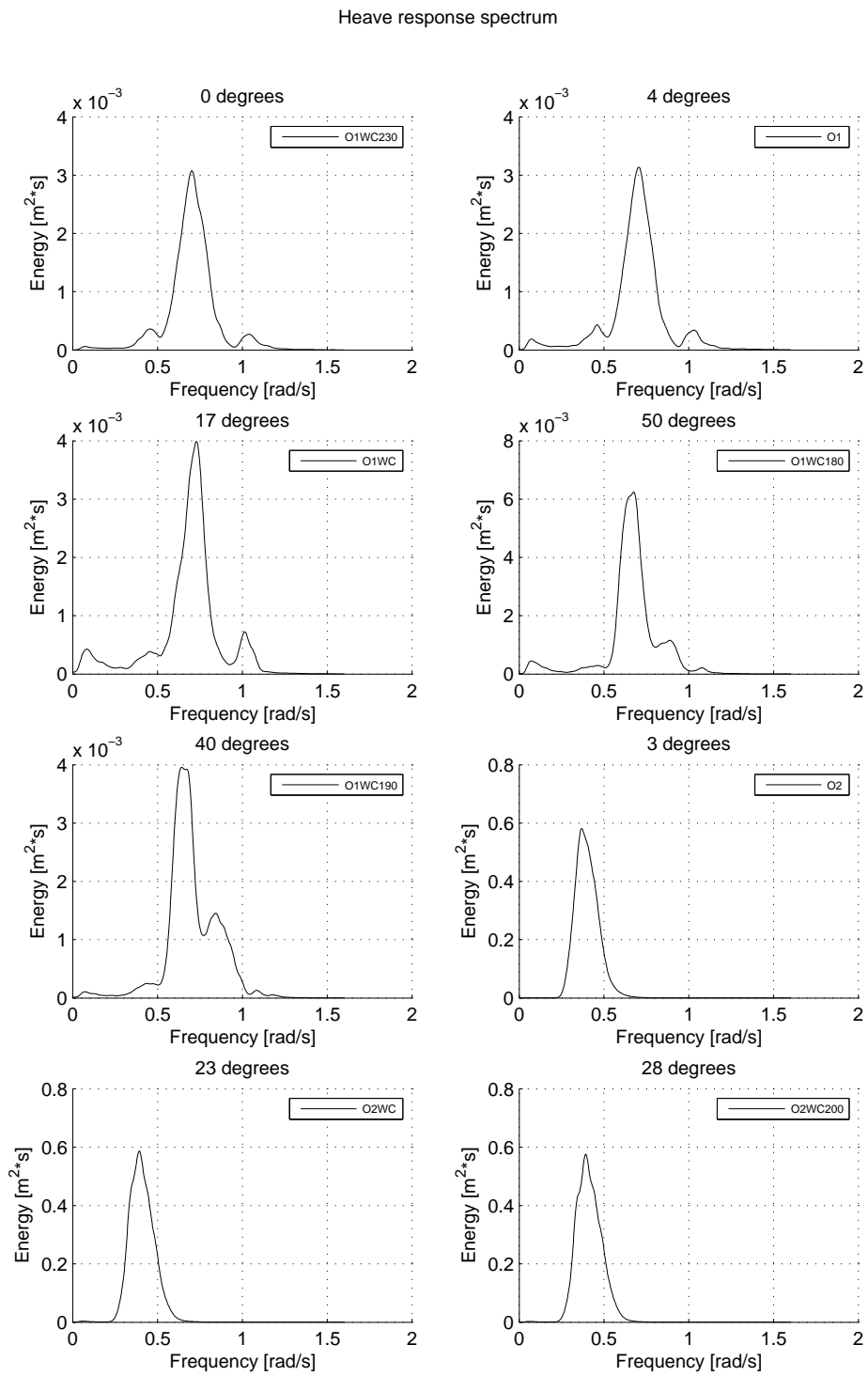
B

RESPONSE SPECTRA

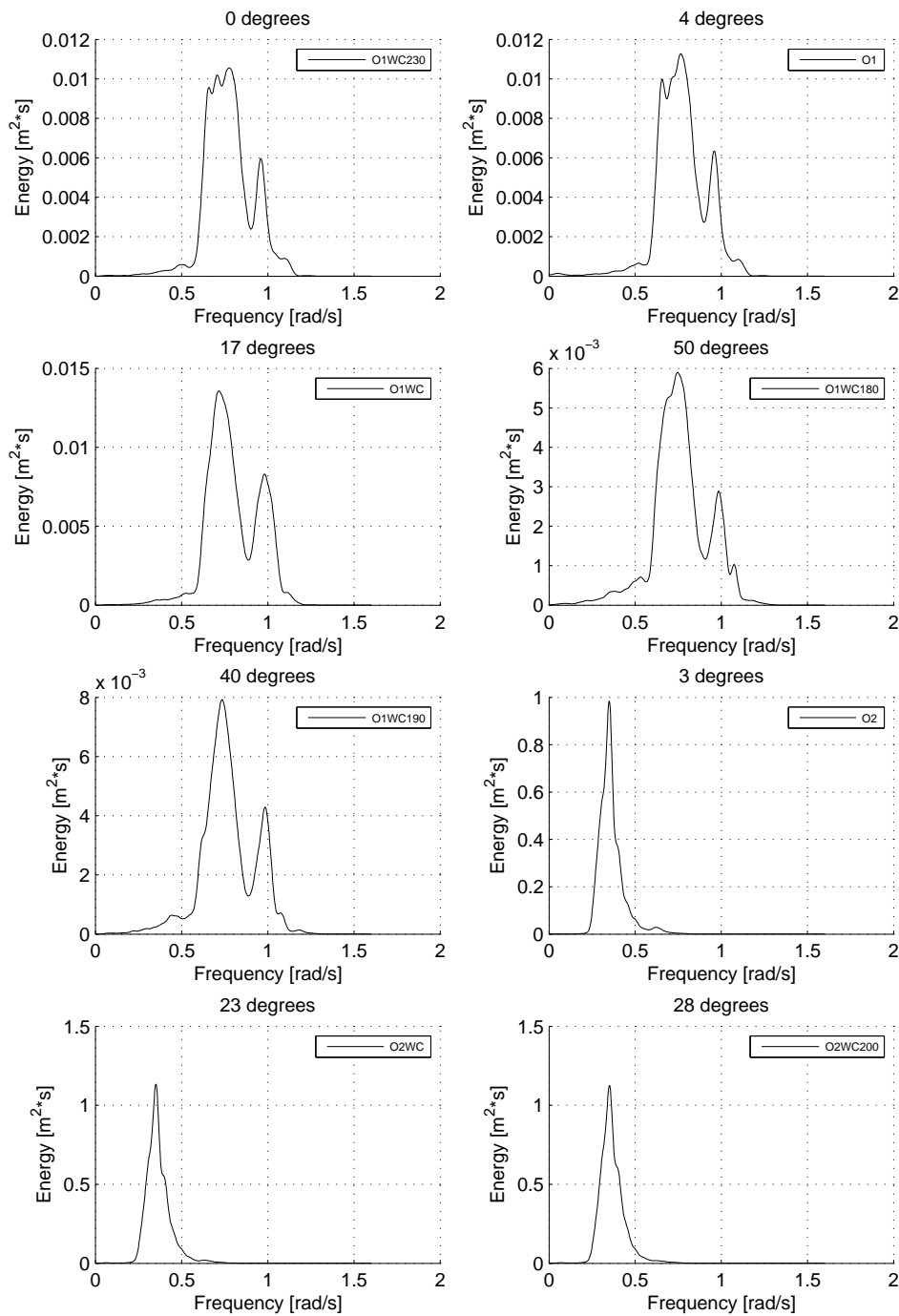


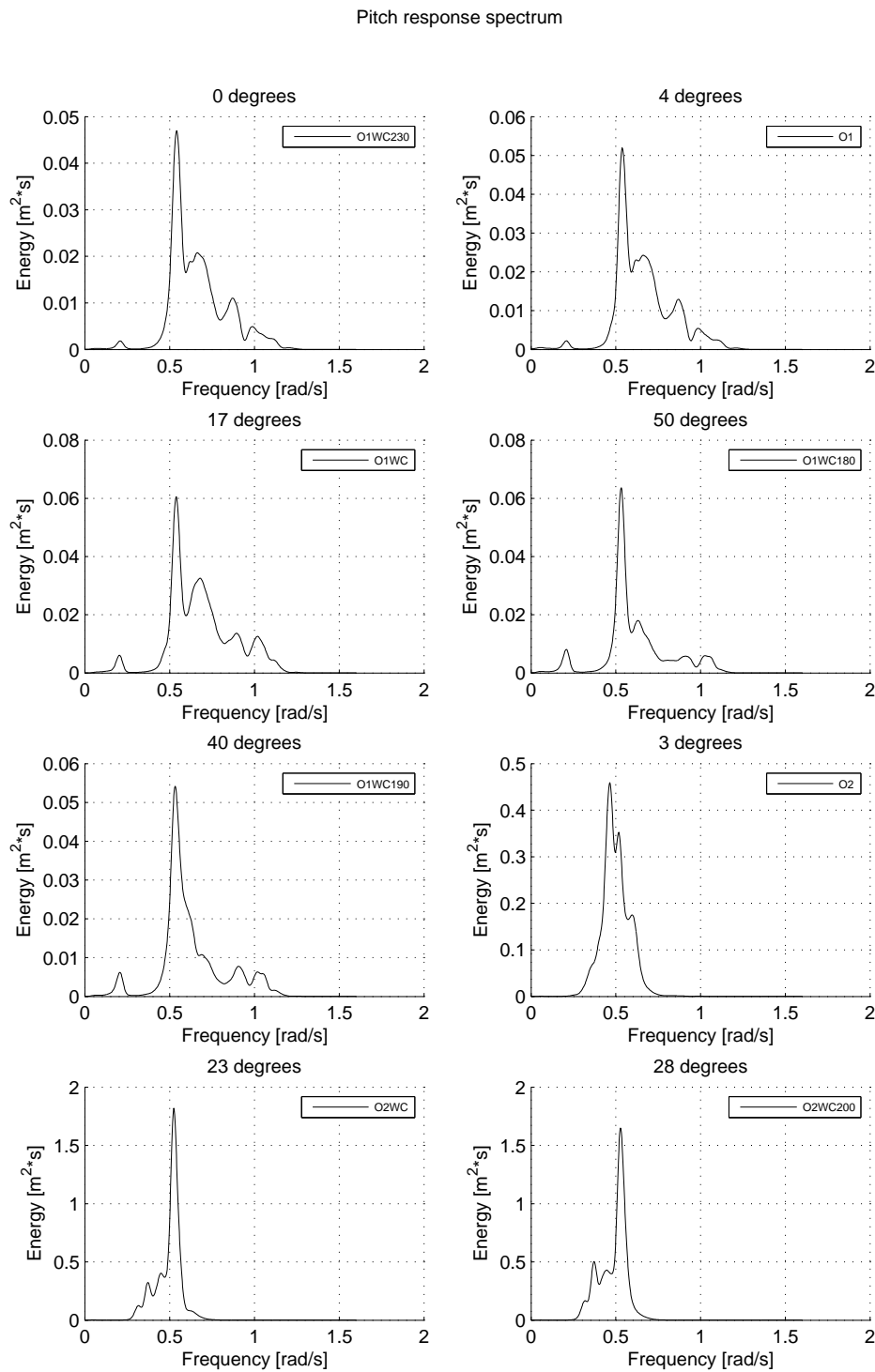
Sway response spectrum



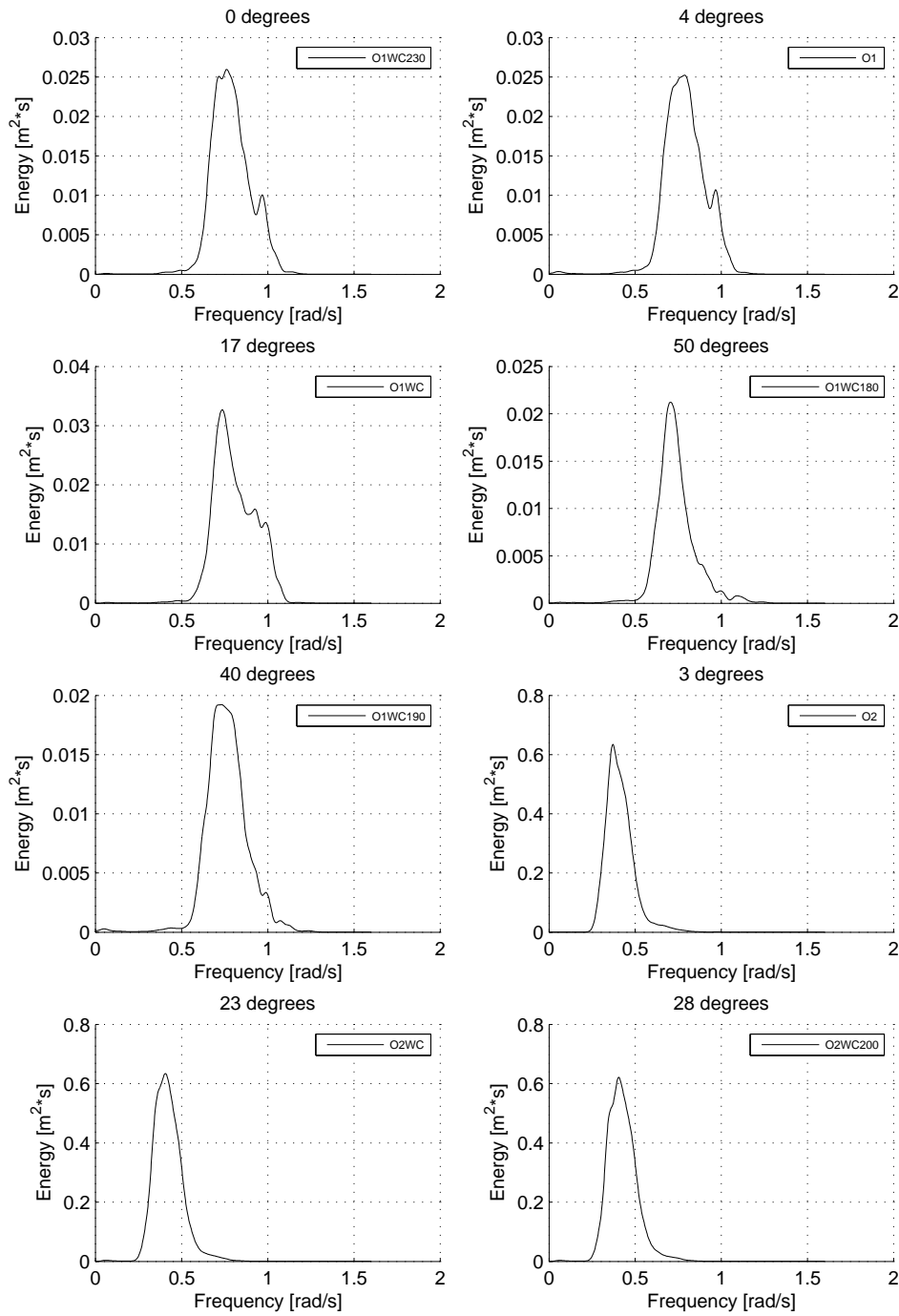


Roll response spectrum



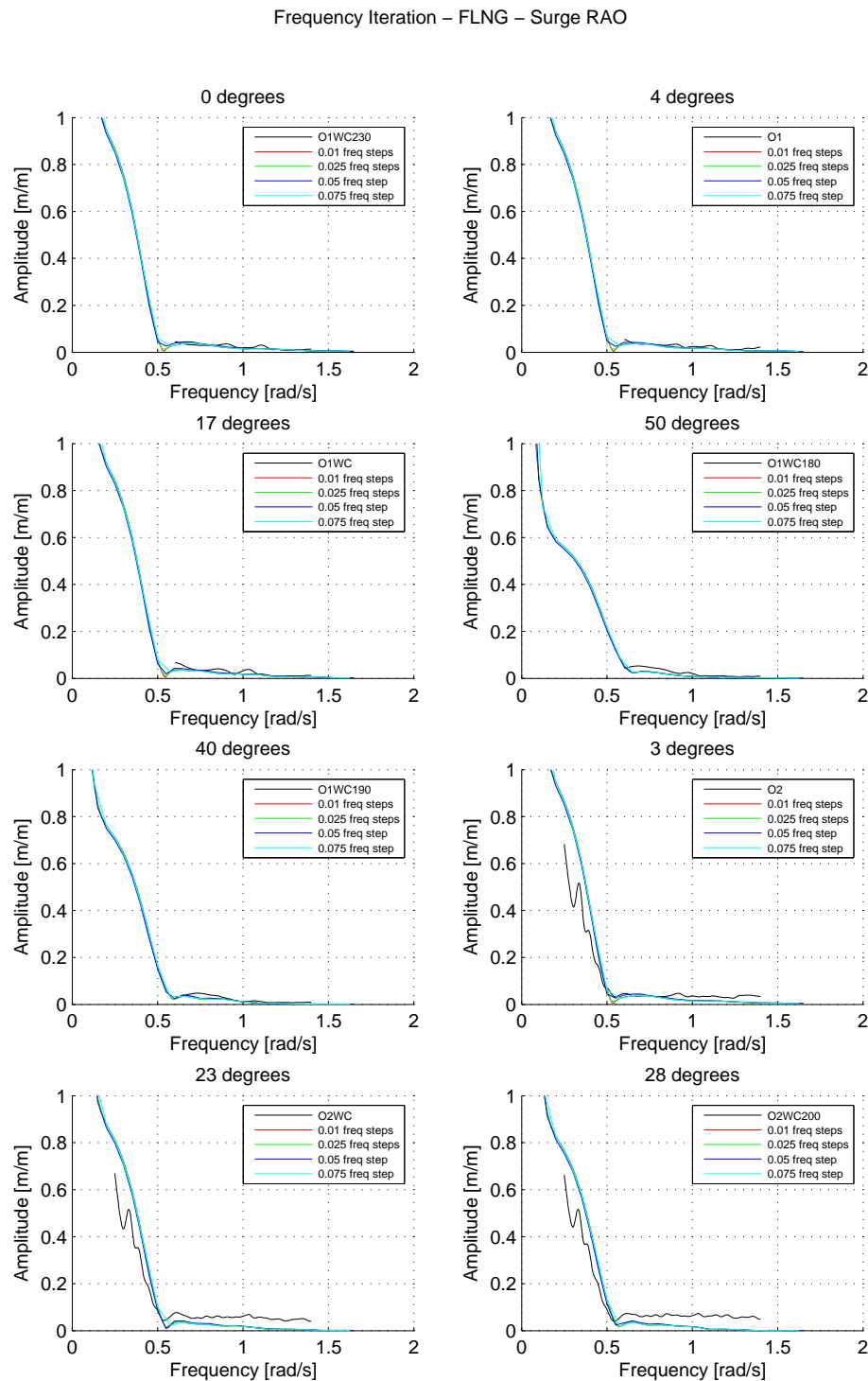


Yaw response spectrum

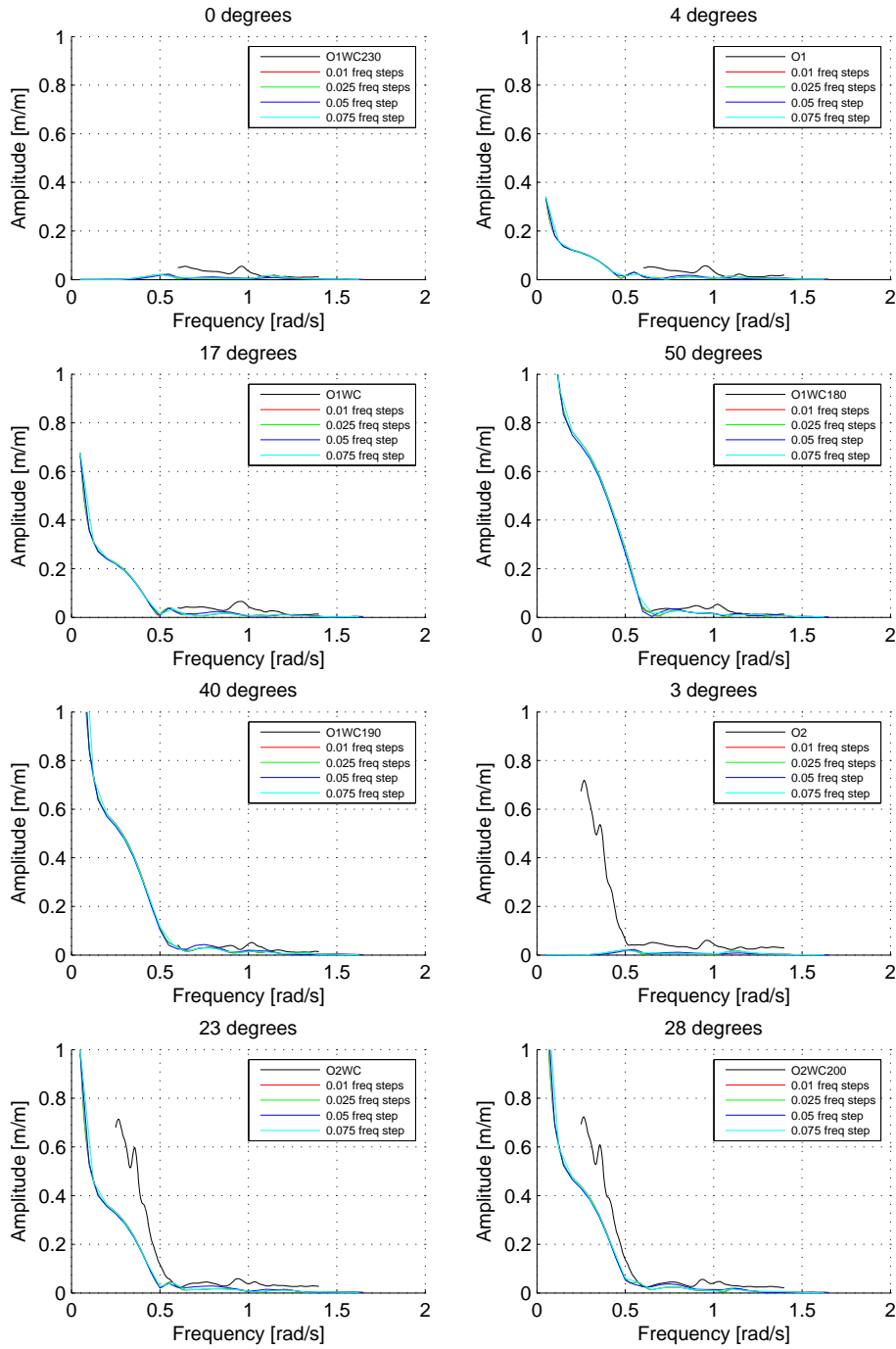


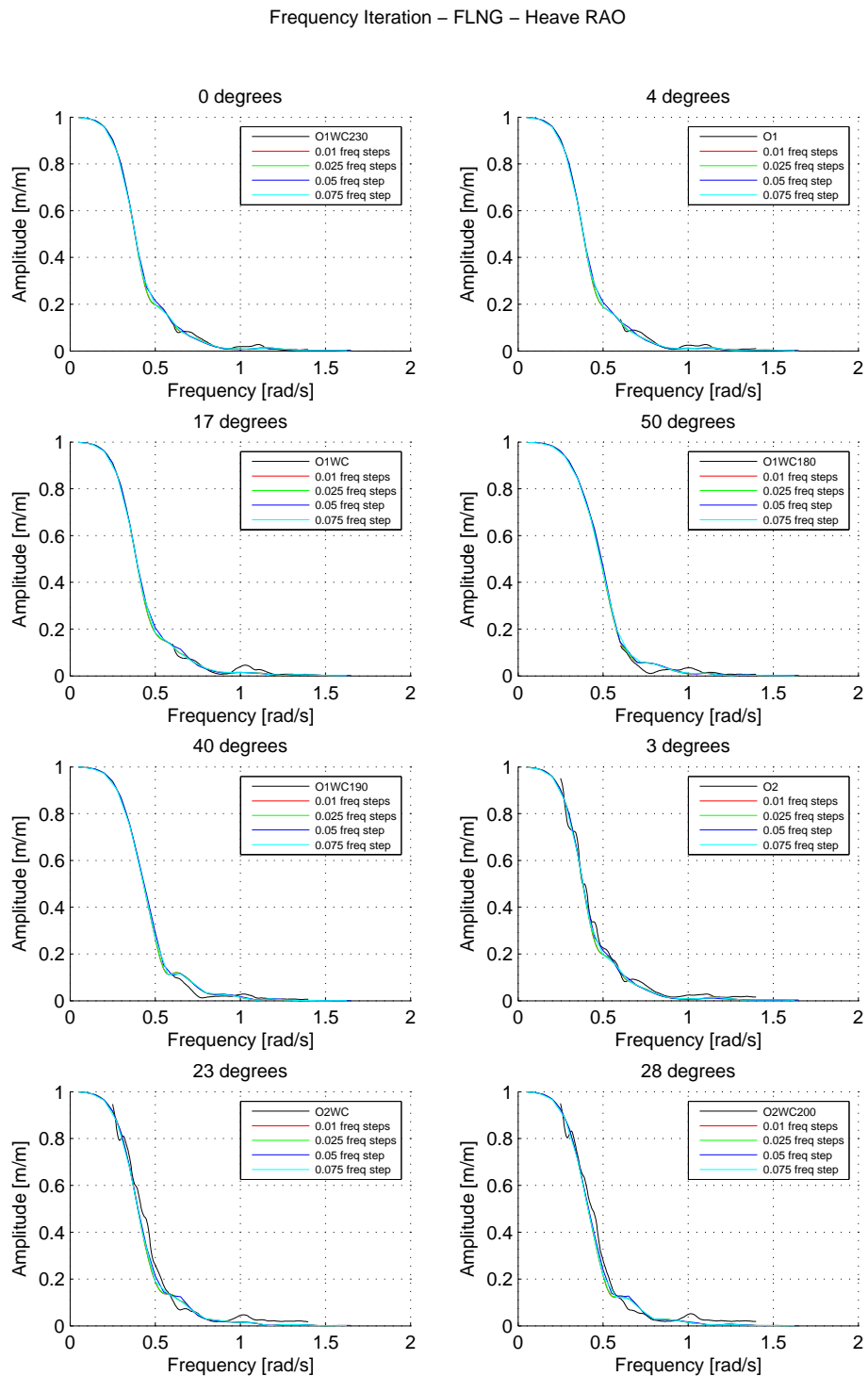
C

FREQUENCY ITERATION RESPONSE

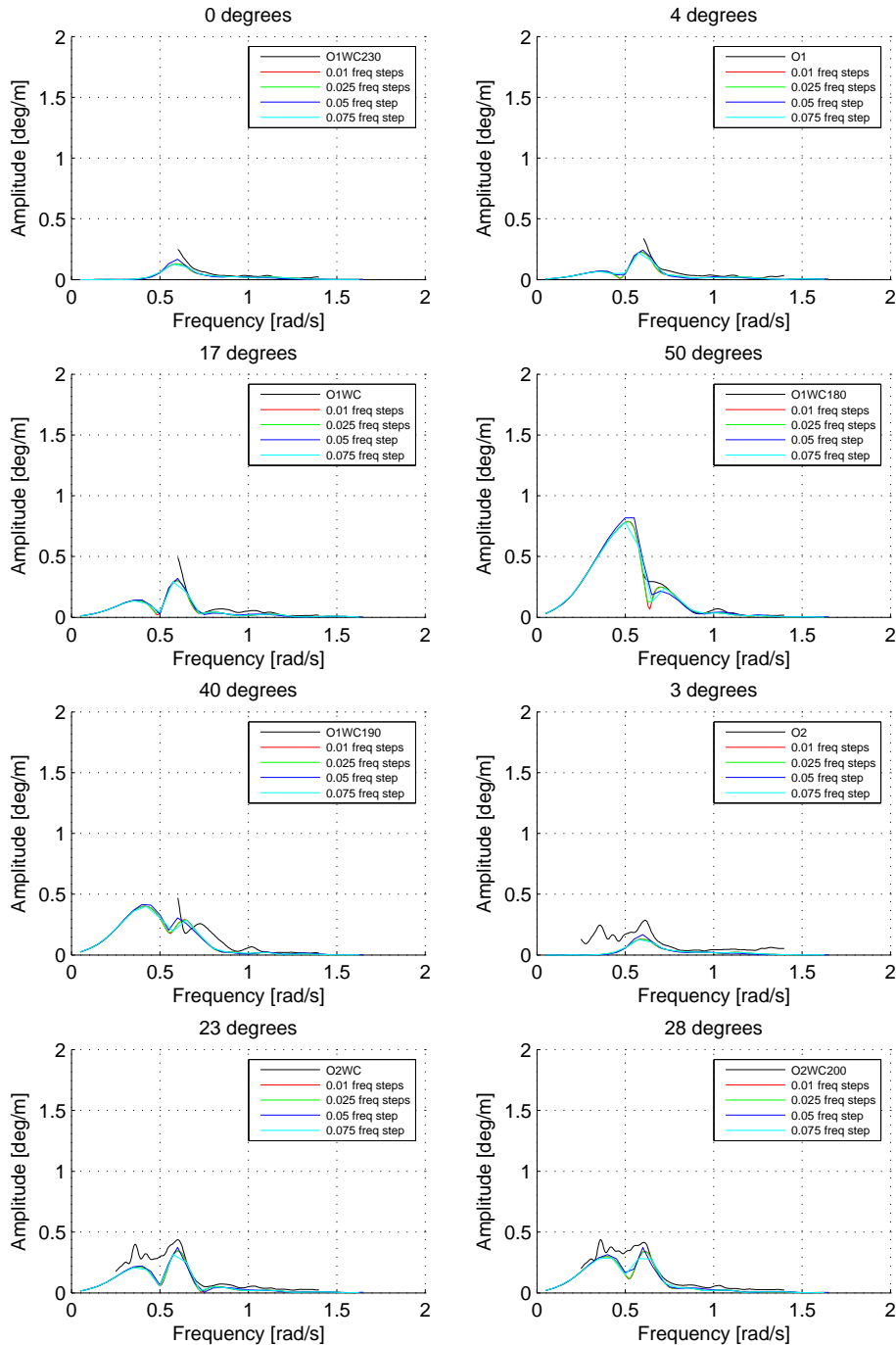


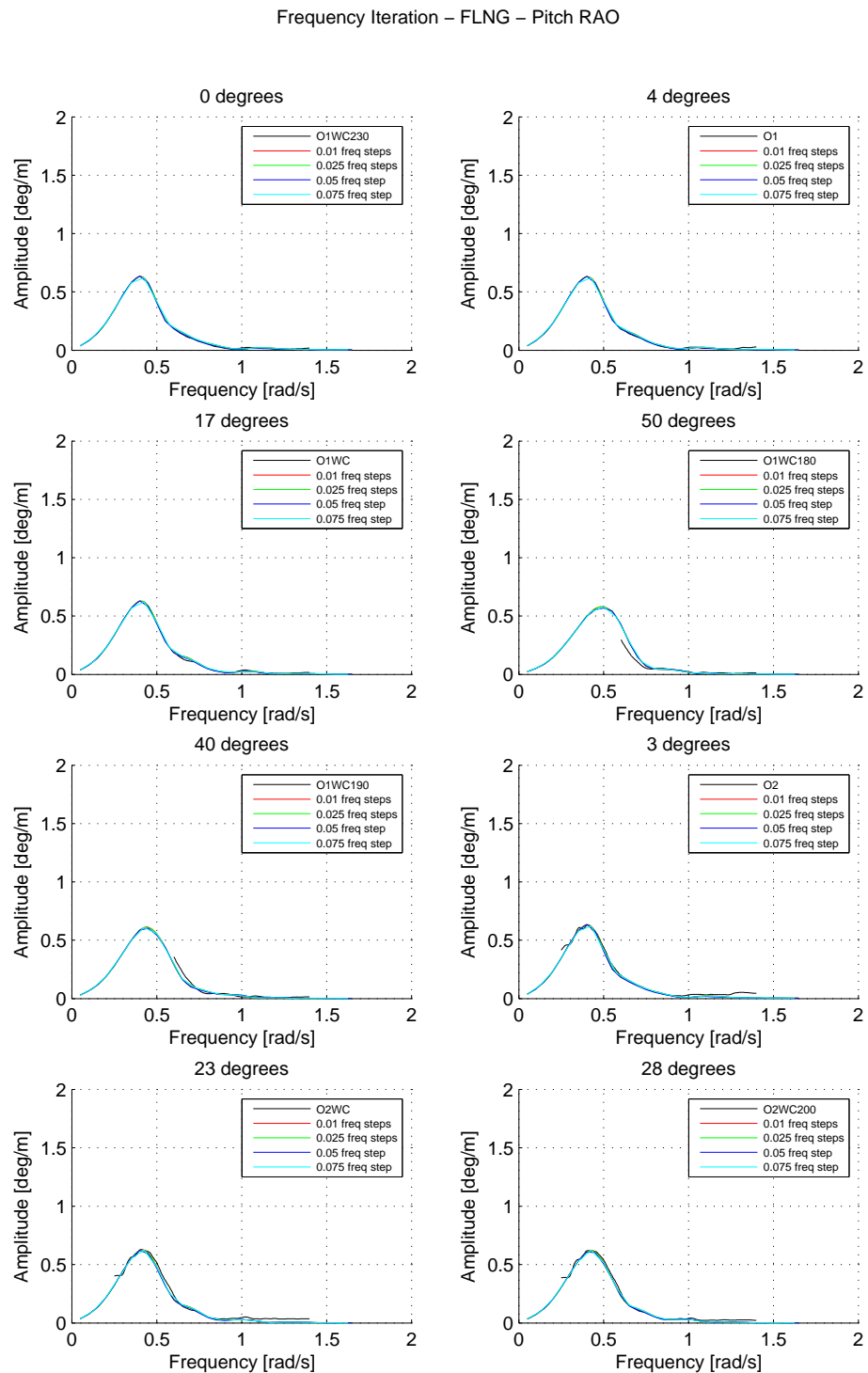
Frequency Iteration – FLNG – Sway RAO



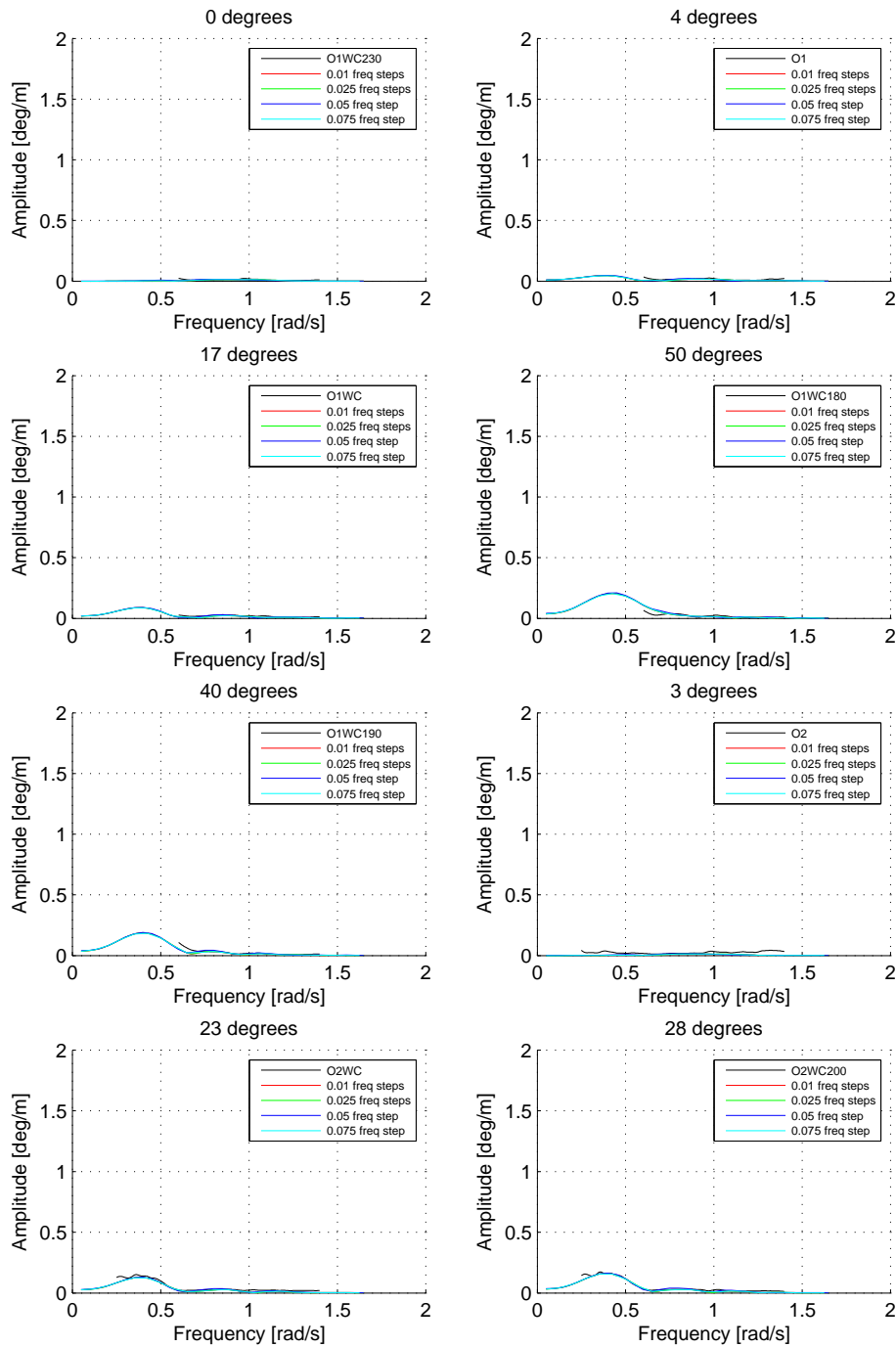


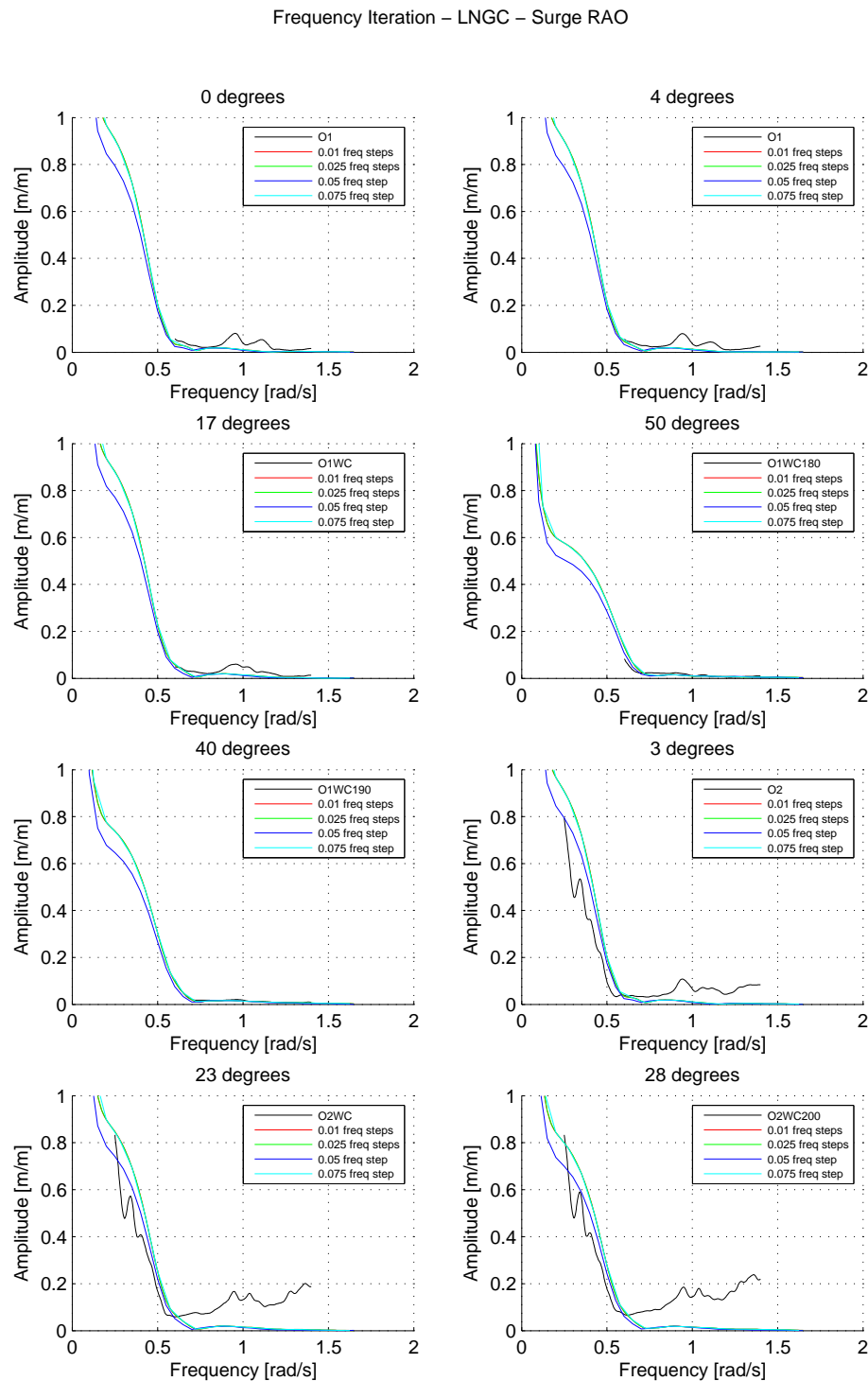
Frequency Iteration – FLNG – Roll RAO



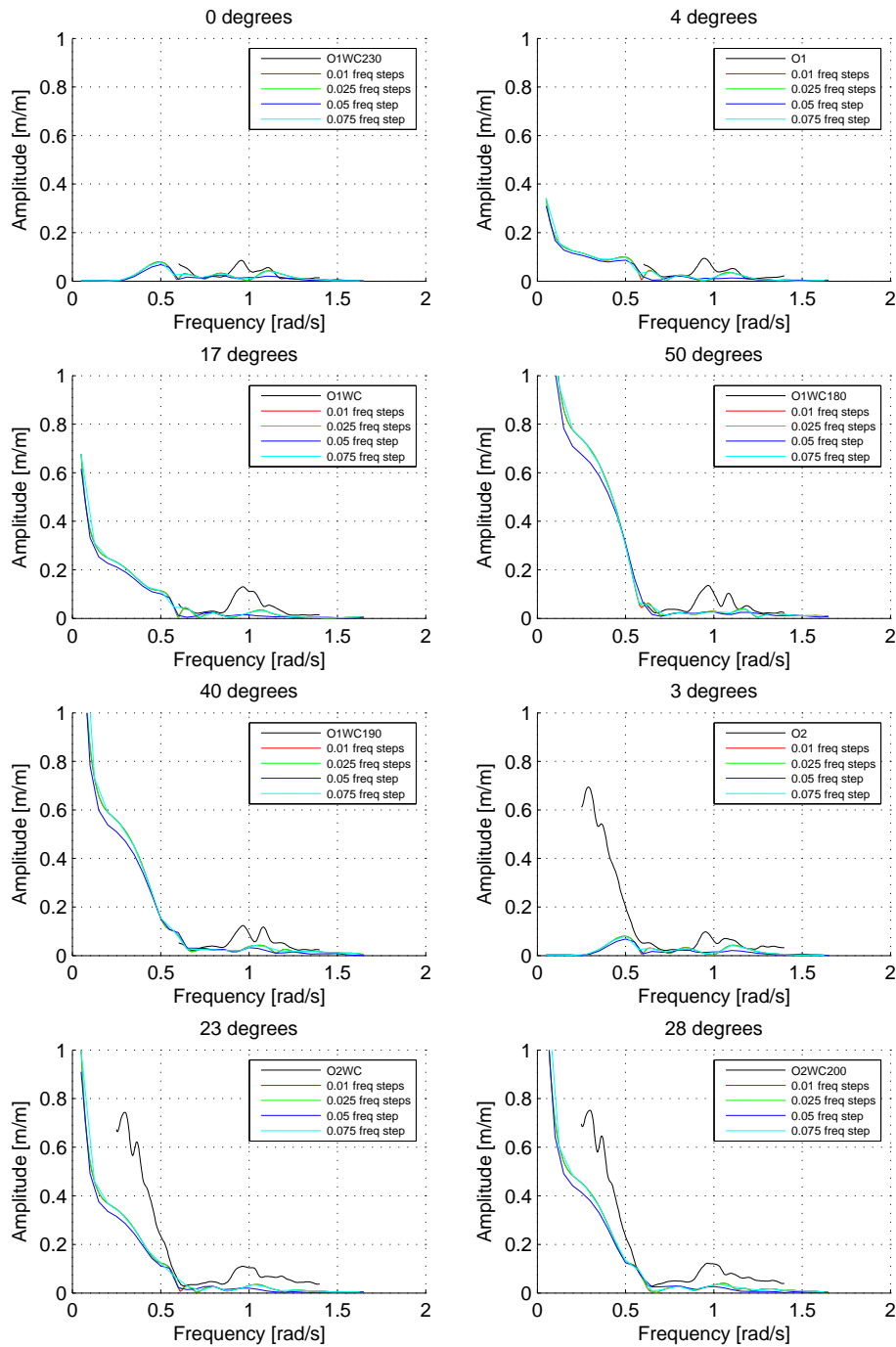


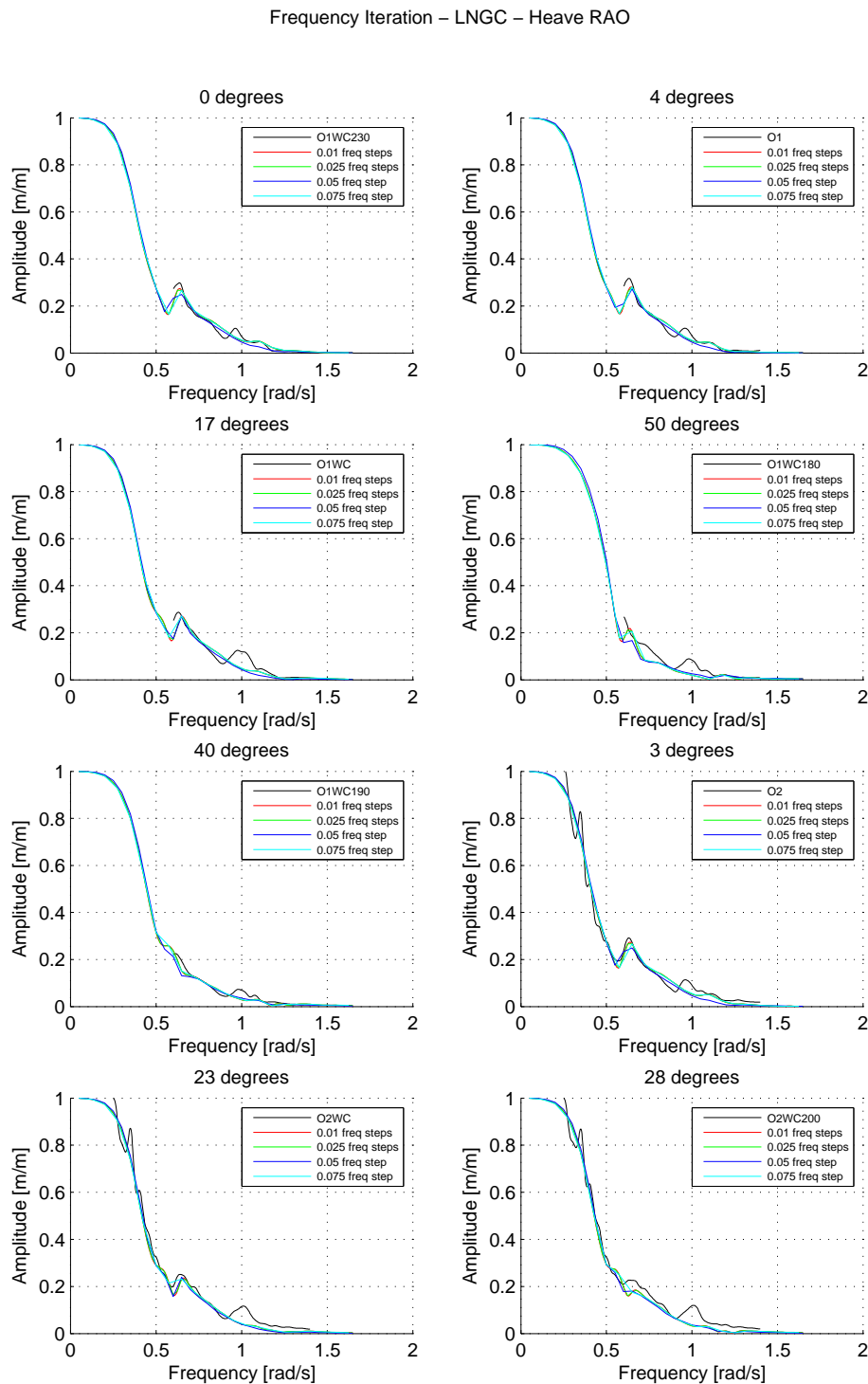
Frequency Iteration – FLNG – Yaw RAO



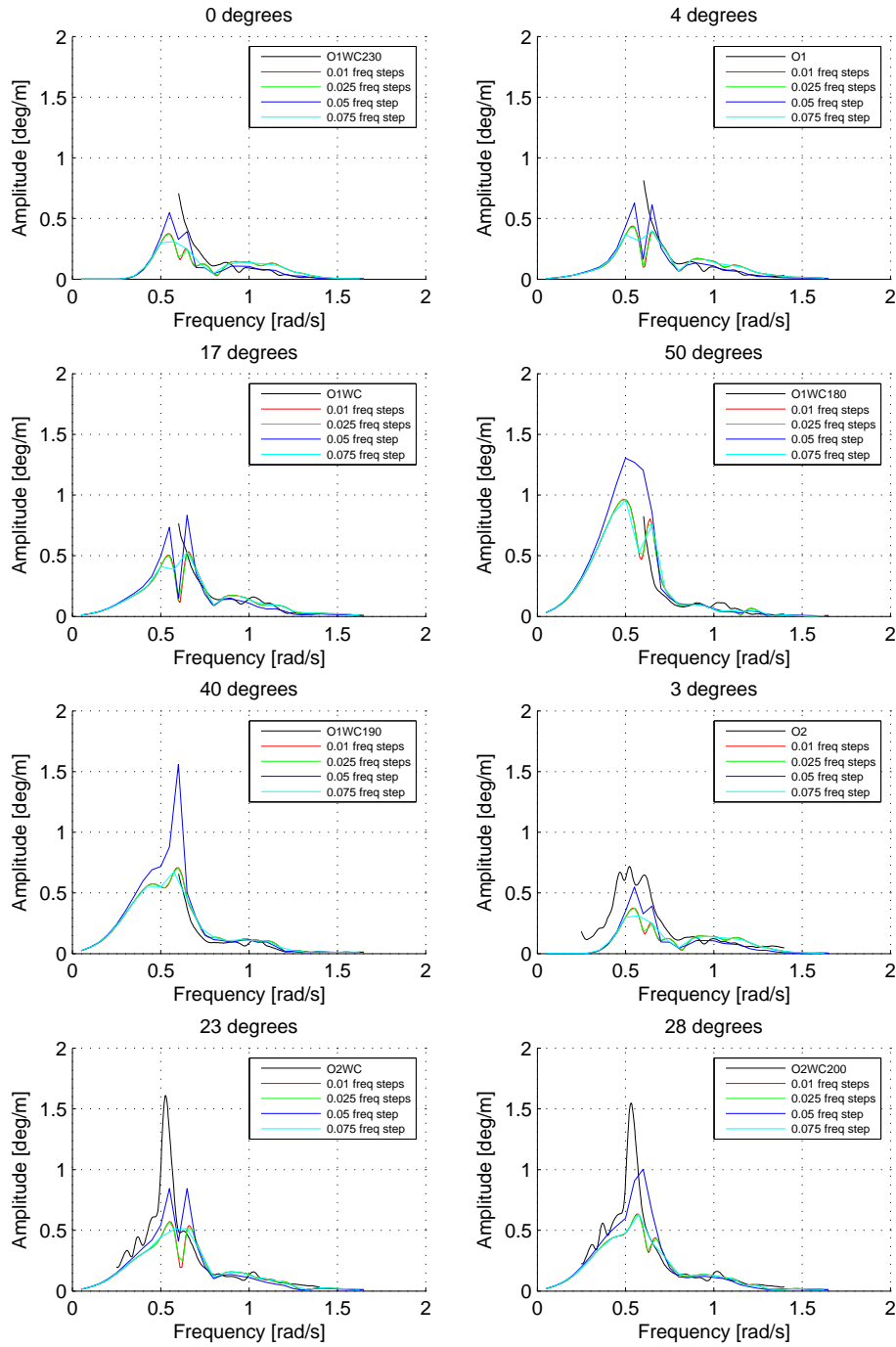


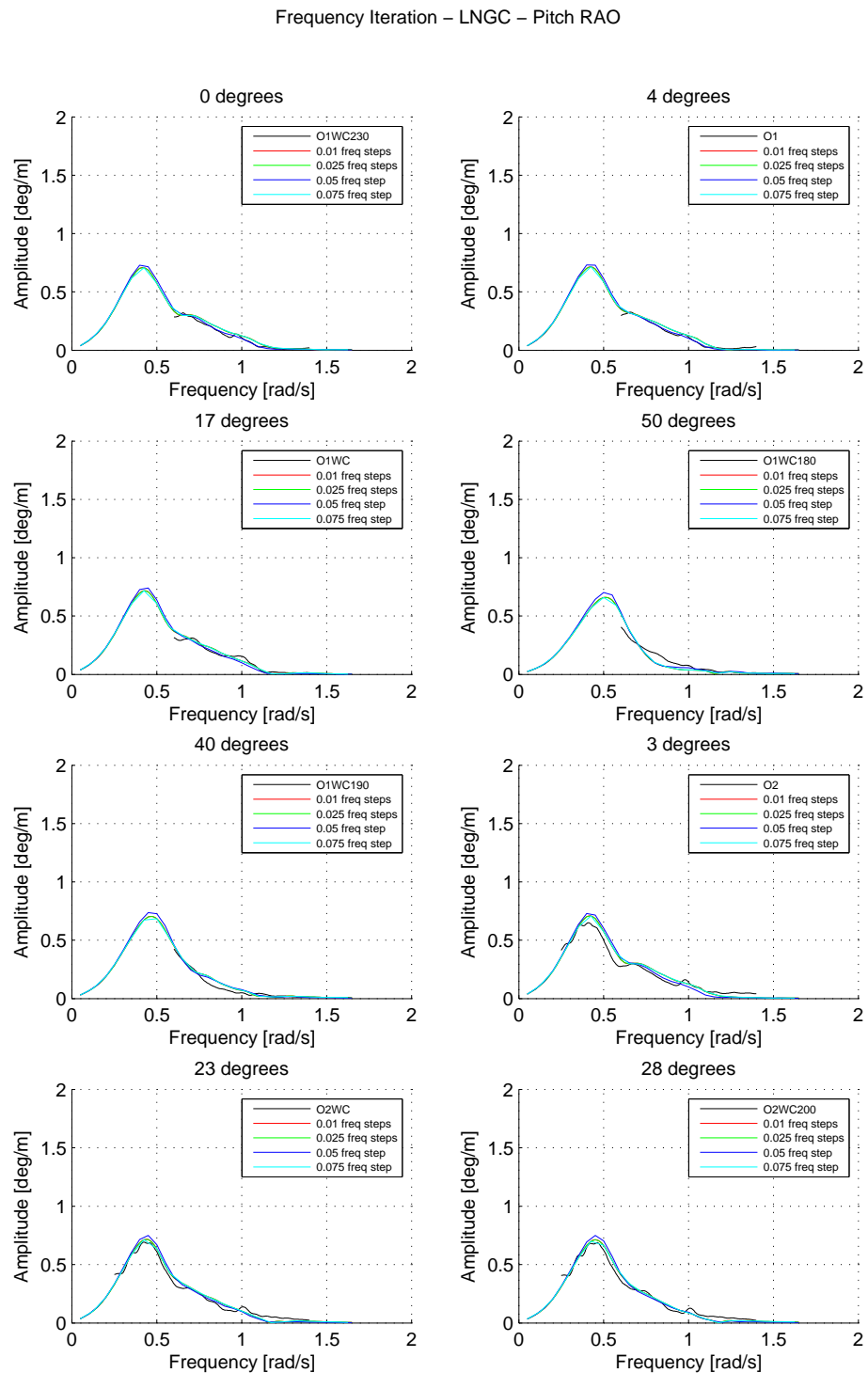
Frequency Iteration – LNGC – Sway RAO



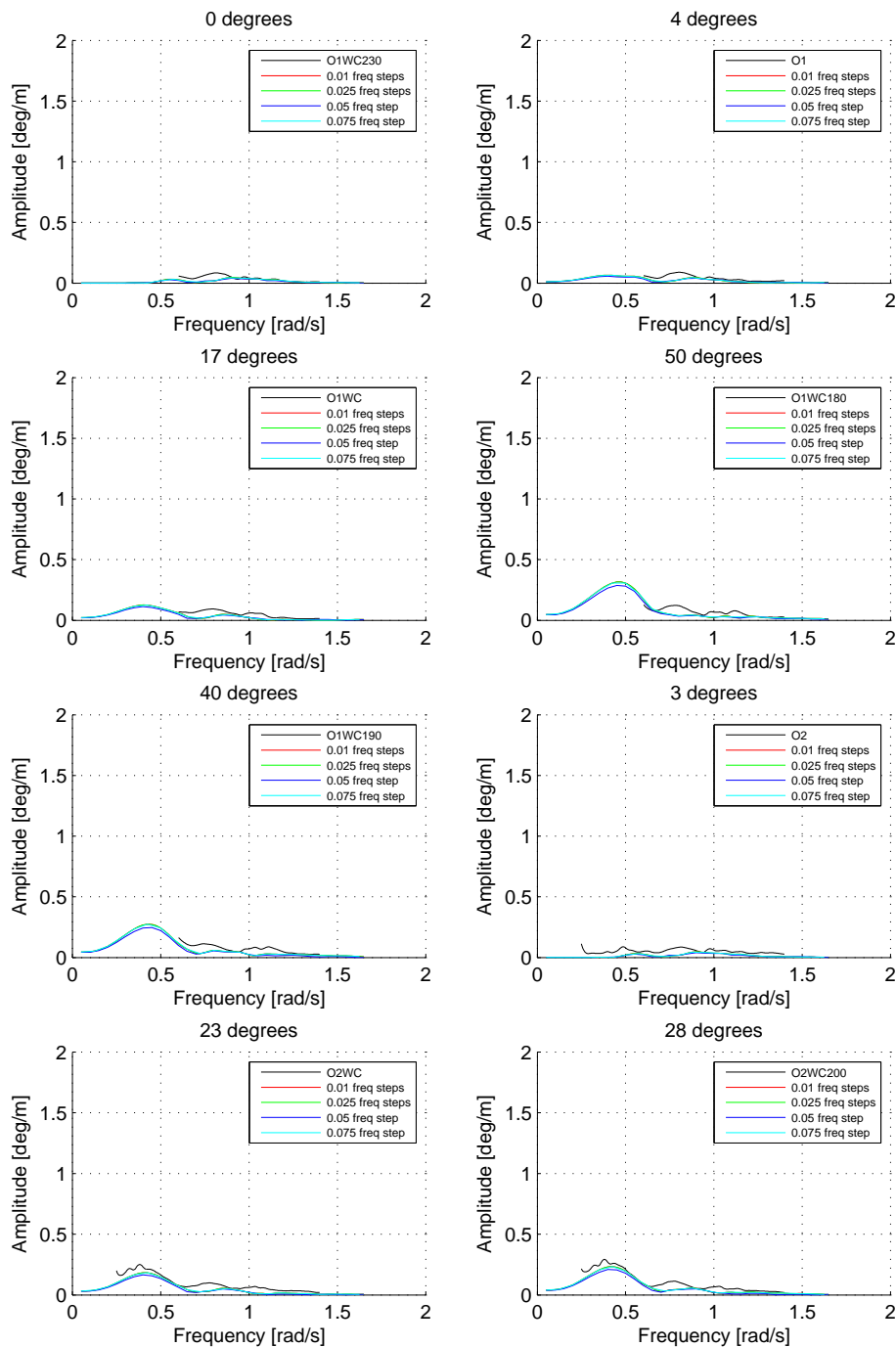


Frequency Iteration – LNGC – Roll RAO





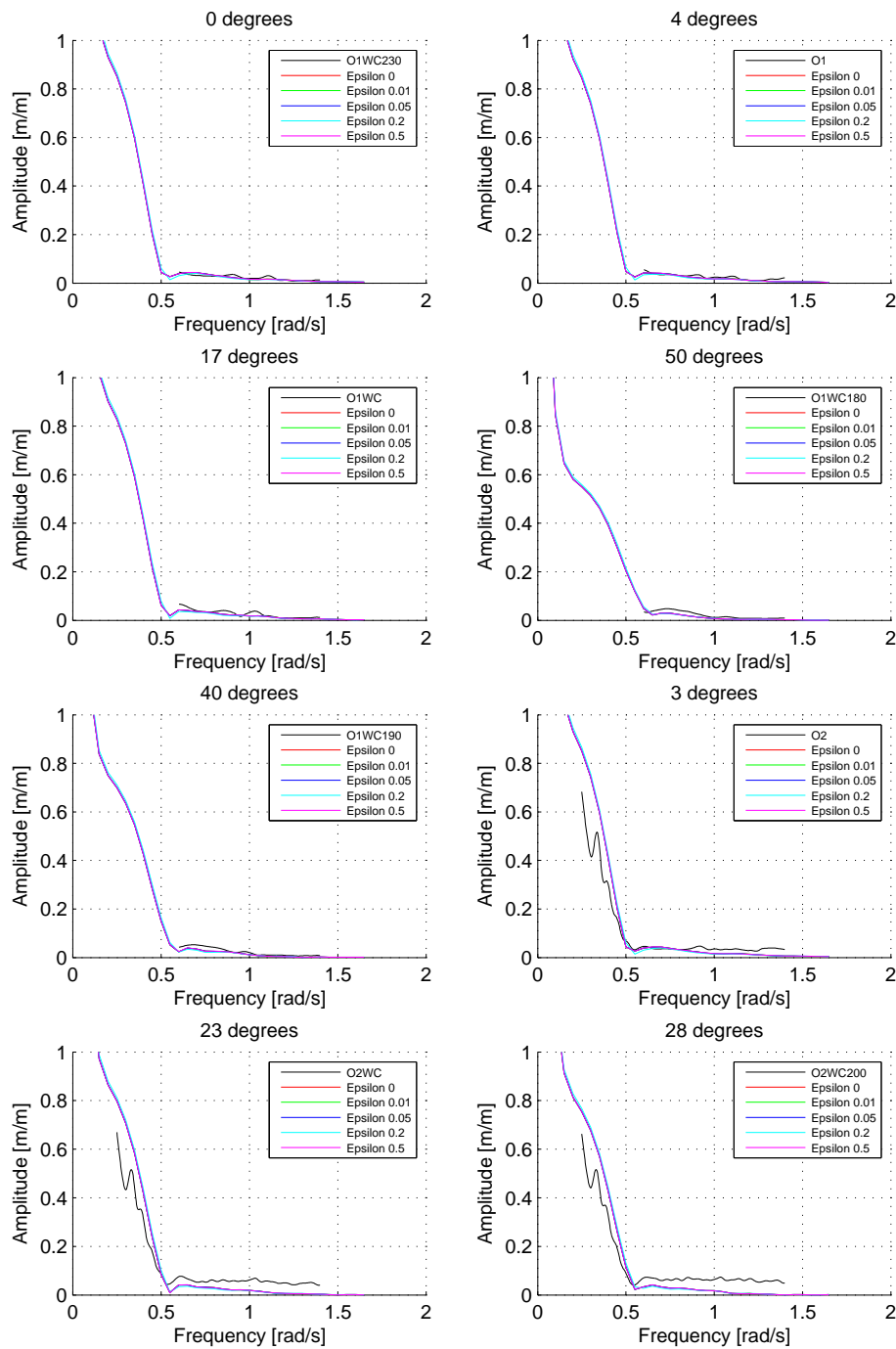
Frequency Iteration – LNGC – Yaw RAO



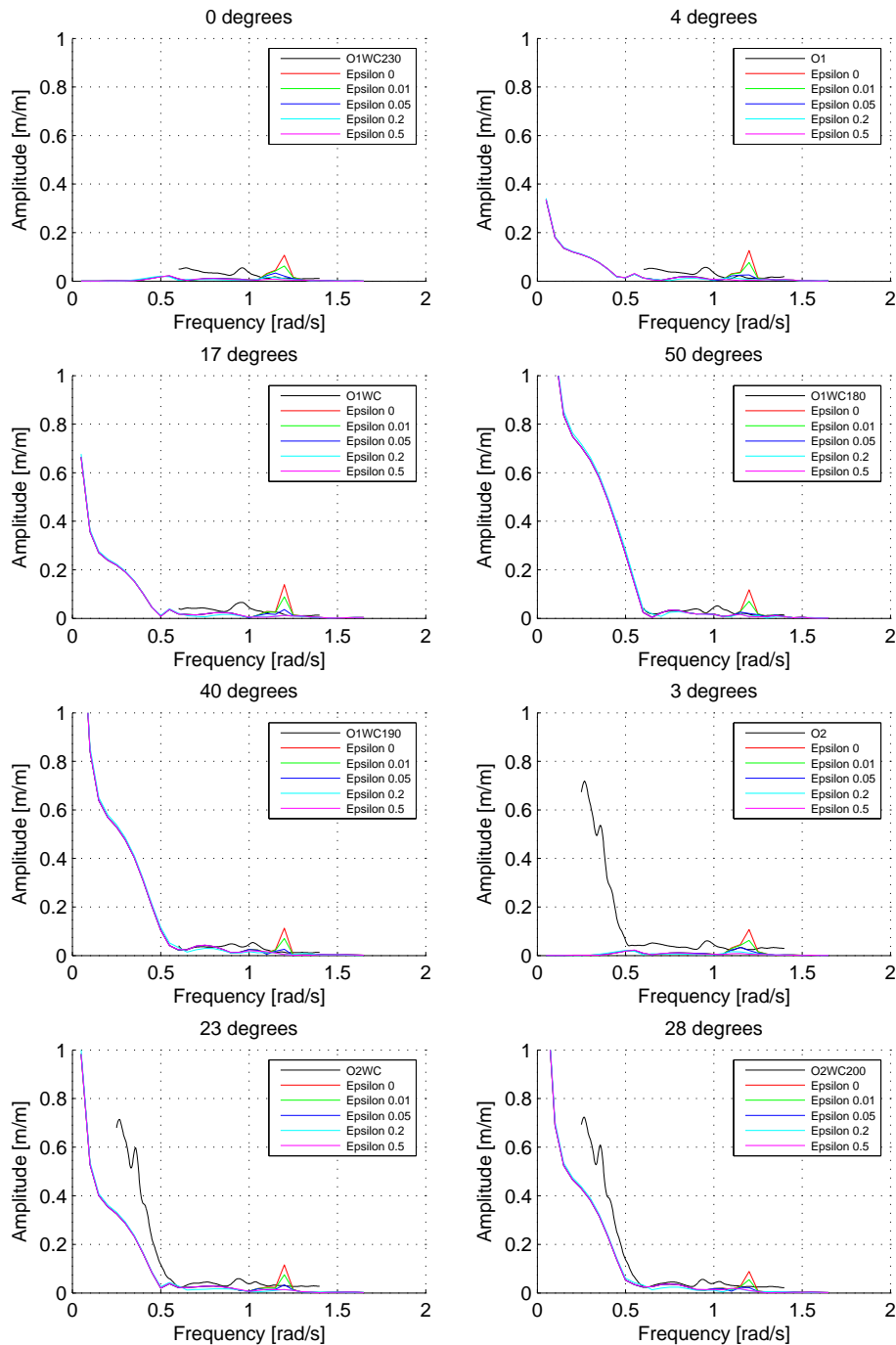
D

VISCOUS LID DAMPING, ϵ DAMPING

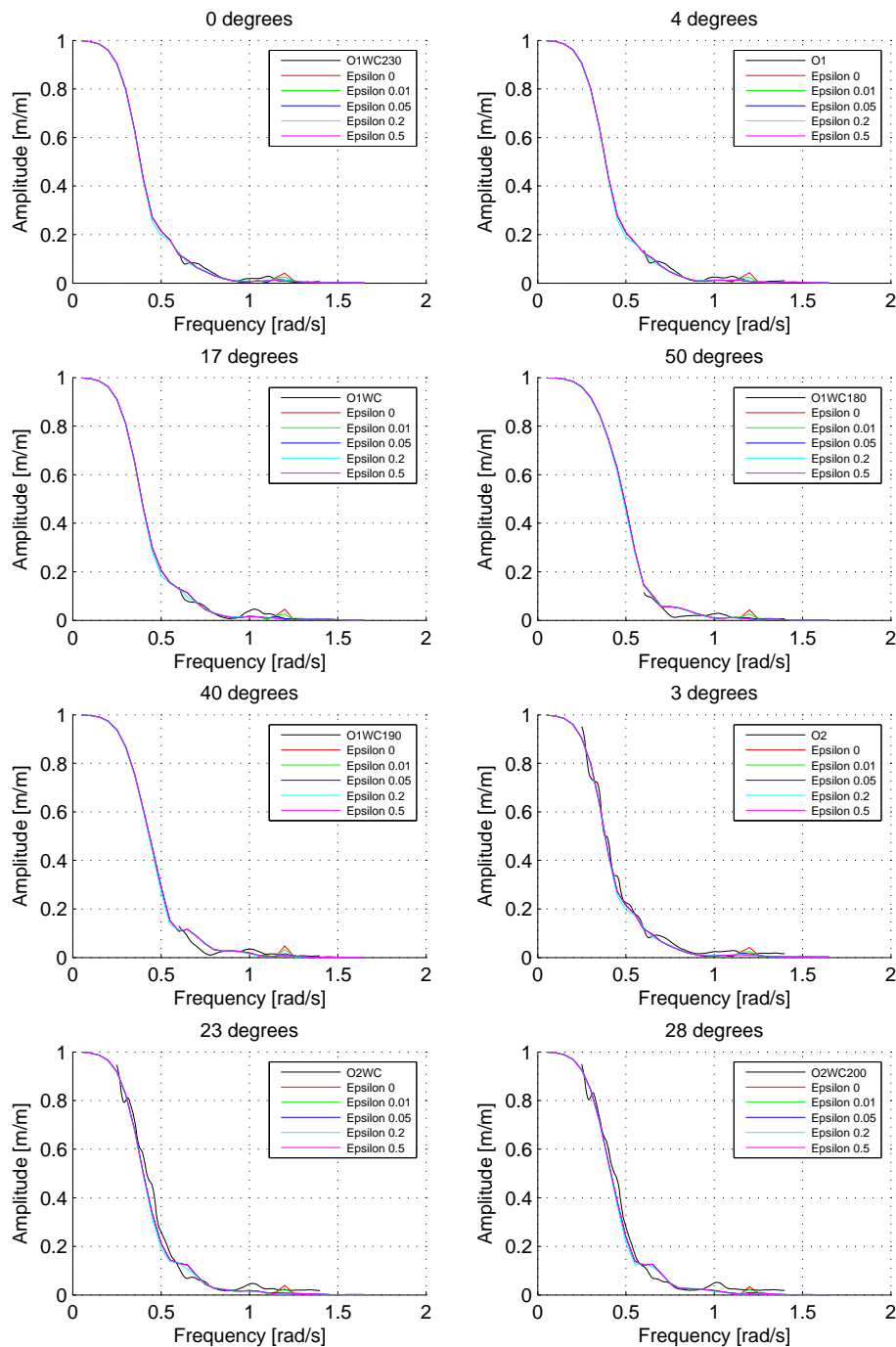
Viscous lid damping Epsilon – FLNG – Surge RAO



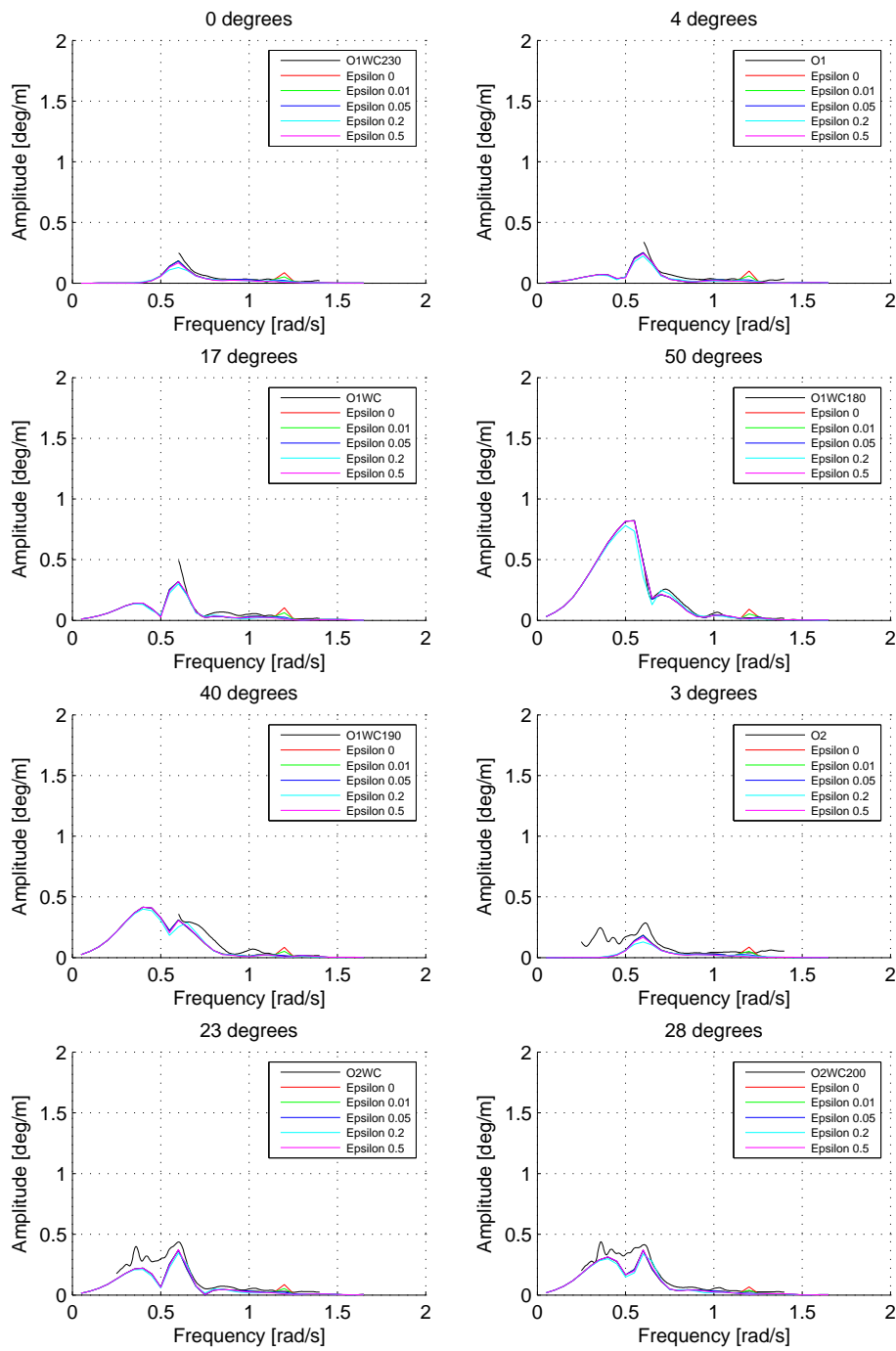
Viscous lid damping Epsilon – FLNG – Sway RAO



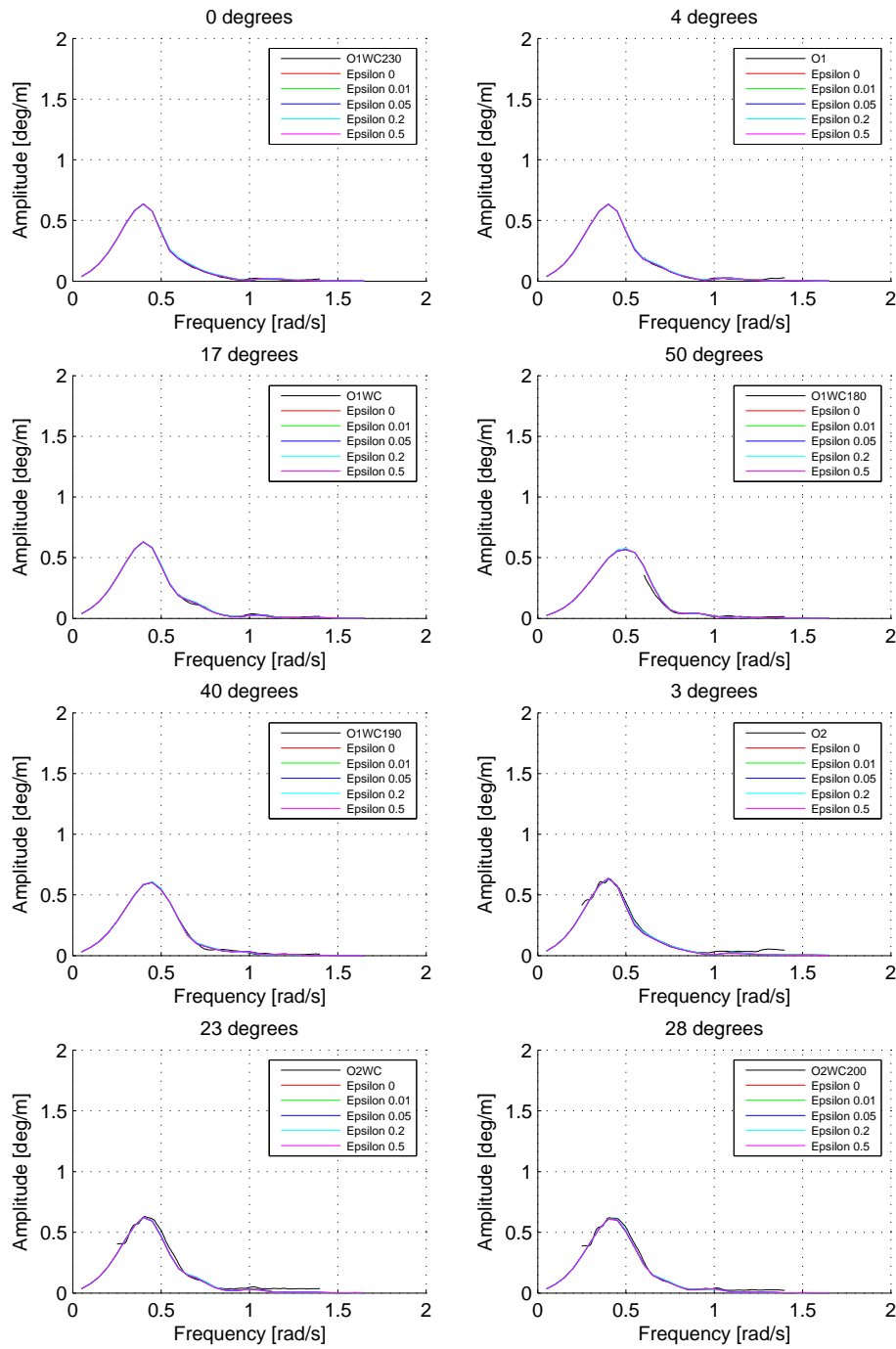
Viscous lid damping Epsilon – FLNG – Heave RAO



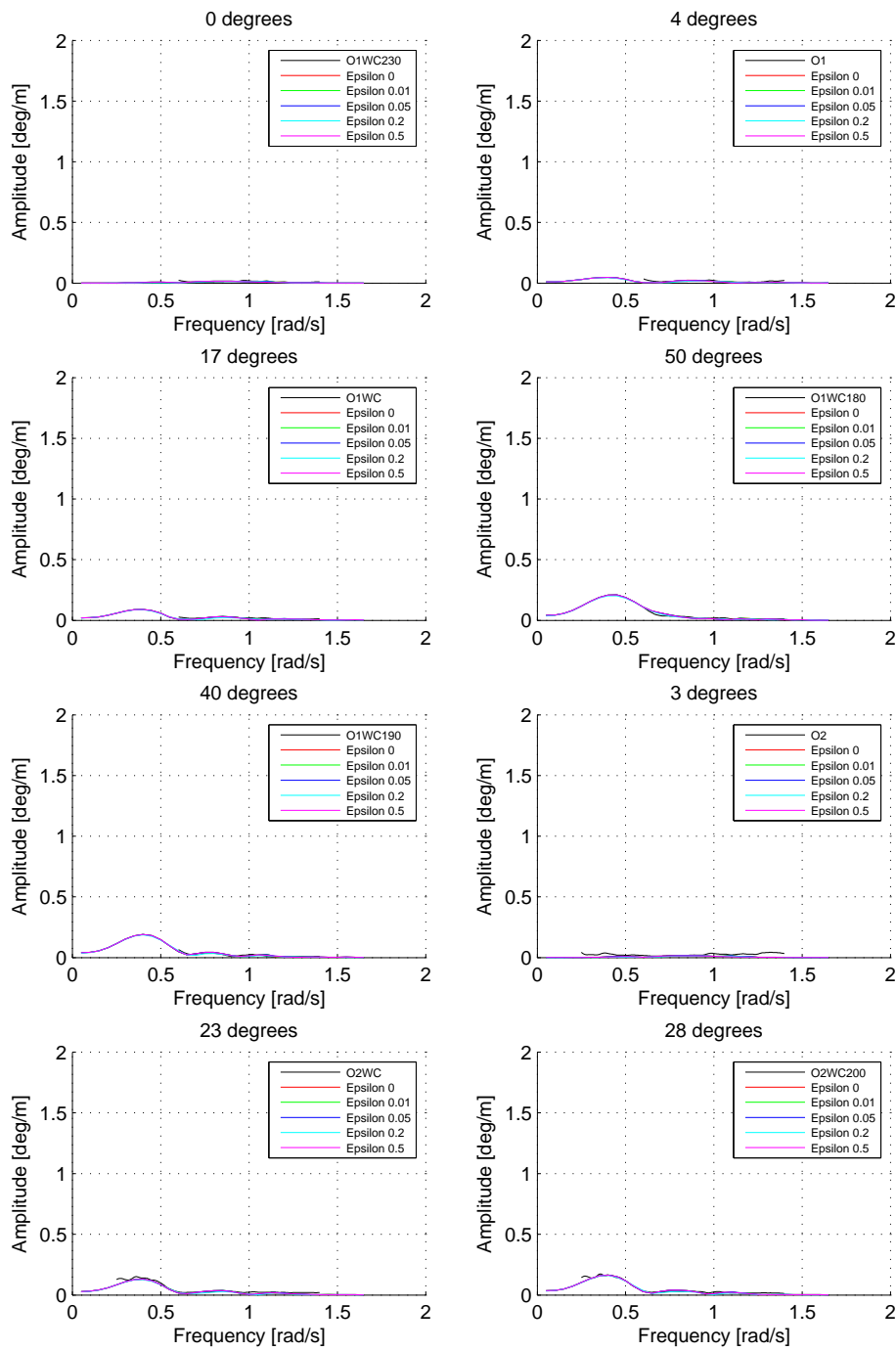
Viscous lid damping Epsilon – FLNG – Roll RAO



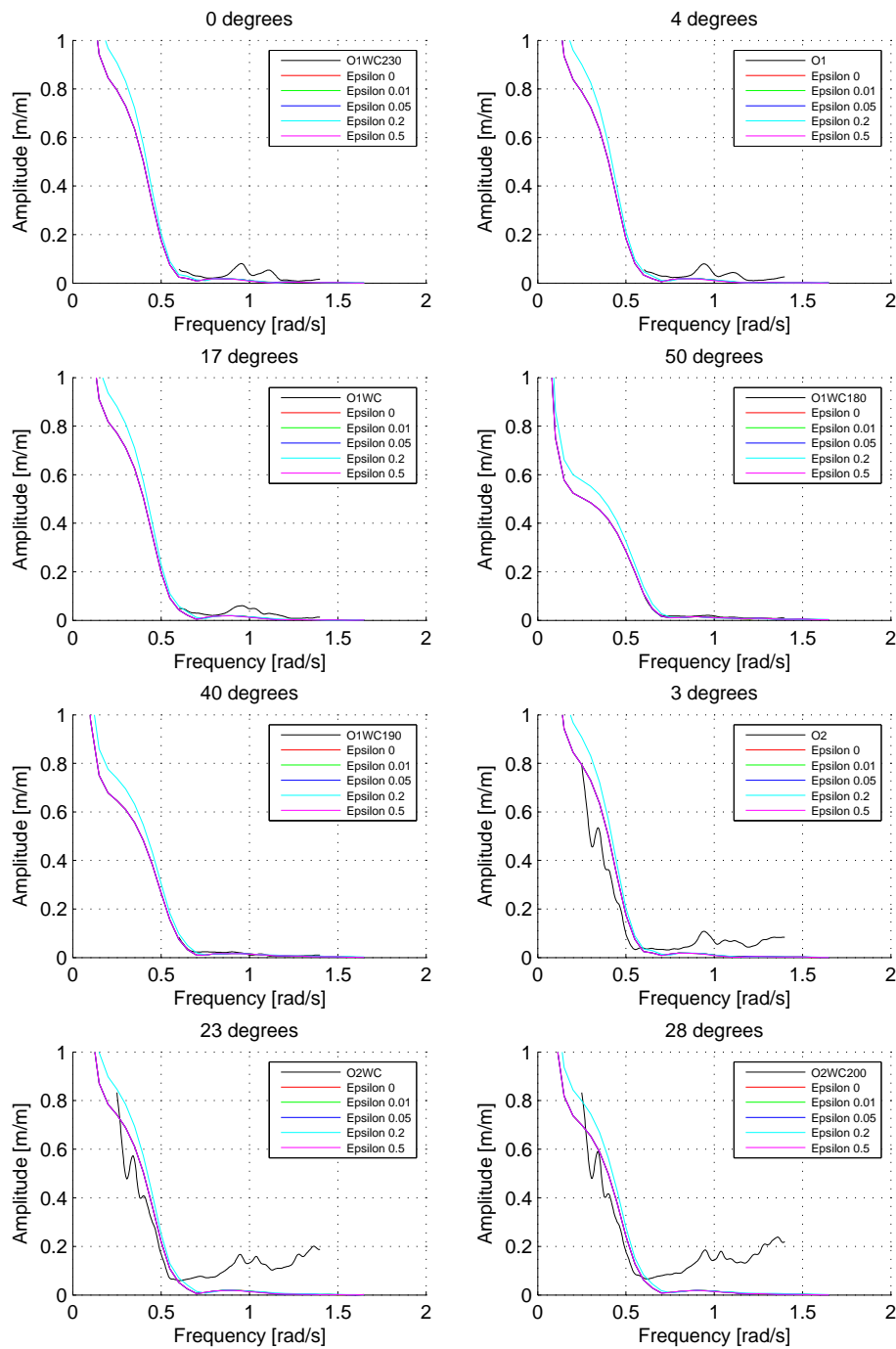
Viscous lid damping Epsilon – FLNG – Pitch RAO



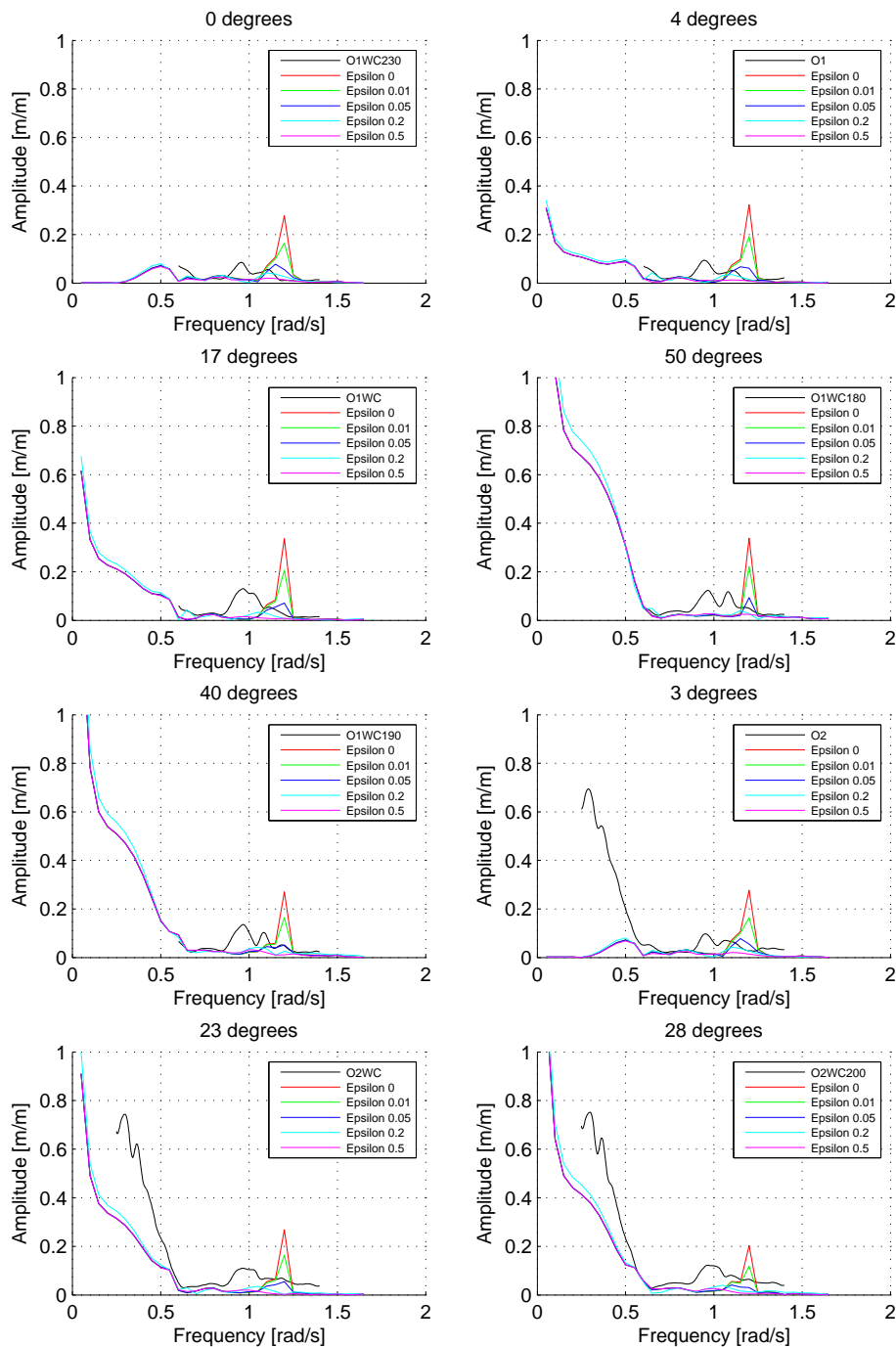
Viscous lid damping Epsilon – FLNG – Yaw RAO



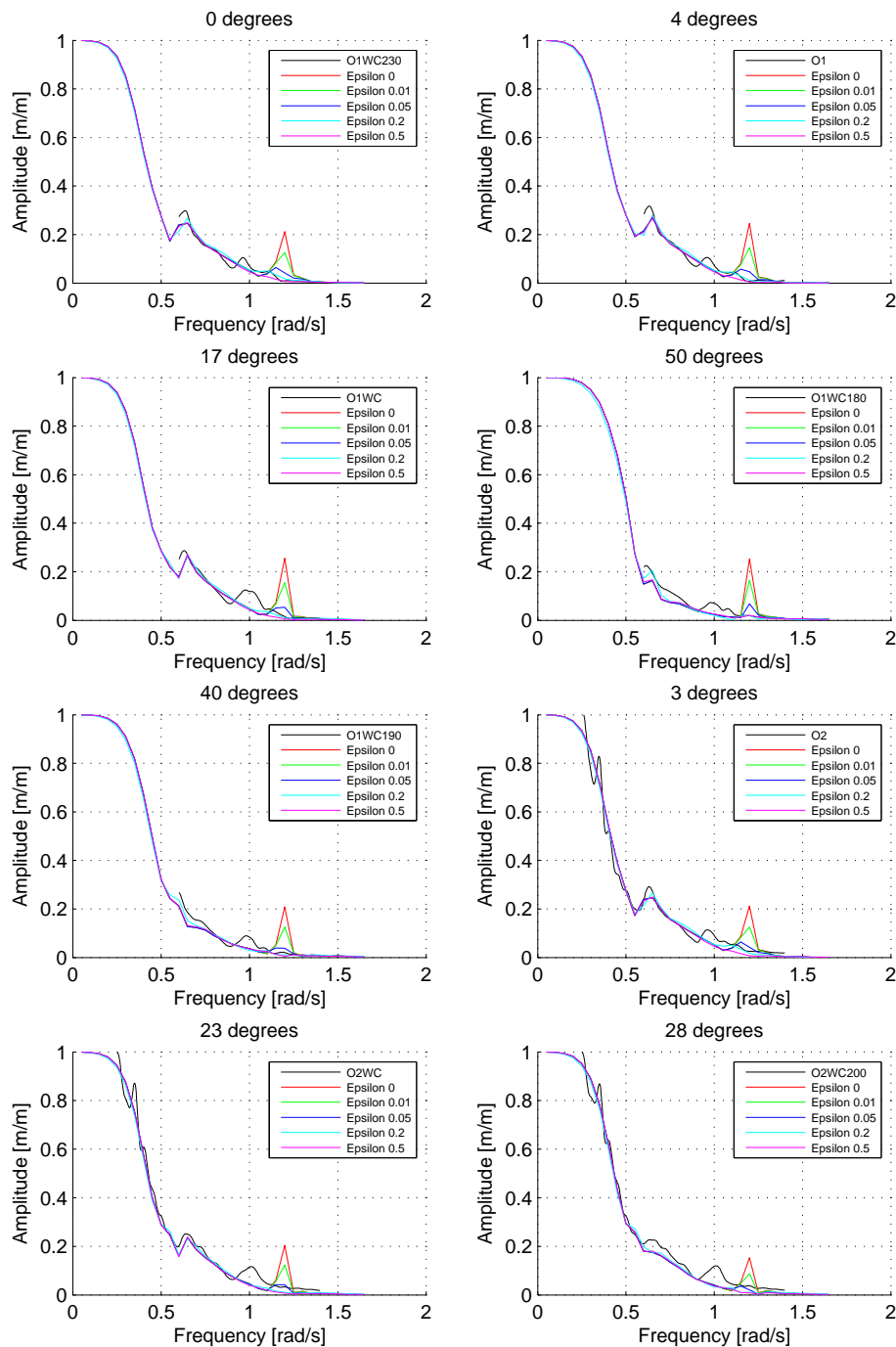
Viscous lid damping Epsilon – LNGC – Surge RAO



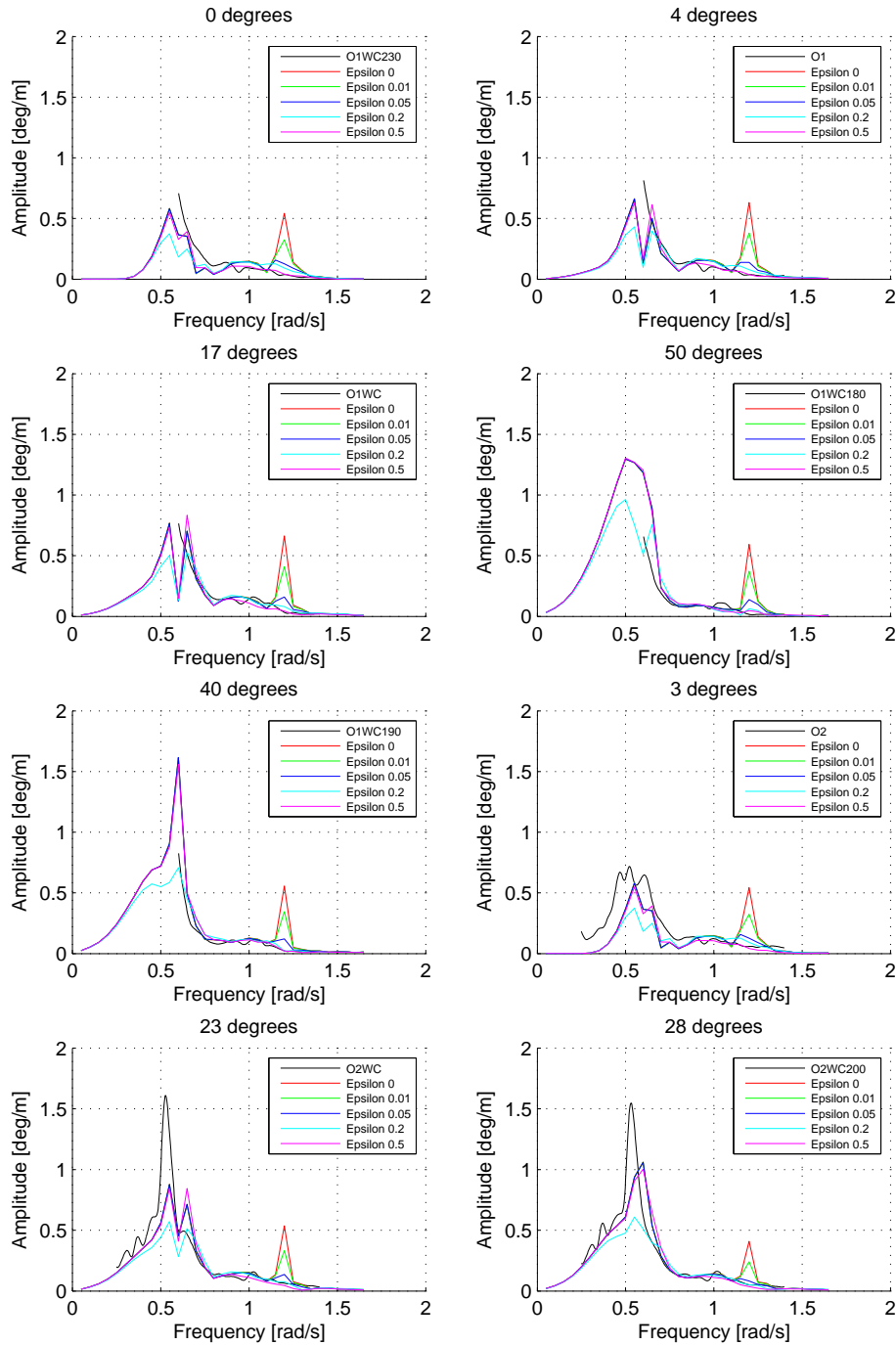
Viscous lid damping Epsilon – LNGC – Sway RAO



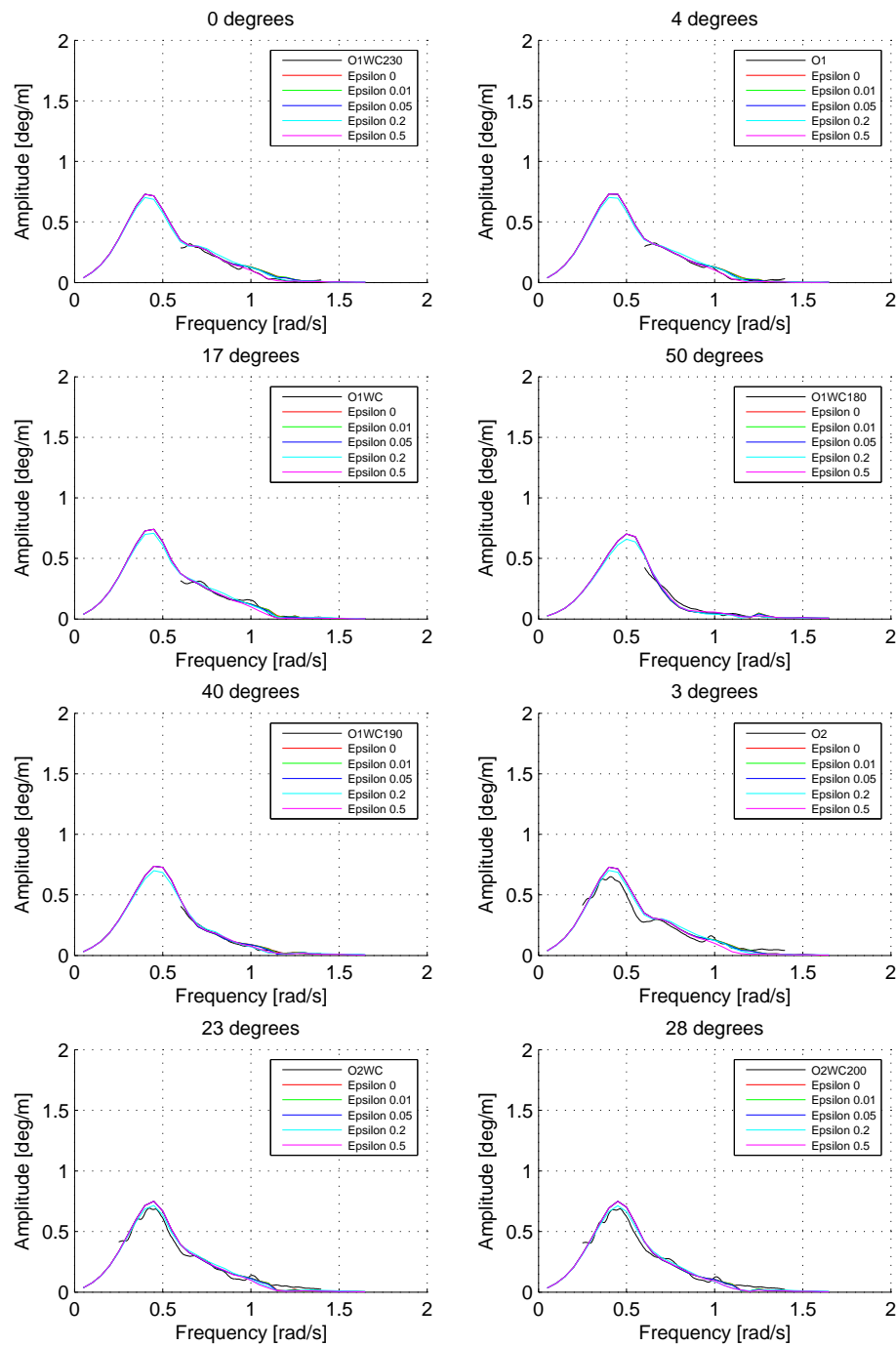
Viscous lid damping Epsilon – LNGC – Heave RAO



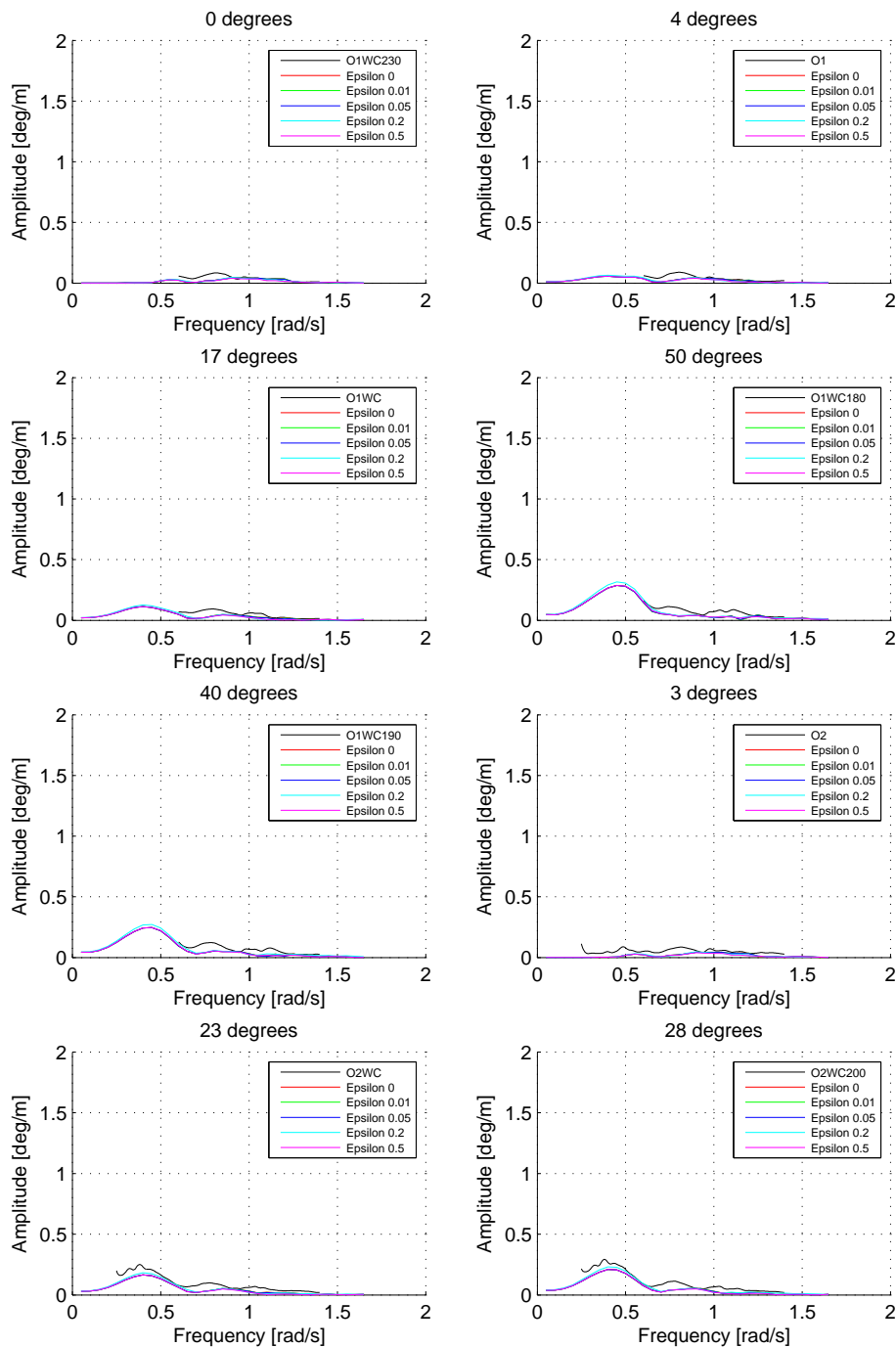
Viscous lid damping Epsilon – LNGC – Roll RAO



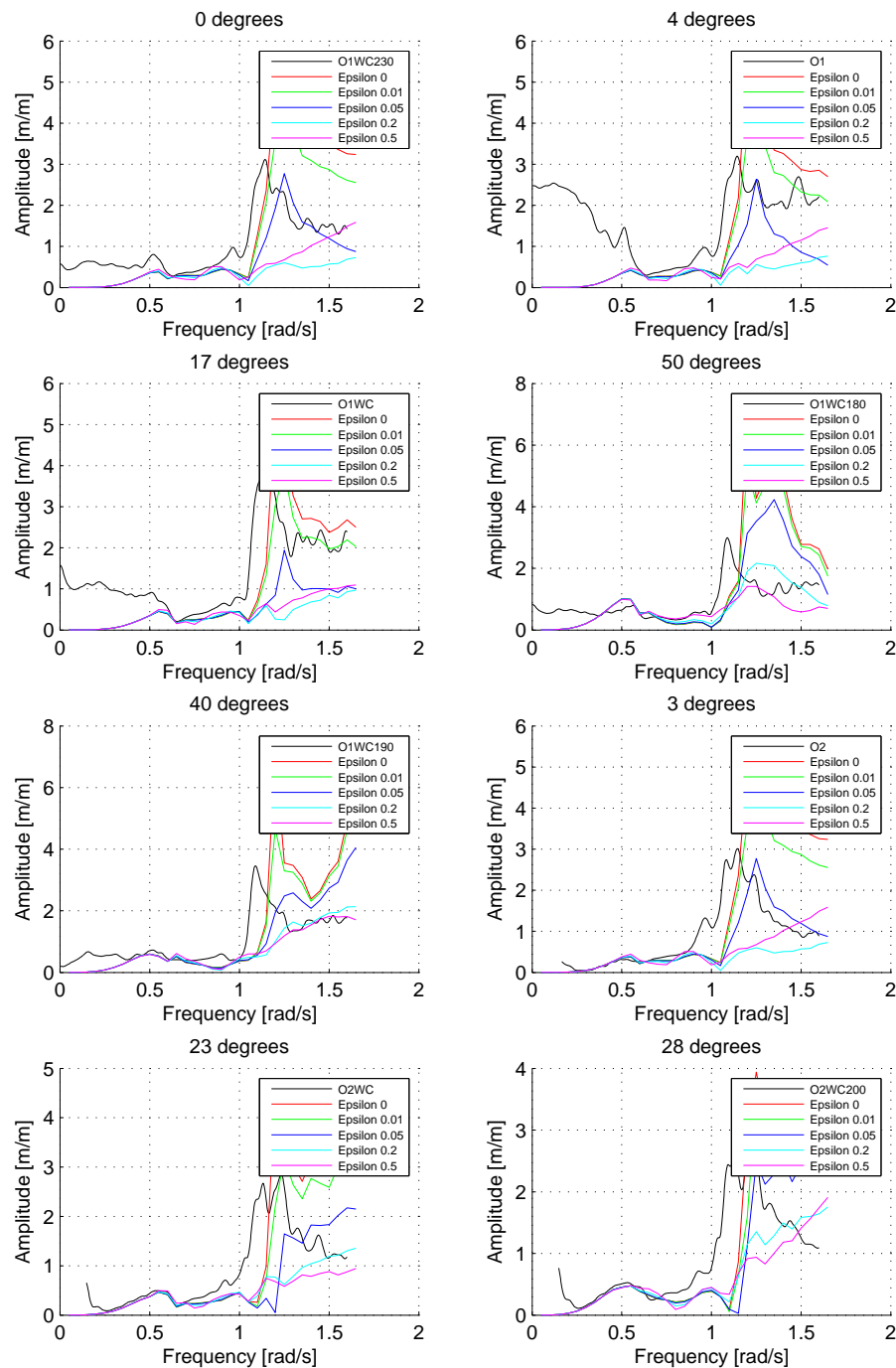
Viscous lid damping Epsilon – LNGC – Pitch RAO



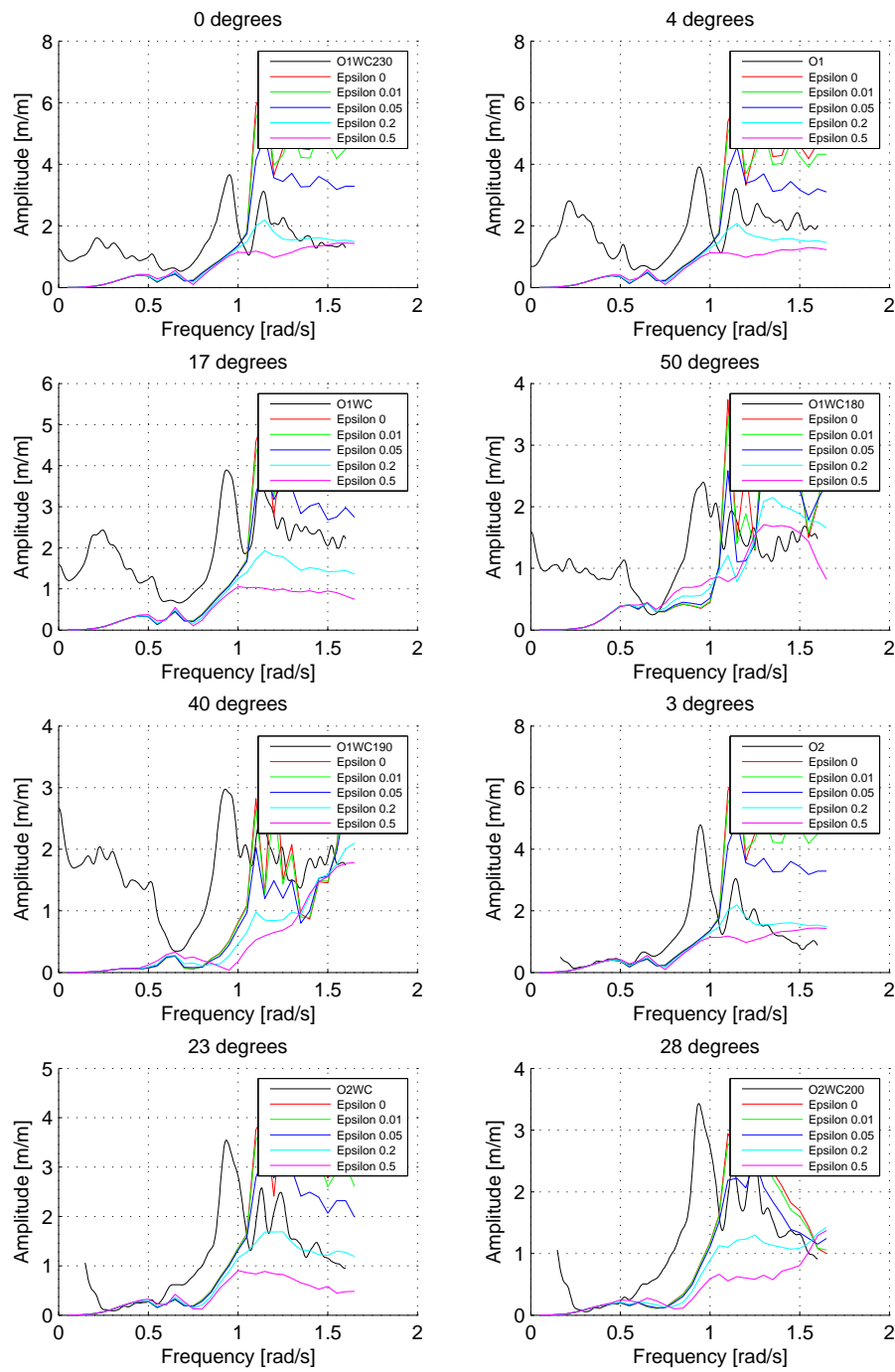
Viscous lid damping Epsilon – LNGC – Yaw RAO



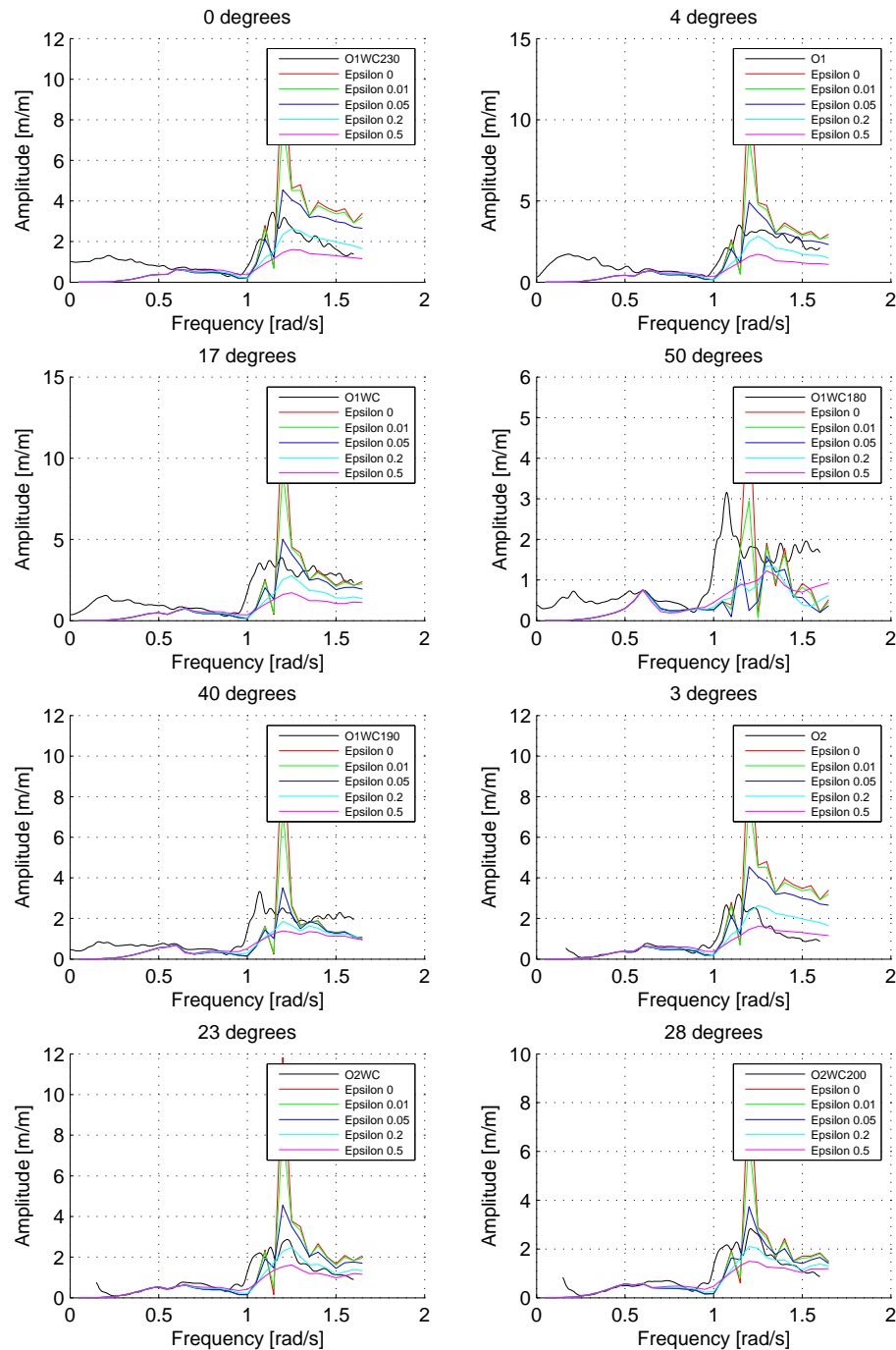
Viscous lid damping Epsilon – Probe 1



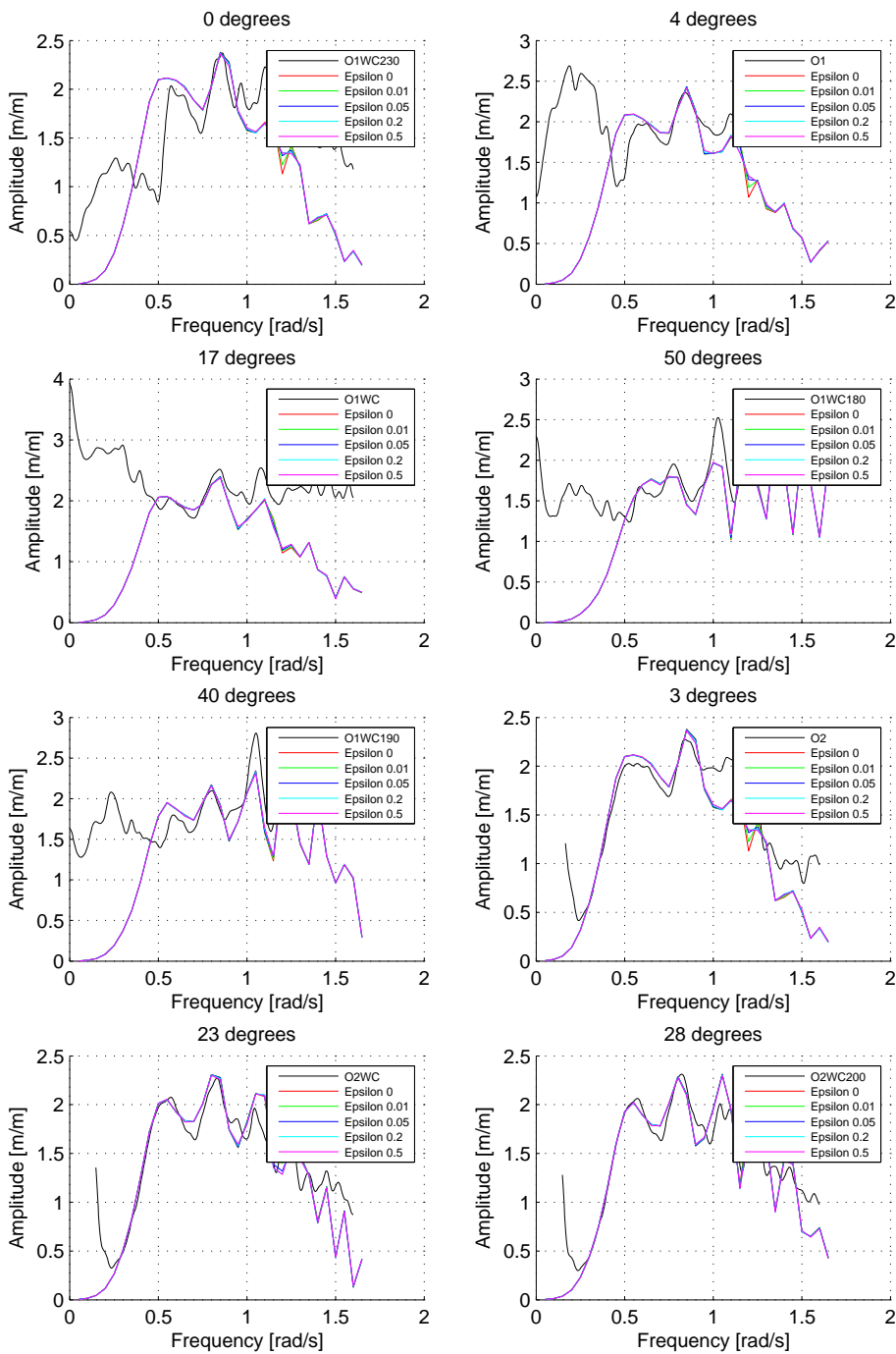
Viscous lid damping Epsilon – Probe 2



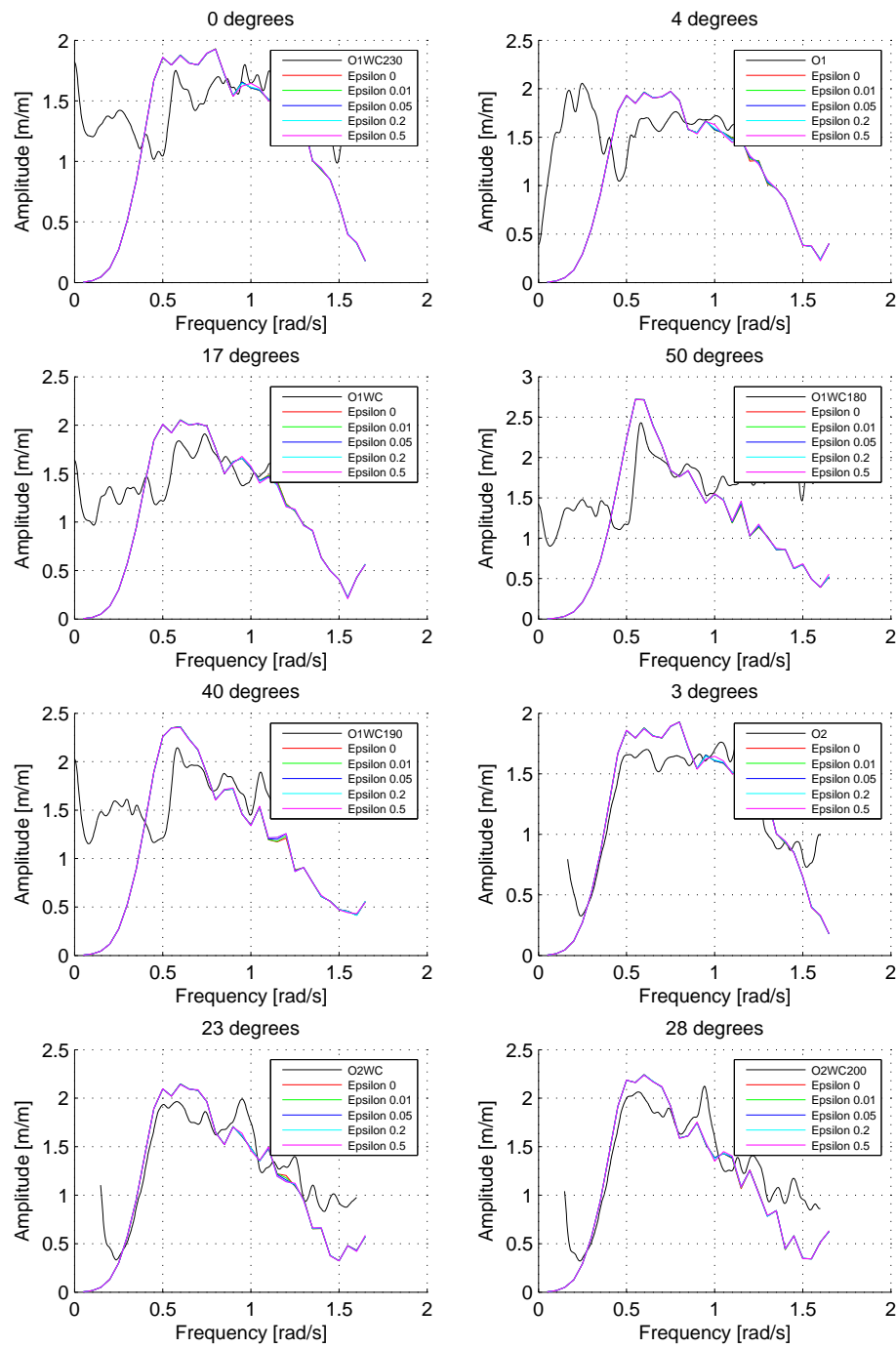
Viscous lid damping Epsilon – Probe 3



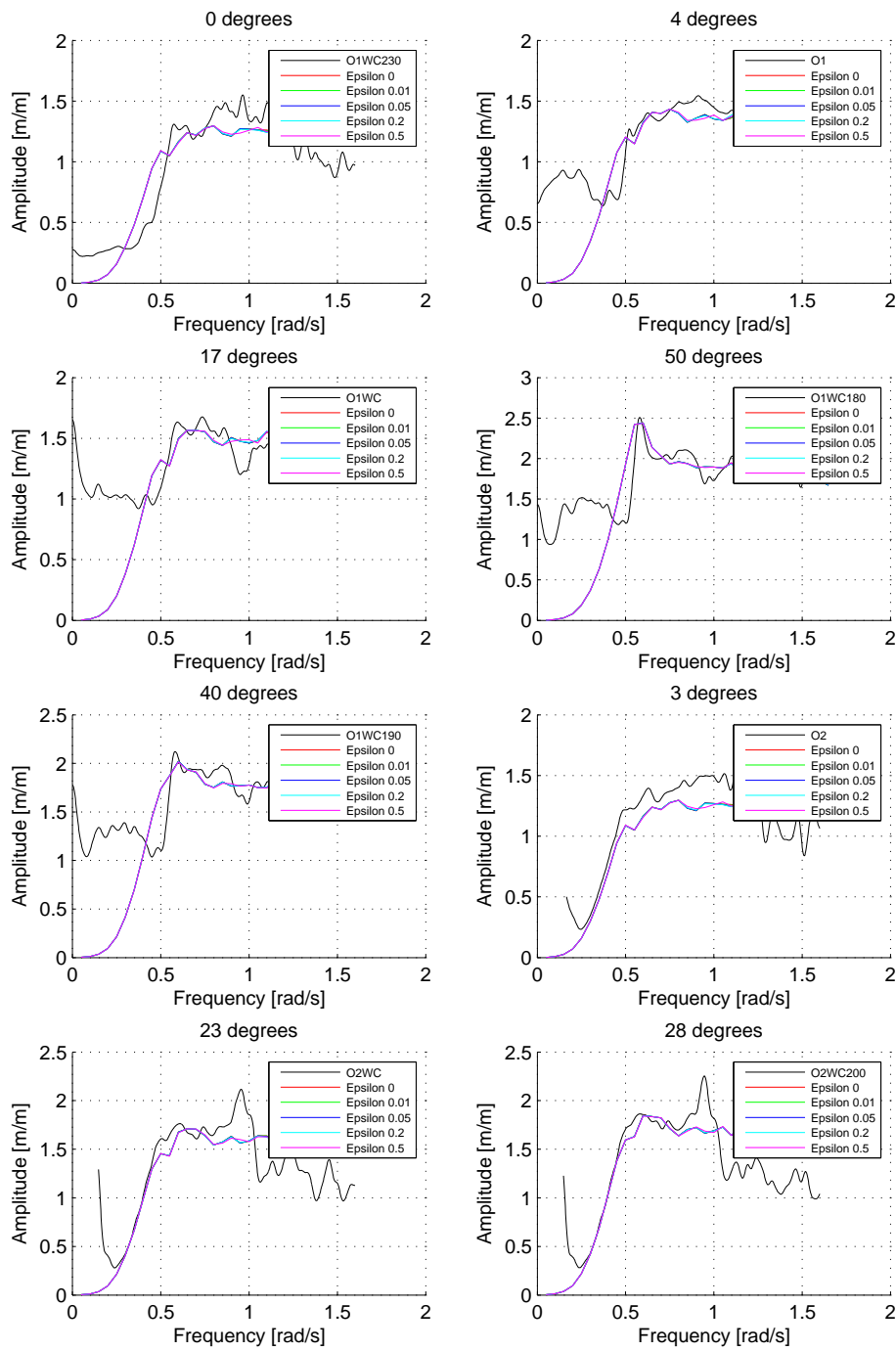
Viscous lid damping Epsilon – Probe 4



Viscous lid damping Epsilon – Probe 5



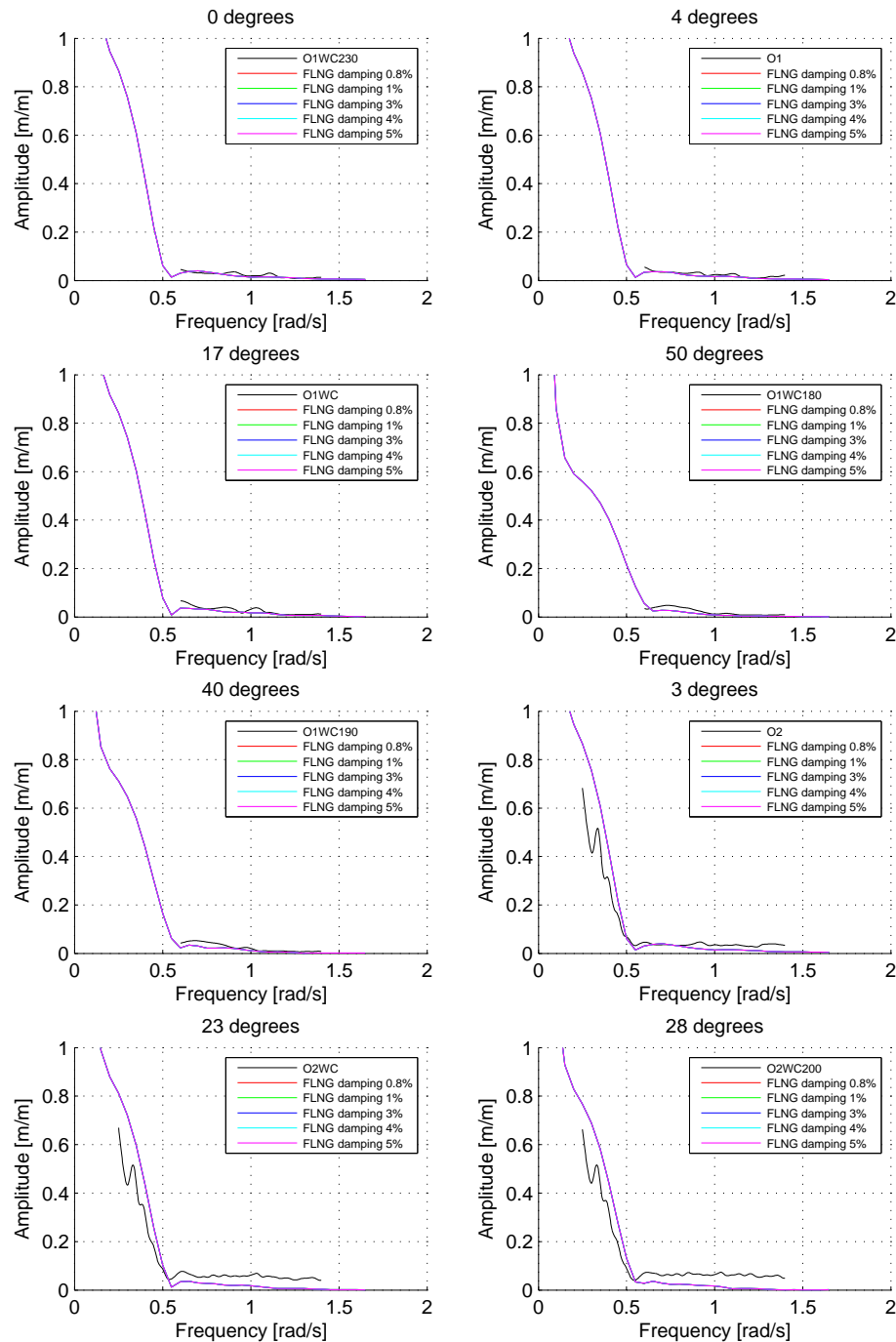
Viscous lid damping Epsilon – Probe 6



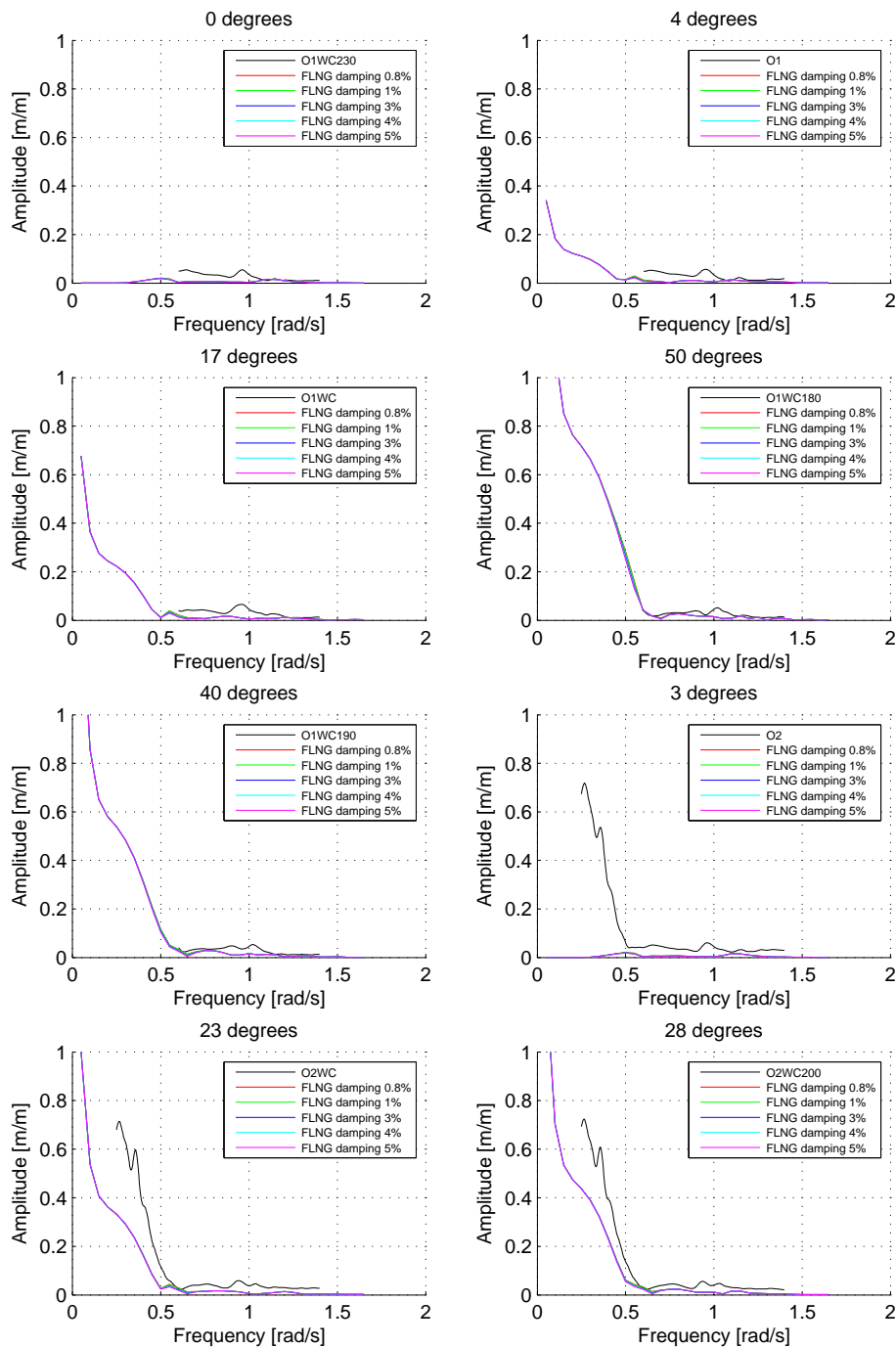
E

VISCOUS ROLL DAMPING

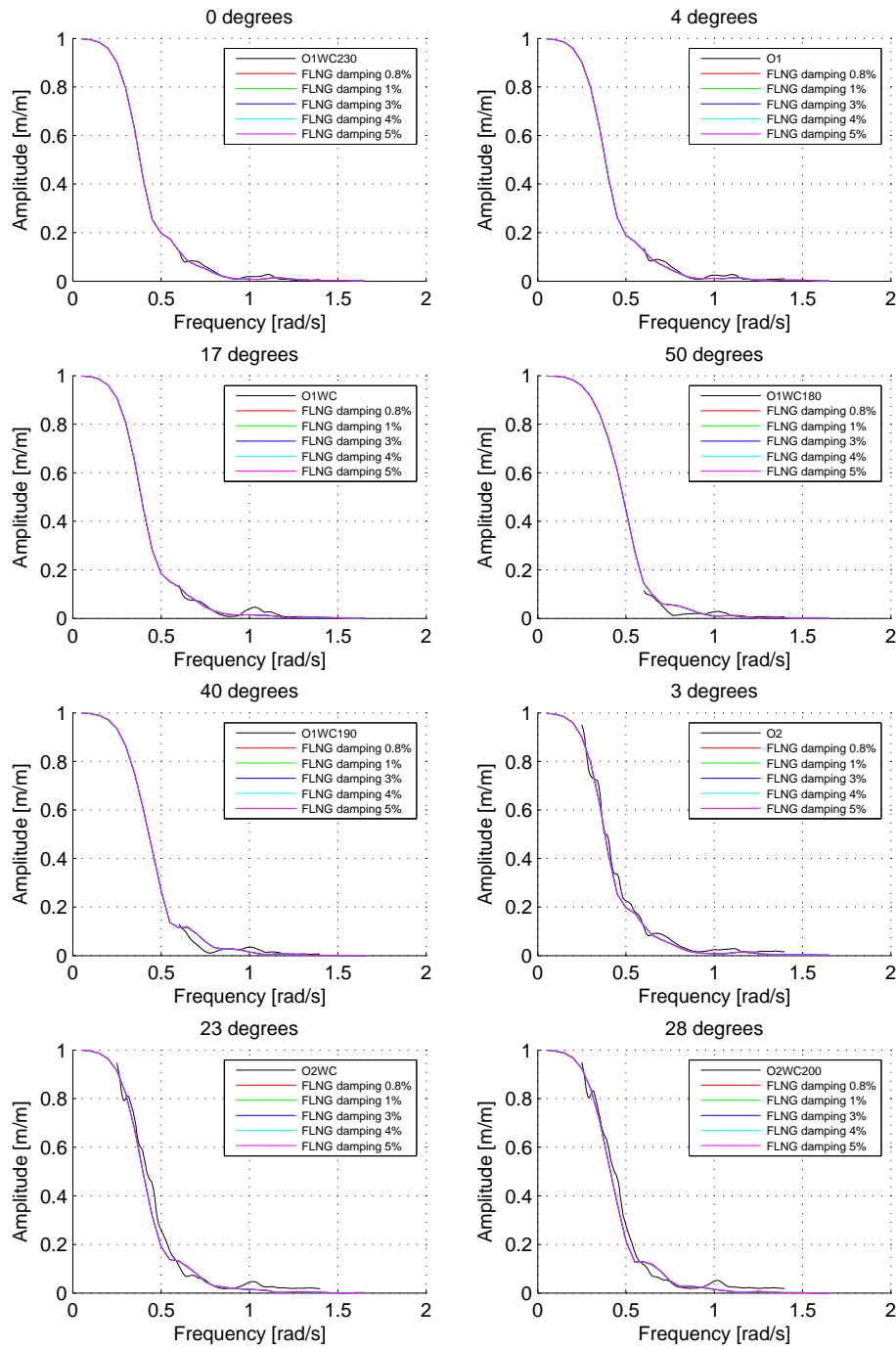
Viscous damping iteration – FLNG – Surge RAO



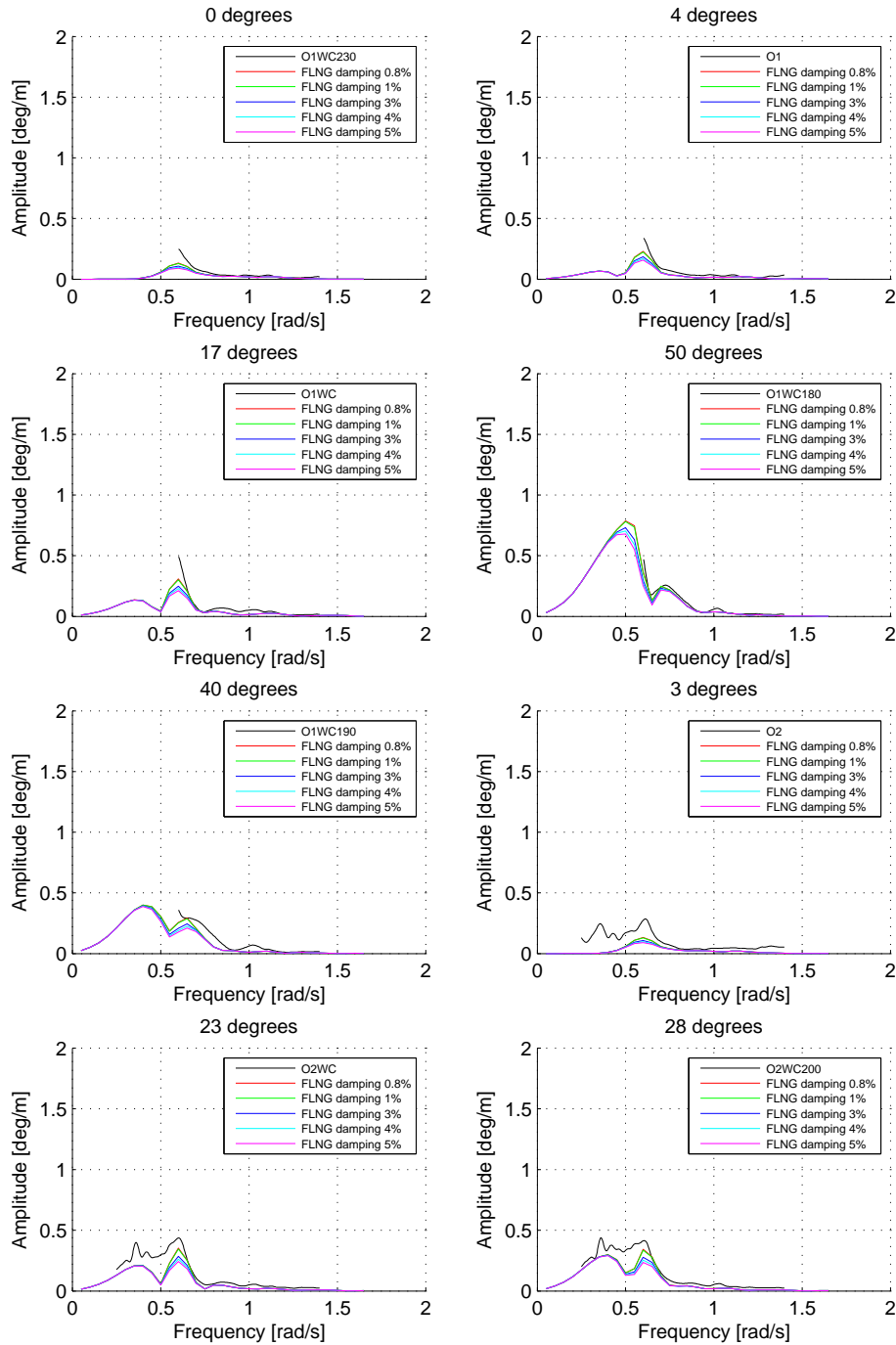
Viscous damping iteration – FLNG – Sway RAO

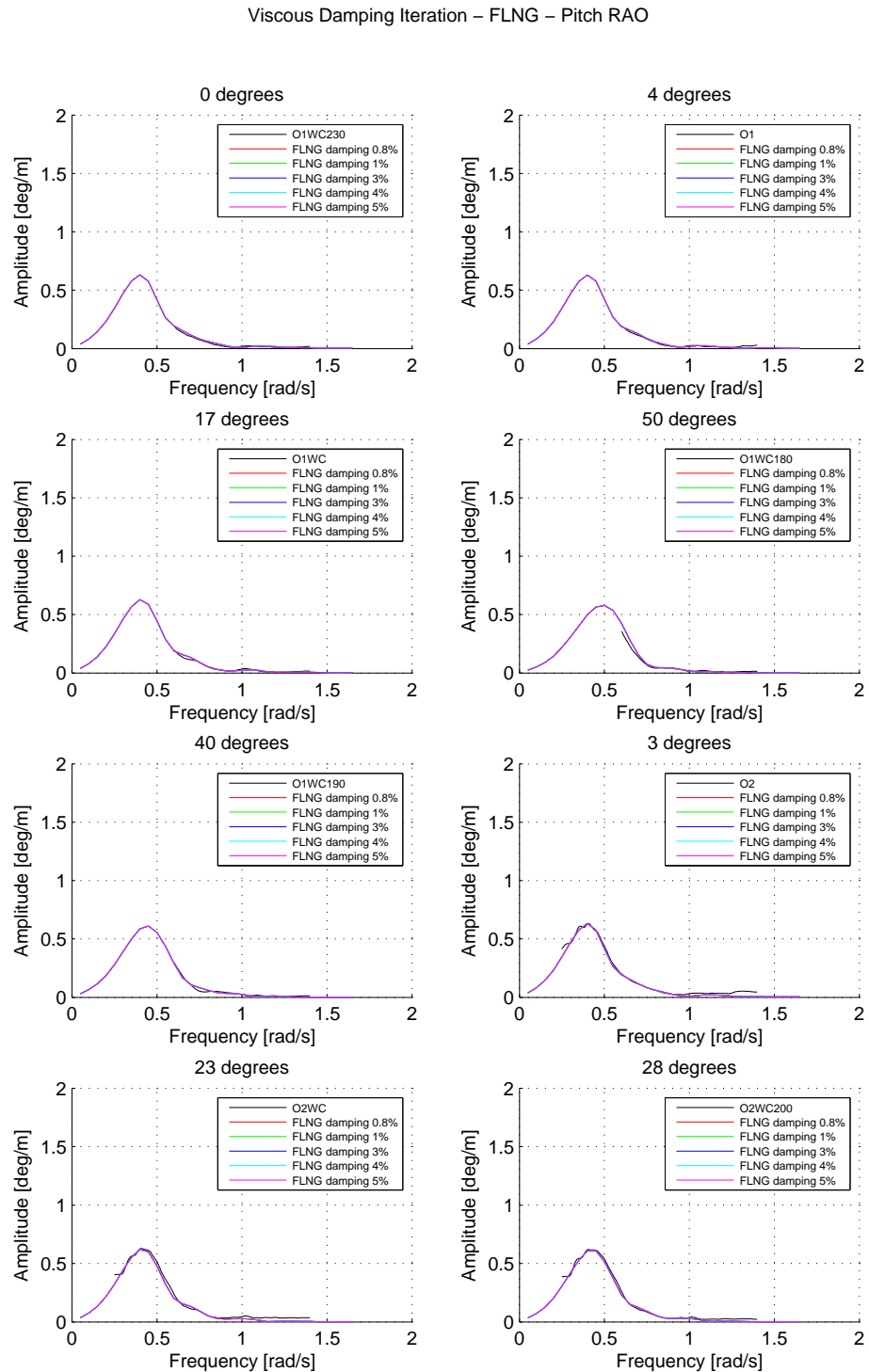


Viscous damping iteration – FLNG – Heave RAO

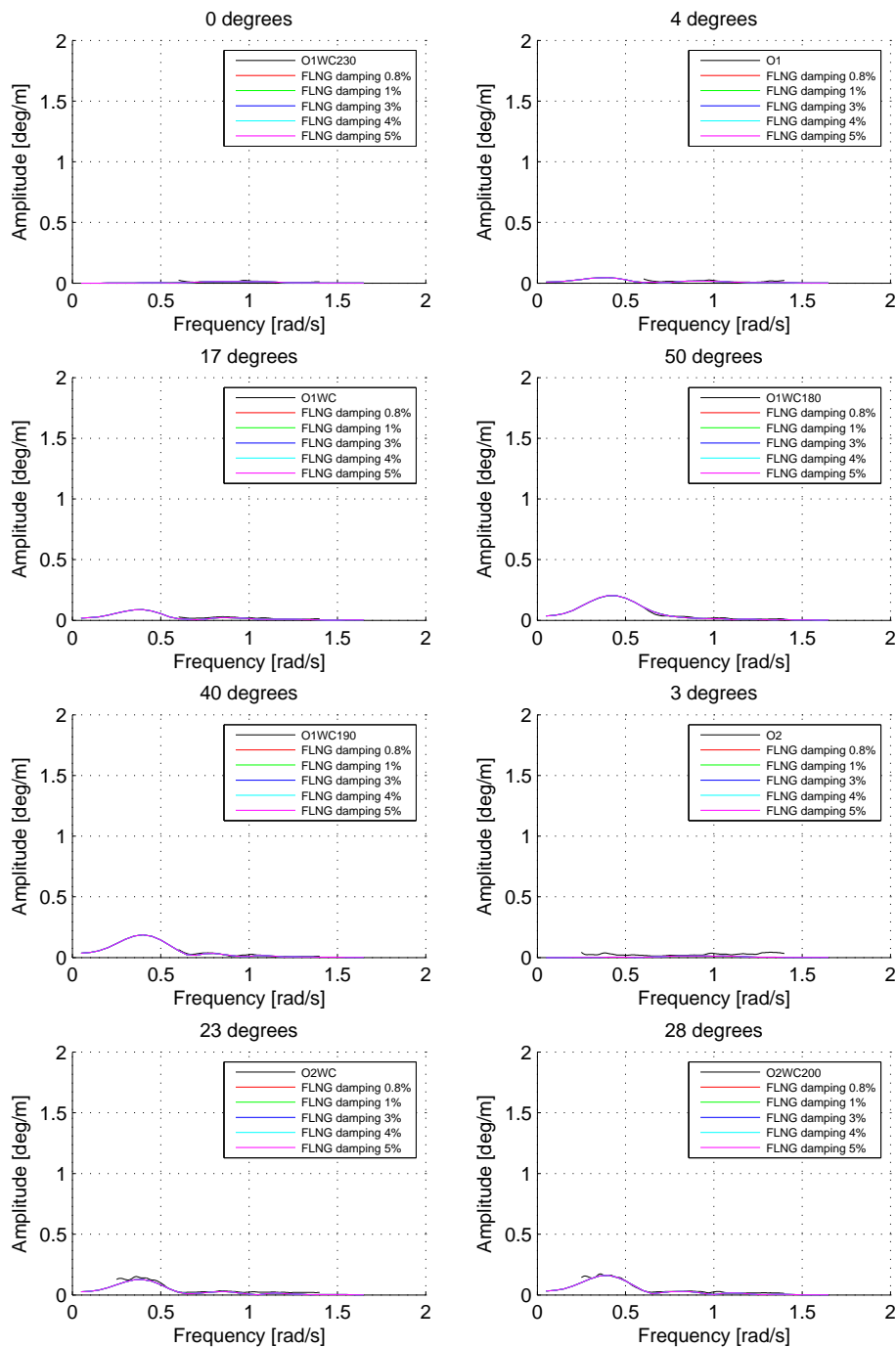


Viscous Damping Iteration – FLNG – Roll RAO

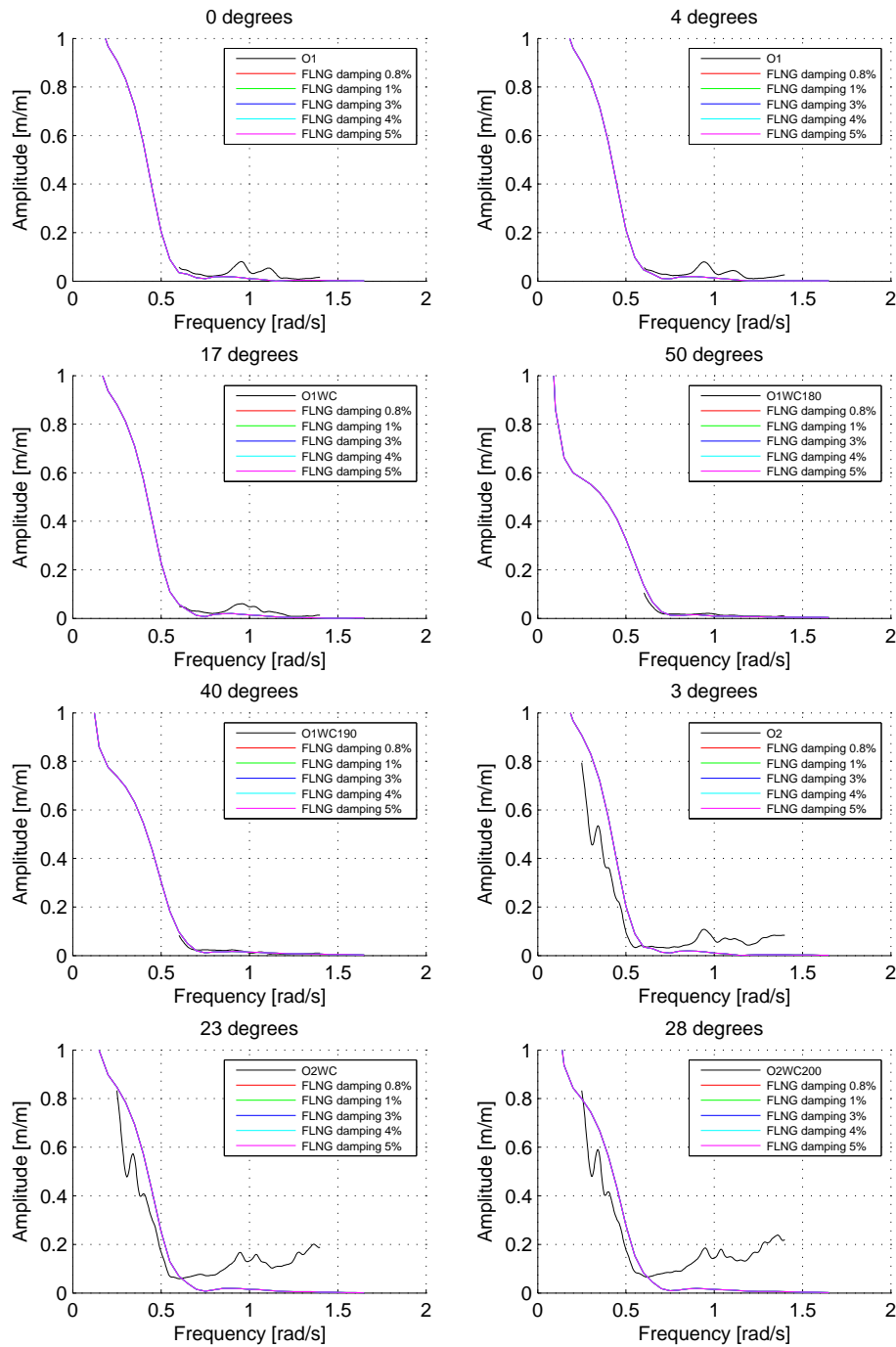




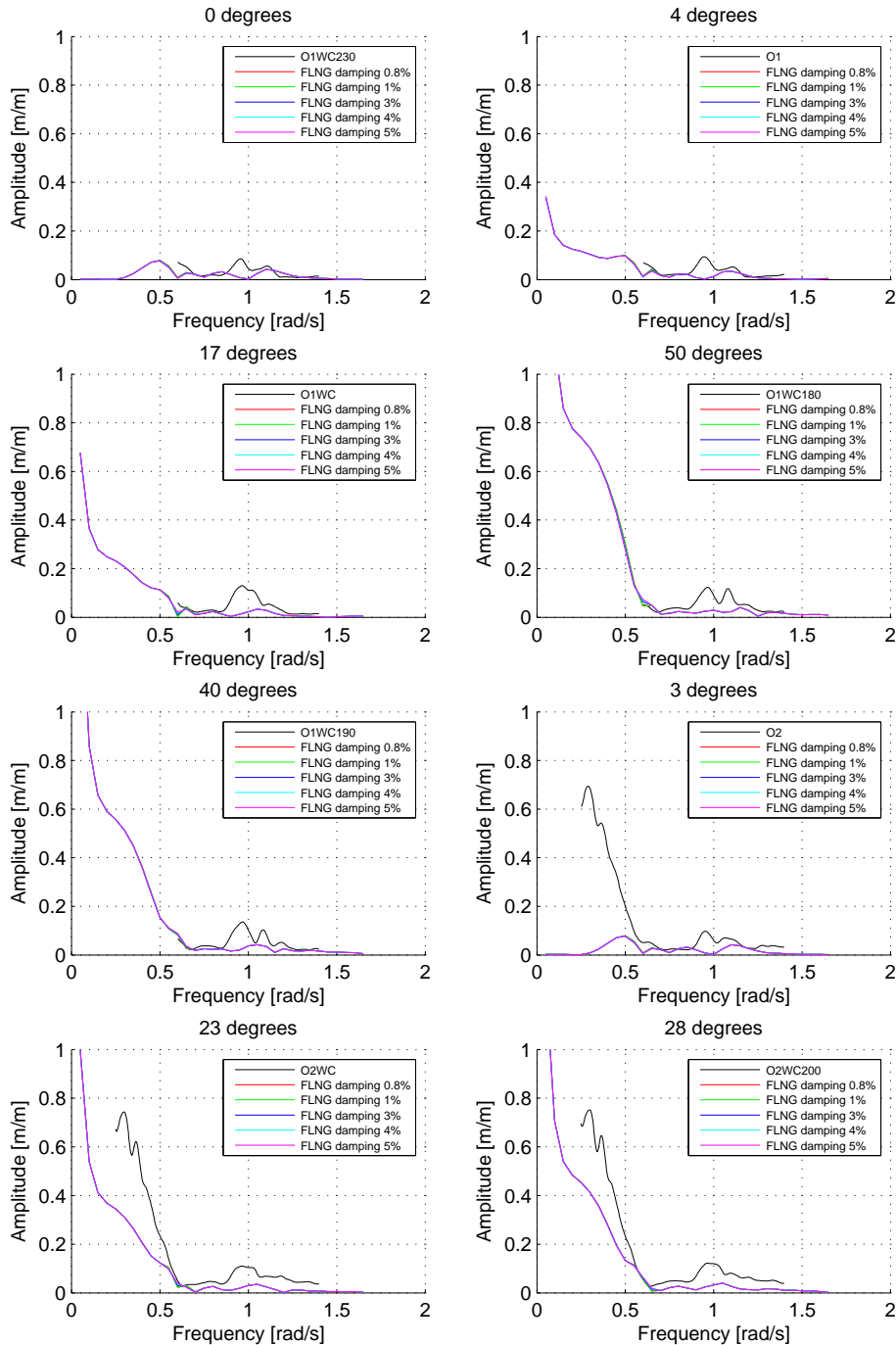
Viscous damping iteration – FLNG – Yaw RAO



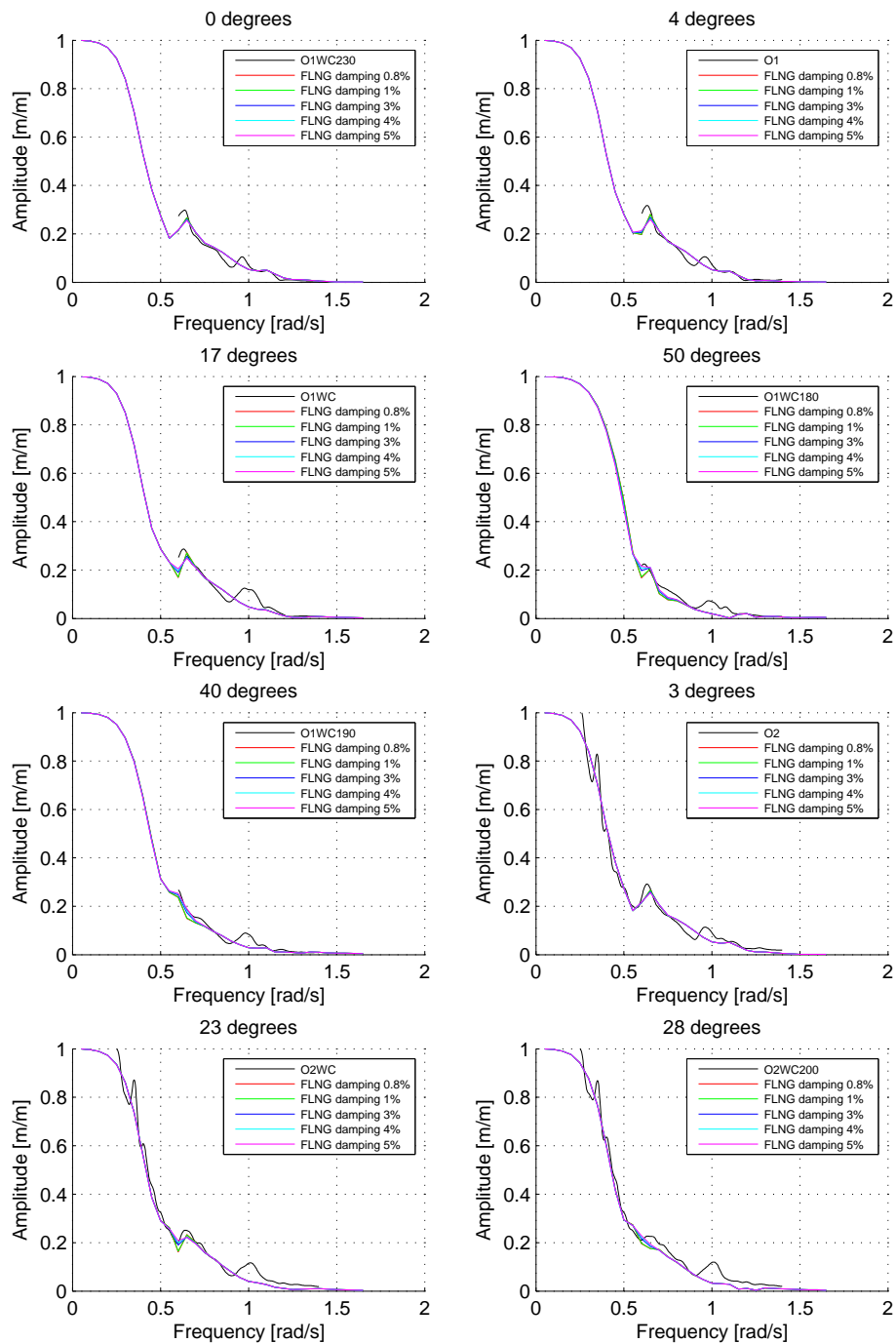
Viscous damping iteration – LNGC – Surge RAO



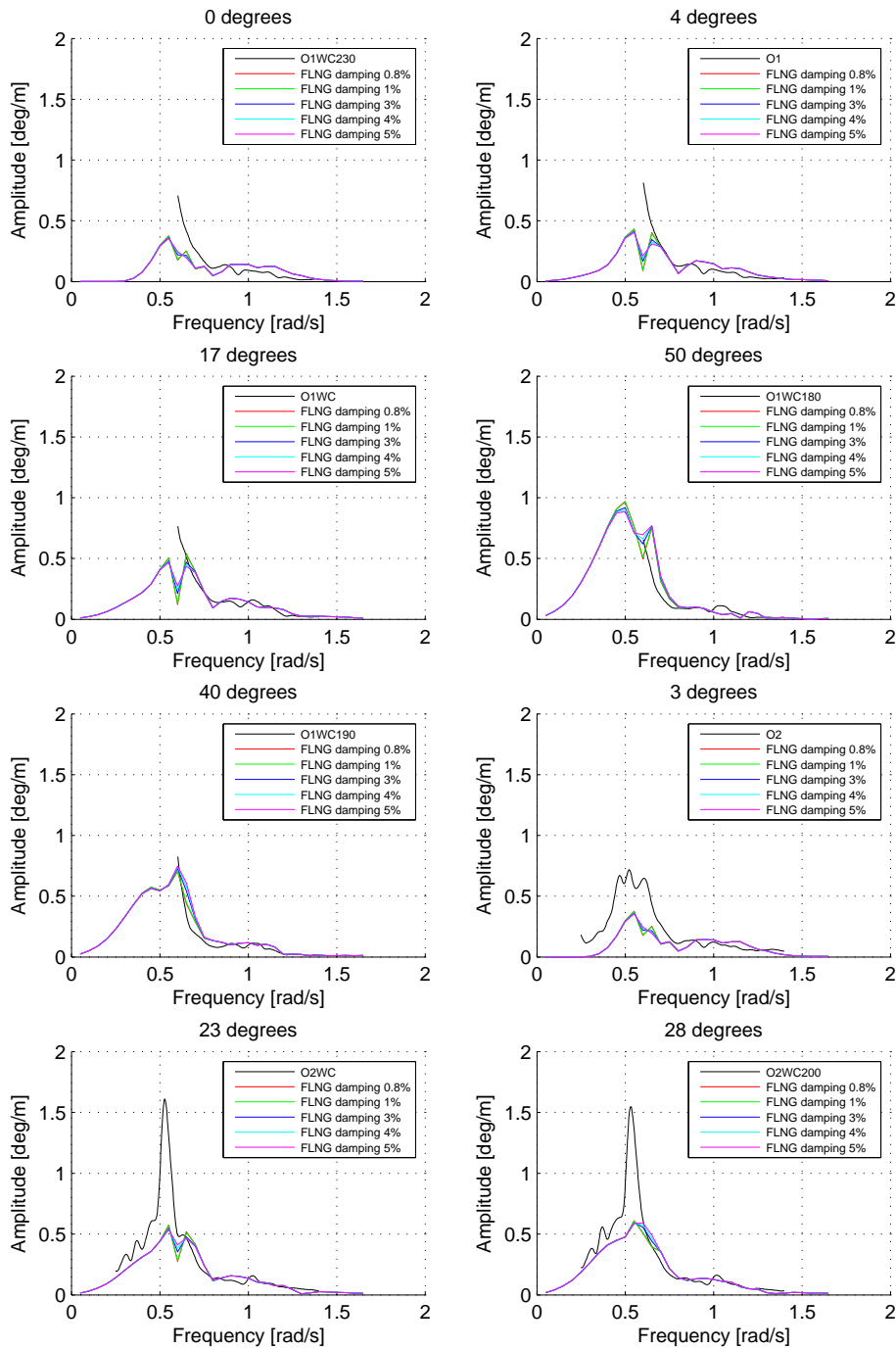
Viscous damping iteration – LNGC – Sway RAO

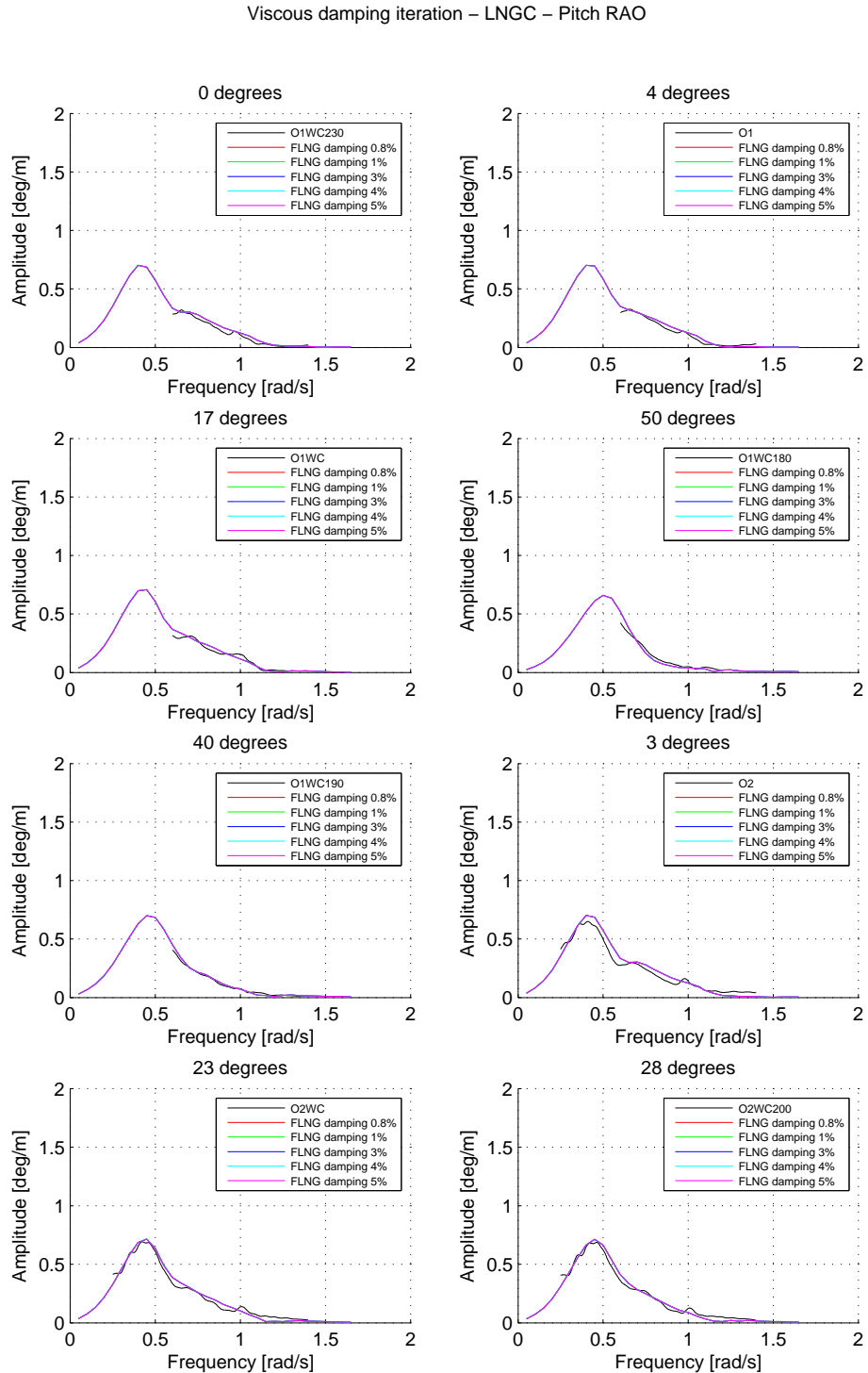


Viscous damping iteration – LNGC – Heave RAO

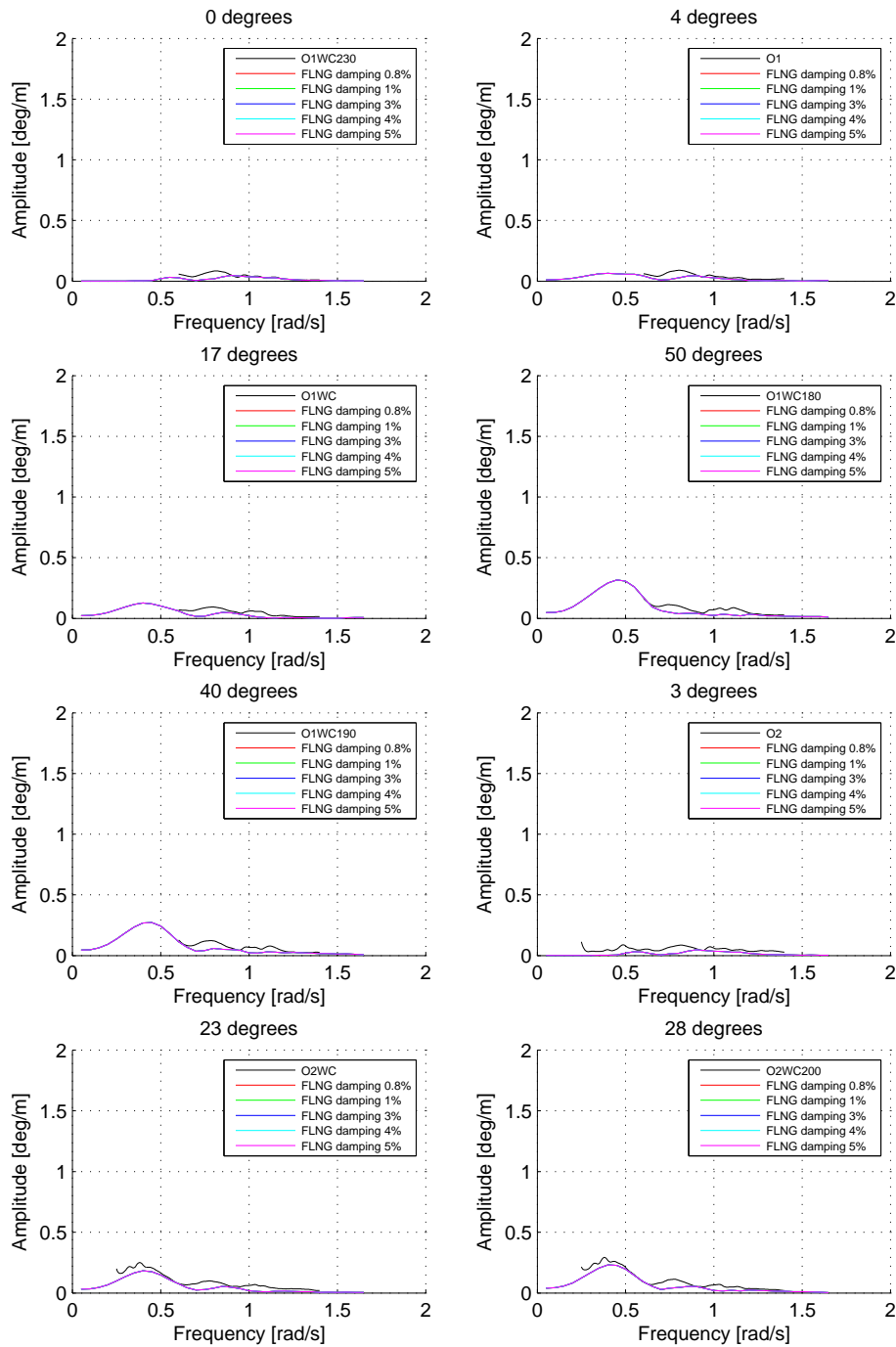


Viscous damping iteration – LNGC – Roll RAO

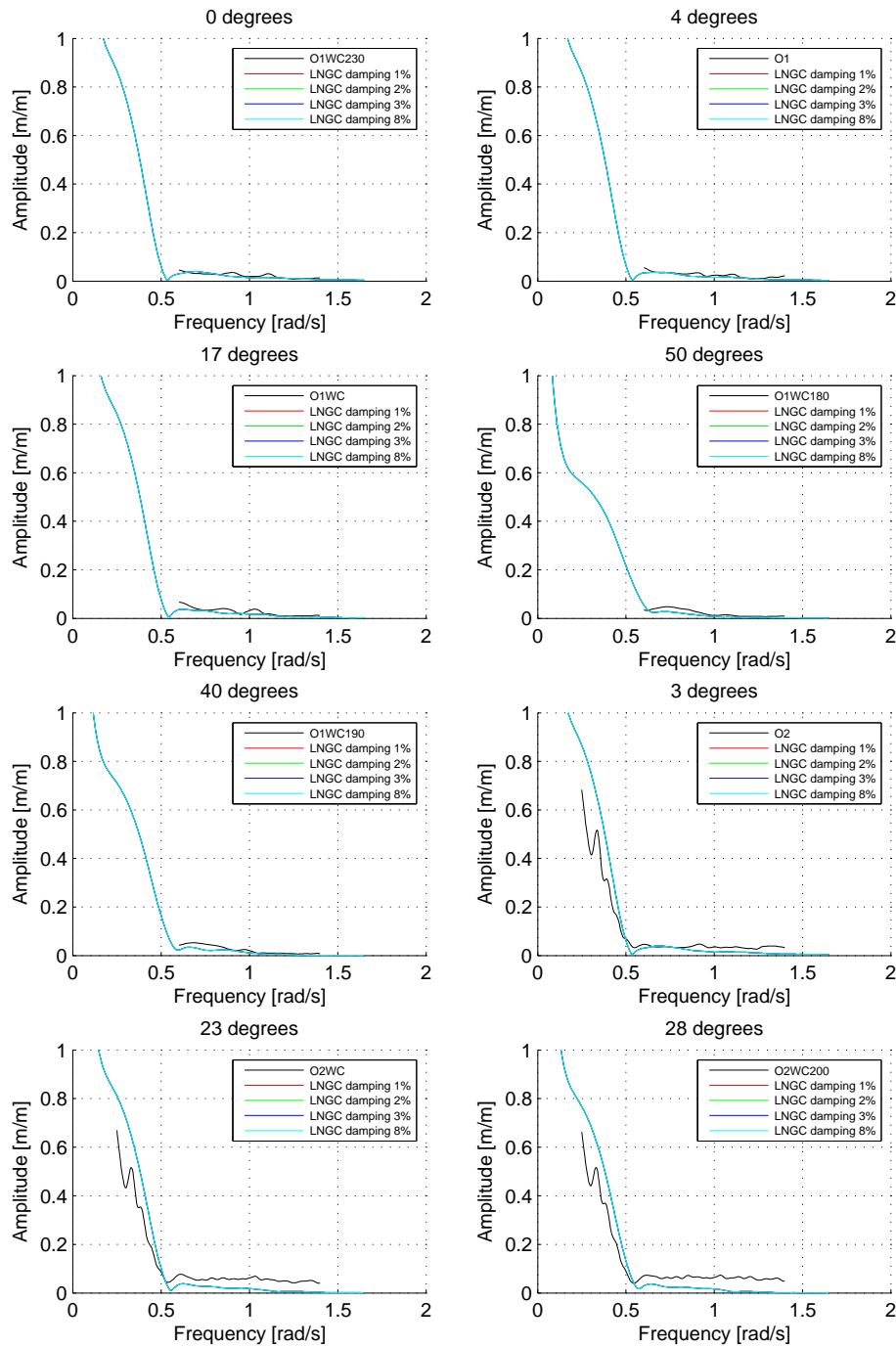




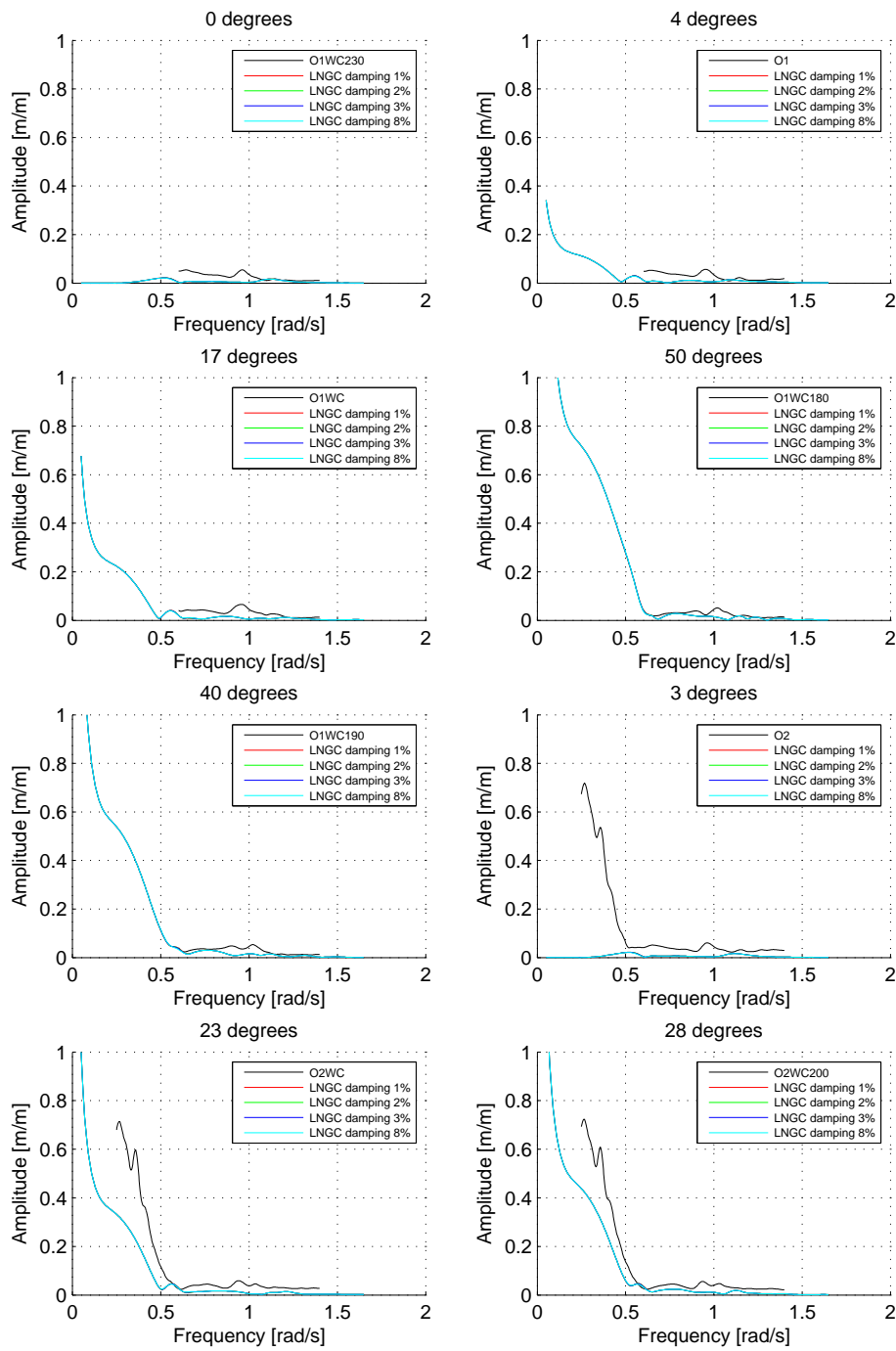
Viscous damping iteration – LNGC – Yaw RAO



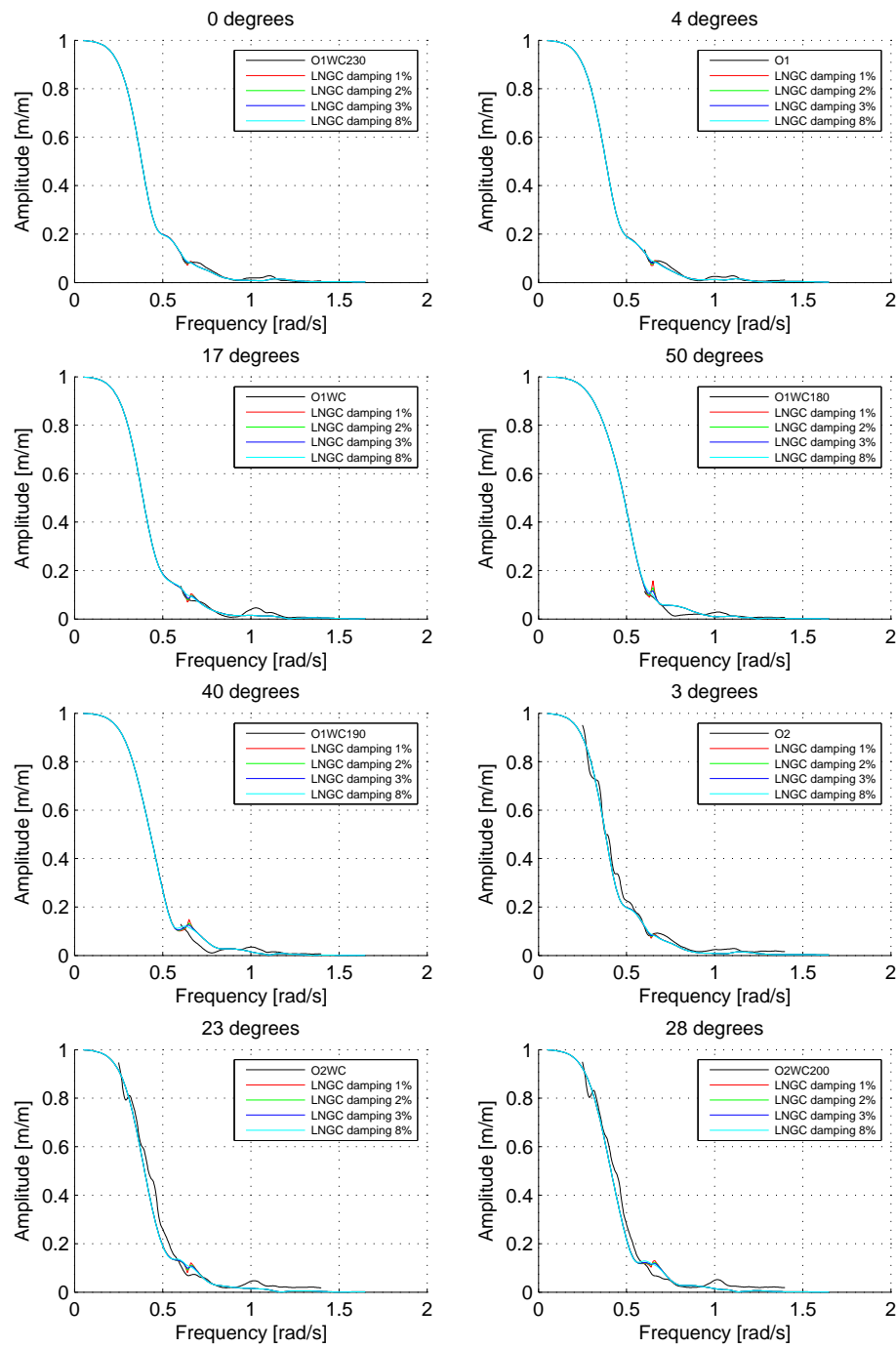
Linear roll viscous damping – FLNG – Surge RAO



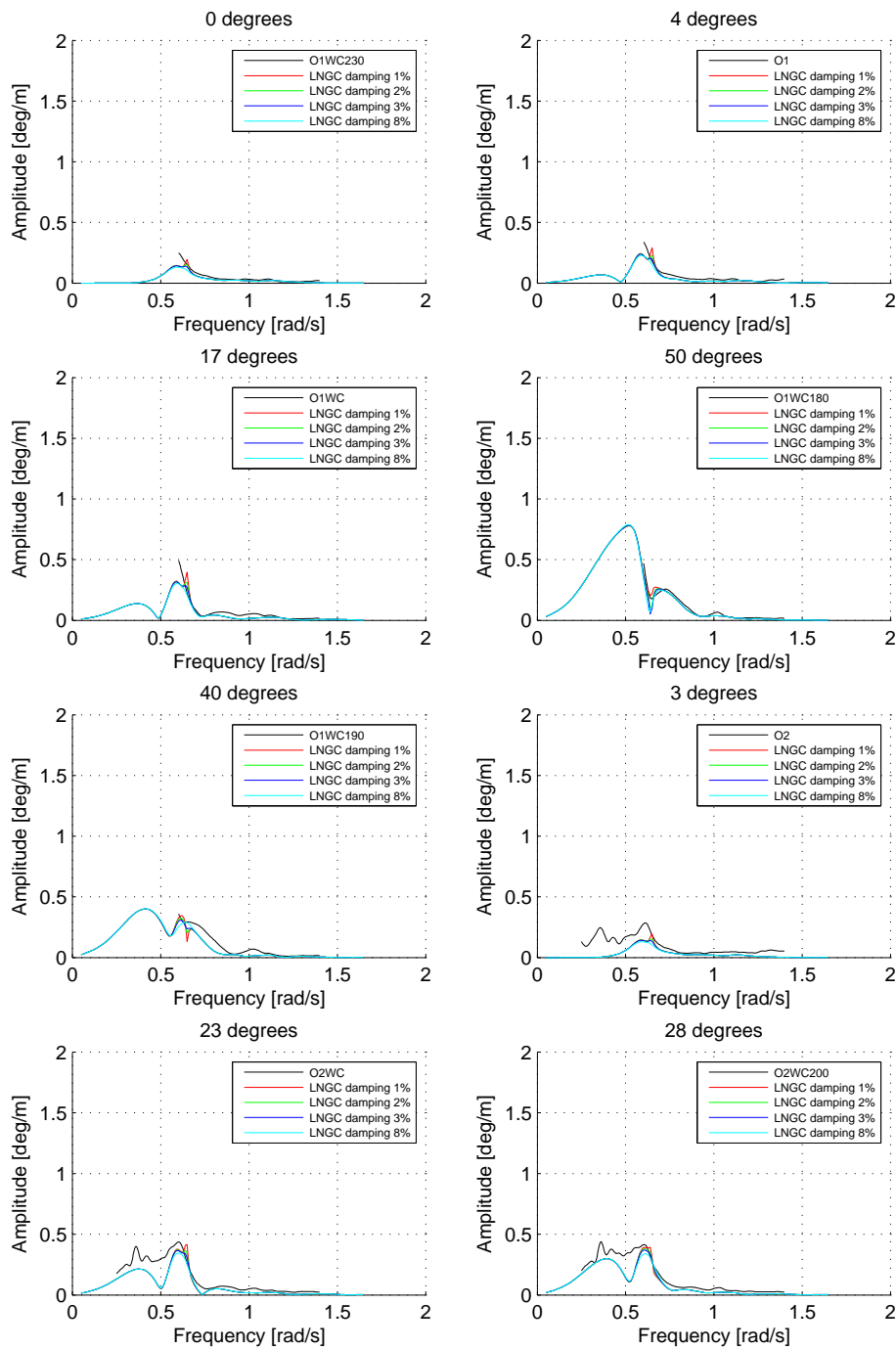
Linear roll viscous damping – FLNG – Sway RAO

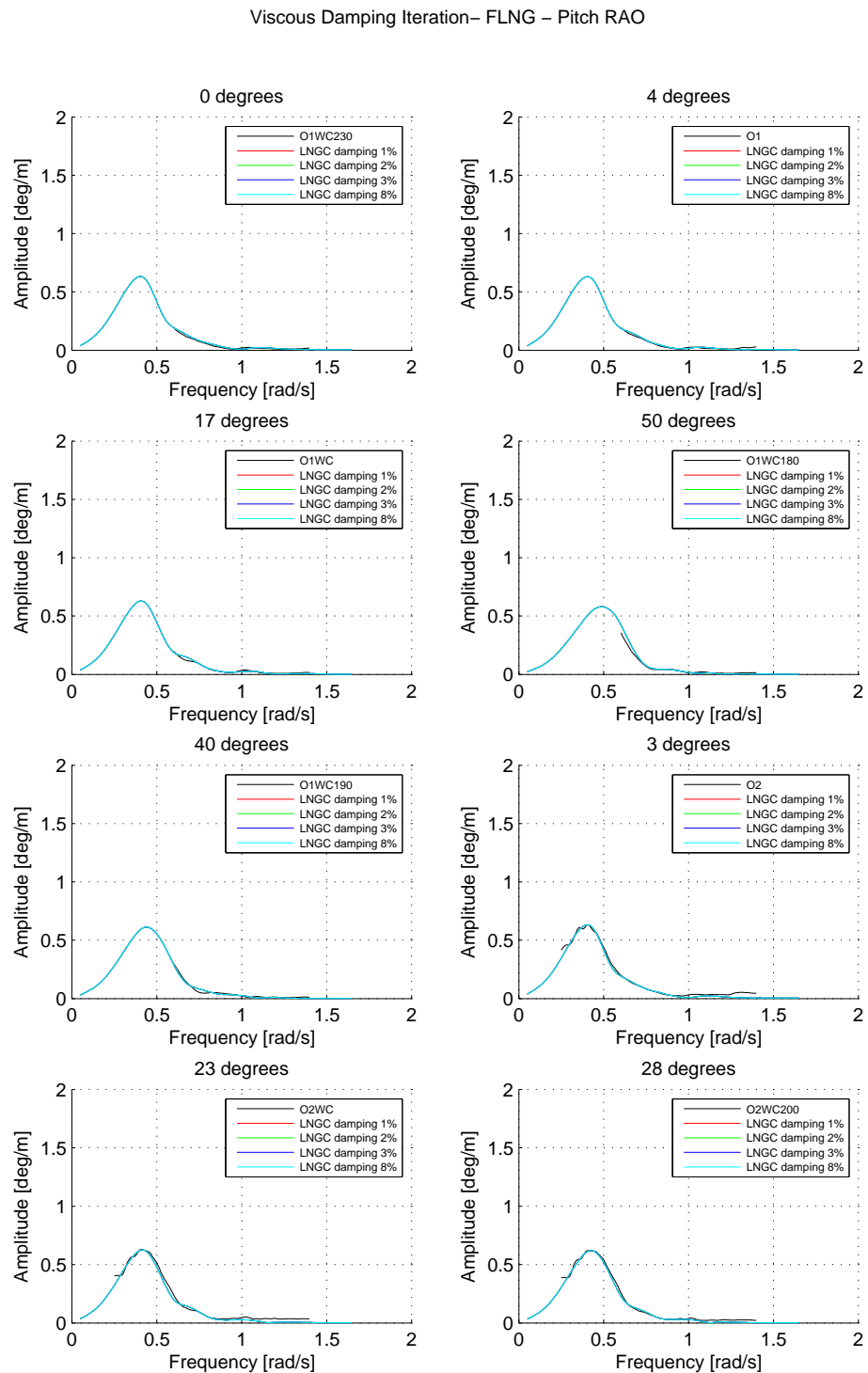


Linear roll viscous damping – FLNG – Heave RAO

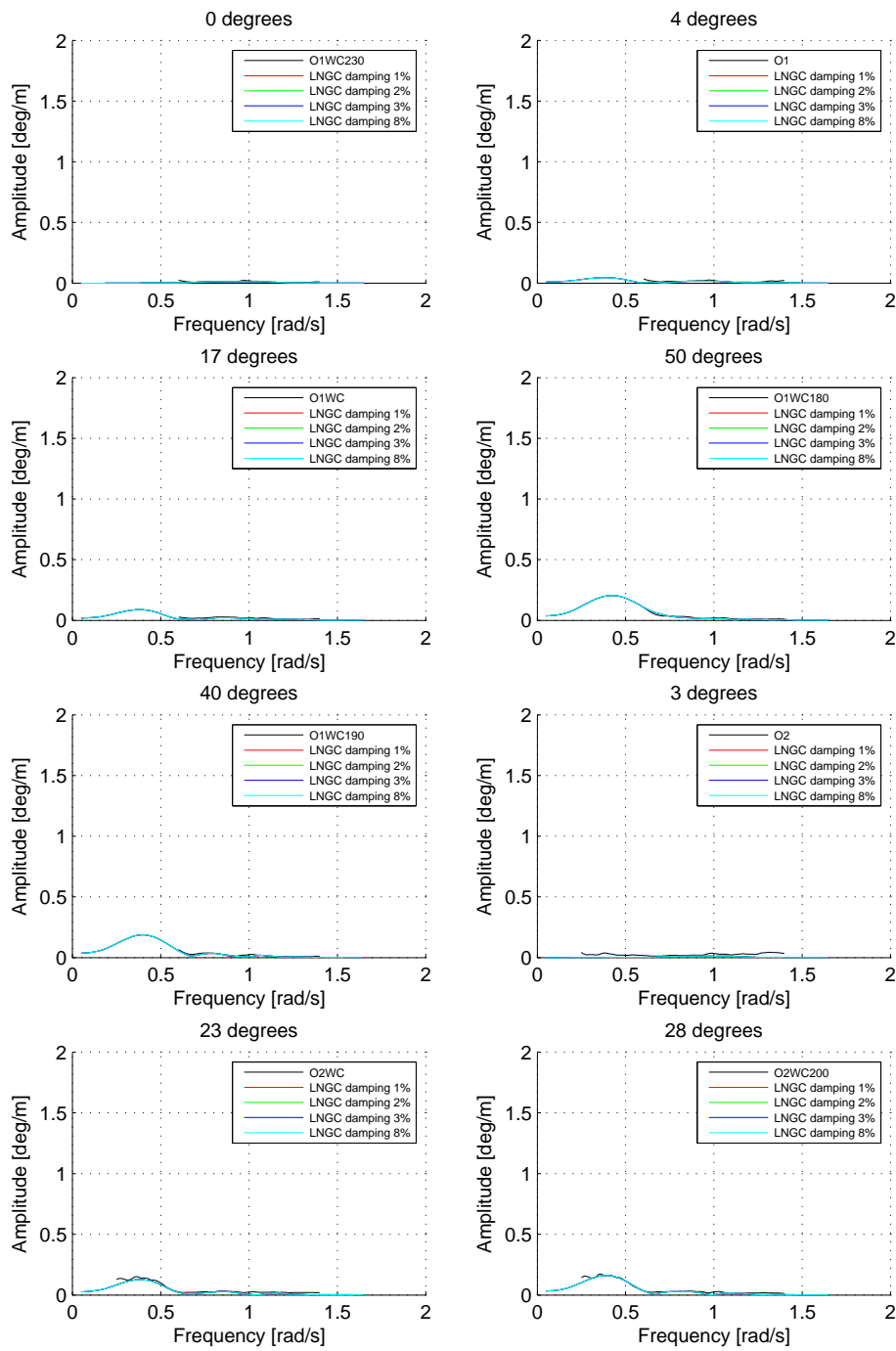


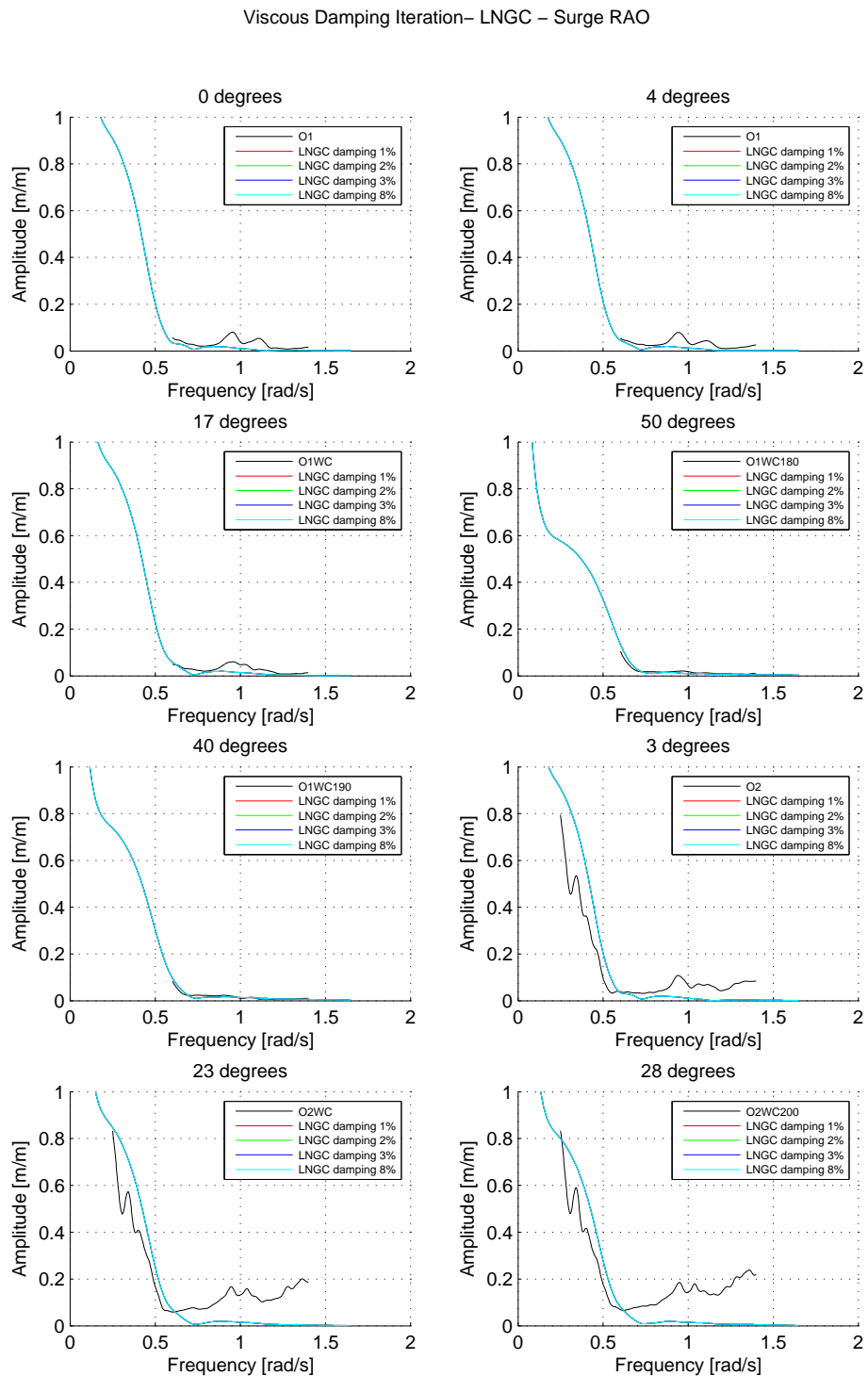
Viscous Damping Iteration– FLNG – Roll RAO



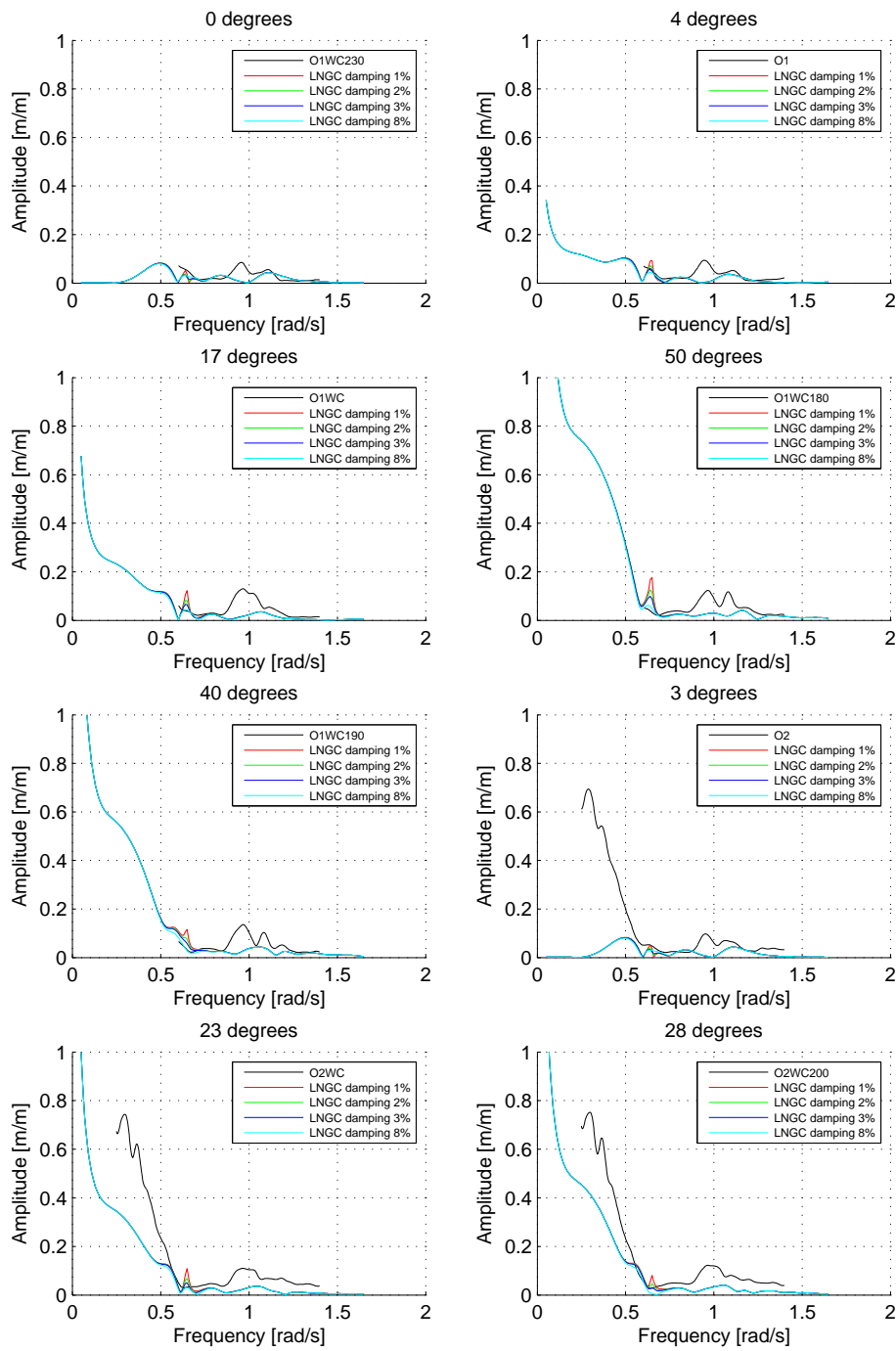


Linear roll viscous damping – FLNG – Yaw RAO

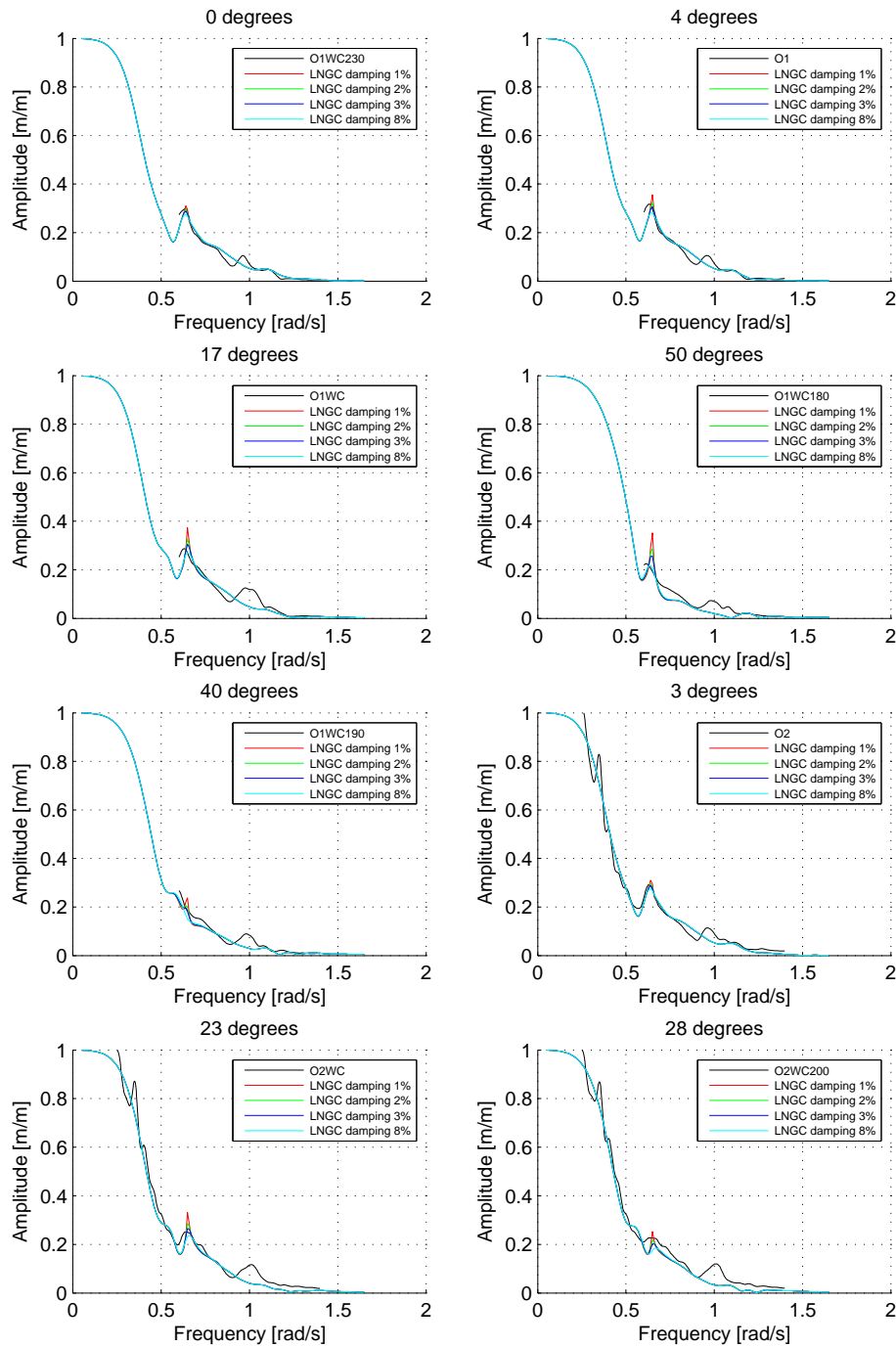




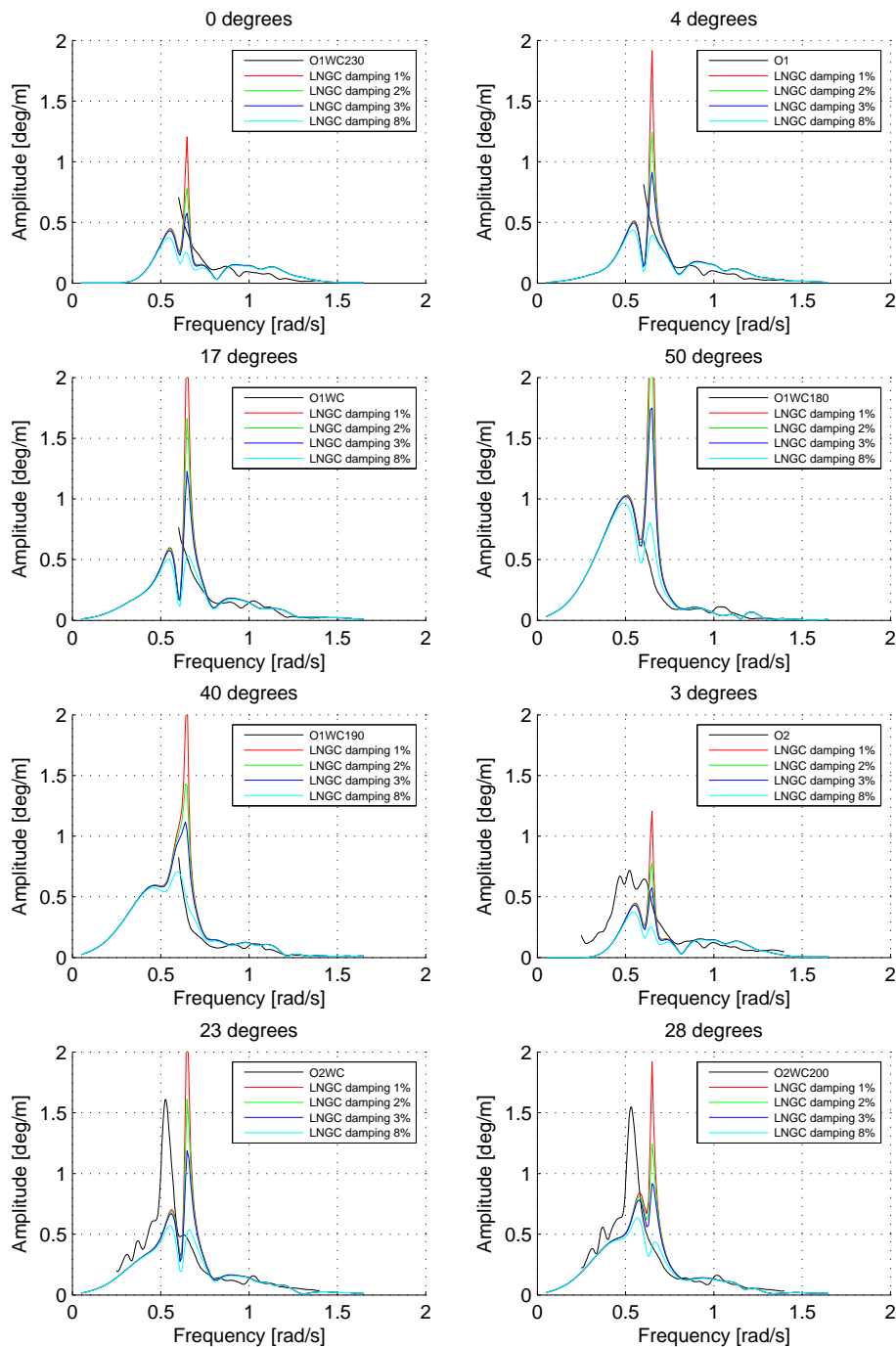
Viscous Damping Iteration – LNGC – Sway RAO

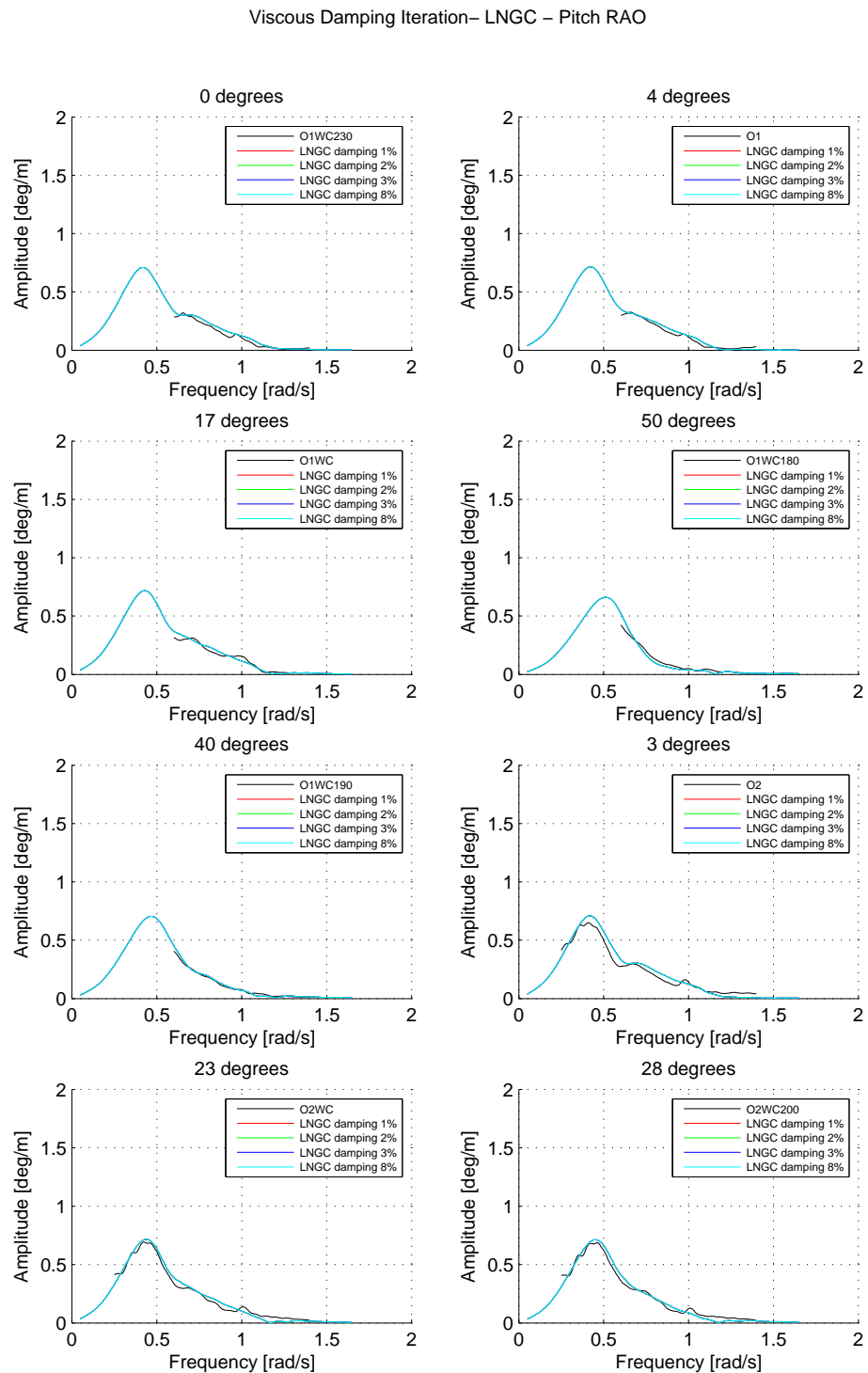


Viscous Damping Iteration– LNGC – Heave RAO

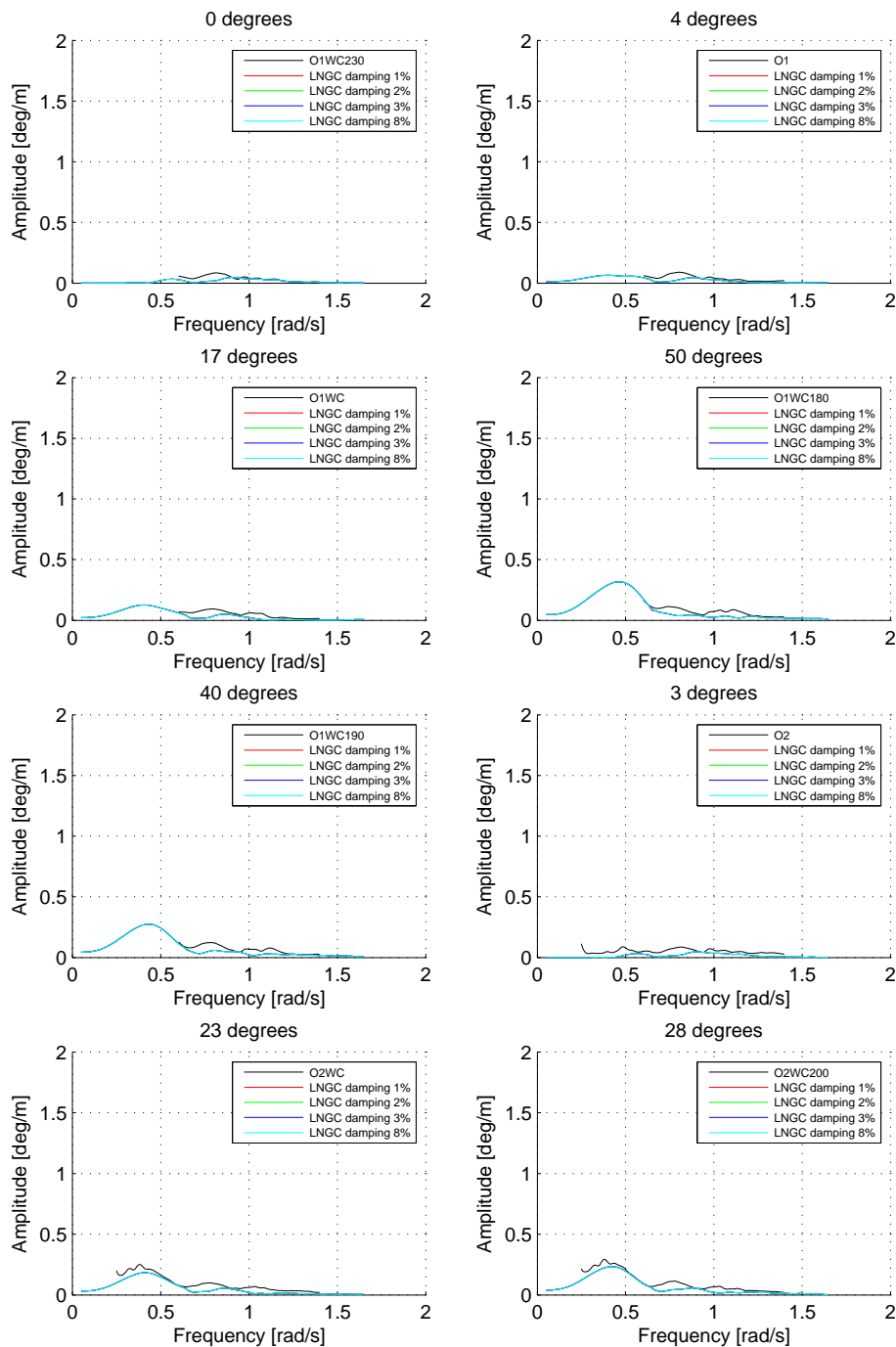


Viscous Damping Iteration– LNGC – Roll RAO



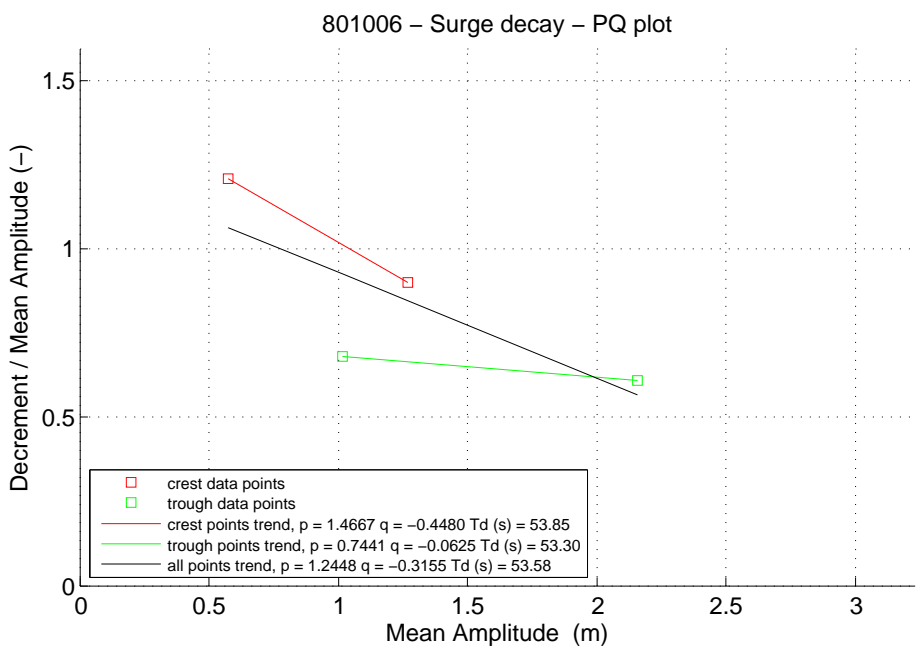
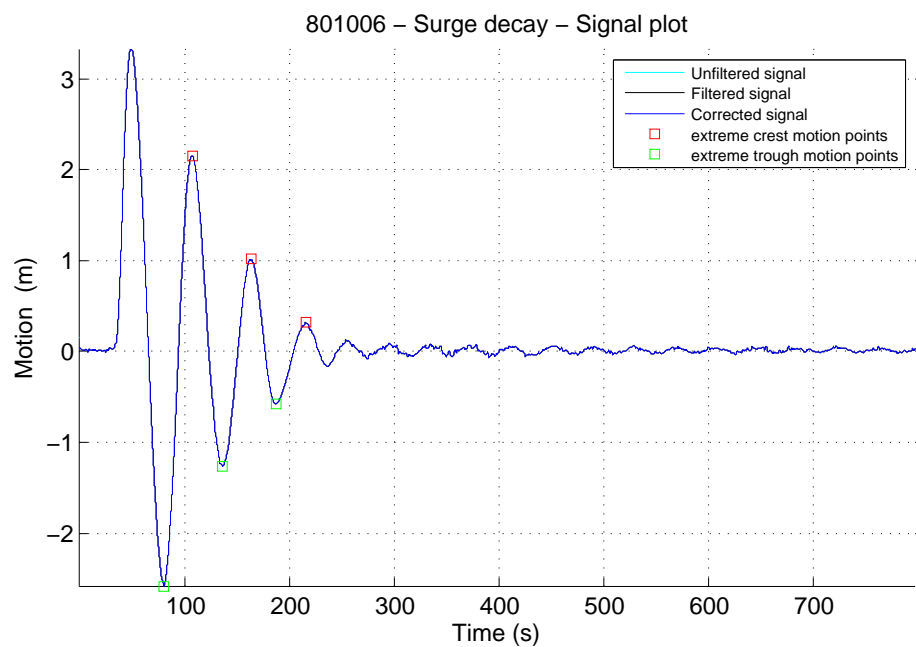


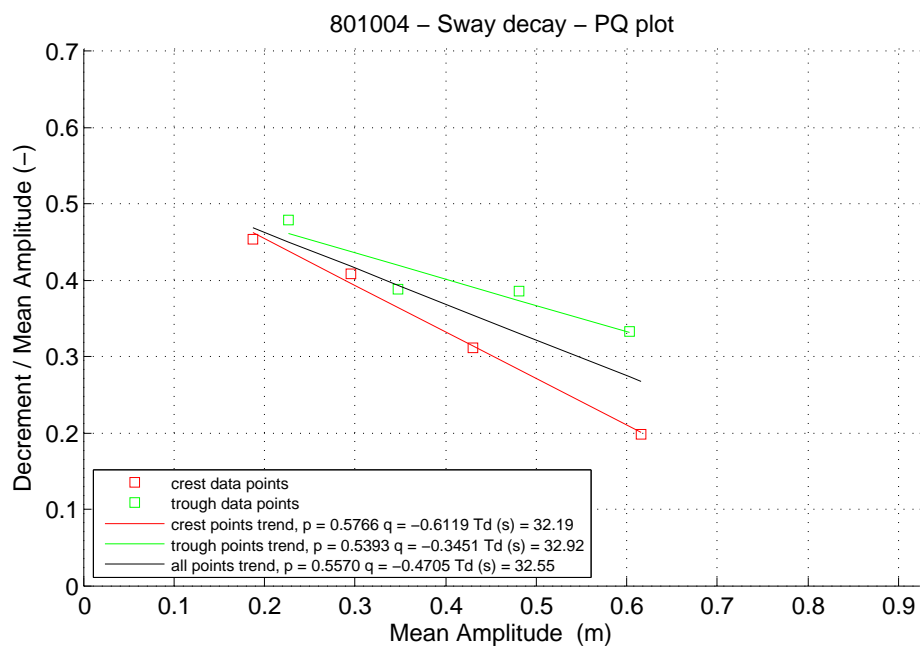
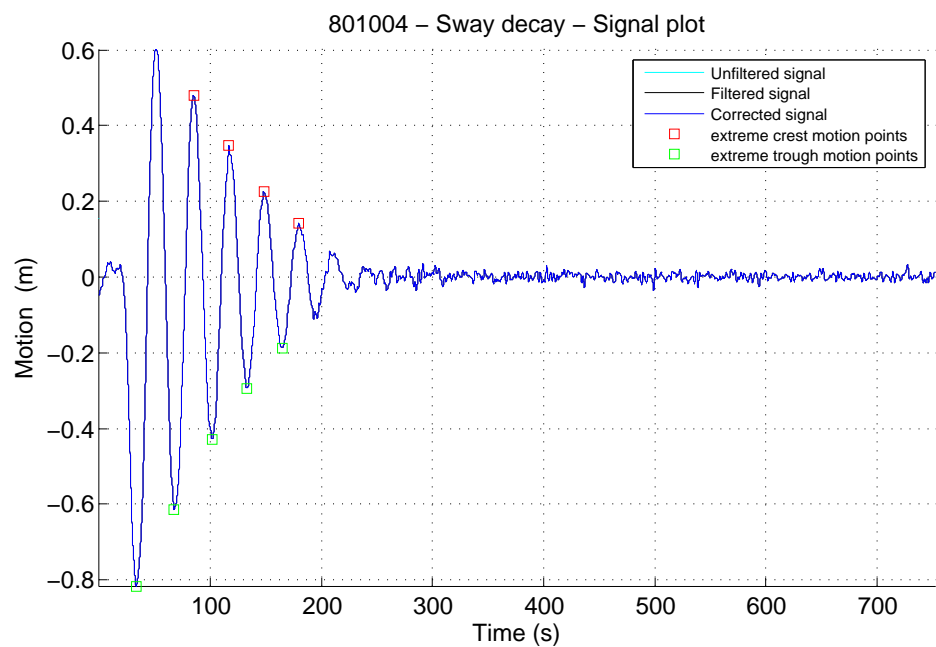
Viscous Damping Iteration– LNGC – Yaw RAO

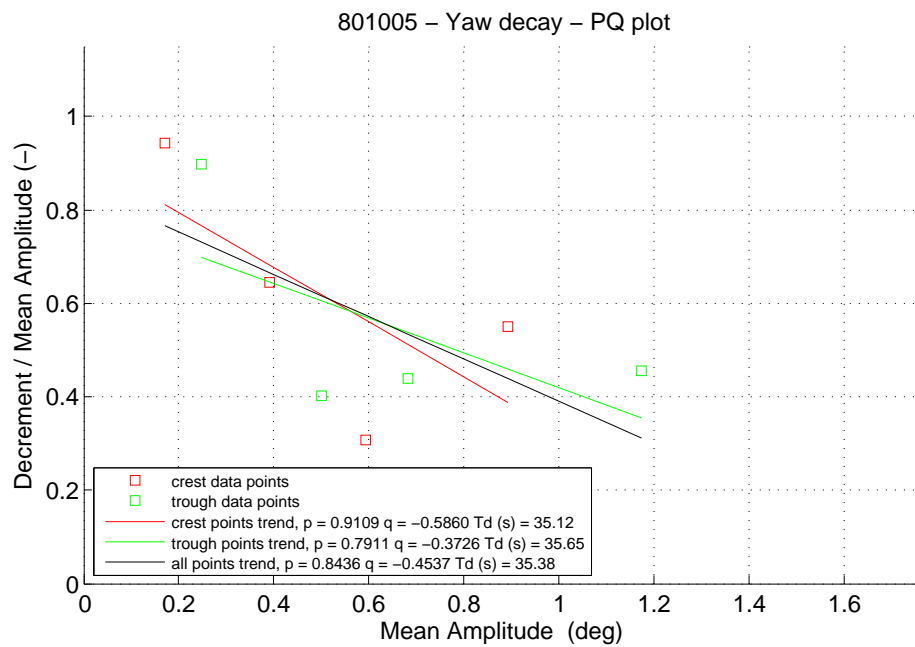
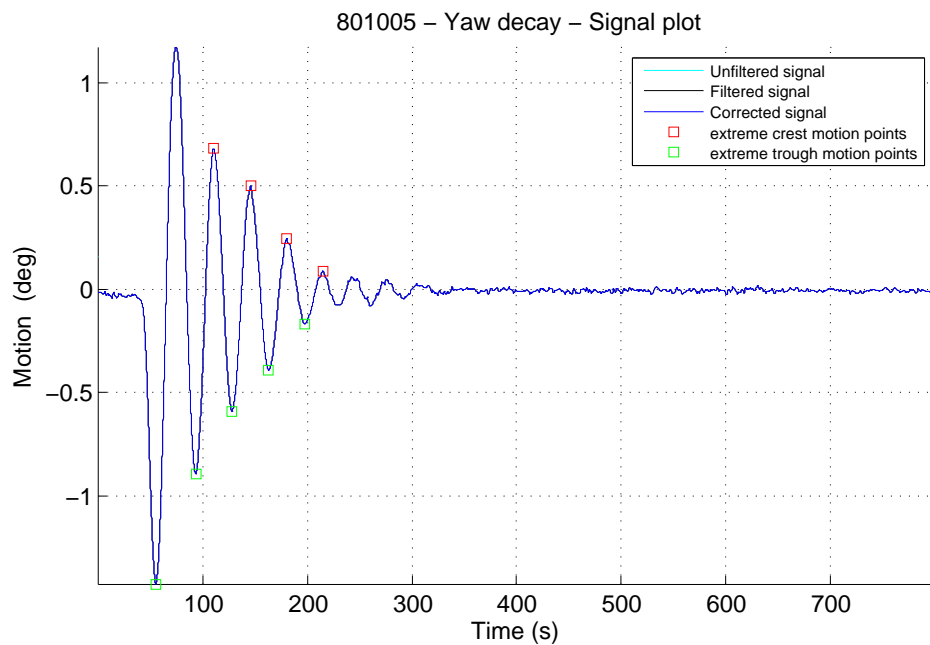


F

DECAY PLOTS



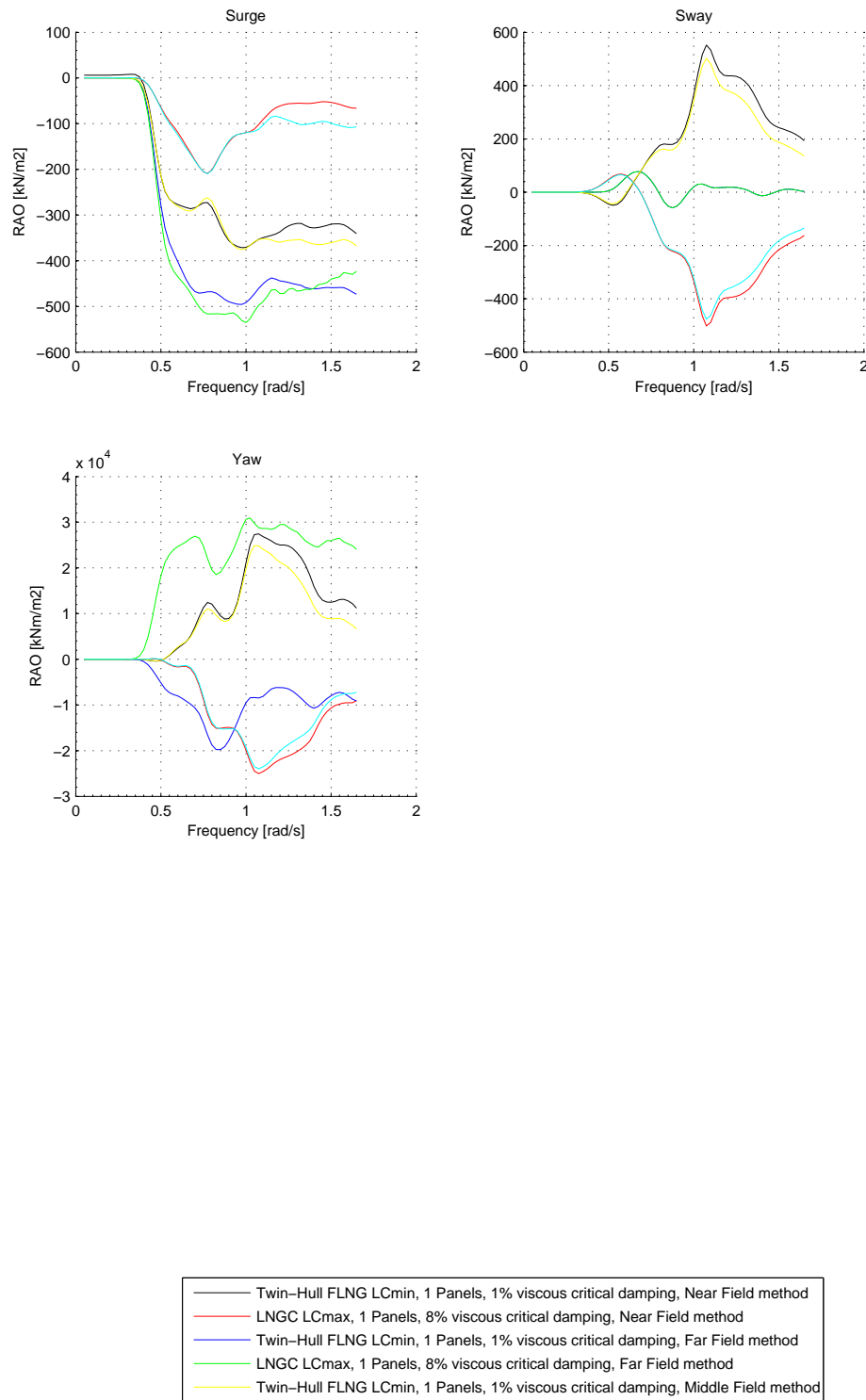




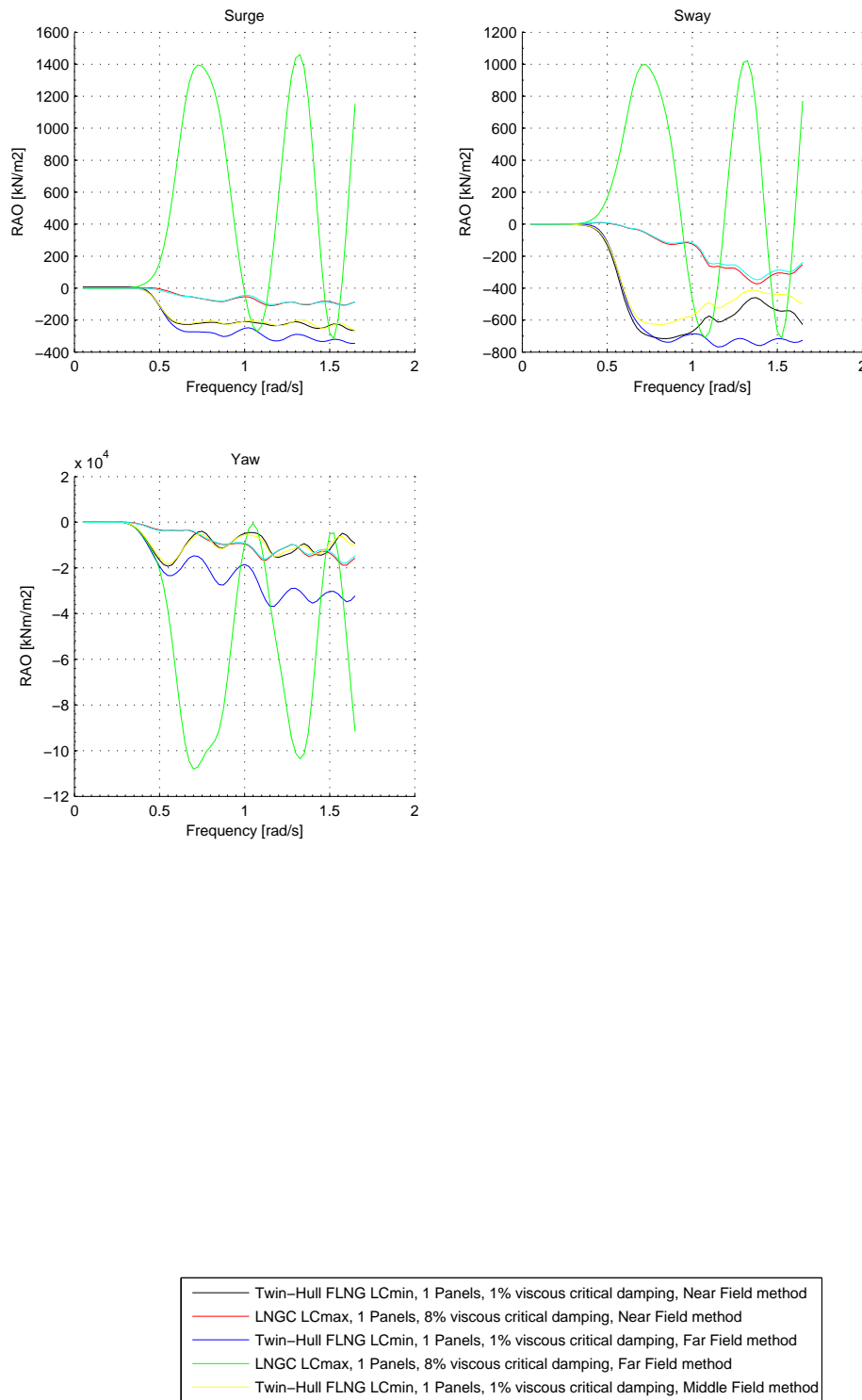
G

DIFFERENT QTF METHODS

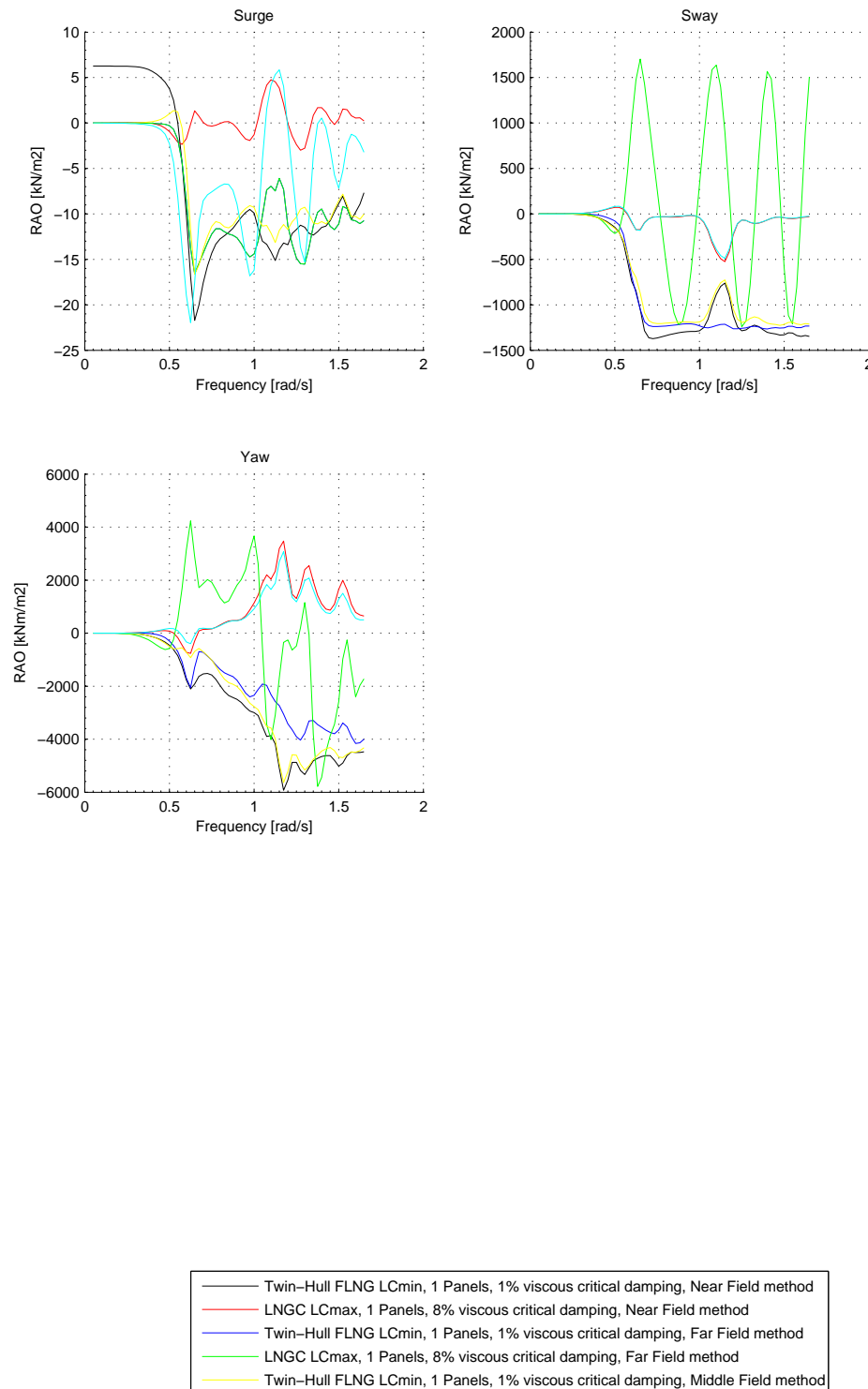
Hydrostar output study, QTFs 0 degrees



Hydrostar output study, QTFs 45 degrees



Hydrostar output study, QTFs 90 degrees



Hydrostar output study, QTFs 135 degrees

